



HAL
open science

Shrinkage and creep of cement-based materials under multiaxial load: poromechanical modeling for application in nuclear industry

Abudushalamu Aili

► **To cite this version:**

Abudushalamu Aili. Shrinkage and creep of cement-based materials under multiaxial load: poromechanical modeling for application in nuclear industry. Materials. Université Paris-Est, 2017. English. NNT: 2017PESC1014 . tel-01682129

HAL Id: tel-01682129

<https://pastel.hal.science/tel-01682129>

Submitted on 12 Jan 2018

HAL is a multi-disciplinary open access archive for the deposit and dissemination of scientific research documents, whether they are published or not. The documents may come from teaching and research institutions in France or abroad, or from public or private research centers.

L'archive ouverte pluridisciplinaire **HAL**, est destinée au dépôt et à la diffusion de documents scientifiques de niveau recherche, publiés ou non, émanant des établissements d'enseignement et de recherche français ou étrangers, des laboratoires publics ou privés.



UNIVERSITÉ PARIS-EST
ÉCOLE DOCTORALE SCIENCE INGÉNIERIE ET ENVIRONNEMENT

THÈSE

présentée pour l'obtention du diplôme de

DOCTEUR

DE

L'UNIVERSITÉ PARIS-EST

Spécialité: *Mécanique*

par Abudushalamu AILI

Sujet de la thèse :

Shrinkage and creep of cement-based
materials under multiaxial load:
poromechanical modeling
for application in nuclear industry

Thèse soutenue le 27 septembre 2017 devant le jury composé de :

<i>Président :</i>	Prof. Farid BENBOUDJEMA
<i>Rapporteurs :</i>	Prof. Alain SELIER Prof. Bernhard PICHLER
<i>Examineurs :</i>	Prof. Kefei LI Mr. Benoît MASSON Dr. Julien SANAHUJA
<i>Invité :</i>	Dr. Laurent CHARPIN
<i>Co-encadrant :</i>	Dr. Matthieu VANDAMME
<i>Directeur de thèse :</i>	Prof. Jean-Michel TORRENTI

To Ayperi, Laila and Yahya ...

*“Truth is ever to be found in simplicity, and not in the multiplicity and
confusion of things.”*

Issac Newton

Remerciements

Cette thèse a été financée par EDF-DIN-SEPTEN et effectuée au sein du Laboratoire Navier (UMR ENPC, IFSTTAR, CNRS) à l'École des Ponts ParisTech. Je souhaite remercier toutes les personnes qui ont contribué à l'aboutissement de ce travail.

Je souhaite exprimer toute ma reconnaissance à mes encadrants de thèse auprès de qui j'ai passé trois années extrêmement enrichissantes. Je remercie en particulier Jean-Michel Torrenti d'avoir accepté ma candidature pour la thèse sans entretien et d'avoir prodigué de précieux conseils scientifiques tout au long de ces 3 années. Il était toujours disponible pour m'aider jusqu'à chercher des matériels au laboratoire. Sans ses vastes connaissances sur les matériaux cimentaires, le chemin de la thèse aurait été plus tortueux. Je remercie également et très sincèrement Matthieu Vandamme tout d'abord pour m'avoir proposé la thèse, puis pour son encadrement régulier et enthousiaste, pour ses idées brillantes, pour la clarté de ses explications et pour sa gentillesse.

J'aimerais également remercier l'ensemble des membres du jury pour l'intérêt qu'ils ont manifesté pour ces travaux et leurs questions et remarques constructives. J'exprime mes plus sincères remerciements aux professeurs Alain Sellier et Bernhard Pichler pour leur lecture détaillée de mon manuscrit. Je remercie également Farid Benboudjema, qui était aussi membre du comité de suivi de ma thèse, d'avoir accepté de présider le jury. Mes remerciements vont aussi au professeur Kefei Li, qui m'a enseigné mon tout premier cours sur les matériaux cimentaires. Je tiens également à remercier les autres membres du jury : Benoît Masson, Julien Sanahuja et Laurent Charpin, qui étaient également membres du comité de suivi de ma thèse.

Je tiens à remercier tous les chercheurs qui m'ont donné des conseils constructifs pour la thèse. Notamment les chercheurs du Laboratoire Navier : merci à Anh Minh Tang pour ses conseils sur la méthode de séchage des éprouvettes. Merci à Robert Leroy pour ses conseils sur la méthode de

coulage des éprouvettes. Merci à Jean-François Caron et Frédéric Tayeb pour leur idée de fabriquer des pièces de support par impression 3D. Merci également à Siavash Ghabezloo pour son aide sur l'estimation du coefficient de Biot par la méthode d'homogénéisation. Je remercie également Bruno Huet du Centre de Recherche de LafargeHolcim pour les échanges sur la perméabilité du béton et sur la cinétique d'auto-dessiccation.

Je remercie tous les techniciens du Laboratoire Navier de leur aide, en particulier pour les travaux expérimentaux de la thèse. Merci à David Hautemayou, Cédric Mezière du site Kepler pour avoir préparé les montages expérimentaux. Merci également à Emmanuel De Laure, Marine Lemaire, Baptiste Chabot, Hocine Delmi pour leur support pour leurs idées très constructives concernant le montage du dispositif expérimental et leur support pour la mesure de l'humidité relative. Merci à Sébastien Gervillers, Christophe Bernard pour leur aide pour la fabrication des supports expérimentaux avec imprimante 3D.

Je remercie tout le personnel du département MAST de l'IFSTTAR. Merci à l'équipe du laboratoire EMMS pour leur aide pour mesurer les déformations différées : Florent Baby, Renaud-Pierre Marin, Jean-Claude Renaud, Franck Guirado, Pierre Marchand. Merci à l'équipe FM2D pour leur aide pour la préparation des éprouvettes de pâte de ciment et la mesure de la résistance en compression : Daniel Simitambe, Jean-François Bouteloup. Merci à l'équipe CPDM pour leur aide pour les essais ATG : Mickaël Saillio, Sandrine Moscardelli, Julien Vincent.

J'exprime ma reconnaissance aussi à l'équipe administrative, et en particulier à Marie-Françoise Kaspi, Rachida Atmani, Sandrine Coqueret, Annie Wei, Pauline Huart, Valérie Fournier et Cécile Blanchemanche.

Je tiens aussi à remercier l'ensemble des chercheurs du laboratoire Navier. En particulier Karam Sab directeur du laboratoire, et Michel Bornert, responsable de l'équipe multi-échelle.

Je remercie chaleureusement toutes les personnes avec qui j'ai partagé un repas, un café ou une discussion durant ces trois ans. Je pense en particulier à mes amis et collègues de bureau : Abdessamad Akkaoui, Nam Nghia Bui, Hafsa Rahoui, Thanh Tung Nguyen, Ababacar Gaye, Houda Friaa, Túlió

Honório de Faria, Sara Bahafid, Hugo Troupel, Yushan Gu. Merci pour les moments inoubliables que nous avons passés ensemble, pour les discussions enrichissantes et pour vos encouragements.

Last but not least, j'exprime également ma gratitude à ma famille pour leurs encouragements et leur soutien permanent. Vous êtes toujours derrière mes réussites et mes différents exploits.

Je ne vais pas finir cette page sans remercier ma très chère Ayperi, pour son amour, sa patience, et pour tout ce qu'elle a fait pour moi. Sans elle, tout cela n'aurait pas été possible. Et bienvenue à Laila et Yahya, qui ont comblé nos jours et nuits de joie et de bonheur.

Abstract

The main interest of the thesis is the long-term mechanical behavior of the containment building of french nuclear power plants. The containment buildings of the power plants are biaxially prestressed concrete structures. Therefore, we summarize the problem of interest into two following key points: biaxiality of load and long-term delayed strain.

In order to characterize the delayed strain under biaxial load, our study first concentrates on the viscoelastic Poisson's ratio of concrete. In this purpose, we start by scrutinizing the definition of Poisson's ratio in non-aging linear isotropic viscoelasticity. Then, from the analysis of experimental results from the literature, we can obtain the viscoelastic Poisson's ratio of concrete. As an extension, we use micromechanics to shed some light on the long-term creep mechanism of the C-S-H gel.

In a second step, we aim at proposing a poroviscoelastic model without postulating a priori the classical decomposition of delayed strains. We start by identifying the major experimental tendencies and physical phenomena that we aim at capturing with the model. From experimental data of autogenous shrinkage and basic creep from the literature, we analyze the possible physical origin of long-term autogenous shrinkage. In the end, a physics-based poroviscoelastic model is proposed, derived from the poromechanics theory. The prediction of the model is compared with experimental results from literature.

Keywords: concrete, cement-based materials, micromechanics, poromechanics, downscaling, viscoelasticity, viscoelastic Poisson's ratio, autogenous shrinkage, basic creep, drying shrinkage, drying creep, capillary effect.

Résumé

L'intérêt principal de la thèse est le comportement mécanique à long terme des enceintes de confinement des centrales nucléaires françaises. Les enceintes de confinement des centrales sont des structures en béton précontraint biaxialement. Nous résumons donc notre problème en deux points clés : la biaxialité du chargement et les déformations différées à long terme.

Afin de caractériser les déformations différées sous chargement biaxial, nous nous concentrons dans un premier temps sur le coefficient du Poisson viscoélastique du béton. Dans ce but, nous commençons par examiner minutieusement la définition du coefficient de Poisson dans le cadre de la viscoélasticité linéaire isotrope non-vieillissante. Puis, en analysant les résultats expérimentaux de la littérature, nous obtenons le coefficient de Poisson viscoélastique du béton. Comme extension, nous amenons une analyse micromécanique et essayons d'éclaircir le mécanisme du fluage à long terme du gel de C-S-H.

Dans un deuxième temps, nous visons à proposer un modèle poroviscoélastique sans supposer préalablement la décomposition classique des déformations différées. Nous commençons par identifier les tendances expérimentales majeures et phénomènes physiques que nous voulons capturer par le modèle. À partir des résultats expérimentaux du retrait endogène et du fluage propre de la littérature, nous analysons l'origine physique possible du retrait endogène à long terme. À la fin, dérivé de la théorie de la poromécanique, un modèle poroviscoélastique basé sur la physique est proposé. La prédiction du modèle est comparée avec les résultats expérimentaux de la littérature.

Mots clés : béton, matériaux cimentaires, micromécanique, poromécanique, changement d'échelle, viscoélasticité, coefficient de Poisson viscoélastique, retrait endogène, fluage propre, retrait de dessiccation, fluage de dessiccation, effet capillaire.

Résumé long

Plus de 70% d'électricité en France est produite par l'énergie nucléaire. De nombreuses centrales nucléaires d'EdF ont été construites initialement pour une durée de service de 40 ans. La plupart d'entre elles arrivent prochainement en fin de vie. Dans l'optique de vouloir évaluer et prolonger la durée de vie de ces centrales nucléaires, on s'intéresse aux enceintes de confinement qui sont des structures en béton précontraint biaxialement. La précontrainte est nécessaire pour que l'enceinte soit capable de résister à une pression interne de 0.5 MPa en cas d'accident et maintenir son étanchéité. Or, avec le temps, le béton flue, et la précontrainte se relaxe. Par conséquent, l'étanchéité doit être vérifiée. Le présent travail se focalise donc sur la déformation différée à long terme des matériaux cimentaires matures sous contrainte multiaxiale.

Pour des comportements uniaxiaux, la complaisance uniaxiale est suffisante pour décrire le comportement du matériau. Dans le cas multiaxial, nous avons besoin de deux paramètres viscoélastiques pour décrire le comportement multiaxial. Cela pourrait être, par analogie avec l'élasticité, la complaisance uniaxiale et le coefficient de Poisson viscoélastique. De nombreuses études et modèles sur la complaisance uniaxiale existent dans la littérature. Quant au coefficient de Poisson viscoélastique, très peu d'études y sont dédiées. En plus, les différents auteurs ont rapporté ou proposé des valeurs assez différentes les unes des autres. Une des raisons qui explique cette divergence est que ces auteurs ont utilisé différentes définitions du coefficient de Poisson. En viscoélasticité linéaire isotrope non-vieillissante, la définition du coefficient de Poisson n'est pas unique non plus. Donc, la première partie de la thèse sera consacrée à la définition du coefficient de Poisson en viscoélasticité, et à ses valeurs et évolutions pour les matériaux cimentaires.

En viscoélasticité linéaire, il est possible de définir un coefficient de Poisson de 7 manières différentes. On s'est limité à comparer les deux définitions les plus intuitives: un coefficient de Poisson de relaxation, défini comme l'opposé du ratio entre la déformation latérale et axiale dans un test de relaxation uniaxiale; un coefficient de Poisson de fluage, défini comme l'opposé

du ratio entre la déformation latérale et axiale dans un test de fluage uniaxial. Ces deux coefficients de Poisson ne sont pas identiques. Nous dérivons la relation qui lie ces deux coefficients de Poisson via la complaisance uniaxiale. Ainsi, on démontre sans aucune hypothèse supplémentaire qu'à l'instant de chargement les valeurs de ces 2 coefficients de Poisson sont identiques, ainsi que leurs dérivées. À long terme, les deux coefficients de Poisson tendent vers une même valeur asymptotique. Le coefficient de Poisson de relaxation est utilisé lorsqu'on résout un problème analytiquement en utilisant le principe de correspondance, puisque c'est la transformée de Laplace du coefficient de Poisson de relaxation qui remplace le coefficient du Poisson élastique. En revanche, presque tous les expérimentalistes ont utilisé le coefficient de Poisson de fluage car son calcul inverse à partir des mesures expérimentales est plus simple que celui du coefficient de Poisson de relaxation. Ensuite, nous avons analysé les résultats expérimentaux de fluage propre sur matériaux cimentaires de la littérature et avons trouvé que la différence entre ces deux coefficients de Poisson est presque négligeable. Par conséquent, dans la suite de la thèse, on ne distingue plus ces deux coefficients de Poisson et on le nomme coefficient de Poisson viscoélastique. On le calcule avec l'expression du coefficient de Poisson de fluage et on applique le principe de correspondance.

Ensuite, nous menons une étude exhaustive des tests de fluage propre dans lesquelles la déformation différée est mesurée dans plus d'une direction. Les 63 tests sur béton et 1 test sur pâte de ciment nous montrent que le coefficient de Poisson à long terme de matériaux cimentaires est inférieur ou égal à la valeur élastique. Pour la plupart des bétons, considérer le coefficient de Poisson viscoélastique comme constant au cours du temps est un bon choix. Le fait que le coefficient de Poisson à long terme est plus petit que 0.5 montre que le fluage à long terme des bétons est à la fois volumétrique et déviatorique. Pour explorer les résultats sur coefficient de Poisson, nous analysons des mécanismes qui peuvent expliquer ce fluage volumétrique à long terme.

Comme l'origine du fluage des matériaux cimentaires se trouve dans le gel de C-S-H, nous calculons le coefficient du Poisson du gel de C-S-H pour

chacune de 64 tests ci-dessus en trois étapes d'homogénéisation par le schéma d'homogénéisation viscoélastique de Mori-Tanaka. Le coefficient de Poisson du gel de C-S-H à long terme est plus petit que 0.2 et a peu d'influence sur le coefficient de Poisson du béton. Le fait d'avoir un coefficient de Poisson plus petit que 0.5 montre qu'à long terme, le fluage du gel de C-S-H possède à la fois un composant volumétrique et un composant déviatorique. Ensuite, différents mécanismes sont analysés en considérant le gel de C-S-H comme un mélange de particules de C-S-H et de pores de gel par un schéma auto-cohérent. Nous retenons que: lorsqu'on considère que le fluage à long terme est dû aux particules de C-S-H, il est nécessaire que soit les particules sont sphériques et il y a un glissement et un rapprochement des feuillets constituant les particules de C-S-H; soit les particules sont asphériques et juste le glissement des feuillets peut être suffisant pour expliquer le fluage volumétrique. Lorsqu'on considère que le fluage à long terme est dû aux points de contact entre des particules, pour avoir un coefficient de Poisson du gel de C-S-H entre 0 et 0.2, sous hypothèse de particule sphérique, il faut qu'il y ait à la fois glissement et pénétration des points de contact.

Après avoir clarifié le coefficient de Poisson des matériaux cimentaires, nous nous intéressons à la modélisation des déformations différées. Tous les codes de calculs réglementaires et la plupart des modèles académiques de la littérature décomposent la déformation différée du béton en quatre composantes: retrait endogène, retrait de dessiccation, fluage propre et fluage de dessiccation. Chacune de ces 4 composantes est calculée séparément et la déformation totale est obtenue en faisant la somme de ces 4 composantes. Or, cette manière de calculer néglige toutes les corrélations possible entre les différentes composantes. Nous avons donc pour objectif de proposer un modèle sans supposer a priori cette décomposition classique de la déformation différée. Pour ce faire, nous allons considérer chacune de ces 4 composantes comme une déformation viscoélastique du matériau.

Il nous a fallu, avant de proposer le modèle, vérifier l'hypothèse constituant à considérer le retrait endogène comme un phénomène de fluage sous l'effet capillaire dû à l'autodessiccation. En analysant toute une série de tests sur les matériaux cimentaires faits avec ciment Portland ordinaire (45

tests de retrait endogène et 59 tests de fluage propre), nous avons calculé une contrainte qui est nécessaire pour expliquer le retrait endogène à long terme comme un phénomène de fluage. Cette contrainte a le même ordre de grandeur que la contrainte capillaire estimée à partir des mesures expérimentales de l'humidité relative à long terme en conditions endogènes à l'aide de la théorie de poromécanique. Ces deux contraintes exhibent une même tendance lorsque le rapport eau-sur-ciment du matériau décroît. Cela nous conduit à conclure qu'on peut modéliser le retrait endogène à long terme comme un phénomène de fluage sous l'effet capillaire dû à l'autodessiccation.

Pour modéliser la déformation différée des matériaux cimentaires en viscoélasticité linéaire, on considère un milieu poreux, dont la porosité peut être totalement ou partiellement saturée. La poromécanique nous permet de prendre en compte les effets de l'eau dans la porosité. La complaisance volumétrique de fluage du matériau est considérée comme une fonction logarithmique du temps, en accord avec la cinétique à long terme du fluage propre. On considère que le module du fluage du matériau est une fonction de l'humidité relative interne du matériau. Pour expliquer le fluage de dessiccation, nous supposons que la contrainte capillaire est transmise au squelette solide en sa totalité dans le cas de séchage avec charge appliquée, tandis que dans le cas de séchage sans charge, la contrainte capillaire n'est transmise qu'en partie au squelette solide. À la fin, le modèle est calibré avec deux tests de la littérature pour montrer qu'on peut modéliser la déformation différée des matériaux cimentaires sans supposer a priori la décomposition classique en 4 composantes indépendantes..

Contents

Contents	17
List of Figures	21
List of Tables	31
1 Context and state of the art	45
1.1 Context of the thesis	48
1.2 Microstructure and hydration of concrete	49
1.2.1 Phases in concrete	49
1.2.2 Pore spaces and water distribution	50
1.2.3 Drying of various types of water	52
1.2.4 Power's hydration model	52
1.3 Delayed strains of concrete	58
1.3.1 Classical decomposition of delayed strains of concrete	59
1.3.2 Some phenomenology	60
1.3.3 Physical origin	61
1.3.4 Multi-axial behavior	63
1.4 Non-aging linear viscoelasticity	65
1.4.1 Basic constitutive relations	66
1.4.2 Extension to the case with environment-dependent properties	68
1.5 Modeling of porous multiscale materials	70
1.5.1 Basics of homogenization	71
1.5.2 Multi-scale scheme of concrete	75

CONTENTS

1.5.3	Poromechanics	78
1.6	Models for creep and shrinkage of cement-based materials . . .	81
1.6.1	B4 Model of Bažant et al.	82
1.6.2	Model of Sellier et al.	84
1.7	Conclusions and thesis outline	86
2	Poisson’s ratio in linear viscoelasticity	89
2.1	Theoretical derivations	92
2.1.1	Viscoelastic constitutive relations	93
2.1.2	Comparison of relaxation Poisson’s ratio and creep Poisson’s ratio	95
2.2	Difference between relaxation and creep Poisson’s ratios for some rheological models	98
2.3	Discussions	104
2.3.1	Poisson’s ratio from multiaxial creep tests on cementitious materials	104
2.3.2	The elastic–viscoelastic correspondence principle	108
2.3.3	Influence of duration of loading phase on apparent creep Poisson’s ratio	110
2.4	Conclusions	112
3	Viscoelastic Poisson’s ratio of concrete	115
3.1	Definition of viscoelastic Poisson’s ratio for creep tests	118
3.1.1	Definition of viscoelastic Poisson’s ratio for isotropic linear non-aging viscoelastic solids	119
3.1.2	Definition based on creep strain	122
3.1.3	Potential anisotropy of time-dependent behavior	123
3.2	Evolution of viscoelastic Poisson’s ratio of concrete	126
3.3	Conclusions	130
4	Long-term viscoelastic Poisson’s ratio of C-S-H gel	133
4.1	Downscaling of long-term viscoelastic Poisson’s ratio	135
4.1.1	Viscoelastic Poisson’s ratio of composite made of matrix embedding non-creeping inclusions	138

4.1.2	Viscoelastic Poisson's ratio of porous medium	141
4.1.3	Long-term viscoelastic Poisson's ratio: from concrete down to C-S-H gel	142
4.2	Discussion	146
4.2.1	Influence of interface	146
4.2.2	Implications for creep mechanism of C-S-H gel at large times	150
4.3	Conclusions	153
5	Is long-term autogenous shrinkage a creep phenomenon in- duced by capillary effects due to self-desiccation?	157
5.1	Introduction	159
5.2	Analysis of autogenous shrinkage and basic creep data	161
5.2.1	Autogenous shrinkage	161
5.2.2	Basic creep	163
5.3	Downscaling of creep compliance from the scale of concrete to the scale of C-S-H gel	165
5.3.1	Multiscale model for concrete	166
5.3.2	Theoretical derivation	166
5.3.3	From concrete to C-S-H gel	169
5.4	In-pore stress necessary to explain long-term kinetics of auto- genous shrinkage	173
5.5	Capillary stress due to self-desiccation	175
5.5.1	Self-desiccation of cementitious materials	175
5.5.2	Estimation of capillary force	178
5.6	Conclusions	181
6	Viscoelastic poromechanical model	183
6.1	Objective of model	186
6.2	Influence of relative humidity	188
6.2.1	Dependence of creep compliance on relative humidity	188
6.2.2	Capillary stress	191
6.3	Constitutive model	195

CONTENTS

6.3.1	Constitutive equations	195
6.3.2	Discussion about the 4 components of delayed strain	199
6.4	Application to concretes	200
6.4.1	Methodology	202
6.4.2	Example of application	205
6.5	Conclusions	213
7	Conclusions and perspectives	215
7.1	Conclusions	215
7.2	Perspectives	217
A	Relaxation and creep Poisson's ratios in rheological models	221
B	Calculation of the two Poisson's ratios from the experimental results	225
C	Comparaison of Poisson's ratio and creep-based Poisson's ratio in different directions	227
D	Experimental data of concrete Poisson's ratio from literature	233
E	Autogenous shrinkage database	241
F	Basic creep database	245
G	Experimental data of evolution of relative humidity with respect to time under autogenous condition	249
H	Experimental study of the influence of relative humidity on creep compliance of cement paste	251
H.1	Material and methods	251
H.2	Results	255
H.3	Discussions	257
	Bibliography	261

List of Figures

1.1	Powers' model of hydration, expressed (a) in mass, (b) in volume	54
1.2	Volume fraction of various phases as a function of hydration degree for cement paste with (a) water-to-cement ratio equal to 0.3(b) water-to-cement ratio equal to 0.5.	57
1.3	Microstructure of cement paste at long term, computed by taking hydration degree equal to (a) long-term hydration degree ξ^p of Powers' model given by Eq. 1.9; (b) long-term hydration degree ξ^∞ given by Eq. 1.10.	58
1.4	Illustration of Pickett effect	61
1.5	Prinple of superposition by (a) horizontal decomposition of stress history and (b) vertical decomposition of stress history, taken from Walraven and Shen (1991)	69
1.6	Strain response to a constant unit stress with various relative humidity histories, constant or varying in time	71
1.7	Multiscale schemes adopted by (a) Bernard et al. (2003b); (b) Constantinides and Ulm (2004); (c)Sanahuja et al. (2007); (d) Pichler et al. (2007); (e) Ghabezloo (2010); (f) Pichler and Hellmich (2011). MT, SC, CS represent Mori-Tanaka scheme, self-consistent scheme and composite sphere, respectively.	77
1.8	Idealized rheological model used in poromechanical model of Sellier et al. (2016)	86

LIST OF FIGURES

2.1	Rheological models used in the parametric study: (a) Both volumetric and deviatoric behaviors governed by the Maxwell unit; (b) Volumetric behavior and deviatoric behavior governed by the Maxwell unit and the Kelvin–Voigt unit, respectively; (c) Volumetric behavior and deviatoric behavior governed by the Kelvin–Voigt unit and the Maxwell unit, respectively; (d) Both volumetric and deviatoric behaviors governed by the Kelvin–Voigt unit.	98
2.2	Relaxation Poisson’s ratio $\nu_r(t)$ and creep Poisson’s ratio $\nu_c(t)$ for a material whose volumetric and deviatoric behaviors are governed by the Maxwell unit and for which $\nu_0 = 0.1$ and $\eta_K/\eta_G = 10$	100
2.3	Characteristic difference $\Delta\nu$ between relaxation Poisson’s ratio $\nu_r(t)$ and creep Poisson’s ratio $\nu_c(t)$: (a) Both volumetric and deviatoric behaviors governed by the Maxwell unit (see Fig. 2.1a); (b) Volumetric behavior and deviatoric behavior governed by the Maxwell unit and the Kelvin–Voigt unit, respectively (see Fig. 2.1b); (c) Volumetric behavior and deviatoric behavior governed by the Kelvin–Voigt unit and the Maxwell unit, respectively (see Fig. 2.1c); (d) Both volumetric and deviatoric behaviors governed by the Kelvin–Voigt unit (see Fig. 2.1d).	102
2.4	Retard factor $f_{\Delta t}$ of the creep Poisson’s ratio $\nu_c(t)$ with respect to the relaxation Poisson’s $\nu_r(t)$: (a) Both volumetric and deviatoric behaviors governed by the Maxwell unit (see Fig. 2.1a); (b) Volumetric behavior and deviatoric behavior governed by the Maxwell unit and the Kelvin–Voigt unit, respectively (see Fig. 2.1b); (c) Volumetric behavior and deviatoric behavior governed by the Kelvin–Voigt unit and the Maxwell unit, respectively (see Fig. 2.1c).	103

2.5	Experimental data of multiaxial creep experiments on cementitious materials: (a) biaxial creep test on cubic concrete sample of Jordaan and Illston (1969) , (b) uniaxial creep test on a cuboid sample of cement paste of Parrott (1974) , (c) triaxial creep tests on cylindrical specimens of leached cement paste and mortar of Bernard et al. (2003a)	106
2.6	Ratio $-\varepsilon_l(t)/\varepsilon_a(t)$ of the lateral to the axial strain (black lines) observed during creep experiments with various durations τ_L of the loading phase, and creep Poisson's ratio ν_c (gray lines) for a material that creeps deviatorically and whose deviatoric creep behavior is modeled by (a) the Maxwell unit, or (b) the Kelvin-Voigt unit.	112
3.1	Dependency of Poisson's ratio on the direction in experiment TC10 in Gopalakrishnan (1968) : (a) Creep-based Poisson's ratio reported in Gopalakrishnan (1968) , calculated from Eq. (3.8) for three directions; (b) viscoelastic Poisson's ratio calculated from Eq. (3.4) for three directions.	125
3.2	Creep experiments on concrete of Gopalakrishnan (1968) ; Jordaan and Illston (1969) ; Kennedy (1975) ; Kim et al. (2005) : Long-term asymptotic value of the viscoelastic Poisson's ratio versus elastic Poisson's ratio (a) for each individual experiment, and (b) averaged over all experiments performed with one mix design. In subfigure (a), y-axis error bars indicate the maximum and minimum values of the viscoelastic Poisson's ratio during the experiment.	129
3.3	Evolution of volumetric strain during creep experiment on concrete. Original data are from Gopalakrishnan (1968) ; Jordaan and Illston (1969) ; Kennedy (1975) ; Ulm et al. (2000) ; Kim et al. (2005)	131

LIST OF FIGURES

4.1	Multiscale structure of concrete: (a) Concrete as a matrix of cement paste embedding aggregates, (b) cement paste as portlandite, calcium sulfoalumintes hydrates and unhydrated clinker embedded into a matrix made of a mixture of C-S-H with capillary pores, (c) mixture of C-S-H with capillary pores as a matrix of C-S-H gel surrounding capillary porosity, and (d) C-S-H gel as a mixture of C-S-H particles and gel pores. The scales (a) (b) (c) are considered in Sec. 4.1 for the downscaling of the long-term Poisson's ratio, while the scale (d) is considered in Sec. 4.2.2 for the analysis of long-term creep mechanism of C-S-H gel.	138
4.2	(a) Long-term viscoelastic Poisson's ratio of a composite made of a creeping matrix that surrounds non-creeping spherical inclusions. f is the volume fraction of inclusions. (b) Long-term viscoelastic Poisson's ratio of a composite made of a creeping matrix that surrounds spherical pores. ϕ is the volume fraction of pores.	140
4.3	Long-term viscoelastic Poisson's ratio ν_c^∞ of concrete versus long-term viscoelastic Poisson's ratio ν_{gel}^∞ of C-S-H gel.	145
4.4	(a) Upscaled long-term viscoelastic Poisson's ratio of concrete as a function of the property of the interface between aggregates and cement paste. (b) Downscaled long-term viscoelastic Poisson's ratio of C-S-H gel as a function of the property of the interface between portlandite, calcium sulfoaluminates hydrates and clinker on one hand, and the mixture of C-S-H with capillary pores on the other hand.	149
4.5	(a) Layered structure of C-S-H particles. (b) Imperfect contact between C-S-H particles.	151
4.6	Long-term viscoelastic Poisson's ratio ν_{gel}^∞ of C-S-H gel: (a) in the case where creep is due to creep of the C-S-H particles themselves, and (b) in the case where creep is due to creep of contact points between neighboring C-S-H particles.	154

5.1	(a) Example of autogenous shrinkage data; (b) Example of basic creep data. Data from Shritharan (1989); De Larrard (1990); Mazloom et al. (2004)	162
5.2	Multiscale structure of concrete: (a) Concrete as a matrix of cement paste embedding aggregates, (b) cement paste as portlandite, calcium sulfoalumintes hydrates and unhydrated clinker embedded into a matrix made of a mixture of C-S-H with capillary pores, (c) mixture of C-S-H with capillary pores as a matrix of C-S-H gel surrounding capillary porosity, and (d) C-S-H gel as a mixture of C-S-H particles and gel pores. The scales (a) (b) (c) are considered in Sec. 5.3.1 for the downscaling of the creep modulus, while the scale (d) is considered in Sec. 5.5.2 for estimating the Biot coefficient of the mixture of C-S-H gel with capillary pores.	167
5.3	Bulk creep modulus as a function water-to-cement ratio, computed from basic creep data in Hanson (1953); Browne (1967); Rostasy et al. (1973); Kommendant et al. (1976); Takahashi and Kawaguchi (1980); Kawasumi et al. (1982); Brooks (1984); Brooks and Wainwright (1983); Bryant and Vadhanavikkitt (1987); De Larrard (1988); Shritharan (1989); De Larrard (1990); Le Roy (1995); Mazloom et al. (2004); Mazzotti et al. (2005); Mu et al. (2009)	172
5.4	Evolution of relative humidity under autogenous condition, data retrieved from Baroghel-Bouny (1994).	177
5.5	Long-term relative humidity under autogenous condition as a function water-to-cement ratio, computed from experimental data in Baroghel-Bouny (1994); Jensen and Hansen (1996, 1999); Persson (1997); Yssorche-Cubaynes and Ollivier (1999); Zhutovsky and Kovler (2013); Wyrzykowski and Lura (2016) and in appendix H.	178

LIST OF FIGURES

5.6 Mechanical stress σ_h that should act on the mixture of C-S-H gel displayed together with capillary pores to explain the long-term kinetics of autogenous shrinkage of data in Brooks (1984); Shrivatharan (1989); De Larrard (1990); Tazawa and Miyazawa (1993, 1995); Weiss et al. (1999); Brooks and Johari (2001); Lee et al. (2003); Zhang et al. (2003); Mazloom et al. (2004); Vidal et al. (2005); Lee et al. (2006) with the capillary stress bS_lP_c 181

6.1 Bulk creep modulus of C-S-H gel as a function of relative humidity obtained from microindentation results of Zhang (2014) and Frech-Baronet et al. (2017) 190

6.2 Desorption isotherm for cement pastes with various water-to-cement ratio. Points are experimental results of Baroghel-Bouny (2007), dashed lines are the model fitted relation with Eq. 6.7, solid line h_r^∞ corresponds to the water content under autogenous condition at long term. 194

6.3 The procedure to predict shrinkage and creep with the proposed model 196

6.4 Application of model on the mixture of C-S-H gel and capillary pores submitted to the histories of relative humidity displayed in Fig. (a). (b) volumetric effective stress acting on the mixture of C-S-H gel with capillary pores. When the specimen is mechanically loaded, the applied stress is uniaxial and of magnitude 12 MPa. 201

6.5 Application of model on the mixture of C-S-H gel and capillary pores submitted to histories of relative humidity and mechanical load displayed in Fig. 6.4. (a) strain of various specimens; (b) illustration of Pickett effect. 202

6.6 Calibration of the model with the experimental results of Flamanville (Granger, 1995): (a) when the coefficient κ is also fitted, (b) when the coefficient κ is set to $\kappa = 0.5$ 208

6.7	Calibration of the model with the experimental results of Chooz (Granger, 1995): (a) when the coefficient κ is also fitted, (b) when the coefficient κ is set to $\kappa = 0.5$	209
6.8	Calibration of the model with the experimental results of Civaux B11 (Granger, 1995): (a) when the coefficient κ is also fitted, (b) when the coefficient κ is set to $\kappa = 0.5$	210
6.9	Calibration of the model with the experimental results of Penly (Granger, 1995): (a) when the coefficient κ is also fitted, (b) when the coefficient κ is set to $\kappa = 0.5$	211
6.10	Calibration of the model with the experimental results on VERCORS concrete: (a) measured desorption isotherm, (b) Calibration of creep properties from basic creep strains and prediction of the strain of non-loaded drying specimen and of loaded drying specimen	212
C.1	Dependency of Poisson's ratio on the direction: (a)(c)(e) creep-based Poisson's ratio reported in Gopalakrishnan (1968), calculated from Eq. (17) for three directions; (b)(d)(f) viscoelastic Poisson's ratio calculated from Eq. (5) for three directions. Data (a)(b) from experiment TC1, (c)(d) from experiment BC4, (e)(f) from experiment TC5 in Gopalakrishnan (1968):	228
C.2	Dependency of Poisson's ratio on the direction: (a)(c)(e) creep-based Poisson's ratio reported in Gopalakrishnan (1968), calculated from Eq. (17) for three directions; (b)(d)(f) viscoelastic Poisson's ratio calculated from Eq. (5) for three directions. Data (a)(b) from experiment TC5R, (c)(d) from experiment TC6, (e)(f) from experiment TC7 in Gopalakrishnan (1968):	229
C.3	Dependency of Poisson's ratio on the direction: (a)(c)(e) creep-based Poisson's ratio reported in Gopalakrishnan (1968), calculated from Eq. (17) for three directions; (b)(d)(f) viscoelastic Poisson's ratio calculated from Eq. (5) for three directions. Data (a)(b) from experiment BC8, (c)(d) from experiment BT9, (e)(f) from experiment TC11 in Gopalakrishnan (1968):	230

LIST OF FIGURES

C.4 Dependency of Poisson’s ratio on the direction in experiment TC12 in Gopalakrishnan (1968): (a) creep-based Poisson’s ratio reported in Gopalakrishnan (1968), calculated from Eq. (17) for three directions; (b) viscoelastic Poisson’s ratio calculated from Eq. (5) for three directions. 231

D.1 Poisson’s ratio of concrete versus time. Data retrieved from Gopalakrishnan (1968) 234

D.2 (a) Poisson’s ratio versus time. Data retrieved from Jordaan and Illston (1969). (b) Poisson’s ratio versus time. Data retrieved from Jordaan and Illston (1971). 235

D.3 (a) Poisson’s ratio versus time for As-Cast concrete specimens. Data retrieved from Kennedy (1975). (b) Poisson’s ratio versus time for Air-Dried specimens. Data retrieved from Kennedy (1975). 235

D.4 (a) Poisson’s ratio versus time for C1 concrete specimens. Data retrieved from Kim et al. (2005). (b) Poisson’s ratio versus time for C2 concrete specimens. Data retrieved from Kim et al. (2005). (c) Poisson’s ratio versus time for C3 concrete specimens. Data retrieved from Kim et al. (2005). 237

G.1 Evolution of relative humidity with respect to time under autogenous condition. Data from (a) Jensen and Hansen (1996, 1999), (b) Persson (1997), (c) Yssorche-Cubaynes and Ollivier (1999), (d) Zhutovsky and Kovler (2013), (e) Wyrzykowski and Lura (2016), (f) appendix H. 250

H.1 (a) Set up to rotate all 12 samples during the first 7 hours after casting. (b) LVDT to measure the strain of specimen. . . 252

H.2 Summary of storage and testing condition of the specimens . . 253

H.3 Mass loss over time. The experimental curve is the mean value of the three specimens in the same desiccator. 255

H.4 Measured total strain of (a) non-loaded specimens (b) loaded specimen. 256

H.5 Evolution of hydration degree and relative humidity under autogenous condition 257

LIST OF FIGURES

List of Tables

1.1	Time-dependent strain of cement-based materials in function of loading condition and hydric condition.	59
4.1	Concrete formulation data used for the downscaling of viscoelastic Poisson's ratio. The volume fraction of aggregates is expressed per unit volume of concrete. The volume fraction of portlandite, calcium sulfoaluminates hydrates and unhydrated clinker is expressed per unit volume of cement paste. The volume fraction of capillary pores is expressed per unit volume of mixture of C-S-H with capillary pores. ¹ OPC is ordinary Portland cement.	144
5.1	Extract of autogenous shrinkage data. ¹ File corresponds to the file number in the database compiled by Prof. Bažant and his collaborators (Bažant and Li, 2008); ² w/c: water-to-cement ratio; ³ a/c: aggregate-to-cement mass ratio; ⁴ c: cement per volume of mixture [kg/m ³]; ⁵ α_{sh} : Fitted parameter in Eq. 5.1, [$\mu\text{m}/\text{m}$]	163
5.2	Extract of basic creep data. ¹ File corresponds to the file number in the database compiled by Prof. Bažant and his collaborators (Bažant and Li, 2008); ² w/c: water-to-cement ratio; ³ a/c: aggregate-to-cement mass ratio; ⁴ c: cement per volume of mixture [kg/m ³]; ⁵ t ₀ : loading age [days]; ⁶ 1/C _c ^E : Fitted parameter in Eq. 5.3, [$\mu\text{m}/\text{m}/\text{MPa}$].	165

LIST OF TABLES

5.3	Summary of experimental data of evolution of relative humidity with respect to time under autogenous condition, and of the fitted parameters. Data from Baroghel-Bouny (1994); Jensen and Hansen (1996, 1999); Persson (1997); Yssorche-Cubaynes and Ollivier (1999); Zhutovsky and Kovler (2013); Wyrzykowski and Lura (2016) and appendix H. ¹ w/c: water-to-cement ratio; ² τ_T : the duration of the test; ³ h_r^∞ : fitted parameter with Eq. 5.18, corresponding to the long-term relative humidity under autogenous conditions; ⁴ τ_{h_r} : fitted parameter with Eq. 5.18.	176
6.1	Young’s modulus of C-S-H gel measured by Acker et al. (2001); Constantinides and Ulm (2004) and computed bulk modulus of C-S-H gel	197
6.2	Mix design of concretes used in Granger (1995)	205
E.1	Details of autogenous shrinkage data (first part). ¹ File corresponds to the file number in the database compiled by Prof. Bažant and his collaborators (Bažant and Li, 2008); ² w/c: water-to-cement ratio; ³ a/c: aggregate-to-cement mass ratio; ⁴ c: cement per volume of mixture [kg/m ³]; ⁵ α_{sh} : Fitted parameter in Eq. 5.1, [$\mu\text{m}/\text{m}$]	242
E.2	Details of autogenous shrinkage data (second part). ¹ File corresponds to the file number in the database compiled by Prof. Bažant and his collaborators (Bažant and Li, 2008); ² w/c: water-to-cement ratio; ³ a/c: aggregate-to-cement mass ratio; ⁴ c: cement per volume of mixture [kg/m ³]; ⁵ α_{sh} : Fitted parameter in Eq. 5.1, [$\mu\text{m}/\text{m}$]	243

F.1 Details of basic creep data (first part). ¹File corresponds to the file number in the database compiled by Prof. Bažant and his collaborators (Bažant and Li, 2008); ²w/c: water-to-cement ratio; ³a/c: aggregate-to-cement mass ratio; ⁴c: cement per volume of mixture [kg/m³]; ⁵t₀: loading age [days]; ⁶1/C_c^E: Fitted parameter in Eq. 5.3, [μm/m/MPa]. 246

F.2 Details of basic creep data (second part). ¹File corresponds to the file number in the database compiled by Prof. Bažant and his collaborators (Bažant and Li, 2008); ²w/c: water-to-cement ratio; ³a/c: aggregate-to-cement mass ratio; ⁴c: cement per volume of mixture [kg/m³]; ⁵t₀: loading age [days]; ⁶1/C_c^E: Fitted parameter in Eq 5.3, [μm/m/MPa]. 247

H.1 Mass loss of specimens per period. A positive value corresponds to decrease of mass whereas a negative value to mass increase. The mass variation during a period is normalized with respect to the mass of sample at the beginning of this period 258

LIST OF TABLES

Nomenclature

α_m	Parameter of Mori-Tanaka homogenization scheme, [-]
α_{hom}	Parameter of self-consistent homogenization scheme, [-]
α_{sh}	Parameter characterizing the long-term kinetics of autogenous shrinkage, [-]
β_m	Parameter of Mori-Tanaka homogenization scheme, [-]
β_{hr}	Fitting parameter related to the evolution of relative humidity under autogenous condition, [Pa]
β_{hom}	Parameter of self-consistent homogenization scheme, [-]
Δ_ν	Characteristic difference between relaxation and creep Poisson's ratios, [-]
η_G	Viscosity of dashpot in viscoelastic unit that controls shear behavior, [Pa · s ⁻¹]
η_K	Viscosity of dashpot in viscoelastic unit that controls bulk behavior, [Pa · s ⁻¹]
κ	A coefficient related to micro-damage in the poroviscoelastic model, [-]
\mathbb{A}_i	Strain localization tensor of phase i , [-]
\mathbb{C}_i	Stiffness tensor of phase i , [Pa]

LIST OF TABLES

\mathbf{v}	Environmental parameters
ν^0	Instantaneous value of Poisson's ratio, [-]
ν^∞	Asymptotic / long-term value of Poisson's ratio, [-]
ν_c^∞	Asymptotic / Long-term value of Poisson's ratio of concrete, [-]
ν_m^∞	Asymptotic / long-term value of Poisson's ratio of matrix phase, [-]
ν_{com}^∞	Asymptotic / long-term value of Poisson's ratio of composite, [-]
ν_{gel}^∞	Asymptotic / Long-term value of Poisson's ratio of the C-S-H gel, [-]
ν_0	Elastic Poisson's ratio, [-]
ν_c	Creep Poisson's ratio, [-]
ν_r	Relaxation Poisson's ratio, [-]
ϕ	Porosity, [-]
ϕ_0	Porosity at reference configuration, [-]
ϕ_c	Volume fraction of capillary pores in the mixture of C-S-H gel and capillary pores, [-]
ϕ_{gel}	Volume fraction of gel pores in the C-S-H gel, [-]
ψ^K	Fitting parameter related to the amplitude of irreversible creep in the model of Sellier et al., [-]
ρ_c	Density of clinker, [kg/m ³]
ρ_w	Density of water, [kg/m ³]
Σ	Equivalent stress at macroscopic level, [Pa]
σ_a	Axial stress, [Pa]
σ_d^0	Constant Von Mises stress, [Pa]

σ_h	Capillary stress, [Pa]
σ_v	Volumetric stress, [Pa]
σ_{dc}	Fitting parameter for drying shrinkage in the Model of Sellier et al., [Pa]
τ^K	Characteristic time related to irreversible creep in the model of Sellier et al., [days]
τ^M	Characteristic time related to reversible creep in the model of Sellier et al., [days]
τ_G	Characteristic viscous time of Kelvin–Voigt unit, [s]
τ_L	Duration of loading phase, [s]
τ_{hr}	Characteristic time related to the decrease of relative humidity under autogenous condition, [s]
$\tilde{\nu}$	Creep-based Poisson’s ratio, [-]
\tilde{t}	Characteristic time related to creep compliance, [s]
$\underline{\underline{\sigma}}$	Stress tensor, [Pa]
$\underline{\underline{\varepsilon}}$	Strain tensor, [-]
ε^E	Elastic strain in the model of Sellier et al., [Pa]
ε^K	Irreversible creep strain in the model of Sellier et al., [Pa]
ε^M	Reversible creep strain in the model of Sellier et al., [Pa]
ε_a	Axial strain, [-]
ε_a^0	Instantaneous value of axial strain, [-]
ε_d	Von Mises strain, [-]
ε_l	Lateral strain, [-]

LIST OF TABLES

ε_l^0	Instantaneous value of lateral strain, [-]
ε_v	Volumetric strain, [-]
$\varepsilon_{a,sh}$	Autogenous shrinkage strain, [-]
$\varepsilon_{d,sh}$	Drying shrinkage strain, [-]
ξ	Degree of hydration, [-]
ξ^∞	Degree of hydration at long term given by Waller, [-]
ξ^p	Degree of hydration at long term given by Powers' model, [-]
a_1	Parameter of Van Genuchten desorption isotherm law, [-]
A_i^{dev}	Deviatoric part of strain localization tensor of phase i , [-]
A_i^{sph}	Spherical part of strain localization tensor of phase i , [-]
$a_{h,r}$	Fitting parameter in empirical model of desorption isotherm, [-]
b	Biot coefficient, [-]
b_1	Parameter of Van Genuchten desorption isotherm law, [Pa]
b_{gel}	Biot coefficient of the C-S-H gel, [-]
$b_{h,r}$	Fitting parameter in empirical model of desorption isotherm, [-]
b_{hom}	Homogenized Biot coefficient of porous heterogeneous medium, [-]
C	Creep modulus, [Pa]
C^G	Shear creep modulus, [Pa]
C_c^K	Bulk creep modulus of concrete, [Pa]
C_i^K	Bulk creep modulus of inclusions, [Pa]
C_m^K	Bulk creep modulus of matrix phase, [Pa]
C_{gel}^K	Bulk creep modulus of the C-S-H gel, [Pa]

C_{hom}^K	Homogenized bulk creep modulus of composite, [Pa]
C^M	Contact creep modulus, [Pa]
C_0	Basic creep function in the B4 model, [Pa ⁻¹]
C_d	Drying creep function in the B4 model, [Pa ⁻¹]
$C_{gel}^{K\infty}$	Value of bulk creep modulus of the C-S-H gel under relative humidity higher than h_c , [Pa]
c_{h_r}	Fitting parameter in empirical model of desorption isotherm, [-]
E	Young's modulus, [Pa]
$E(t)$	Uniaxial relaxation modulus, [Pa]
E_0	Uniaxial elastic modulus at the age of loading, [-]
E_{CSH}	Relaxation modulus related to variation of the space between layers in C-S-H particles, [Pa]
e_{ij}	Deviatoric part of the strain tensor, [-]
f_a	Volume fraction of aggregates in concrete, [-]
f_b	Volume fraction of portlandite, calcium sulfoaluminates and unhydrated clinker in cement paste, [-]
f_i	Volume fraction of phase i , [-]
$f_{\Delta\nu}$	Retard factor between relaxation and creep Poisson's ratios, [-]
f_{am}	Volume fraction of physically adsorped water, [-]
f_{ck}	Volume fraction of unhydrated clinker, [-]
f_{cs}	Volume fraction of chemical shrinkage, [-]
f_{cw}	Volume fraction of capillary water, [-]
f_c	Volume fraction of capillary pores, [-]

LIST OF TABLES

$f_{hyd,s}$	Volum fraction of solid hydrates, [-]
f_{hyd}	Volume fraction of bulk hydrates, [-]
G	Shear modulus, [Pa]
$G(t)$	Shear relaxation modulus, [Pa]
G^∞	Asymptotic / long-term value of shear relaxation modulus, [Pa]
G_i^∞	Asymptotic / long-term value of shear relaxation modulus of inclusions, [Pa]
G_m^∞	Asymptotic / long-term value of shear relaxation modulus of matrix phase, [Pa]
G_{com}^∞	Asymptotic / long-term value of shear relaxation modulus of composite, [Pa]
G_0	Shear modulus at time 0, [Pa]
G_{CSH}	Relaxation modulus related to sliding of layers in C-S-H particles, [Pa]
G_{hom}	Homogenized shear modulus of composite, [Pa]
h_c	Critical relative humidity above which the bulk creep modulus of the C-S-H gel is independent from relative humidity, [-]
h_r	Relative humidity, [-]
h_r^∞	Long-term relative humidity under autogenous condition, [-]
h_{cr}	Critical relative humidity below which desorption isotherm is independent from water-to-cement ratio, [-]
$J^E(t)$	Uniaxial creep compliance, [Pa ⁻¹]
$J^G(t)$	Shear creep compliance, [Pa ⁻¹]
$J^K(t)$	Bulk creep compliance, [Pa ⁻¹]

J_2^ε	Second invariant of the deviatoric strain tensor, [-]
$J_2^{\sigma^0}$	Second invariant of the deviatoric stress tensor, [Pa ²]
J_E^{cu}	Uniaxial creep compliance measured from uniaxial test, [Pa ⁻¹]
J_G^0	Shear compliance at time 0, [Pa ⁻¹]
J_G^∞	Asymptotic / long-term value of shear creep compliance, [Pa ⁻¹]
J_K^0	Bulk compliance at time 0, [Pa ⁻¹]
J_K^∞	Asymptotic / long-term value of bulk creep compliance, [Pa ⁻¹]
J_N	Corresponding viscoelastic parameter of the inverse of Biot modulus, [Pa ⁻¹]
K	Bulk modulus, [Pa]
$K(t)$	Bulk relaxation modulus, [Pa]
K^∞	Asymptotic / long-term value of bulk relaxation modulus, [Pa]
K_i^∞	Asymptotic / long-term value of bulk relaxation modulus of inclusions, [Pa]
K_m^∞	Asymptotic / long-term value of bulk relaxation modulus of matrix phase, [Pa]
K_{com}^∞	Asymptotic / long-term value of bulk relaxation modulus of composite, [Pa]
K_0	Bulk modulus at time 0, [Pa]
K_n	Normal stiffness between two particles, [Pa]
K_t	Tangential stiffness between two particles, [Pa]
K_t	Tangential stiffness of the interface between inclusion and matrix, [Pa]
K_{hom}	Homogenized bulk modulus of composite, [Pa]

LIST OF TABLES

$L(t)$	Contact creep compliance, [Pa ⁻¹]
M_0	Elastic contact modulus, [Pa]
M_w	Molar mass of water, [g/mol]
m_θ	Dimensionless parameter related to interface properties, [-]
N	Biot modulus of skeleton, [Pa]
P	Pore pressure, [-]
p	Volume fraction of water in the initial mixture of water and clinker, [-]
P_c	Capillary pressure, [Pa]
P_w	Water pressure in pores at saturated state, [Pa]
R	Ideal gas constant, [J · K ⁻¹ · mol ⁻¹]
R_i	Radius of inclusions, [m]
s	Laplace variable
S_l	Saturation degree, [-]
s_{ij}	Deviatoric part of the stress tensor, [Pa]
T	Temperature, [K]
t	Current age, [days]
t	Time since loading, [days]
t'	Age at the start of environmental exposure, [days]
t_0	Age at loading, [days]
t_c	Time related to median value of creep Poisson's ratio, [s]
t_r	Time related to median value of relaxation Poisson's ratio, [s]

V_V	Volume of pores, [m ³]
V_w	Volume occupied by water, [m ³]
V_{V0}	Volume of pores at reference configuration, [m ³]
w	Water content per unit mass of dried hardened cement paste, [g/g]
w/c	Water-to-cement mass ratio, [-]
w_{cr}	Value of water content corresponding to critical relative humidity h_{cr} , [g/g]
w_{sat}	Value of water content at saturated state, [g/g]

LIST OF TABLES

Chapter 1

Context and state of the art

THIS CHAPTER *aims at presenting the context and scientific background of the thesis subject and the basic notions and useful tools that are needed in the thesis. The long-term shrinkage and creep behavior of concrete depends on the microstructure of concrete. Hence, we start by introducing the microstructure of concrete. The hydration model of Powers' is then presented in detail as it is going to be used in several parts of the thesis. Then, we describe the classical decomposition of the delayed behavior of concrete, then some observed phenomenology and some proposed physical origin for this delayed behavior. After understanding the delayed strain of concrete, we present three useful tools (or framework) that are necessary to model shrinkage and creep behavior of cement-based materials. The first one is the theory of isotropic linear viscoelasticity, which is well adapted to cement-based materials loaded to less than 40% of their compressive strength. The second one is Micromechanics, called also homogenization. Concrete is a heterogeneous multi-scale materials as it is composed of different phases whose size varies from the scale of centimeters to the scale of nanometers. Micromechanical analysis, which is a tool that predicts the properties of an heterogeneous material, is widely used to analyze mechanical behavior of cement-based materials. The third one is Poromechanics. Composed from solid phase and pore spaces, concrete is a porous material that is submitted to mechanical*

and hydric load. Poromechanics is a powerful tool to describe the mechanical behavior of such porous materials. Understanding these theoretical tools that are used in modeling of delayed behavior of concrete, in final section we look at the existing models in literature that predict shrinkage and creep behavior of concrete. Emphasis are given on the following two models: B₄ model of Bazant and his collaborators and the model of Sellier and his collaborators. The chapter is concluded and objectives of the thesis are presented in the end.

CE CHAPITRE a pour objectif de présenter le contexte industriel et scientifique de la thèse ainsi que les notions de base et les outils utiles à la thèse. Le retrait et fluage à long terme du béton dépend de la microstructure du béton. Nous commençons donc par introduire la microstructure du béton. Le modèle d'hydratation de Powers est ensuite présenté en détail comme il sera utilisé à plusieurs reprises dans la thèse. Ensuite, nous passons à la déformation différée du béton. Nous décrivons d'abord la décomposition classique de la déformation différée du béton, puis quelques observations phénoménologiques et des propositions sur l'origine physique du comportement différé. Puis, nous présentons trois outils utiles qui sont nécessaires pour modéliser le retrait et fluage des matériaux cimentaires. Le premier est la théorie de la viscoélasticité linéaire isotrope, qui est bien adaptée aux matériaux cimentaires chargés à moins de 40% de leur résistance en compression. Le deuxième est la micromécanique, appelée aussi méthode d'homogénéisation. Le béton est un matériau hétérogène à plusieurs échelles car il est composé de différentes phases dont la taille varie de l'échelle des centimètres à l'échelle du nanomètre. L'analyse micromécanique, un outil qui prédit les propriétés macroscopiques d'un matériau hétérogène, est largement utilisée pour analyser le comportement mécanique des matériaux cimentaires. Le troisième est la poromechanique. Composé d'une phase solide et d'un espace poreux, le béton est un matériau poreux soumis à une charge mécanique et hydrique. La poromécanique est un outil puissant pour décrire le comportement mécanique de ce type de matériaux poreux. Après avoir introduit ces outils théoriques

qui sont utilisés dans la modélisation du comportement différé du béton, à la fin du chapitre, nous examinons les modèles existants de la littérature qui prédisent le retrait et fluage du béton. L'accent est mis sur les deux modèles suivants : le modèle B_4 de Bazant et de ses collaborateurs et le modèle de Sellier et de ses collaborateurs. Le chapitre se termine par les objectifs de la thèse.

In this chapter we are going to present first the context of the thesis. Then, we introduce basic notions and useful tools that are needed in the thesis. We start by presenting the microstructure and hydration model of cement-based material. Then, the delayed strain of cement-based materials are presented as well as their classical decomposition. Some phenomenology and physical origin of these delayed strains are described. Next, we introduce the theory of non-aging linear isotropic viscoelasticity which will be the main framework of the thesis. Short introductions also are given for micromechanics and poromechanics. In the end, we draw a state of the art on the models that predict the delayed strain of cement-based materials and finish by presenting the objectives of the thesis.

1.1 Context of the thesis

Around 75% of the electricity in France is produced by means of nuclear energy. The initial service life of the French nuclear power plants (NPP) is 40 years and an important part of the NPPs will attain their age in the following years. So, the extension of their service life is an economical challenge for EDF (in French *Électricité de France*). The most restrictive aspect is to fully respect the safety requirements of nuclear power stations.

In the context of extension of the service life of the current nuclear power stations, EDF started the project VERCORS to study the behavior of the containment buildings. This PhD thesis is a part of the VERCORS project.

The containment buildings are made with biaxially prestressed concrete and are meant to insure the tightness. The biaxial prestress is designed so that the containment building is able to resist an internal pressure of 0.5 MPa in case of accident. In order to avoid tensile stresses in concrete, the applied prestress corresponds to compressive stresses in concrete of around 8.5 MPa and 12 MPa along vertical and orthoradial axes, respectively. However, as time goes by, the delayed strains of concrete continue to accumulate and the prestress may be lost. That is why the evolution of prestressing forces with respect to time is critical for the operation of nuclear power plants and for the extension of their service life. Consequently, a good prediction of

the evolution of delayed strains of the containment under a biaxial stress condition is needed.

The PhD thesis is launched in this context with the aim of better understanding long-term delayed strain behavior of matured cement-based materials under biaxial load.

1.2 Microstructure and hydration of concrete

Concrete is a heterogeneous materials that is composed from solid and pore spaces. The solid phase is not homogenous and composed form various phases depending on hydration state. The sizes of these components vary across a wide range of scale. The pore space can contain both gas (mostly air) and liquid (mostly water). Understanding the microstructure of concrete is important to interpret and explain the macroscopic behavior. In this section, we present first the microstructure of hardened cement paste. Then, the hydration model of Powers' is explained in order to characterize the microstructure from the composition of cement paste.

1.2.1 Phases in concrete

Concrete is a mixture of aggregates and cement paste. The aggregates compose usually about 70% volume of the concrete. The size of aggregates depends on the case but usually varies from tens of micrometers to tens of millimeters. As to the cement paste, it plays the role of binder and has microstructure that is itself multiscale and heterogeneous.

The cement paste is obtained by mixing water and cement clinker powder. It is possible to add other constituent, such as silica fume, fly ashes, slag or admixture. In this thesis we restrict ourselves on the cement pastes made from only water and ordinary Portland cement (i.e., without supplementary cementitious materials). The microstructure of hardened cement paste depends on the mass ratio of mixed water over mixed clinker, noted as water-to-cement ratio, and the degree of hydration, which is defined as the mass ratio of reacted clinker over the total clinker of mixture. The hardened

cement paste is composed from hydration products, unhydrated clinker and pores space, in which we can find unhydrated water and air.

Hydration product of ordinary Portland cement includes calcium silicate gel, portlandite and calcium sulfoaluminates hydrates.

The exact structure of calcium silicate hydrate (C-S-H) gel is not well known. According to [Jennings \(2000\)](#), C-S-H gel is made of (approximately) spherical C-S-H particles and porosity. Each of C-S-H particle has a layered structure. The C-S-H particles tend to form clusters. The clusters can be divided into two categories: low density and high density. On the contrary, [Feldman and Sereda \(1968\)](#); [Mehta and Monteiro \(2006\)](#) consider the C-S-H gel as an amorphous structure that contains C-S-H solid and porosity in which we find water. This C-S-H solid has a surface area of 100 to 700 m²/g. In this thesis, we adopt the same point of view as [Jennings \(2000\)](#): C-S-H gel is made of spherical C-S-H particles and pores. C-S-H gel constitutes about 60% volume of the hydration product.

Portlandite is a calcium hydroxide crystal with well defined stoichiometry. Portlandite tends to form large crystals with a distinctive hexagonal-prism morphology ([Mehta and Monteiro, 2006](#)). Portlandite constitutes 20 to 25 percent of the volume of hydration product ([Mehta and Monteiro, 2006](#)).

Calcium sulfoaluminates hydrate forms hexagonal-plate crystals and occupies 15 to 20 percent of the volume of hydration product ([Mehta and Monteiro, 2006](#)).

In addition to these hydration products, we usually have unhydrated clinker in cement paste. In ordinary Portland cement, the size of unhydrated clinker grain is in the range of 1 to 50 μm ([Mehta and Monteiro, 2006](#)).

1.2.2 Pore spaces and water distribution

The pore spaces in cement paste are filled by either air or water.

According to size, the pore spaces in cement paste can be divided into air voids, capillary porosity, gel porosity and interlayer porosity.

Air voids are the largest pores in cement paste. The size of air voids varies from 50 to 200 μm .

Capillary pores are much smaller than air voids. The size of capillary pores ranges from 10 nm to 10 μm (Mehta and Monteiro, 2006).

Gel pores are smaller than capillary pores. Jennings (2000) defines the space between C-S-H particles in a cluster as gel porosity. The size of gel pores ranges from 2 nm to 10 nm.

Interlayer space is the space between the layers in a particle of C-S-H. The size of interlayer space is around 0.1 nm to 1 nm. However, according to their description of C-S-H gel, Mehta and Monteiro (2006) defines all the spaces in C-S-H gel as interlayer space. Therefore, the so-called interlayer space by Mehta and Monteiro (2006) includes both gel pores and interlayer space defined by Jennings (2000).

In this thesis, we follow the classification of Jennings (2000) and distinguish gel pores from interlayer space.

After classifying the pore spaces, the classification of water becomes straight forward. In fact, water is divided into four categories based on the pores space where the water locates: capillary water, adsorbed water, interlayer water and chemically adsorbed water.

Capillary water is the water present in capillary pores. It is called also bulk water as this water is free from the influence of the attractive forces exerted by the solid surface (Mehta and Monteiro, 2006).

Adsorbed water is the water near to the solid surface. The molecules of this water are under the attractive forces of solid surface. It has been suggested that six molecular layers (thickness of 1.5 nm) of water can be physically held by hydrogen bonding (Mehta and Monteiro, 2006).

Gel water is the water that occupies the gel pores.

Inter-layer water is the water that occupies the space between the layers of C-S-H. The interlayer water is strongly bounded by hydrogen bonding and Mehta and Monteiro (2006) suggested that the inter-layer water should be a monomolecular water layer.

In addition to the above categories, cement paste contain chemically combined water, which is an integral part of various hydration product. Mehta and Monteiro (2006) stated that this water is not lost on drying while Mantellato et al. (2015) consider that strong drying can cause dehydration of

gypsum.

1.2.3 Drying of various types of water

As seen in the previous section, water in cement paste is subjected to various constraints in function of the pores in which it is located. When relative humidity decreases, the evaporation does not happen to all types of water simultaneously. Instead, the various types of water evaporates at different stages of drying.

As soon as the relative humidity drops below 100%, the capillary water starts to evaporate. [Jennings \(2000\)](#) stated that when relative humidity decrease to around 40%, almost all of the capillary water evaporated. The cement paste starts to lose its gel water when relative humidity drops around 40%. Around 20% of relative humidity almost all gel water and physically adsorbed water is lost ([Jennings, 2000](#)). According to [Jennings \(2000\)](#), drying from 20% to 0% of relative humidity causes loss of interlayer water ([Jennings, 2000](#)), while [Mehta and Monteiro \(2006\)](#) claimed that interlayer water (knowing that the interlayer water defined by [Mehta and Monteiro \(2006\)](#) includes gel water defined by [Jennings \(2000\)](#)) starts to leave only when relative humidity drop below 11%.

For the concretes that are used in nuclear industry, the relative humidity inside the concrete drops rarely below 40%. Hence, we are limited in this thesis only for the desiccation in which the relative humidity varies between 40% and 100%.

1.2.4 Power's hydration model

Powers' model of hydration ([Powers and Brownyard, 1947](#)) is one of the most widely used model of hydration due its simplicity. More sophisticated models exist in literature, for example the model of [Tennis and Jennings \(2000\)](#). However, for our needs in the thesis, the model of Powers' is sufficient.

For ordinary Portland cement, knowing water-to-cement ratio w/c and degree of hydration ξ , Powers' model can give an estimation of mass and

volume of capillary water, physically adsorbed water, solid hydrates and unhydrated clinker and also the volume of chemical shrinkage. Recent measurements (Muller et al., 2012) using NMR have shown that despite of simplicity, Powers' model give a correct evaluation of the evolution of the microstructure.

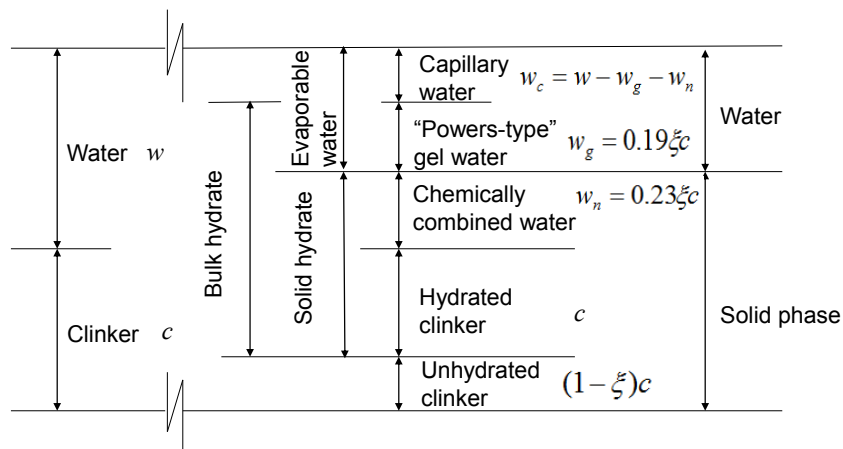
Based on evaporability, Powers and Brownyard (1947) classified water into two categories: evaporable water and non-evaporable water. Based on specific volume, Powers and Brownyard (1947) classified water into two categories: adsorbed water and free water. Hence, in Powers' hydration model, water in a cement paste can be classified into three categories (see Fig. 1.1): capillary water, physically adsorbed water and chemically adsorbed water.

Capillary water is free of forces from solid. It is also called free water. In fact, this definition of capillary water is not totally consistent with the definition in section 1.2 since the former definition excludes a part of water that is physically adsorbed on the surface of solid in capillary pores. However, supposing that the volume of physically adsorbed water in capillary pores is much smaller than the total volume of capillary pores, we take the amount of capillary water computed with Powers' hydration model equal to the amount of capillary water defined in section 1.2. Powers and Brownyard (1947) got the amount of capillary water by subtracting the amount of physically adsorbed water from the total amount of water loss at 105°C. The amount w_c of capillary water is equal to total mass w of mixed water minus mass w_n of chemically adsorbed water and of w_g physically adsorbed water.

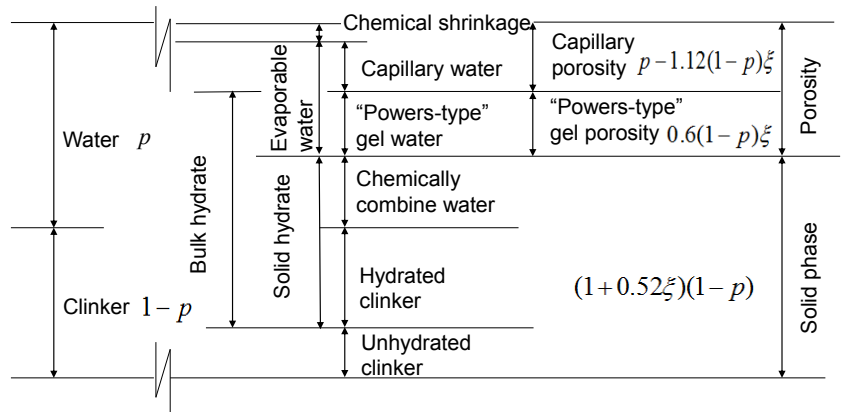
Physically adsorbed water is water that is adsorbed on the surface of solid in cement paste by surface force. It is also called *gel water*, which may cause confusion with the definition of gel water in section 1.2. In fact, the physically adsorbed water defined by Powers and Brownyard (1947) includes four layers of water that are adsorbed to solid surface in all type of pores, including capillary pores. Hence, using Powers' hydration model, the amount of physically adsorbed water cannot give any information about the amount of gel water defined in section 1.2. Powers and Brownyard (1947) computed the amount of physically adsorbed water as four layers of water that is needed to cover the surface area of hydrates. The amount w_g of physically adsorbed

water per reacted clinker is equal to 0.19 g/g (this value is valid only for cement pastes that exchange no water with outside).

Chemically adsorbed water is the water that has chemically reacted with clinker. It is also called non-evaporable water, water of constitution. Powers and Brownyard (1947) measured the amount of chemically adsorbed water by ignition at 1000°C and found that per gram of reacted clinker, the amount w_n of chemically adsorbed water is equal to 0.23 g/g.



(a)



(b)

Figure 1.1 – Powers' model of hydration, expressed (a) in mass, (b) in volume

In the following, the Powers' model of hydration, which is expressed in mass relation, is going to be expressed in volume fraction (see Fig. 1.1b). In

1.2. MICROSTRUCTURE AND HYDRATION OF CONCRETE

the initial mixture, the volume fraction p of water is:

$$p = \frac{w/c}{w/c + \rho_w/\rho_c} \quad (1.1)$$

w/c is the water-to-cement mass ratio; ρ_w and ρ_c are density of water and of clinker grains, and are taken to be equal 1 g/cm^3 and 3.15 g/cm^3 , respectively.

[Powers and Brownyard \(1947\)](#) measured that the volume reduction due to the full hydration of 100 g of clinker is approximately 6.4 mL. Thus, the volume f_{cs} of chemical shrinkage per volume of cement paste, which corresponds to the part of the porosity which is not filled with water, for a cement paste with hydration degree of ξ is:

$$f_{cs} = \rho_c 6.4(1 - p)\xi/100 = 0.20(1 - p)\xi \quad (1.2)$$

The volume fraction f_{cw} of capillary water reads:

$$f_{cw} = p - (\rho_c/\rho_w)(0.19 + 0.23)(1 - p)\xi = p - 1.32(1 - p)\xi \quad (1.3)$$

Taking the density of physically adsorbed water approximately equal to the density ρ_w of bulk water, the volume fraction f_{aw} of physically adsorbed water reads:

$$f_{aw} = 0.19(\rho_c/\rho_w)(1 - p)\xi = 0.60(1 - p)\xi \quad (1.4)$$

Subtracting the volume of chemical shrinkage from the total volume of reacted water and reacted clinker, we get the volume fraction $f_{hyd,s}$ of solid hydrates:

$$f_{hyd,s} = (1 - 6.4\rho_c/100 + 0.23(\rho_c/\rho_w))(1 - p)\xi = 1.52(1 - p)\xi \quad (1.5)$$

The volume fraction f_{ck} of unhydrated clinker reads:

$$f_{ck} = (1 - p)(1 - \xi) \quad (1.6)$$

In addition to the volumes of different phase computed with Eqs. 1.2-1.6, volume fraction f_c of capillary pores and f_{hyd} of bulk hydrates are useful. The volume fraction f_p of capillary pores are defined as the sum of the volume fraction f_{cw} of capillary water and f_{cs} of chemical shrinkage:

$$f_c = f_{cw} + f_{cs} = p - 1.32(1 - p)\xi \quad (1.7)$$

The volume fraction f_{hyd} of bulk hydrates is equal to sum of the volume fraction f_{aw} of physically adsorbed water and $f_{hyd,s}$ of solid hydrates:

$$f_{hyd} = f_{hyd,s} + f_{aw} = 2.12(1 - p)\xi \quad (1.8)$$

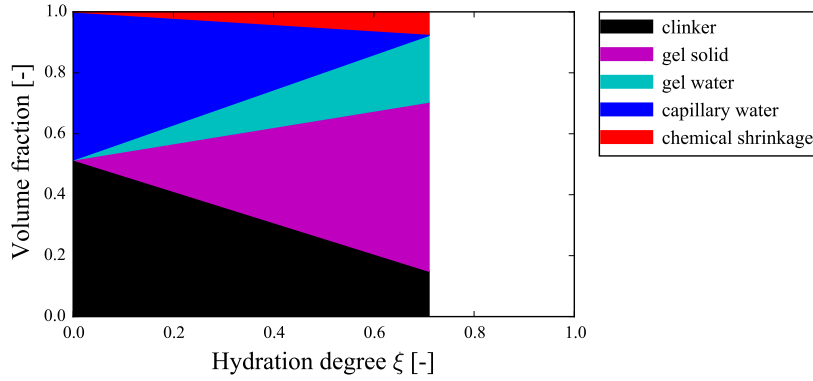
According to Powers' model, as long as there is capillary water inside cement paste, the hydration will progress until all the capillary water is consumed. Letting the volume fraction f_{cw} of capillary water equal to 0, we get the limit of hydration degree for a given water-to-cement ratio while there is no external water supply during hydration. The limit of hydration degree, i.e., long-term hydration degree ξ^p given by Powers' model reads:

$$\xi^p(w/c) = \begin{cases} w/c/0.42, & \text{if } w/c < 0.42, \\ 1, & \text{if } w/c \geq 0.42 \end{cases} \quad (1.9)$$

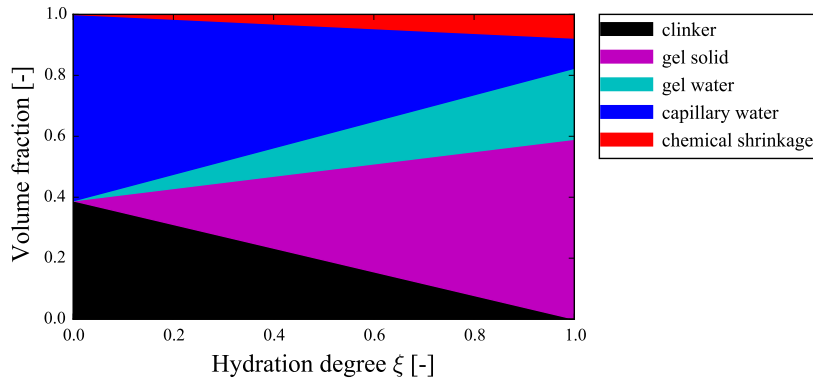
As shown in above Eqs. 1.2-1.8, the microstructure, i.e., volume fraction of each phase, depends not only water-to-cement ratio w/c but also the degree of hydration ξ . Figure 1.2 displays the volume fraction of each phase as a function of hydration degree ξ for two water-to-cement ratio, 0.3 and 0.5 respectively. As shown in Eq. 1.9, clinker cannot be fully hydrated for water-to-cement ratio 0.3, but stops at $\xi^p = 0.3/0.42 = 0.71$ (see Fig. 1.2a).

In practice, Powers and Brownyard (1947); Jensen (1995); Flatt et al. (2011) showed that hydration stops below a certain relative humidity. Since the consumption of water decreases the relative humidity, hydration may stop due to the lower relative humidity before consumption of all of the capillary water. In other words, the long-term hydration degree is lower than the long-term hydration degree ξ^p of Powers' model which is obtained

1.2. MICROSTRUCTURE AND HYDRATION OF CONCRETE



(a)



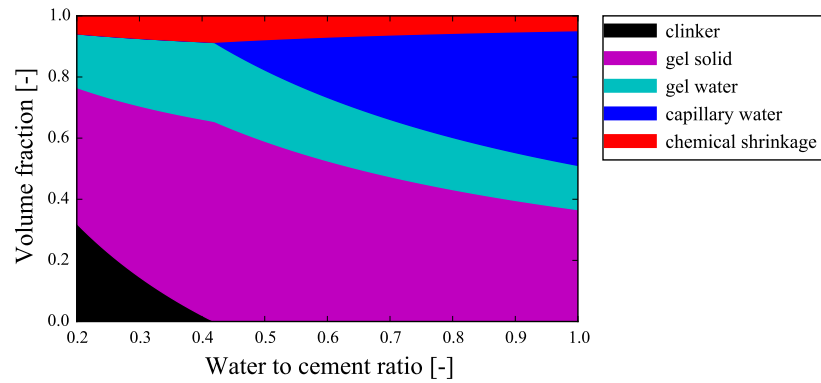
(b)

Figure 1.2 – Volume fraction of various phases as a function of hydration degree for cement paste with (a) water-to-cement ratio equal to 0.3 (b) water-to-cement ratio equal to 0.5.

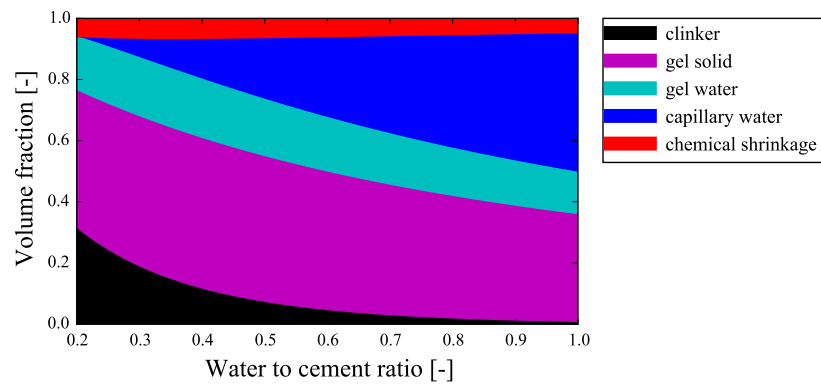
by supposing that hydration stops when capillary water is fully consumed. Based on experimental measurement, Waller (1999) proposed an empirical relation for long-term hydration ξ^∞ :

$$\xi^\infty(w/c) = 1 - \exp(-3.3w/c) \quad (1.10)$$

This long-term hydration degree ξ^∞ is slightly lower than ξ^p given by Powers' model. The microstructure of cement paste at long term is displayed in Fig. 1.3a and 1.3b, as a function of water-to-cement ratio, by considering that the long-term hydration degree is ξ^p and ξ^∞ , respectively.



(a)



(b)

Figure 1.3 – Microstructure of cement paste at long term, computed by taking hydration degree equal to (a) long-term hydration degree ξ^p of Powers' model given by Eq. 1.9; (b) long-term hydration degree ξ^∞ given by Eq. 1.10.

1.3 Delayed strains of concrete

Cement-based materials deform during all their service life, due to applied load or water exchange with outside or temperature variation. In this section, we are going to present first various delayed strain under isothermal condition. Then follow some observed phenomenology about physical origin of each type of delayed strain.

1.3. DELAYED STRAINS OF CONCRETE

Loading condition Hydric condition	No load	Under load
No water exchange with outside	Autogenous shrinkage	Autogenous shrinkage + Basic creep
Water exchange with outside	Autogenous shrinkage + Drying shrinkage	Autogenous shrinkage +Drying shrinkage +Basic creep + Drying creep

Table 1.1 – Time-dependent strain of cement-based materials in function of loading condition and hydric condition.

1.3.1 Classical decomposition of delayed strains of concrete

Conventionally, under isothermal condition, time-dependent strain of cement-based material is decomposed into following four components (see Tab. 1.1): autogenous shrinkage, basic creep, drying shrinkage and drying creep.

Autogenous shrinkage is the time dependent strain of a non-loaded specimen exchanging no water with outside.

Basic creep is the difference between the strain of a loaded specimen exchanging no water with outside and the autogenous shrinkage. The basic creep is regarded as the strain due to the applied load.

Drying shrinkage is the difference between the strain of a non-loaded specimen exchanging water with outside and the autogenous shrinkage. The drying shrinkage is regarded as the strain due to drying of specimen.

Drying creep is the additional time-dependent strain of a loaded specimen exchanging water with outside with respect to the sum of autogenous shrinkage, basic creep and drying shrinkage. Drying creep is also known under the name of Pickett effect as it was observed at first by [Pickett \(1942\)](#).

Many design codes ([FIB, 2013](#); [ACI Committee 209, 2008](#)) obtain the total delayed strain by summing the 4 components described above without questioning the correlation between them. In the next section, we provide some phenomenological observations related to these 4 components.

1.3.2 Some phenomenology

As mentioned in the previous section, the classical decomposition of delayed strain of cement-based materials neglects the correlation between the various components. In the following, we explain the correlation between various components via the role of hydration degree, relative humidity and structural effect.

The autogenous shrinkage is influenced by the degree of hydration (Lura et al., 2003; Wu et al., 2017). The specimen exchanging water with outside does not necessarily have same hydration degree as the one kept sealed due to the possible variation of available water for hydration. Hence, the autogenous shrinkage of the specimen exchanging water with outside is not exactly same as the autogenous shrinkage of the specimen kept sealed.

The delayed strain behavior of cement-based materials depend on relative humidity of the material. For the loaded specimen exchanging water with outside, the part of strain due to load is not exactly the same as basic creep strain of the loaded specimen exchanging no water with the outside. This is because the creep of cement-based material depend on water content (or, relative humidity) of the material (Bažant et al., 1976; Bažant and Chern, 1985; Abiar, 1986): If the specimen is kept sealed, i.e., there is no exchange of water with outside, a wet specimen creeps much more than a pre-dried specimen. Therefore, to predict the delayed strain of loaded and drying specimen, taking same basic creep as a loaded but sealed specimen is arguable.

The delayed strain behavior of cement-based material is submitted to structural effect. For the loaded specimen exchanging water with the outside, the part of strain due to drying is not exactly the same as the drying shrinkage of the non-loaded specimen exchanging water with outside. This is because the non-loaded specimen exchanging water with outside cracks due to drying while cracking of the loaded specimen exchanging water with the outside is limited by the load (Bažant and XI, 1994). Therefore, to predict the delayed strain of loaded and drying specimen, taking same drying shrinkage as a drying but non-loaded specimen is arguable.

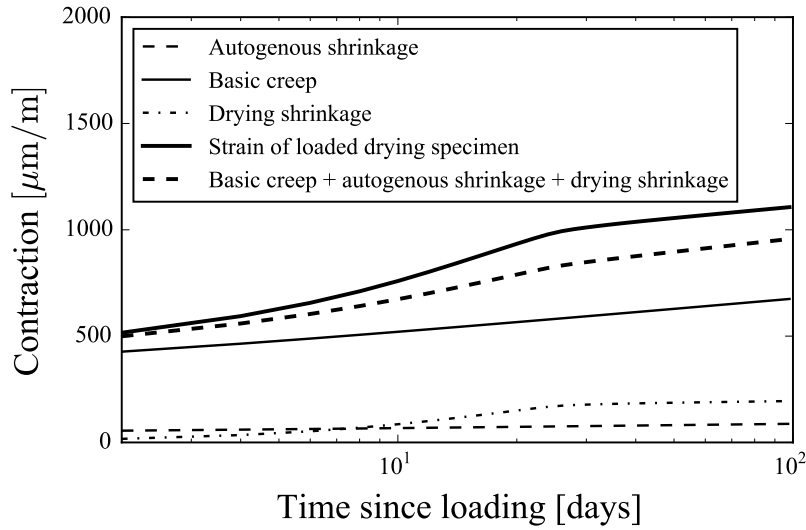


Figure 1.4 – Illustration of Pickett effect

In conclusion, the 4 component of classical decomposition are in fact correlated.

1.3.3 Physical origin

This section is dedicated to present the physical origin of delayed strain.

The origin of autogenous shrinkage is not fully understood. [Lura et al. \(2003\)](#); [Lin and Meyer \(2008\)](#); [Stefan et al. \(2009\)](#); [Zhang et al. \(2012\)](#); [Wu et al. \(2017\)](#) consider that the autogenous is the elastic response to the capillary effect due to self-desiccation of cement-based materials due to hydration of cement. [Hua et al. \(1995\)](#); [Luan et al. \(2013\)](#) consider that the autogenous shrinkage as viscoelastic response to the capillary effect due to self-desiccation.

Drying shrinkage is considered to be caused by the capillary effects due to drying of cement-based materials. [Benboudjema et al. \(2007\)](#); [Sellier and Buffo-Lacarrière \(2009\)](#); [Grasley and Leung \(2011\)](#); [Sellier et al. \(2016\)](#) model the drying shrinkage as viscoelastic response of material to the capillary effects while [Di Bella et al. \(2017\)](#) consider the drying shrinkage as elastic strain under capillary effect.

Basic creep is explained as a result of relaxation of microprestress, called *microprestress theory*, by Bažant et al. (1997). In this theory, Bažant et al. (1997) postulate that, for loading level below 40% of the strength, the origin of the creep is the shear slip at localized overstressed creep sites, represented by bridges across the micropores. As a result of progressive relaxation of the shear stress at the creep sites and exhaustion of the available overstressed creep sites causes the creep rate under a constant applied stress to decline.

Drying creep, defined as the extra strain of the loaded drying specimen with respect to the sum of basic creep, drying shrinkage and autogenous shrinkage, can be divided into two parts: the intrinsic part and the part due to structural effect. In the following, whenever drying creep is mentioned, we mean the intrinsic part.

The definition of drying creep due to structural effect is as following: the drying is much important on the surface than in the center of specimen. In case of drying with no load, the surface cracks whereas cracking is limited by the load in case of drying under load. The measured strain of non-loaded drying specimen is less than the potential strain of material (Acker, 1988; Bažant and XI, 1994). When the specimen is loaded and cracking is limited by the load, the supplementary part of strain is mobilized. This part of strain is called drying creep related to structural effect.

The structural effect is not enough to explain the totality of drying creep. The rest of drying creep is considered as intrinsic drying creep.

The origin of the intrinsic drying creep is still not known. Bažant and Chern (1985) consider that microdiffusion of water due to drying promotes shear slip in microprestress theory Bažant et al. (1997) so that the creep with drying is more important. This explanation is also supported by Vlahinić et al. (2012) who suggest that the migration of water molecules plays a lubricant role that amplifies delayed strain. On the contrary, Sellier et al. (2016) consider that the capillary effect due to drying is amplified in presence of load, which explains the drying creep.

As discussed in previous section, classical prediction method by summing up the 4 components has its shortage that is to neglect the correlation between them. Therefore, we would like to propose a model without decom-

posing the delayed strain to overcome the above shortage of classical model. In the next section, we present the necessary tools that we need in the thesis.

1.3.4 Multi-axial behavior

As we are interested in mainly the containment buildings that are biaxially prestressed concrete, we need to predict the creep of concrete under biaxial load. Therefore, we need to know its full 3-dimensional creep behavior. Within the framework of isotropic linear viscoelasticity, this 3-dimensional creep behavior is fully characterized by two creep compliances or relaxation moduli: for instance, on top of the uniaxial creep compliance considered in most models, we can use a viscoelastic (i.e., time-dependent) Poisson's ratio. However, although numerous studies (e.g., (RILEM Technical Committee, 1995, 2015)) and models (e.g., FIB (2013), 1992-1-1:2005 (2004), ACI Committee 209 (2008)) are devoted to the uniaxial creep compliance, the evolution of the viscoelastic Poisson's ratio of concrete with time has been much less scrutinized.

A first issue when considering a viscoelastic Poisson's ratio is that its definition is not unique. In the framework of linear isotropic viscoelasticity, Hilton (2001) enumerated five different ways of defining a time-dependent Poisson's ratio. The most widely used two Poisson's ratios are the creep Poisson's ratio ν_c and the relaxation Poisson's ratio ν_r , defined from a uniaxial creep experiment and to a uniaxial relaxation experiment, respectively:

$$\nu_c(t) = -\frac{\varepsilon_l(t)}{\varepsilon_a(t)} \text{ during a uniaxial creep experiment for which } \sigma_a(t) = \sigma_{a0} \quad (1.11a)$$

$$\nu_r(t) = -\frac{\varepsilon_l(t)}{\varepsilon_{a0}} \text{ during a uniaxial relaxation experiment for which } \varepsilon_a(t) = \varepsilon_{a0} \quad (1.11b)$$

where $\varepsilon_a(t)$ and $\varepsilon_l(t)$ are the time-dependent axial and lateral strains, respectively, $\sigma_a(t)$ is the axial load, and σ_{a0} and ε_{a0} are constants.

These two Poisson's ratios are not equal (Tschoegl et al., 2002; Lakes and

Wineman, 2006). However, little is known on how significant the difference between them is.

As to cement-based materials, Neville et al. (1983) define it through a ratio of the creep strains only, while Jordaan and Illston (1969) define it through a ratio of the total mechanical strains (which are equal to the sum of the elastic strains and of the creep strains). For uniaxial creep tests, Neville et al. (1983) defined a uniaxial creep-based Poisson's ratio as:

$$\tilde{\nu}(t) = -\frac{\varepsilon_l(t) - \varepsilon_l^0}{\varepsilon_a(t) - \varepsilon_a^0} \quad (1.12)$$

where $\varepsilon_l(t)$, $\varepsilon_a(t)$ are the total lateral and axial strain, respectively, and where $\varepsilon_l^0 = \varepsilon_l(0)$ and $\varepsilon_a^0 = \varepsilon_a(0)$ are the lateral and axial elastic strains, respectively. Thus, $\varepsilon_l(t) - \varepsilon_l^0$ and $\varepsilon_a(t) - \varepsilon_a^0$ are the lateral and axial creep strains, respectively.

The main interest of the creep-based Poisson's ratio $\tilde{\nu}(t)$ is that only creep strains are needed to compute it. Thus, it can be reported for any creep experiment, even in absence of any information on the elastic properties of the material.

For what concerns the value of the Poisson's ratio or its evolution over time, a very large scatter is observed. For instance, with the definition he chose, Neville et al. (1983) gathered the following values for the viscoelastic Poisson's ratio: close to 0 (Ross, 1954; Furr, 1967), equal to 0.05 (Glanville and Thomas, 1939; L'Hermite, 1959), equal to the elastic Poisson's ratio (Duke and Davis, 1944; Polivka et al., 1963), increasing with time (Evans and Wood, 1937), or decreasing with time (York et al., 1972). A possible reason that could partly explain this large scatter is that the various experiments gathered by Neville were performed under various —and sometimes uncontrolled— hydric conditions. In our present work, we will focus on the evolutions of a viscoelastic Poisson's ratio during basic creep experiments, during which no water is exchanged between sample and environment. Such condition is achieved either by sealing the sample (Jordaan and Illston, 1969, 1971; Kennedy, 1975; Ulm et al., 2000; Kim et al., 2005), or by controlling the relative humidity of the environment to the same relative humidity as

that of the sample (Gopalakrishnan, 1968).

In this thesis, we would like quantify the difference between the relaxation Poisson's ratio and the creep Poisson's ratio and define well the viscoelastic Poisson's ratio that we will consider in this thesis. Then, we compare it with alternative definitions found in the literature specific to cement-based materials. In the end, we perform an analysis of basic creep data on concrete from the literature, to determine how this viscoelastic Poisson's ratio evolves with time.

1.4 Non-aging linear viscoelasticity

Concrete is an aging material, i.e., its mechanical properties depend on its age (Mehta and Monteiro, 2006; Grasley and Lange, 2007). However, mature concrete can reasonably be considered non-aging. Also, up to about at least 40% of its strength, concrete can reasonably be assumed to be linear viscoelastic (Neville et al., 1983). The *linearity* here means that the response to a sum of two stress (or strain) histories is the sum of the responses to each of them taken separately, from which the Boltzmann superposition principle is derived (Christensen, 1982).

Hence, the non-aging linear viscoelasticity would be the framework in which we develop the model for predicting of shrinkage and creep behavior of cement-based materials. In this section, we present first the constitutive relation for an isotropic non-aging linear viscoelastic solid submitted to infinitesimal strains in isothermal conditions.

One of the characteristic that we would like to include in our model is the dependence on relative humidity of creep properties of cement-based materials. Therefore, in second part of this section, we aim at extending the above strain-stress relation to the case where viscoelastic behavior depends on environmental parameters, by comparing two ways of considering the superposition principle as already compared by Bažant (1988); Walraven and Shen (1991).

1.4.1 Basic constitutive relations

For an isotropic non-aging linear viscoelastic solid submitted to infinitesimal strains in isothermal conditions, the time-dependent state equations that link the stress tensor $\underline{\underline{\sigma}}$ (decomposed into the volumetric stress $\sigma_v = \text{tr}(\underline{\underline{\sigma}})/3$ and the deviatoric stress tensor $\underline{\underline{s}}$ such that $\underline{\underline{\sigma}} = \sigma_v \underline{\underline{1}} + \underline{\underline{s}}$, where tr is the trace operator and $\underline{\underline{1}}$ is the unit tensor) to the strain tensor $\underline{\underline{\varepsilon}}$ (decomposed into the volumetric strain $\varepsilon_v = \text{tr}(\underline{\underline{\varepsilon}})$ and the deviatoric strain tensor $\underline{\underline{e}}$ such that $\underline{\underline{\varepsilon}} = (\varepsilon_v/3)\underline{\underline{1}} + \underline{\underline{e}}$) are (Christensen, 1982):

$$\sigma_v(t) = K(t) \otimes \dot{\varepsilon}_v(t) \quad (1.13a)$$

$$s_{ij}(t) = 2G(t) \otimes \dot{e}_{ij}(t) \quad (1.13b)$$

where t is the time since loading; \otimes denotes for the convolution product defined as $f \otimes g = \int_{-\infty}^t f(t-\tau)g(\tau)d\tau$ and \dot{f} is for derivatives with respect to time, $\dot{f} = df(t)/dt$. Those state equations can equivalently be written as (Christensen, 1982):

$$\varepsilon_v(t) = J_K(t) \otimes \dot{\sigma}_v(t) \quad (1.14a)$$

$$e_{ij}(t) = \frac{1}{2}J_G(t) \otimes \dot{s}_{ij}(t) \quad (1.14b)$$

where $J_K(t)$ and $J_G(t)$ are called the bulk creep compliance and the shear creep compliance, respectively. Creep compliances are linked to relaxation moduli through (Christensen, 1982):

$$s\widehat{J}_K = \frac{1}{s\widehat{K}} \quad (1.15a)$$

$$s\widehat{J}_G = \frac{1}{s\widehat{G}} \quad (1.15b)$$

where s is the Laplace variable and $\widehat{f}(s)$ is the Laplace transform of a function $f(t)$.

Starting from the state equations 2.4a-2.4b, in uniaxial testing, we can show that the axial stress history $\sigma_a(t)$ and the axial strain history $\varepsilon_a(t)$ are related by (Christensen, 1982):

$$\sigma_a(t) = E(t) \otimes \dot{\varepsilon}_a(t) \quad (1.16a)$$

$$\varepsilon_a(t) = J_E(t) \otimes \dot{\sigma}_a(t) \quad (1.16b)$$

where $E(t)$ and $J_E(t)$ are called the uniaxial relaxation modulus and the uniaxial creep compliance, respectively. The creep function, defined by $J_E(t) - J_E(0)$ is also widely used in literature (Bažant et al., 1993; Vandamme and Ulm, 2009; Zhang, 2014).

For a uniaxial relaxation or creep test, by solving Eqs. (2.3) and Eqs. (2.4) in the Laplace domain, we obtain an analytic expression for the uniaxial relaxation modulus E and the uniaxial creep compliance J_E in the Laplace domain, respectively, the latter being transformed back directly (Christensen, 1982):

$$\widehat{E}(s) = \frac{9\widehat{K}(s)\widehat{G}(s)}{3\widehat{K}(s) + \widehat{G}(s)} \quad (1.17a)$$

$$J_E(t) = \frac{1}{9}J_K(t) + \frac{1}{3}J_G(t) \quad (1.17b)$$

1.4.2 Extension to the case with environment-dependent properties

From the definition of compliance, we write the viscoelastic strain $\varepsilon(t, t_0)$ at time t due to a constant stress σ_0 that is applied since time t_0 as following:

$$\varepsilon(t, t_0) = \sigma_0 J(t, t_0) \quad (1.18)$$

where $J(t, t_0)$ is the compliance. Note that Eq. 1.18 is for 1D case for the sake of simplicity. For the stress $\sigma(t, t_0)$ which stands hereby applied at time t_0 and varies over time, we can write the strain response by making use of the principle of superposition by decomposing the stress history either horizontally as shown in Fig. 1.5a, or vertically as shown in Fig. 1.5b.

When we follow the horizontal decomposition as in Fig. 1.5a, the strain is the sum of the $n + 1$ strain responses due to $n + 1$ constant stress σ_0 and $\Delta\sigma_i$ (i.e., the stress increment at time step t_i) with $i = 1, 2, \dots, n$:

$$\varepsilon(t, t_0) = \sigma_0 J(t, t_0) + \sum_{i=1}^n \Delta\sigma_i J(t, t_i) \quad (1.19)$$

When the stress is differentiable, we can write in form of integral:

$$\varepsilon(t, t_0) = \sigma_0 J(t, t_0) + \int_{t_0}^t J(t, \tau) \frac{d\sigma(\tau)}{d\tau} d\tau = \int_{-\infty}^t J(t, \tau) \frac{d\sigma(\tau)}{d\tau} d\tau = J(t) \otimes \dot{\sigma}(t) \quad (1.20)$$

which is the same as Eq. 2.6b.

Or, following the vertical decomposition as in Fig. 1.5b, we decompose the stress into sum of n impulse stress σ_i each of which lasts from time t_i to t_{i+1} . The strain response then can be written as the sum of n strain responses, each of which is due to impulse stress σ_i :

$$\varepsilon(t, t_0) = \sum_{i=0}^{n-1} \varepsilon(t, t_{i+1}, t_i) = - \sum_{i=0}^{n-1} \bar{\sigma}_i (J(t - t_{i+1}, \mathbf{v}) - J(t - t_i, \mathbf{v})) \quad (1.21)$$

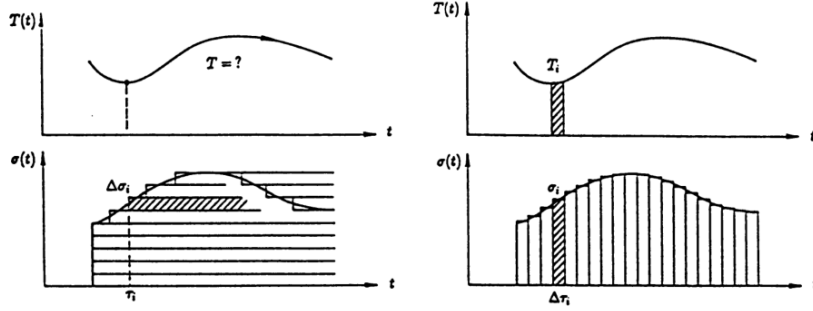


Figure 1.5 – Principle of superposition by (a) horizontal decomposition of stress history and (b) vertical decomposition of stress history, taken from [Walraven and Shen \(1991\)](#)

where $\bar{\sigma}_i$ is the mean stress at the time step i ; \mathbf{v} is the environmental parameters on which the viscoelastic properties depend, for instance relative humidity. When the stress is differentiable, we can write in form of integral:

$$\varepsilon(t, t_0) = \int_{-\infty}^t \sigma_i(\tau) \frac{\partial J(t - \tau, \mathbf{v}|_{t-\tau})}{\partial \tau} d\tau \quad (1.22)$$

As shown in Fig. 1.5, when we follow the horizontal decomposition, the dependence on environmental parameter \mathbf{v} (e.g. temperature in Fig. 1.5) cannot be taken into consideration as the environmental parameter is changing for each stress increment $\Delta\sigma_i$. Hence, in order to be able to take into account the dependence on environmental parameter, we follow the vertical decomposition of stress history, but not the horizontal decomposition. However, it is worth to notice that when the environmental parameter \mathbf{v} is constant over time, Eq. 1.22 can be reduced to Eq. 1.20 ([Walraven and Shen, 1991](#)).

In order to take into account the fact that the creep properties of cement-based material depend on relative humidity, we will use the vertical decomposition, i.e., Eq. 1.22 in our model in chapter 6. In the following, we illustrate how to consider the environmental parameter by an example.

Let's take a material whose viscoelastic behavior depends on relative humidity h_r . The compliance is given by: $J(t) = \frac{1}{K} + \frac{1}{C} \log(1 + t)$ with the creep modulus C depending on relative humidity h_r . For relative humidities

h_r between 100% and 75%, $C(h_r) = C_0$. When relative humidity h_r drop below 75%, i.e.; $h_r < 75\%$, $C(h_r) = C_0 - \alpha(h_r - 75)$. Now we compute the strain due to a constant unit stress $\sigma = 1$ applied at time $t = 0$. The relative humidity $h_r = 100\%$ in the beginning for time $t < t_d$ and drops suddenly to 25% at time $t = t_d$ and is kept constant since. Using Eq. 1.22, the strain reads:

$$\varepsilon(t) = \frac{1}{K} + \int_0^t \frac{1}{C} \left(\frac{1}{1+t-\tau} \right) d\tau \quad (1.23)$$

It is important to keep in mind that using Eq. 1.23 is delicate when the viscoelastic properties of the material depend on the environment. By comparing three different possibilities, we found that the creep compliance C in Eq. 1.23 should be evaluated at time $t - \tau$ according to Eq. 1.22. Evaluating the creep compliance C at time t or τ gives unphysical results. But our comparison is not a definite proof of the validity of the use of Eq. 1.23 when properties are environment-dependent. How to use the correspondence principle in general when the viscoelastic properties of the material depend on the environment is a delicate question, which would deserve further scrutiny.

Figure 1.6 shows in the same figure the strain response calculated from Eq. 1.23 and the compliance at constant relative humidity at $h_r = 100\%$ and at $h_r = 25\%$, respectively.

1.5 Modeling of porous multiscale materials

As seen in section 1.2, concrete is a heterogeneous material and made of various solid phases whose characteristic lengths vary from nanometers to centimeters. The time-dependent properties at the scale of concrete depend on those components that have a smaller scale than concrete. In this section, we are going to present first homogenization, called also micromechanics, which is a method to predict the properties of a heterogeneous material from the properties of its components. In the first section basic procedure of micromechanical analysis is going to be presented. Mori-Tanaka scheme and self-consistent scheme are also going to be discussed as they are going to be

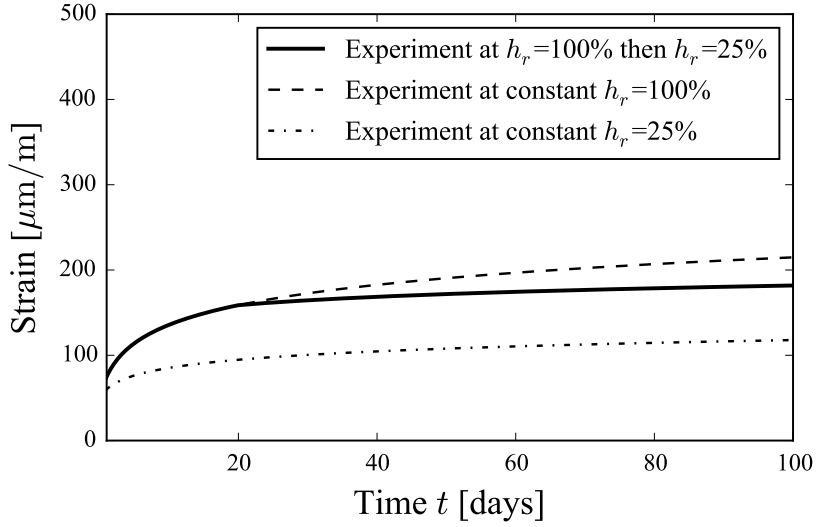


Figure 1.6 – Strain response to a constant unit stress with various relative humidity histories, constant or varying in time

used in the thesis. The second section is dedicated to multi-scale schemes that are used for simulation of concrete.

As seen in section 1.2, concrete is composed from solid and pores that are fully or partially saturated by water. Hence, concrete is subjected to capillary effects and surface effects that is related to the movement of water inside pores. The poromechanics suits well to study the behavior of such a porous material. Hence, in the third section, basic idea and equations of poromechanics are going to be presented.

1.5.1 Basics of homogenization

As mentioned above, the objective of micromechanics is to predict the properties of a composite from the properties of its components. In general, micromechanical analysis follows three steps: definition of representative elementary volume (REV), localization and homogenization.

In the first step, we define REV as a volume at whose scale we are going to look for an equivalent homogenous volume that responds to a load the same manner as the original heterogeneous material. First we define the

characteristic length d of heterogeneity and l of REV. In order to consider homogenous behavior of REV, the characteristic length d of heterogeneity should be much smaller than l of REV, i.e., $d \ll l$. As to the characteristic length l of REV, it should be much smaller comparing to the characteristic length L of structure, i.e., $l \ll L$, so that the gradient of strain and stress fields can be neglected over the REV. Second, we describe the internal composition of the REV by the geometrical shape, distribution and orientation of each phase.

In the second step, we localize the stress or strain tensor which consists to determine the local stress $\underline{\underline{\sigma}}(\underline{x})$ or strain $\underline{\underline{\varepsilon}}(\underline{x})$ tensor of each phase from the applied strain $\underline{\underline{E}}$ or stress $\underline{\underline{\Sigma}}$ at the scale of VER. The vector \underline{x} represents the coordinate of the point.

$$\underline{\underline{\varepsilon}}(\underline{x}) = \mathbb{A}_i(\underline{x}) : \underline{\underline{E}} \quad (1.24)$$

where \mathbb{A} is the fourth order strain localization tensor. Let f_i denote for the volume fraction of phase i and $\langle z \rangle_i$ for volume average of quantity z over the volume V_i of phase i , i.e., $\langle z \rangle_i = 1/V_i \int_{V_i} z dV_i$, then strain localization tensors should satisfy: ;

$$\sum_i f_i \langle \mathbb{A}_i(\underline{x}) \rangle_i = \mathbb{I} \quad (1.25)$$

The third step, which is homogenization, consists to link the behavior of the equivalent homogenous medium to the properties of heterogeneous phase by combining the above localization, constitutive behavior of heterogeneous phases and relation of mean values.

At the end of a micromechanical analysis, we get the stiffness tensor \mathbb{C}_{hom} of the equivalent homogenous medium as a function of stiffness tensor \mathbb{C}_i of each heterogeneous phase:

$$\mathbb{C}_{hom} = \sum_i f_i \mathbb{C}_i : \mathbb{A}_i \quad (1.26)$$

For isotropic linear elastic material, the fourth order stiffness tensor has only two independent components: bulk modulus K and shear modulus G .

In other words, stiffness tensor \mathbb{C} can be written as: $\mathbb{C} = 3K\mathbb{J} + 2G\mathbb{K}$, with \mathbb{J} and \mathbb{K} the volumetric and deviatoric part of the fourth-order symmetric unit tensor \mathbb{I} , respectively. \mathbb{I} is defined as $I_{ijkl} = 1/2(\delta_{ik}\delta_{jl} + \delta_{il}\delta_{jk})$ in which and δ_{ij} stands for the Kronecker delta. Then, the Eq. 1.26 can be reduced to following two scalar equations:

$$K_{hom} = \sum_i f_i A_i^{sph} K_i \quad (1.27a)$$

$$G_{hom} = \sum_i f_i A_i^{dev} G_i \quad (1.27b)$$

where A_i^{sph} and A_i^{dev} are the spherical and deviatorical part of strain localization tensor \mathbb{A}_i of phase i .

Hence, the question is to determine the strain localization tensor \mathbb{A}_i , i.e., A_i^{sph} and A_i^{dev} , which depends on the description of the VER and the hypothesis that are supposed at the step of localization. In the following, we are going present two homogenization schemes that are going to be used in this thesis: Mori-Tanaka's scheme and self-consistent scheme. Both of the two schemes are based on the solution of Eshelby's inclusion problem (Eshelby, 1957). In this thesis we restrict ourselves only on the cases where all inclusions are spherical.

The Mori-Tanaka's scheme (Mori and Tanaka, 1973) is intended for materials which are composed from a matrix that embeds inclusions inside. The matrix phase, noted $i = m$ for subscript, is continuous and totally incloses each of the inclusions. The main hypothesis is that the inclusions do not influence each other. Therefore, by considering each inclusion as embedded into an infinite matrix, the phase m , and making use of the solution of Eshelby's inclusion problem, we get the strain localization tensor of Mori-

Tanaka's scheme (Zaoui, 1999):

$$A_i^{sph} = \frac{(1 + \alpha_m(K_i/K_m - 1))^{-1}}{\sum_i f_i(1 + \alpha_m(K_i/K_m - 1))^{-1}} \quad (1.28a)$$

$$A_i^{dev} = \frac{(1 + \beta_m(G_i/G_m - 1))^{-1}}{\sum_i f_i(1 + \beta_m(G_i/G_m - 1))^{-1}} \quad (1.28b)$$

with $\alpha_m = 3K_m/(3K_m + 4G_m)$ and $\beta_m = 6(K_m + 2G_m)/(15K_m + 20G_m)$.

For a composite made from matrix m and one type of inclusions i , inserting Eq. 4.2 into Eq. 1.27, the bulk modulus K_{hom} and shear modulus G_{hom} of a composite made from an elastic matrix and elastic spherical inclusions can be computed as following:

$$K_{hom} = \frac{(1 - f_i)(K_m + \alpha_m(K_i - K_m)) + f_i K_i}{(1 - f_i)(K_m + \alpha_m(K_i - K_m)) + f_i K_m} K_m \quad (1.29a)$$

$$G_{hom} = \frac{(1 - f_i)(G_m + \beta_m(G_i - G_m)) + f_i G_i}{(1 - f_i)(G_m + \beta_m(G_i - G_m)) + f_i G_m} G_m \quad (1.29b)$$

where K_m and G_m are the bulk and shear modulus of matrix, respectively; K_i and G_i are the bulk and shear modulus of inclusions, respectively; f_i is the volume fraction of inclusions.

Self-consistent scheme (Budiasky, 1965; Hill, 1965) is intended for materials in which none of the phase plays dominating a role. It is supposed that each of the phase is surrounded by the equivalent homogenous materials that we are looking for. Therefore, by considering each phase as embedded into an infinite matrix, i.e., the equivalent homogenous medium hom , and making use of the solution of Eshelby's inclusion problem, we get the strain

localization tensor of Self-consistent scheme:

$$A_i^{sph} = \frac{(1 + \alpha_{hom}(K_i/K_{hom} - 1))^{-1}}{\sum_i f_i(1 + \alpha_{hom}(K_i/K_{hom} - 1))^{-1}} \quad (1.30a)$$

$$A_i^{dev} = \frac{(1 + \beta_{hom}(G_i/G_{hom} - 1))^{-1}}{\sum_i f_i(1 + \beta_{hom}(G_i/G_{hom} - 1))^{-1}} \quad (1.30b)$$

with $\alpha_{hom} = 3K_{hom}/(3K_{hom}+4G_{hom})$ and $\beta_{hom} = 6(K_{hom}+2G_{hom})/(15K_{hom}+20G_{hom})$.

For a composite made from phase 1 and phase 2, inserting Eq. 1.30 into Eq. 1.27, the bulk modulus K_{hom} and shear modulus G_{hom} of a composite made from two phases can be obtained by solving the following implicit Eqs.:

$$K_{hom} = \frac{(1 - \alpha_{hom})(f_1 K_1 + (1 - f_1) K_2) K_{hom} + \alpha_{hom} K_1 K_2}{(1 - \alpha_{hom}) K_{hom} + \alpha_{hom} ((1 - f_1) K_1 + f_1 K_2)} \quad (1.31a)$$

$$G_{hom} = \frac{(1 - \beta_{hom})(f_1 G_1 + (1 - f_1) G_2) G_{hom} + \beta_{hom} G_1 G_2}{(1 - \beta_{hom}) G_{hom} + \beta_{hom} ((1 - f_1) G_1 + f_1 G_2)} \quad (1.31b)$$

where K_1 and G_1 are the bulk and shear modulus of the phase 1, respectively; K_2 and G_2 are the bulk and shear modulus of the phase 2, respectively; f_1 is the volume fraction of phase 1.

1.5.2 Multi-scale scheme of concrete

As presented in section 1.2, the size of component of concrete varies from centimeters (size of aggregates) to nanometers (size of C-S-H particles). Hence, micromechanical modeling of concrete is normally achieved by several steps of homogenization. This section aims at resuming homogenization schemes for concrete in literature.

Based on length of various phases in microstructure of concrete, researchers adapted different multi-scale scheme of concrete, depending on the problem they want to resolve or on the method of observation they used on concrete.

The different schemes that are found in literature differ slightly from each other, but still can be resumed as following (in the order of from larger scale to smaller scale):

1. At the largest scale of concrete, the aggregates are considered as spherical inclusions and are embedded into a matrix made of cement paste. Given the matrix-inclusion morphology, Mori-Tanaka scheme is used (Bernard et al., 2003b; Pichler et al., 2007; Sanahuja et al., 2007; Pichler and Hellmich, 2011).
2. At the scale below of cement paste, due to different consideration of size of clinker and portlandite, different schemes are adapted by different authors:
 - (a) Bernard et al. (2003b) consider the cement paste as a mixture of unhydrated clinker grains, portlandite crystals and C-S-H matrix (including gel porosity) and used self-consistent scheme. At the scale below of C-S-H matrix, low density (LD) C-S-H phase is considered to be the matrix that embeds high density (HD) C-S-H phase (see Fig. 1.7a).
 - (b) Constantinides and Ulm (2004) consider unhydrated clinker grains and portlandite crystals as inclusions that are embedded in C-S-H matrix (including gel porosity) and used Mori-Tanaka's scheme. At the scale below of C-S-H matrix, low density (LD) C-S-H phase is considered to be the matrix that embeds high density (HD) C-S-H phase (see Fig. 1.7b).
 - (c) Sanahuja et al. (2007) consider matrix-inclusions morphology, where the matrix and inclusion phase are as following: the matrix is a mixture of capillary pores and low density (LD) C-S-H phase and used mori-Tanaka scheme; the inclusion phase is composed of spheres, with the unhydrated clinker is the core that is coated by a layer of high density (HD) C-S-H phase (see Fig. 1.7c).
 - (d) Pichler et al. (2007) consider unhydrated clinker grains, portlandite, gypsum, ettringite, monosulfate as spherical inclusions

1.5. MODELING OF POROUS MULTISCALE MATERIALS

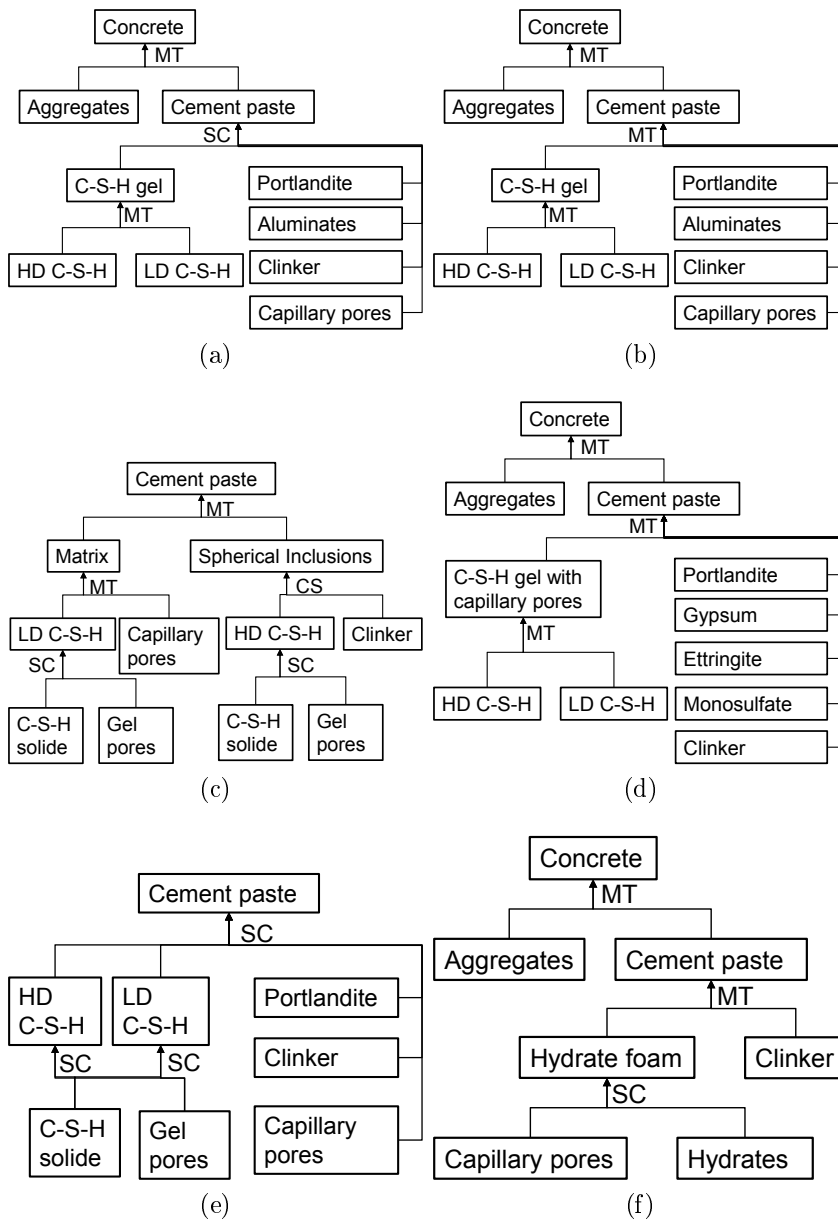


Figure 1.7 – Multiscale schemes adopted by (a) Bernard et al. (2003b); (b) Constantinides and Ulm (2004); (c) Sanahuja et al. (2007); (d) Pichler et al. (2007); (e) Ghabezloo (2010); (f) Pichler and Hellmich (2011). MT, SC, CS represent Mori-Tanaka scheme, self-consistent scheme and composite sphere, respectively.

that are embedded in a matrix of the mixture of C-S-H gel and capillary pores. The Mori-Tanaka's scheme is used. At the scale below, spherical capillary pores are considered as inclusions that are embedded in C-S-H gel. At the scale below of C-S-H gel, low density (LD) C-S-H is considered as a matrix that surrounds high density (HD) C-S-H that is considered to be spherical (see Fig. 1.7d).

- (e) [Ghabezloo \(2010\)](#) consider unhydrated clinker grains, portlandite, low density (LD) C-S-H phase and high density (HD) C-S-H phase as same scale particles that are arranged together and used self-consistent scheme. At the scale below, both low density (LD) C-S-H phase and high density (HD) C-S-H phase are respectively considered to be the mixture of C-S-H particles and gel pores. At this scale, self-consistent scheme is used (see Fig. 1.7e).
- (f) [Pichler and Hellmich \(2011\)](#) consider unhydrated clinker grains as inclusions that are embedded in a matrix of hydrate foam and used Mori-Tanaka's scheme. At the scale below of hydrate foam, hydrates and capillary pores are considered to be particles that arranged together and used self-consistent scheme. The hydrates are considered to be needle-shaped while capillary pores are considered to be spherical (see Fig. 1.7f).

In conclusion, there is several types of multi-scale scheme that can simulate the mechanical behavior of concrete. At the scale of concrete, matrix-inclusion morphology with Mori-Tanaka's scheme seems mostly appropriate. At other scales below, depending on the authors, different options are available. As the microstructure of cement-based materials is not exactly same as the hypothesis of homogenization schemes, we cannot judge which of the above homogenization schemes is the best.

1.5.3 Poromechanics

This chapter is intended to present basic knowledge about poromechanics which describes the mechanical behavior of porous solids. By porous solid,

we mean here a solid with pore networks through which fluid can flow across.

For a porous solid, the non-loaded state is noted as reference state. At this reference state, the volume of porous solid V_0 and the volume of pore space V_{V_0} are noted as reference volume of porous solid and reference volume of pores, respectively. The porosity of porous solid is defined as:

$$\phi = \frac{V_V}{V_0} \quad (1.32)$$

where V_V is the volume of pores at any state. At reference state, taking pore volume V_{V_0} we obtain the reference porosity ϕ_0 .

When an isotropic elastic porous solid is submitted to a mechanical load $\underline{\underline{\sigma}}$, the strain response is given by (Coussy, 2004):

$$\sigma_v = K\varepsilon_v - bP \quad (1.33a)$$

$$\phi - \phi_0 = b\varepsilon_v + \frac{P}{N} \quad (1.33b)$$

$$s_{ij} = 2Ge_{ij} \quad (1.33c)$$

where b and N are the Biot coefficient and Biot skeleton modulus, respectively; P is the pressure in pores; K and G are the elastic bulk modulus and elastic shear modulus of porous solid, respectively; the stress and strain components are defined exactly in the same way as in Eq. 2.3.

From Eq. 1.33a, we can see that the strain of porous solid is caused by

$$\sigma'_v = \sigma_v + bP, \quad (1.34)$$

which is defined as Biot's effective stress. When the solid phase is incompressible, the Biot coefficient of porous solid is equal to 1, from where the effective stress equals to Terzaghi's effective stress, $\sigma'_v = \sigma_v + P$.

For porous solid in which the pore space is filled by water and air, the

degree of saturation S_l is defined as:

$$S_l = \frac{V_w}{V_V} \quad (1.35)$$

When the porous solid is fully saturated, i.e., $S_l=1$, the pore pressure P equals to the pressure of water $P = P_w$. When the porous solid is partially saturated, i.e., $S_l < 1$, the pore pressure P can be computed to be equal to $S_l P_c$ (Coussy, 2004) or $\int P_c dS_l$ (Coussy et al., 2004). The latter expression takes into account surface effects while the former expression neglects these effects. In the thesis, as we are dealing mainly the cases where relative humidity stays over 40%, we choose to use the former expression, $P = S_l P_c$.

The bulk modulus K , shear modulus G or Biot coefficient b of porous solid can be computed using micromechanics. Taking Mori-Tanaka homogenization scheme, we can use Eq. 1.29 to obtain the bulk modulus K and shear modulus G . The Biot coefficient b , meanwhile, reads as following (Ghabezloo, 2010):

$$b = \phi A_\phi^{sph} \quad (1.36)$$

where A_ϕ^{sph} is the spherical part of strain localization tensor of pores.

When the Poisson's ratio ν_s of solid skeleton equals to 0.2, using the Mori-Tanaka scheme, the bulk modulus K , shear modulus G and Biot coefficient of porous solid reads as following:

$$K = \frac{1 - \phi}{1 + \phi} K_s \quad (1.37a)$$

$$G = \frac{1 - \phi}{1 + \phi} G_s \quad (1.37b)$$

$$b = \frac{2\phi}{1 + \phi} \quad (1.37c)$$

The micromechanical analysis can be used also to compute the Biot coefficient of a porous material with double porosity which is composed from l ($l < m$) porous phase, $m - l$ solid phase and pores. It should be noted that

the size of the pores is much larger than the size of the pores of the porous phase. For such a material, the Biot coefficient b_{hom} reads:

$$b_{hom} = 1 - \sum_{i=1}^m (f_i A_i^{sph} (1 - b_i)) \quad (1.38)$$

where b_i is the Biot coefficient of phase i . For porous phase, the Biot coefficient b_i is computed from Eq. 1.36; for solid phase, the Biot coefficient b_i equals to 1.

Coussy (2004) also extended poroelasticity to viscoelastic porous materials. When the porous solid is viscoelastic, the constitutive law in Eq. 1.33 reads as following:

$$\sigma_v(t) = K(t) \otimes \dot{\epsilon}_v(t) - b(t) \otimes \dot{P}(t) \quad (1.39a)$$

$$\phi(t) - \phi_0 = b(t) \otimes \dot{\epsilon}_v + J_N(t) \otimes \dot{P}(t) \quad (1.39b)$$

$$s_{ij}(t) = 2G(t) \otimes \dot{\epsilon}_{ij} \quad (1.39c)$$

where $b(t)$ and $J_N(t)$ are viscoelastic parameters that corresponds in elastic case the Biot coefficient b and the inverse of Biot skeleton modulus, $1/N$; $K(t)$ and $G(t)$ are the bulk and shear relaxation modulus of porous solid, respectively. The stress and strain components are defined exactly in the same way as in Eq. 2.3.

1.6 Models for creep and shrinkage of cement-based materials

Most of design codes predict shrinkage and creep of cement-based materials as they have to be take into account in design. Moreover, since the physical mechanism and influencing parameter of shrinkage and creep behavior is not fully understood yet, researchers have been trying to propose new models in order to better take into account new findings since decades. The prediction

model of creep and shrinkage can be divided into two groups: the models that follow the classical decomposition of delayed strain of cement-based materials. Examples of this type of models can be found in the work of RILEM Technical Committee (1995); Granger (1995); Le Roy (1995); Gardner and Lockman (2001); 1992-1-1:2005 (2004); Benboudjema et al. (2005); ACI Committee 209 (2008); FIB (2013); RILEM Technical Committee (2015); and the models that do not presuppose the decomposition of delayed strain. As far as we know, the only model of this type is the model of Sellier et al. (2016) and its previous version Sellier and Buffo-Lacarrière (2009).

In the following, we present the B4 model of RILEM Technical Committee (2015) and the model of Sellier et al. (2016) as examples of each type of model.

1.6.1 B4 Model of Bažant et al.

The B4 model of RILEM Technical Committee (2015) is fourth in a series of progressively improved model at Northwestern University. It is based on solidification theory, theory of microporestress relaxation in nano-structure, activation energy concept, moisture diffusion theory and damage models for microcracking (Bažant, 1988; Bažant and Prasannan, 1989; Bažant et al., 1997; Jirásek and Bazant, 2002). The same mathematical form as B3 model is used. The model is formulated for 1D problem. For a specimen in reference temperature 20°C, time-dependent strain $\varepsilon(t)$ is computed as following:

$$\varepsilon(t) = \left(\frac{1}{E_0} + C_0(t, t') + C_d(t, t', t - t_0) \right) \sigma_0 + \varepsilon_{d,sh}(t - t_0, t_0) + \varepsilon_{a,sh}(t - t_0, t_0) \quad (1.40)$$

where t, t', t_0 are current age, age at loading and age at the start of environmental exposure in days, respectively; σ_0 is the constant load applied at the age t' ; $E_0, C_0(t, t'), C_d(t, t', t - t_0)$ are the instantaneous creep modulus (i.e., Young's modulus) at the age of loading, basic creep function and drying creep function, respectively; $\varepsilon_{d,sh}(t - t_0, t_0), \varepsilon_{a,sh}(t - t_0, t_0)$ are strain due to drying shrinkage and autogenous shrinkage, respectively.

Autogenous shrinkage is supposed to be asymptotic and evolves as a

1.6. MODELS FOR CREEP AND SHRINKAGE OF CEMENT-BASED MATERIALS

power function. The final value of autogenous shrinkage depends on water-to-cement ratio, aggregate-to-cement mass ratio and the type of cement.

Drying shrinkage is also considered to be asymptotic. The final value of drying shrinkage depends on water-to-cement ratio, aggregate-to-cement mass ratio, the volume fraction of cement in mixture and the type of cement. The kinetics of drying shrinkage is influenced by the size of sample that influences the kinetics of drying.

Basic creep is considered as non-asymptotic and evolves as a logarithmic function of time. In fact, the model supposes that the derivative of basic creep compliance is a function of the inverse of time since loading. The basic creep depends on also water-to-cement ratio, aggregate-to-cement mass ratio and the type of cement.

Drying creep is considered to be asymptotic. The final value of drying creep depends on water-to-cement ratio, aggregate-to-cement mass ratio and the type of cement. The final value of drying creep is considered to be proportional to the final value of drying shrinkage.

The model parameters are fitted to database of Northwestern University that contains 1400 creep tests and 1050 shrinkage tests and also includes data on 69 bridges. To predict time-dependent strain of a concrete specimen at a given age t , the input parameters are as following: cement type, age at loading, age when drying begins, mean cylinder compressive strength, volume-surface ratio of specimen, cement content, water-cement mass ratio, aggregate-cement mass ratio, applied compressive stress, admixture content.

For practical reasons in engineering design, the B4 model is also proposed in a simplified form B4s which predicts shrinkage and creep based on only the mean strength that is required in the structure.

As to non-isothermal condition, temperature is considered to have acceleration or deceleration effects on creep and shrinkage rate. Thus, temperature effect is taken into account, using the concept of thermo-activation of the process, by horizontal shift of the curves of the reference temperature in logarithmic scale.

The B4 model predicts the long-term delayed strain of concrete rather well as it is based on large data base that includes significant number of

long-term tests.

1.6.2 Model of Sellier et al.

Rather different from the B4 model, [Sellier et al. \(2016\)](#) do not decompose the delayed strain. Instead, the model is based on poromechanics, where the effect of drying is integrated via the concept of effective stress. The effect of drying also reflects on the material properties.

The model is formulated for 3D case. In a Cartesian coordinate system whose three axes are same as the eigen-directions of stress tensor, the effective stress reads as:

$$\frac{\partial \sigma_i}{\partial t} = \frac{\partial \sigma'_i}{\partial t} + \frac{\partial (bS_l P_c)}{\partial t} \left(1 + \frac{|\sigma_i|}{\sigma_{dc}} \right) \quad (1.41)$$

where σ_i is the total normal stress in the direction i ; b is Biot coefficient; S_l is saturation degree; P_c is capillary pressure; σ_{dc} is a fitting parameter such that the equivalent capillary pressure effects are doubled when the material is subjected to a compression.

Then, elastic strain ε_i^E due to effective stress σ'_i in the direction i is computed. The delayed strain is computed from the elastic strain ε_i^E and material creep properties. In fact, using idealized rheological model (see Fig. 1.8), [Sellier et al. \(2016\)](#) decomposed the time-dependent strain $\varepsilon_i(t)$ into three parts:

$$\varepsilon_i(t) = \varepsilon_i^E + \varepsilon_i^M(t) + \varepsilon_i^K(t) \quad (1.42)$$

where ε_i^M and ε_i^K are the permanent creep and reversible creep, and correspond to Maxwell chain and Kelvin chain in Fig. 1.8, respectively. Both of the permanent creep ε_i^M and reversible creep ε_i^K depend on elastic strain ε_i^E :

$$\frac{\partial \varepsilon_i^M}{\partial t} = \frac{\varepsilon_i^E}{\tau_i^M} \quad (1.43a)$$

$$\frac{\partial \varepsilon_i^K}{\partial t} = \frac{1}{\tau^K} \left(\frac{\varepsilon_i^E}{\psi^K} - \varepsilon_i^K \right) \quad (1.43b)$$

where τ_i^M and τ_i^K are the characteristic times that are associated with permanent creep and reversible creep, respectively. ψ^K is a fitting parameter so that the amplitude of reversible creep equals to ε_i^K/ψ^K . The characteristic times τ_i^M and τ_i^K depend on temperature and water content (hence, relative humidity).

It is noteworthy that the decomposition of delayed strain used by [Sellier et al. \(2016\)](#) is not at all the same as the classical decomposition. In the former case, the decomposition is same for various hydric conditions and loading condition. The delayed strain of any hydric and loading case cannot be obtained by summing up the delayed strains of other cases.

The strain of a non-loaded specimen exchanging no water with outside, i.e., autogenous shrinkage, is not considered in this model.

The drying shrinkage, i.e., when the non-loaded specimen is exchanging water with outside, is the sum of elastic strain, permanent creep and reversible creep under the effective stress due to capillary pressure, which is computed from Eq. 1.41.

The basic creep, i.e., when specimen is loaded but not exchanging water with outside, is the sum of elastic strain, permanent creep and reversible creep under the stress due to applied load, as effective stress equals to applied load according to Eq. 1.41. Under isothermal condition, the basic creep under a constant load evolves as a logarithmic function of time at long term.

The strain of the specimen that is loaded and exchanging water with outside is computed by the same way as drying shrinkage and basic creep. The only difference lies in effective stress: in this case, the effective stress is greater than the sum of the effective stresses for the case of drying shrinkage and basic creep, due to the fitting parameter σ_{dc} in Eq. 1.41. Therefore, the delayed strain of the loaded specimen exchanging water is greater than the sum of the delayed strain of a loaded specimen with exchanging no water with outside and of a non-loaded specimen exchanging water with outside. In other words, the drying creep (i.e., Pickett effect) is captured.

The model is also coupled with damage model to take into account the part of structural effect in drying creep.

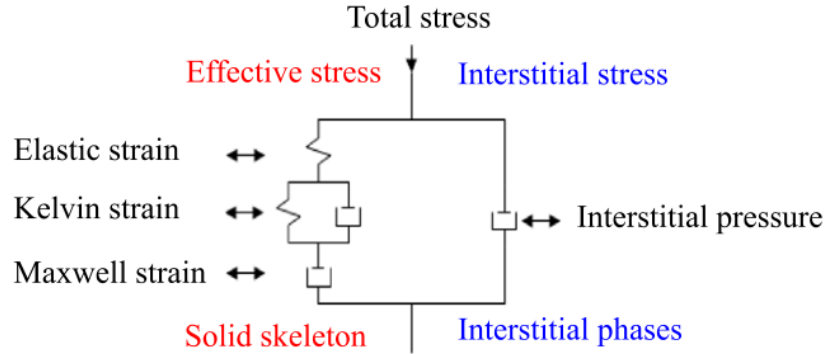


Figure 1.8 – Idealized rheological model used in poromechanical model of Sellier et al. (2016)

1.7 Conclusions and thesis outline

In this chapter, we presented first the microstructure and hydration model of cement-based materials. Then, briefly presented are the useful tools that are going to be used in the thesis: non-aging isotropic linear viscoelasticity, micromechanics and poromechanics.

In the thesis we aim at understanding long-term shrinkage and creep behavior of concrete under multiaxial load without postulating the classical decomposition of delayed strain. Concrete is regarded as poroviscoelastic multi-scale material, on which applied are the mechanical load and hydric load. The mechanical behavior of concrete is modeled within the framework of non-aging isotropic linear viscoelasticity. We use the micromechanics to interpret involving physical phenomena at microscale from the macroscopic observations. Poromechanics is also going to be used to take into account the effect of hydric load.

In order to characterize the delayed strain under biaxial load, our study first concentrates on the viscoelastic Poisson's ratio of concrete. The chapters 2 and 3 are dedicated to the definition of Poisson's ratio in non-aging linear isotropic viscoelasticity and experimental results in literature from which we can obtain the viscoelastic Poisson's ratio of concrete, respectively. As an extension, in chapter 4, we use micromechanics to shed some lights on the long-term creep mechanism of concrete at the scale of C-S-H.

1.7. CONCLUSIONS AND THESIS OUTLINE

In the second step, we aim at proposing a poroviscoelastic model without decomposing the delayed strain. In chapter 5, we analyze experimental data of basic creep and autogenous shrinkage from literature to find out possible physical origin of long-term autogenous shrinkage. Then, based on poromechanics and physical phenomena, a poroviscoelastic model is going to be proposed in chapter 6.

We end up by concluding the findings of the thesis work and giving some perspectives for the future.

Chapter 2

Poisson's ratio in linear viscoelasticity

THE POISSON'S RATIO is a well-defined parameter in elasticity. For time-dependent materials, multiple definitions based on the ratios between lateral and axial deformations are available. Here, we focus on the two most widely used definitions in the time domain, which define time-dependent functions that we call relaxation Poisson's ratio and creep Poisson's ratio. Those two ratios are theoretically different, but are linked in an exact manner through an equation that we derive. We show that those two functions are equal at both initial and large times, and that their derivatives with respect to time also are. Based on simple rheological models for both the deviatoric and volumetric creep behaviors, we perform a parametric study and show that the difference between those two time-dependent Poisson's ratios can be significant. However, based on creep data available in the literature, we show that, for cementitious materials, this difference can be negligible or not, depending on the case.¹

¹This chapter is published as Aili, A., Vandamme, M., Torrenti, J.-M., & Masson, B. (2015). Theoretical and practical differences between creep and relaxation Poisson's ratios in linear viscoelasticity. *Mechanics of Time-Dependent Materials*, 19(4), 537-555.

LE COEFFICIENT DE POISSON est un paramètre bien défini en élasticité. Pour les matériaux dépendant du temps, il est possible de définir un coefficient de Poisson en se basant sur les rapports entre les déformations latérales et axiales. Nous nous intéressons ici aux deux définitions les plus utilisées dans le domaine temporel, qui définissent des fonctions dépendant du temps que nous appelons le coefficient de Poisson de relaxation et le coefficient de Poisson de fluage. Ces deux coefficients de Poisson sont théoriquement différents, mais sont liés de manière exacte par une équation que nous dérivons. Nous montrons que ces deux fonctions sont égales au temps initial et à l'infini, et que leurs dérivées par rapport au temps le sont également. Supposant des modèles rhéologiques simples pour les comportements déviatorique et volumétrique, nous menons une étude paramétrique et montrons que la différence entre ces deux coefficients de Poisson dépendant du temps peut être significative. Cependant, en se basant sur des données de fluage de la littérature, nous montrons que, pour les matériaux cimentaires, selon le cas, cette différence peut être négligeable ou non.

For an isotropic body, the elastic Poisson's ratio ν_0 is defined unambiguously as the ratio of the lateral contraction $-\varepsilon_l$ to the elongation ε_a in the infinitesimal deformation under uniaxial load, that is:

$$\nu_0 = -\frac{\varepsilon_l}{\varepsilon_a}. \quad (2.1)$$

By extension, for linear viscoelastic materials, we can aim at defining a time-dependent Poisson's ratio (Varst and Kortsmiit, 1992; Hilton, 2001; Tschoegl et al., 2002; Lakes and Wineman, 2006; Hilton, 2011). However, such an aim can generate some ambiguity, since Hilton (2001) enumerated five different ways of defining a time-dependent Poisson's ratio. Here, by using a direct extension of Eq. 2.1 to a uniaxial creep experiment and to a uniaxial relaxation experiment, we define what we will call the creep Poisson's ratio ν_c and the relaxation Poisson's ratio ν_r :

$$\nu_c(t) = -\frac{\varepsilon_l(t)}{\varepsilon_a(t)} \text{ during a uniaxial creep experiment for which } \sigma_a(t) = \sigma_{a0} \quad (2.2a)$$

$$\nu_r(t) = -\frac{\varepsilon_l(t)}{\varepsilon_{a0}} \text{ during a uniaxial relaxation experiment for which } \varepsilon_a(t) = \varepsilon_{a0} \quad (2.2b)$$

where $\varepsilon_a(t)$ and $\varepsilon_l(t)$ are the time-dependent axial and lateral strains, respectively, $\sigma_a(t)$ is the axial load, and σ_{a0} and ε_{a0} are constants. Note that these definitions are specific to the case of creep and relaxation with an instantaneous loading: indeed, even in the case of uniaxial compression only, various load histories lead to various evolutions of the ratio of the lateral dilation to the axial contraction over time.

With respect to the terminology used by Hilton (2001), our creep Poisson's ratio ν_c corresponds to his type I definition restricted to a uniaxial creep experiment, whereas our relaxation Poisson's ratio corresponds to his type II definition. These two Poisson's ratios are not equal (Tschoegl et al., 2002; Lakes and Wineman, 2006). However, little is known on how significant the difference between them is. Quantifying such a difference is the main goal of

this work.

Better understanding how Poisson's ratios evolve with time is relevant for a variety of applications, among which we find the estimation of service life of the containment of French nuclear power plants. Indeed, the containment of French nuclear power plants is made of a biaxially prestressed concrete and designed to withstand an internal pressure of 0.5 MPa in case of an accident. In order to avoid tensile stresses in concrete, the applied prestress corresponds to compressive stresses in concrete of around 8.5 MPa and 12 MPa along vertical and orthoradial axes, respectively (Torrenti et al., 2014). To limit cracking of concrete, tensile stresses should remain below the tensile strength of concrete in case of accident. That is why the evolution of prestressing forces with respect to time is critical for the operation of nuclear power plants and for the optimization of their service life. Consequently, a good prediction of the evolution of delayed strains of the containment under a biaxial stress condition is needed.

In this chapter, starting from the basic equations of linear viscoelasticity, we derive a relationship between the two time-dependent Poisson's ratios just introduced. We specifically consider how their values and their derivatives can be compared at short and long times. Then, a parametric study of the difference between them over all times is performed, based on common rheological models. In the last section, we consider the practical case of cementitious materials (on which creep data in both axial and lateral directions are available from the literature): for this specific class of materials, the difference between the two time-dependent Poisson's ratios is scrutinized.

2.1 Theoretical derivations

This section is devoted to derive analytical relations pertaining to the creep Poisson's ratio ν_c and the relaxation Poisson's ratio ν_r . First, from the basic equations of viscoelasticity we derive expressions of the two Poisson's ratios. Then, we derive relation between them and compare their initial and long-time asymptotic values and derivatives with respect to time.

2.1.1 Viscoelastic constitutive relations

We restrict ourselves to an isotropic nonaging linear viscoelastic solid submitted to infinitesimal strains in isothermal conditions. For such a case, the time-dependent state equations that link the stress tensor $\underline{\underline{\sigma}}$ (decomposed into the volumetric stress $\sigma_v = \text{tr}(\underline{\underline{\sigma}})/3$ and the deviatoric stress tensor $\underline{\underline{s}}$ such that $\underline{\underline{\sigma}} = \sigma_v \underline{\underline{1}} + \underline{\underline{s}}$, where tr is the trace operator, and $\underline{\underline{1}}$ is the unit tensor) to the strain tensor $\underline{\underline{\varepsilon}}$ (decomposed into the volumetric strain $\varepsilon_v = \text{tr}(\underline{\underline{\varepsilon}})$ and the deviatoric strain tensor $\underline{\underline{e}}$ such that $\underline{\underline{\varepsilon}} = (\varepsilon_v/3)\underline{\underline{1}} + \underline{\underline{e}}$) are (Christensen, 1982):

$$\sigma_v(t) = K(t) \otimes \dot{\varepsilon}_v(t) \quad (2.3a)$$

$$s_{ij}(t) = 2G(t) \otimes \dot{e}_{ij}(t) \quad (2.3b)$$

where \otimes denotes for the convolution product defined as $f \otimes g = \int_{-\infty}^t f(t - \tau)g(\tau)d\tau$ and \dot{f} is for derivatives with respect to time, $\dot{f} = df(t)/dt$. Those state equations can equivalently be written as (Christensen, 1982):

$$\varepsilon_v(t) = J_K(t) \otimes \dot{\sigma}_v(t) \quad (2.4a)$$

$$e_{ij}(t) = \frac{1}{2}J_G(t) \otimes \dot{s}_{ij}(t) \quad (2.4b)$$

where $J_K(t)$ and $J_G(t)$ are called the bulk creep compliance and the shear creep compliance, respectively. Creep compliances are linked to relaxation moduli through (Christensen, 1982):

$$s\widehat{J}_K = \frac{1}{s\widehat{K}} \quad (2.5a)$$

$$s\widehat{J}_G = \frac{1}{s\widehat{G}} \quad (2.5b)$$

where s is the Laplace variable, $\widehat{f}(s)$ is the Laplace transform of a function $f(t)$.

Starting from the state equation 2.4, in uniaxial testing, we can show that the axial stress history $\sigma_a(t)$ and the axial strain history $\varepsilon_a(t)$ are related by (Christensen, 1982):

$$\sigma_a(t) = E(t) \otimes \dot{\varepsilon}_a(t) \quad (2.6a)$$

$$\varepsilon_a(t) = J_E(t) \otimes \dot{\sigma}_a(t) \quad (2.6b)$$

where $E(t)$ and $J_E(t)$ are called the uniaxial relaxation modulus and the uniaxial creep compliance, respectively. For a uniaxial relaxation or creep test, by solving Eqs. 2.3 and 2.4 in the Laplace domain, we obtain an analytic expression for the uniaxial relaxation modulus E and the uniaxial creep compliance J_E in the Laplace domain, respectively, the latter being transformed back directly:

$$\widehat{E}(s) = \frac{9\widehat{K}(s)\widehat{G}(s)}{3\widehat{K}(s) + \widehat{G}(s)} \quad (2.7a)$$

$$J_E(t) = \frac{1}{9}J_K(t) + \frac{1}{3}J_G(t) \quad (2.7b)$$

In the uniaxial relaxation test, for which $\varepsilon_a(t) = \varepsilon_{a0}$, by substituting this condition into Eq. 2.3 and solving it in Laplace domain, the relaxation Poisson's ratio is found:

$$\widehat{\nu}_r(s) = \frac{3\widehat{K}(s) - 2\widehat{G}(s)}{2s(3\widehat{K}(s) + \widehat{G}(s))} \quad (2.8)$$

For the uniaxial creep test, for which $\sigma_a(t) = \sigma_{a0}$, Eq. 2.4 is solved directly in the time domain, which yields an analytic expression of the creep Poisson's

ratio ν_c in time:

$$\nu_c(t) = \frac{3J_G(t) - 2J_K(t)}{2(3J_G(t) + J_K(t))} \quad (2.9)$$

In the creep test, the ratio between the Laplace transform $\widehat{\varepsilon}_l$ of the lateral strain to the Laplace transform $\widehat{\varepsilon}_a$ of the axial strain is evaluated and found to be equal to $-s\widehat{\nu}_r$. By transforming this equality back to the time domain we have:

$$\widehat{\varepsilon}_l = -s\widehat{\nu}_r\widehat{\varepsilon}_a \Rightarrow \varepsilon_l(t) = -\nu_r(t) \otimes \dot{\varepsilon}_a(t) \quad (2.10)$$

Comparing Eq. 2.10 with Eq. 2.2a, and combining them with Eq. 2.6b, we get the relation between the two Poisson's ratios:

$$\nu_c(t) = \frac{\nu_r(t) \otimes \dot{J}_E(t)}{J_E(t)} \quad (2.11)$$

Varst and Kortsmit (1992) also found this relation by writing the equilibrium of a cylindrical bar subjected to a uniaxial load. Salençon (1983) also demonstrated this relation, but in the Laplace domain. Note that this relationship is only valid to relate the creep and relaxation Poisson's ratios as defined by Eqs. 2.2a and 2.2b, respectively. In contrast, if the loading is not applied instantaneously, then how the ratio between lateral and axial strains evolves over time during the creep phase is related in a different manner to how this same ratio evolves over time during the relaxation phase.

2.1.2 Comparison of relaxation Poisson's ratio and creep Poisson's ratio

Equations 2.8 and 2.9 indicate that both the relaxation Poisson's ratio ν_r and the creep Poisson's ratio ν_c can be expressed as functions of the relaxation moduli, even though they are defined with reference to a specific loading path. In order to evaluate the difference between the relaxation Poisson's ratio ν_r and the creep Poisson's ratio ν_c , their initial and long-time asymptotic values are compared first.

At time $t = 0$, the relaxation modulus and creep compliance are equal to their elastic values, that is, $K(t = 0) = K_0$, $G(t = 0) = G_0$, $J_K(t = 0) = J_{K0} = K_0^{-1}$, $J_G(t = 0) = J_{G0} = G_0^{-1}$. By using the initial value theorem (Auliac et al., 2000), the value of the relaxation Poisson's ratio ν_r at time 0 is evaluated:

$$\nu_r(0) = \lim_{s \rightarrow +\infty} s\widehat{\nu}_r(s) = \lim_{s \rightarrow +\infty} \frac{3\widehat{K} - 2\widehat{G}s}{6\widehat{K} + 2\widehat{G}s} = \frac{3K_0 - 2G_0}{6K_0 + 2G_0} = \nu_0. \quad (2.12)$$

What concerns the creep Poisson's ratio ν_c , evaluating Eq. 2.9 at time $t = 0$ is straightforward:

$$\nu_c(0) = \frac{3J_{G0} - 2J_{K0}}{6J_{G0} + 2J_{K0}} = \frac{3K_0 - 2G_0}{6K_0 + 2G_0} = \nu_0 \quad (2.13)$$

Therefore, the value of both the relaxation Poisson's ratio ν_r and the creep Poisson's ratio ν_c at time 0 is equal to the elastic Poisson's ratio ν_0 .

At large times (i.e., $t \rightarrow +\infty$), the bulk and shear relaxation moduli tend toward K_∞ and G_∞ , respectively. Hence, an asymptotic Poisson's ratio ν_∞ can be defined:

$$\nu_\infty = \frac{3K_\infty - 2G_\infty}{6K_\infty + 2G_\infty}. \quad (2.14)$$

The asymptotic value of the relaxation Poisson's ratio is evaluated by using the final value theorem (Auliac et al., 2000):

$$\lim_{t \rightarrow +\infty} \nu_r(t) = \lim_{s \rightarrow 0} s\widehat{\nu}_r(s) = \lim_{s \rightarrow 0} \frac{3\widehat{K} - 2\widehat{G}s}{6\widehat{K} + 2\widehat{G}s} = \frac{3K_\infty - 2G_\infty}{6K_\infty + 2G_\infty} = \nu_\infty, \quad (2.15)$$

whereas since $\lim_{t \rightarrow +\infty} J_K(t) = 1/K_\infty$ and $\lim_{t \rightarrow +\infty} J_G(t) = 1/G_\infty$:

$$\lim_{t \rightarrow +\infty} \nu_c(t) = \frac{3/G_\infty - 2/K_\infty}{6/G_\infty + 2/K_\infty} = \frac{3K_\infty - 2G_\infty}{6K_\infty + 2G_\infty} = \nu_\infty. \quad (2.16)$$

Therefore, both relaxation Poisson's ratio ν_r and creep Poisson's ratio ν_c tend toward the same value ν_∞ at large times.

2.1. THEORETICAL DERIVATIONS

The relation between their derivatives with respect to time will be derived from Eq. 2.11. The uniaxial creep compliance $J_E(t)$ is a continuous function for times $t \geq 0$, but exhibits a discontinuity at $t = 0$: $J_E(t < 0) = 0$ whereas $J_E(t = 0) = J_{E0} > 0$. The existence of this discontinuity implies that the convolution integral on the right-hand side of Eq. 2.11 is a hereditary integral. By multiplying both sides of Eq. 2.11 by J_E and simplifying the hereditary integral, we get:

$$\nu_c(t) J_E(t) = \nu_r(t) J_E(0) + \int_{0+}^t \nu_r(t - \tau) \frac{dJ_E(\tau)}{d\tau} d\tau. \quad (2.17)$$

Differentiating this equation with respect to time yields:

$$\dot{\nu}_c(t) J_E(t) + \nu_c(t) \dot{J}_E(t) = \dot{\nu}_r(t) J_E(0) + \nu_r(0) \dot{J}_E(t) + \int_{0+}^t \frac{d\nu_r(t - \tau)}{dt} \frac{dJ_E(\tau)}{d\tau} d\tau, \quad (2.18)$$

which, after evaluation at $t = 0$, yields $\dot{\nu}_r(0) = \dot{\nu}_c(0)$.

The relaxation Poisson's ratio ν_r and creep Poisson's ratio ν_c are known to be bounded. In addition, in most cases, considering that, after a certain time, those two Poisson's ratios are monotonic functions of time is a reasonable assumption. Under such an assumption, we can therefore conclude that their derivatives with respect to time must tend to zero, i.e.: $\lim_{t \rightarrow \infty} \dot{\nu}_r(t) = \lim_{t \rightarrow \infty} \dot{\nu}_c(t) = 0$.

In conclusion, the initial values of the relaxation Poisson's ratio ν_r and of the creep Poisson's ratio ν_c are equal to each other. So are their long-time asymptotic value, their initial derivative with respect to time, and the long-time asymptotic values of their derivatives with respect to time. However, in spite of these similarities, over all times, those two Poisson's ratios differ from each other. Quantifying how different those quantities are is the main objective of the next section.

2.2 Difference between relaxation and creep Poisson's ratios for some rheological models

This section is devoted to assessing how different the relaxation Poisson's ratio ν_r and the creep Poisson's ratio ν_c are over all times. To do so, we perform a parametric study in which the shear and volumetric behaviors are modeled with the most common rheological units.

Here, we consider virtual materials for which the volumetric behavior and the deviatoric behavior are modeled with either the Maxwell unit (to model a creep behavior that diverges with time) or the Kelvin–Voigt unit (to model a creep behavior with an asymptotic value). All four combinations of those units are considered (see Fig. 2.1). For simplicity, when the Kelvin–Voigt unit is considered, then the stiffness of the two springs it contains are set equal to each other.

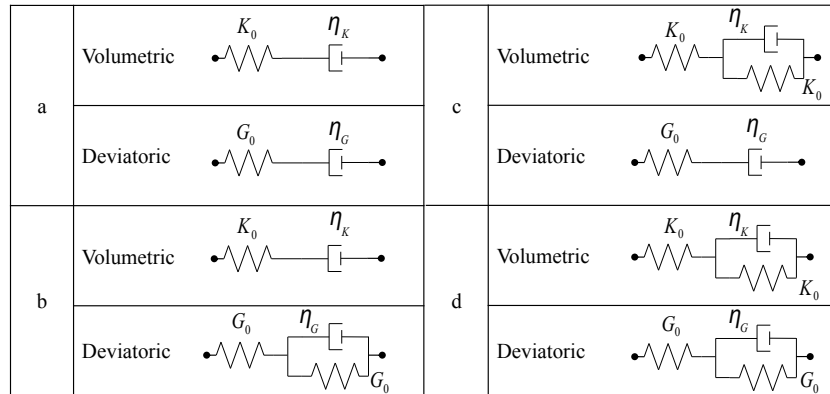


Figure 2.1 – Rheological models used in the parametric study: (a) Both volumetric and deviatoric behaviors governed by the Maxwell unit; (b) Volumetric behavior and deviatoric behavior governed by the Maxwell unit and the Kelvin–Voigt unit, respectively; (c) Volumetric behavior and deviatoric behavior governed by the Kelvin–Voigt unit and the Maxwell unit, respectively; (d) Both volumetric and deviatoric behaviors governed by the Kelvin–Voigt unit.

If the bulk behavior is modeled with the Maxwell unit, then the bulk relaxation modulus $\widehat{K}(s)$ in the Laplace domain and the bulk creep compliance

2.2. DIFFERENCE BETWEEN RELAXATION AND CREEP POISSON'S RATIOS FOR SOME RHEOLOGICAL MODELS

$J_K(t)$ in the time domain read:

$$\widehat{K}(s) = \left(\frac{s}{K_0} + \frac{1}{\eta_K} \right)^{-1} \quad (2.19a)$$

$$J_K(t) = \frac{t}{\eta_K} + \frac{1}{K_0}. \quad (2.19b)$$

In contrast, if the bulk behavior is modeled with a Kelvin–Voigt unit, the bulk relaxation modulus $\widehat{K}(s)$ in the Laplace domain and the bulk creep compliance $J_K(t)$ in the time domain read:

$$\widehat{K}(s) = \left(\frac{s}{K_0} + \frac{s}{K_0 + s\eta_K} \right)^{-1} \quad (2.20a)$$

$$J_K(t) = \frac{1}{K_0} \left(2 - \exp\left(-\frac{K_0}{\eta_K}t\right) \right). \quad (2.20b)$$

Equivalent equations can be derived for the shear behavior.

For every combination of rheological units considered (see Fig. 2.1), by applying the inverse Laplace transform to Eq. 2.8, in which the corresponding time-dependent moduli have been injected, we obtain the relaxation Poisson's ratio ν_r over all times. The creep Poisson's ratio ν_c is obtained by injecting the corresponding creep compliances into Eq. 2.9. Details of all calculations are provided in appendix A.

The relaxation Poisson's ratio ν_r and the creep Poisson's ratio ν_c depend on the stiffnesses K_0 and G_0 of the springs, and on the viscosities η_K and η_G of the dashpots. In fact, dimensional analysis shows that those two Poisson's ratios ν_r and ν_c can be expressed with the following dimensionless parameters:

$$\nu_c(t, K_0, G_0, \eta_K, \eta_G) = \nu_c(\tilde{t}, \nu_0, \eta_K/\eta_G) \quad (2.21)$$

$$\nu_r(t, K_0, G_0, \eta_K, \eta_G) = \nu_r(\tilde{t}, \nu_0, \eta_K/\eta_G) \quad (2.22)$$

where $\tilde{t} = tG_0/\eta_G$ is a dimensionless time. This dimensional analysis defines the rationale for the parametric study: For the four combinations of rheological units considered, the difference between the two Poisson's ratios is studied for various values of the elastic initial Poisson's ratio $\nu_0 \in [-1, 0.5]$ and for a wide range of values of the ratio η_K/η_G (i.e., $\eta_K/\eta_G \in [0.01, 100]$).

Figure 2.2 displays the two Poisson's ratios ν_r and ν_c for the specific case of a material whose both the volumetric and deviatoric behaviors are governed by the Maxwell unit and for which $\nu_0 = 0.1$ and $\eta_K/\eta_G = 10$. We observe that, in this case, the relaxation Poisson's ratio ν_r increases more rapidly and reaches its asymptotic value earlier than the creep Poisson's ratio ν_c .

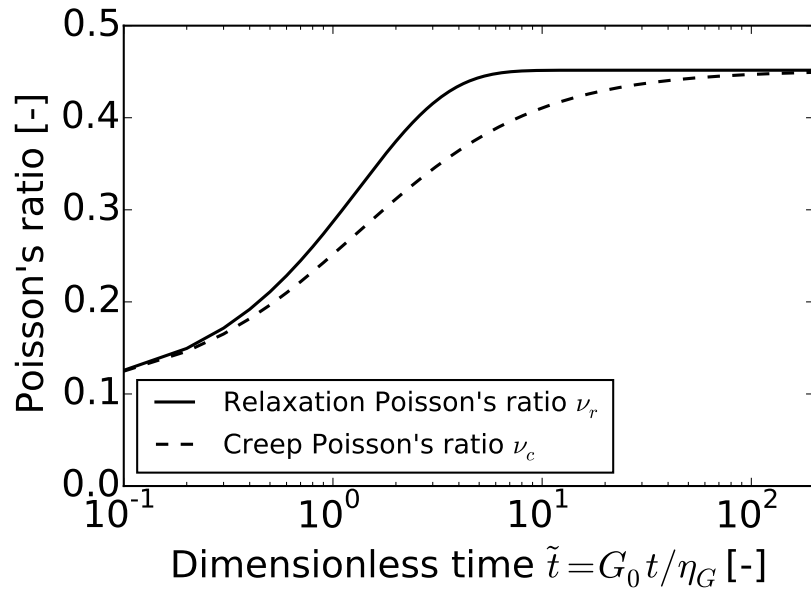


Figure 2.2 – Relaxation Poisson's ratio $\nu_r(t)$ and creep Poisson's ratio $\nu_c(t)$ for a material whose volumetric and deviatoric behaviors are governed by the Maxwell unit and for which $\nu_0 = 0.1$ and $\eta_K/\eta_G = 10$.

In the following parametric study, the difference in the evolutions of the two Poisson's ratios over time is characterized by two parameters: a characteristic difference $\Delta\nu$ and a retard factor $f_{\Delta t}$ that captures the retard of the

2.2. DIFFERENCE BETWEEN RELAXATION AND CREEP POISSON'S RATIOS FOR SOME RHEOLOGICAL MODELS

creep Poisson's ratio ν_c with respect to the relaxation Poisson's ratio ν_r :

$$\Delta\nu = \nu_r(t_m) - \nu_c(t_m) \quad (2.23a)$$

$$f_{\Delta t} = \frac{t_c}{t_r} \quad (2.23b)$$

where t_m is such that $|\nu_r(t_m) - \nu_c(t_m)| = \max_t |\nu_r(t) - \nu_c(t)|$, and t_r and t_c are such that $\nu_r(t_r) = \nu_c(t_c) = (\nu_0 + \nu_\infty)/2$.

Figure 2.3 displays the characteristic difference $\Delta\nu$. For a material whose both volumetric and deviatoric behaviors are governed by the Maxwell unit (see Figs. 2.3a and 2.1a), the characteristic difference $\Delta\nu$ is an increasing function of the ratio η_K/η_G and a decreasing function of the initial Poisson's ratio ν_0 . For this material, the characteristic difference $\Delta\nu$ is comprised between -0.3 and 0.3. For a material whose volumetric and deviatoric behaviors are governed by the Maxwell unit and the Kelvin–Voigt unit, respectively (see Figs. 2.3b and 2.1b), the characteristic difference $\Delta\nu$ is a decreasing function of the initial Poisson's ratio ν_0 . The minimum characteristic difference is equal to -0.3 and is observed for the material for which $\nu_0 = 0.5$. For a material whose volumetric and deviatoric behaviors are governed by the Kelvin–Voigt unit and the Maxwell unit, respectively (see Fig. 2.1c and Fig. 2.3c), the characteristic difference $\Delta\nu$ is an increasing function of the initial Poisson's ratio ν_0 . The maximum characteristic difference is equal to 0.3 and is observed for the material for which $\nu_0 \rightarrow -1$. For a material whose both volumetric and deviatoric behaviors are governed by the Kelvin–Voigt unit (see Figs. 2.1d and 2.3d), the characteristic difference $\Delta\nu$ is almost 0. The observation of such a small characteristic difference is likely due to the fact that we chose identical stiffnesses for the two springs of the Kelvin–Voigt unit, for both the volumetric and deviatoric behaviors.

Figure 2.4 displays the retard factor $f_{\Delta t}$. For a material whose both volumetric and deviatoric behaviors are governed by the Maxwell unit (see Figs. 2.1a and 2.4a), the retard factor $f_{\Delta t}$ is constant and equal to 1.44 for the various values of the initial Poisson's ratio ν_0 and the ratio η_K/η_G . For a ma-

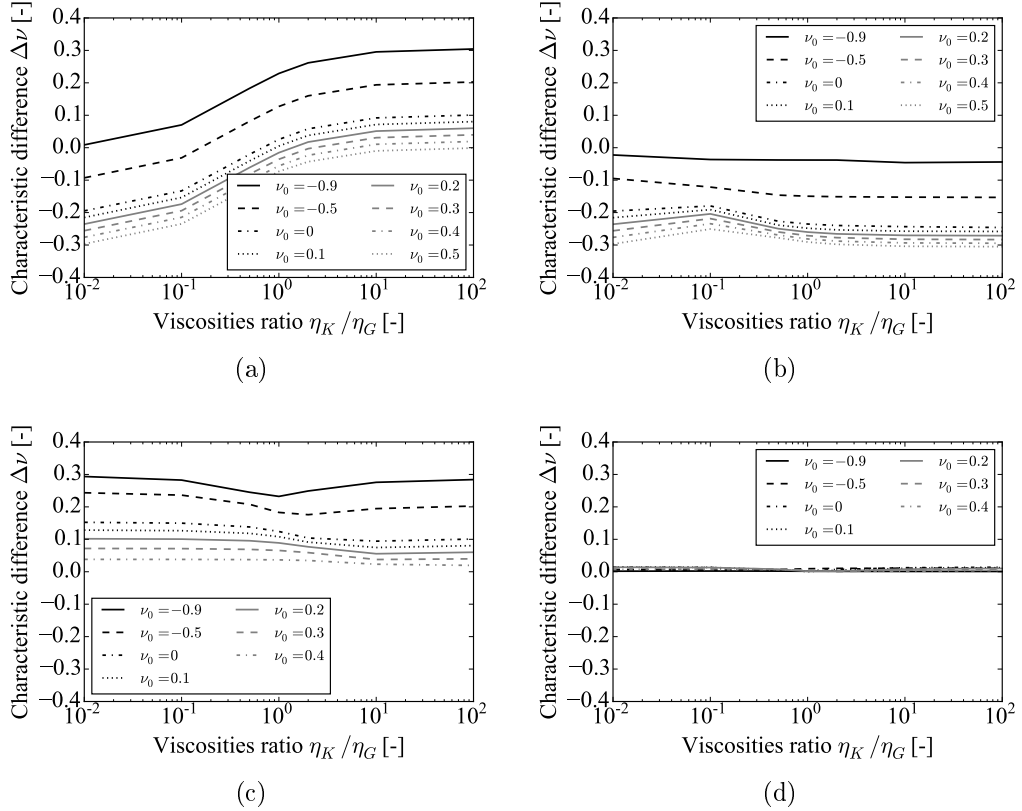


Figure 2.3 – Characteristic difference $\Delta\nu$ between relaxation Poisson's ratio $\nu_r(t)$ and creep Poisson's ratio $\nu_c(t)$: (a) Both volumetric and deviatoric behaviors governed by the Maxwell unit (see Fig. 2.1a); (b) Volumetric behavior and deviatoric behavior governed by the Maxwell unit and the Kelvin-Voigt unit, respectively (see Fig. 2.1b); (c) Volumetric behavior and deviatoric behavior governed by the Kelvin-Voigt unit and the Maxwell unit, respectively (see Fig. 2.1c); (d) Both volumetric and deviatoric behaviors governed by the Kelvin-Voigt unit (see Fig. 2.1d).

material whose volumetric and deviatoric behaviors are governed by the Maxwell unit and the Kelvin-Voigt unit, respectively (see Figs. 2.1b and 2.4b), and for a material whose volumetric and deviatoric behaviors are governed by the Kelvin-Voigt unit and the Maxwell unit, respectively (see Figs. 2.1c and 2.4c), the retard factor $f_{\Delta t}$ is a monotonic function of neither the initial Poisson's ratio ν_0 , nor the ratio η_K/η_G . For each of those two types of materials, the retard factor $f_{\Delta t}$ is comprised between 1.44 and 2.08. For the material whose

2.2. DIFFERENCE BETWEEN RELAXATION AND CREEP POISSON'S RATIOS FOR SOME RHEOLOGICAL MODELS

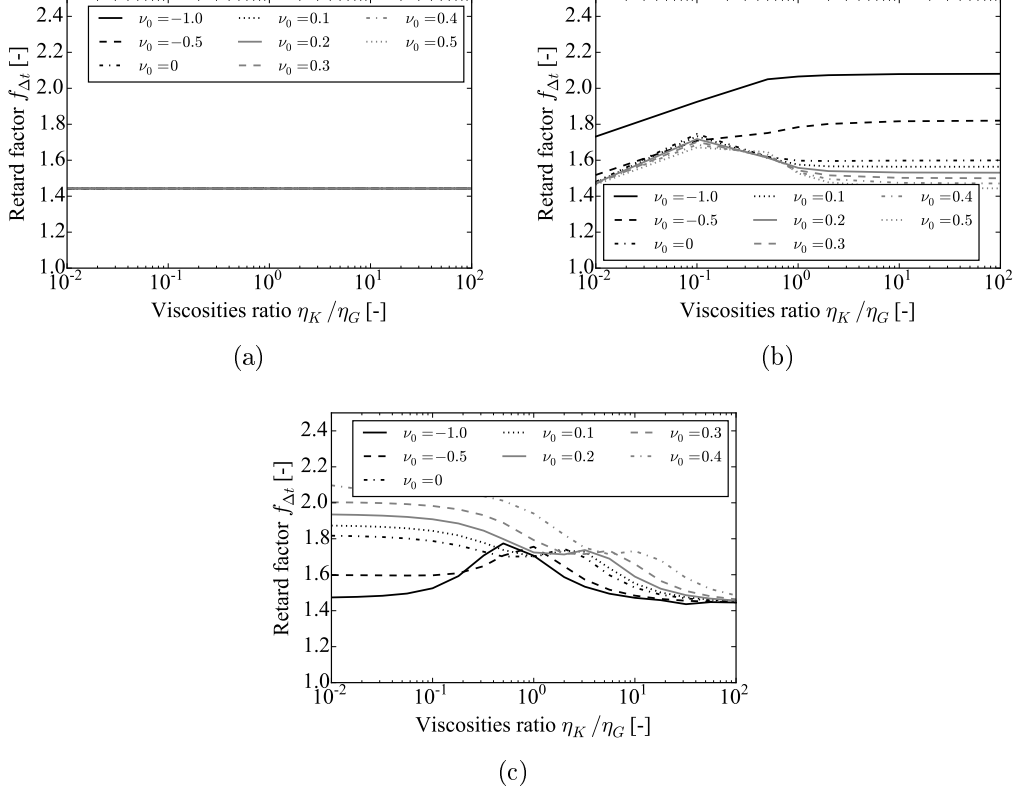


Figure 2.4 – Retard factor $f_{\Delta t}$ of the creep Poisson's ratio $\nu_c(t)$ with respect to the relaxation Poisson's $\nu_r(t)$: (a) Both volumetric and deviatoric behaviors governed by the Maxwell unit (see Fig. 2.1a); (b) Volumetric behavior and deviatoric behavior governed by the Maxwell unit and the Kelvin–Voigt unit, respectively (see Fig. 2.1b); (c) Volumetric behavior and deviatoric behavior governed by the Kelvin–Voigt unit and the Maxwell unit, respectively (see Fig. 2.1c).

both volumetric and deviatoric behaviors are governed by the Kelvin-Voigt unit (see Fig. 2.1d and 2.3d), since the characteristic difference $\Delta\nu$ between the two Poisson's ratios is almost 0, the retard factor is not studied.

To sum up this parametric study, for some materials, the creep Poisson's ratio $\nu_c(t)$ can differ significantly from the relaxation Poisson's ratio $\nu_r(t)$ (see, e.g., the case of a material whose both volumetric and deviatoric behaviors are governed by the Maxwell unit in Fig. 2.3a). In contrast, for other materials, the difference can be negligible (see, e.g., the case of a material

whose both volumetric and deviatoric behaviors are governed by the Kelvin-Voigt unit in Fig. 2.3d). For all cases considered, the characteristic difference $\Delta\nu$ between the two Poisson's ratios lies in the range $[-0.3, 0.3]$. In terms of kinetics, the creep Poisson's ratio $\nu_c(t)$ always evolves slower than the relaxation Poisson's ratio $\nu_r(t)$: for all cases for which the difference between the two Poisson's ratios is not negligible, the retard factor $f_{\Delta t}$ that we introduced is always comprised in the range $[1.44, 2.08]$.

2.3 Discussions

This section discusses the difference between the two Poisson's ratios ν_r and ν_c , first in practice in the case of multiaxial creep tests on cementitious materials, and then with respect to the elastic-viscoelastic correspondence principle (Christensen, 1982). A brief conclusion on the different usage of the two Poisson's ratios is drawn at the end of this latter section, in which the influence of the duration of the loading phase on the creep strains is also discussed.

2.3.1 Poisson's ratio from multiaxial creep tests on cementitious materials

In order to compare the two Poisson's ratios ν_r and ν_c in practice, we consider cementitious materials (i.e., cement paste, mortar and concrete), for which multiaxial creep tests are available in the literature (Gopalakrishnan et al., 1969; Jordaan and Illston, 1969; Parrott, 1974; Kennedy, 1975; Neville et al., 1983; Bernard et al., 2003a; Kim et al., 2005). The tests here considered characterize the so-called "basic" creep of the cementitious materials (Neville, 1995), which is measured in absence of any hydric transfer and to which any time-dependent deformation observed on a nonloaded specimen (i.e., autogenous shrinkage) is subtracted.

We consider that the coordinate frame is oriented in the principal directions, which are numbered from 1 to 3. The principal stresses and strains in those principal directions are denoted $\sigma_i(t)$ and $\varepsilon_i(t)$, respectively, with

$i = 1, 2, 3$. For a multiaxial creep test, the stresses are kept constant over time, that is, $\sigma_i(t) = \sigma_{i0}$. For such a test, the linearity of the material makes it possible to extend Eqs. 2.2a and 2.10 to find out the viscoelastic stress-strain relations valid in the case of multiaxial solicitation, expressed in terms of either the relaxation Poisson's ratio $\nu_r(t)$ or the creep Poisson's ratio $\nu_c(t)$:

$$\varepsilon_i(t) = J_E(t)\sigma_{i0} - (\sigma_{j0} + \sigma_{k0})\nu_r(t) \otimes \dot{J}_E(t), \text{ where } i \neq j \neq k \in \{1, 2, 3\} \quad (2.24a)$$

$$\varepsilon_i(t) = J_E(t)\sigma_{i0} - (\sigma_{j0} + \sigma_{k0})\nu_c(t)J_E(t), \text{ where } i \neq j \neq k \in \{1, 2, 3\}. \quad (2.24b)$$

Here, we consider experimental results available in the literature (see Fig. 2.5), and by using Eqs. 2.24a and 2.24b, we compute the experimental values of the Poisson's ratios ν_r and ν_c . The details of the computation are given in appendix B. Note that the Poisson's ratios displayed on Figs. 2.5a-c exhibit very different trends over time: some increase, one decreases, and one remains constant. For such a variety of cases, we compare the relaxation and creep Poisson's ratios with each other.

Figure 2.5a displays results of a biaxial creep test on a cubic concrete sample of [Jordaan and Illston \(1969\)](#). The two Poisson's ratios reach their asymptotic value in less than 10 days, during which they vary by about 0.004. The difference between them is smaller than 0.0002, which is negligible: they can be considered as equal to each other. Note that such a trend of almost constant Poisson's ratios is observed with other experimental data on concrete available in the literature (i.e., namely the data in [Kennedy \(1975\)](#); [Stockl et al. \(1989\)](#); [Kim et al. \(2005\)](#)): with such data, relaxation and creep Poisson's ratio can again be considered as equal to each other. The results from a uniaxial creep test on a cuboid sample of cement paste of [Parrott \(1974\)](#) are displayed in Fig. 2.5b. Both Poisson's ratios decrease by about 0.05 in about a dozen of days. The difference between the two Poisson's ratios is always smaller than 0.004, which, depending on the applications, can be considered as negligible or not. The last case displayed in Fig. 2.5c is that

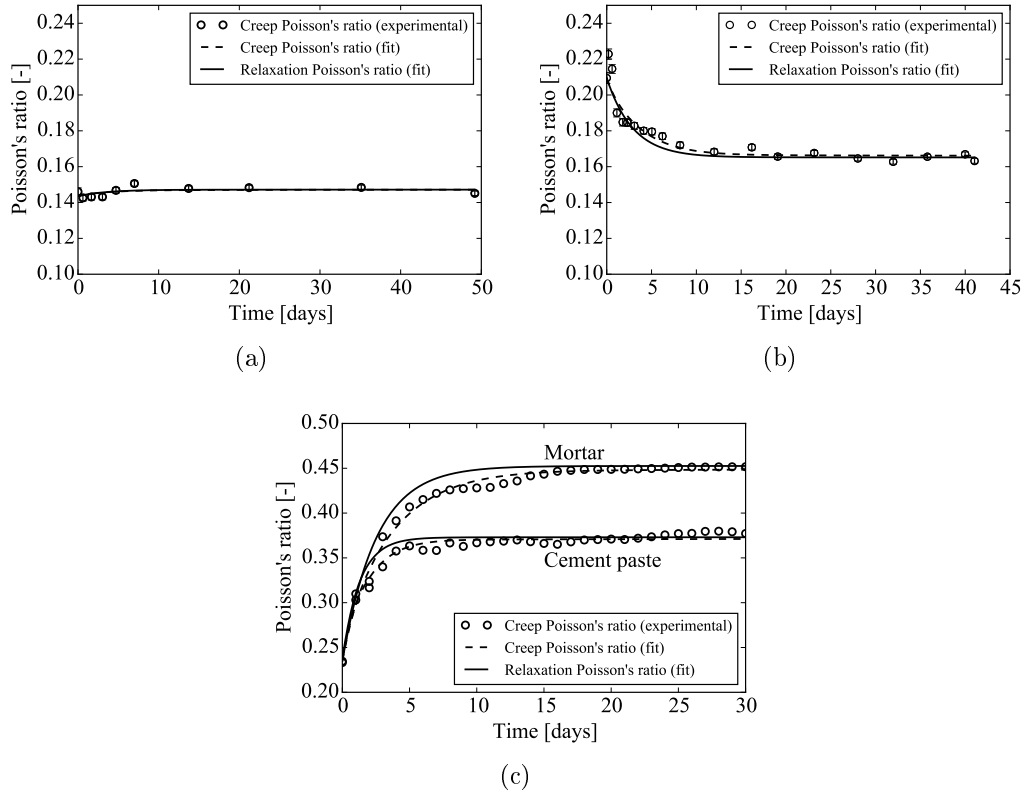


Figure 2.5 – Experimental data of multiaxial creep experiments on cementitious materials: (a) biaxial creep test on cubic concrete sample of [Jordaan and Illston \(1969\)](#), (b) uniaxial creep test on a cuboid sample of cement paste of [Parrott \(1974\)](#), (c) triaxial creep tests on cylindrical specimens of leached cement paste and mortar of [Bernard et al. \(2003a\)](#).

of triaxial creep tests on cylindrical specimens of leached cement paste and mortar of [Bernard et al. \(2003a\)](#). In this last case, the Poisson's ratios are increasing functions of time and vary by about 0.157 for the cement paste specimen and by about 0.218 for the mortar specimen². Here, the difference between the two Poisson's ratios can be as large as 0.017 for the cement paste specimen and 0.025 for the mortar specimen: for those specimens the differ-

²[Bernard et al. \(2003a\)](#) reported only creep strains. We estimated the elastic strains that are necessary for the computation of the creep Poisson's ratio by considering the Young's modulus equal to 0.7 GPa and the elastic Poisson's ratio equal to 0.24 for the leached cement paste, the Young's modulus equal to 0.5 GPa and the elastic Poisson's ratio equal to 0.24 for mortar ([Heukamp, 2003](#); [Le Bellego, 2001](#)).

ence between the relaxation Poisson's ratio and the creep Poisson's ratio is no more negligible. From this back-analysis of creep tests on cementitious materials, we conclude that if the Poisson's ratios vary little over time, then the difference between the relaxation Poisson's ratio and the creep Poisson's ratio is negligible. In contrast, when the Poisson's ratios vary significantly over time, the difference between the two Poisson's ratios can be no more negligible: whether this difference must be taken into account in practice needs to be assessed case by case, that is, for each application considered.

The significance of the difference between the two Poisson's ratios must also be assessed by keeping in mind the accuracy of the measurement of creep strains, which results from the accuracy of strain gauges and of temperature control. For instance, the accuracy of the strain gauges that were used in the biaxial creep test reported on concrete sample (see Fig. 2.5a) is 1×10^{-6} (Jordaan and Illston, 1969): this accuracy leads to an uncertainty on the creep Poisson's ratio of about 0.002, which is ten times larger than the difference between the two Poisson's ratios in that experiment. The temperature was controlled with an accuracy of $\pm 1^\circ$ C in that experiment. Considering a thermal dilatation coefficient of $14.5 \times 10^{-6} \text{ K}^{-1}$ for concrete, uncorrected variations of temperatures would lead to an uncertainty on the measured strain that would be 15 times larger than the accuracy of the strain gauges. However, in that experiment, variations of temperature were corrected so that the uncertainty induced by variations of temperatures would be much smaller than 15 times the accuracy of the strain gauges, although probably nonnegligible. Also, what concerns the uniaxial creep test reported on cement paste (see Fig. 2.5b), for which the accuracy of the strain gauges they used was 3×10^{-6} (Parrott, 1974), we found an uncertainty on the creep Poisson's ratio of about 0.003, which is of the same order of magnitude as the maximum difference between the two Poisson's ratios in that experiment. In contrast, for what concerns the experiments performed on leached specimens (see Fig. 2.5c), since the strains are about two orders of magnitude greater than the strains in the experiments displayed in Figs. 2.5a and 2.5b, the uncertainty on the Poisson's ratio becomes truly negligible: with respect to this uncertainty, the difference between the creep and relaxation Poisson's

ratios in that experiment is significant.

2.3.2 The elastic–viscoelastic correspondence principle

For an isotropic elastic material with bulk modulus K_0 and shear modulus G_0 , the stress–strain relations read:

$$\sigma_v = K_0 \varepsilon_v \tag{2.25a}$$

$$s_{ij} = 2G_0 e_{ij} \tag{2.25b}$$

We observe that these elastic relations are analogous to the viscoelastic stress–strain relations 2.3 and 2.4. In fact, we could have inferred these latter viscoelastic stress–strain relations in the Laplace domain directly from the elastic stress–strain relations 2.25, simply by replacing all elastic coefficients by the s -multiplied Laplace transform (also called the Carson transform) of their corresponding viscoelastic relaxation functions (Tschoegl et al., 2002).

In terms of Poisson's ratio, for an isotropic elastic material, we have the following relation:

$$\nu_0 = \frac{3K_0 - 2G_0}{2(3K_0 + G_0)}. \tag{2.26}$$

We observe that applying the correspondence principle to this equation makes it possible to retrieve Eq. 2.8 if one replaces the elastic Poisson's ratio ν_0 with the s -multiplied Laplace transform of the relaxation Poisson's ratio $\nu_r(t)$. Therefore, we infer that the corresponding viscoelastic operator of the elastic Poisson's ratio is the relaxation Poisson's ratio $\nu_r(t)$ and not the creep Poisson's ratio $\nu_c(t)$; in other words, the correspondence principle can be applied to elastic relations that involve the Poisson's ratio if this latter is replaced with the s -multiplied Laplace transform $s\hat{\nu}_r(s)$ of the relaxation Poisson's ratio $\nu_r(t)$ in the corresponding viscoelastic equation.

The validity of correspondence principle is due to the fact that the viscoelastic relations are “of the convolution type whose integral transforms lead

to algebraic relations similar to the elastic ones” (Hilton, 2001). Considering the specific example of a uniaxial creep test, we observe that the lateral strain $\varepsilon_l(t)$ and the axial strain $\varepsilon_a(t)$ can be related through the use of either the relaxation Poisson’s ratio $\nu_r(t)$ or the creep Poisson’s ratio $\nu_c(t)$, through Eqs. 2.10 or 2.2a, respectively. Of those two equations, the former involves a convolution, whereas the latter does not, which shows that the correspondence principle is not applicable to the creep Poisson’s ratio ν_c , as already noted by Hilton (2001); Tschoegl et al. (2002); Hilton (2009, 2011). Note that Lakes and Wineman (2006) found a relationship between the two Poisson’s ratios ν_r and ν_c that differs from that given in Eq. 2.11. We believe that their equation is not valid and that the error in their derivation stems from the fact that they applied the correspondence principle not only to the relaxation Poisson’s ratio ν_r (which is valid), but also to the creep Poisson’s ratio ν_c (which is not valid) (Tschoegl et al., 2002). This example shows that we can easily get confused in how to manipulate the various Poisson’s ratios that can be defined: in consequence, in the generic case, to perform a viscoelastic characterization, avoiding as much as possible the use of viscoelastic Poisson’s ratios and restricting oneself to the use of creep compliances and relaxation moduli seems to be a wise choice.

Since the relaxation Poisson’s ratio ν_r is the only Poisson’s ratio to which the correspondence principle can be applied, solving viscoelastic problems analytically can be performed much more easily by using the relaxation Poisson’s ratio rather than the creep Poisson’s ratio. In contrast, since the relationship between the creep Poisson’s ratio ν_c and the time-dependent strains does not involve any convolution (see Eq. 2.24b in comparison with Eq. 2.24a), back-calculating the creep Poisson’s ratio from experimental data is more straightforward than back-calculating the relaxation Poisson’s ratio. This is the reason why, when experimentalists report a Poisson’s ratio, they almost exclusively report the creep Poisson’s ratio (see, e.g., Benboudjema (2002); Torrenti et al. (2014); Hilaire (2014)).

For a uniaxial experiment performed on an elastic material, the lateral strain ε_l is linked to the axial strain σ_a through $\varepsilon_l = -(\nu/E)\sigma_a$. Based on this elastic relation, the fact that the correspondence principle is applicable to

the relaxation Poisson's ratio makes it possible to derive how, for a uniaxial experiment with a generic load history $\sigma_a(t)$ performed on a viscoelastic solid, the lateral strain $\varepsilon_l(t)$ must evolve over time. Thus, we find that, in the Laplace domain, the following relation holds:

$$\widehat{\varepsilon}_l = -s\widehat{\nu}_r \left(s\widehat{J}_E\widehat{\sigma}_a \right). \quad (2.27)$$

This relation can be translated back into the time domain:

$$\varepsilon_l(t) = -\nu_r(t) \otimes \left(\frac{d}{dt}(J_E(t) \otimes \dot{\sigma}_a(t)) \right). \quad (2.28)$$

Thus, for a uniaxial experiment with a generic load history, we can use the relaxation Poisson's ratio to calculate the evolution of the lateral strain over time. Note that we did not succeed in deriving such an equation based on the creep Poisson's ratio, which is a direct consequence of the fact that the correspondence principle cannot be applied to the creep Poisson's ratio.

For triaxial loadings with a generic load history, starting from Eqs. 2.6b and 2.28, using the principle of superposition makes it possible to derive the following equation:

$$\varepsilon_i(t) = J_E(t)\otimes\dot{\sigma}_i(t) - \nu_r(t)\otimes\left(\frac{d}{dt}(J_E(t)\otimes(\dot{\sigma}_j(t) + \dot{\sigma}_k(t)))\right) \text{ where } i \neq j \neq k \in \{1, 2, 3\} \quad (2.29)$$

which is a direct extension of Eq. 2.24a. Thus, if we know the uniaxial creep compliance and the relaxation Poisson's ratio of the material, this equation makes it possible to predict the evolution of the principal strains over time from the history of the triaxial stresses. Note that, again, we did not succeed in deriving such equation based on the creep Poisson's ratio.

2.3.3 Influence of duration of loading phase on apparent creep Poisson's ratio

In order to identify the creep Poisson's ratio, we may want to perform a creep experiment and calculate the ratio $-\varepsilon_l(t)/\varepsilon_a(t)$ of the lateral dilation to the

axial contraction measured during the creep phase. By doing so, we identify a time-dependent function to which we will refer as to an “apparent” creep Poisson’s ratio since, in practice, for any creep experiment, the duration of the loading phase is finite, whereas the creep Poisson’s ratio was defined with respect to a creep experiment with an instantaneous loading (see Eq. 2.2a). Therefore, we can wonder by how much an apparent creep Poisson’s ratio identified on an actual creep experiment differs from *the* creep Poisson’s ratio of the material. The study of such a difference is the focus of this section.

To study this difference, we consider two virtual materials whose rheological behaviors are those described in Figs. 2.1a and 2.1b in the specific case where $\eta_K \rightarrow +\infty$. Therefore, the volumetric behavior of the two virtual materials is elastic since they only creep deviatorically. The deviatoric behavior of the first virtual material is governed by the Maxwell unit (see Fig. 2.1a), whereas the deviatoric behavior of the second virtual material is governed by the Kelvin–Voigt unit (see Fig. 2.1b). Their characteristic viscous time is $\tau_G = \eta_G/G_0$. The elastic stiffnesses are chosen such that the elastic Poisson’s ratio is $\nu_0 = 0.2$.

On each of those two materials, we consider creep experiments in which the load is increased linearly over time in a duration τ_L , after which the load is kept constant. For various durations τ_L of the loading phase, Fig. 2.6 displays what the ratio of the lateral dilation to the axial contraction is, together with the creep Poisson’s ratio of the material. We observe that the apparent creep Poisson’s ratio differs from *the* creep Poisson’s ratio: the slower the loading, the greater this difference. Also, this difference is maximum at the end of the loading phase (i.e., at the dimensionless time $t/\tau_L = 1$), but we note that this difference is significant only for times that are smaller than about 10 times the duration of the loading phase: at times greater than 10 times the duration of the loading phase, the difference between the creep Poisson’s ratio and the apparent creep Poisson’s ratio is negligible.

In conclusion, if we aim at identifying the creep Poisson’s ratio as the ratio $-\varepsilon_l(t)/\varepsilon_a(t)$ of a lateral dilation to an axial contraction measured during the creep phase of an actual creep experiment, one will commit some error. However, the difference between *the* creep Poisson’s ratio and the apparent

we may only be significant for times smaller than about 10 times the duration of the loading phase; for larger times, this difference will be negligible.

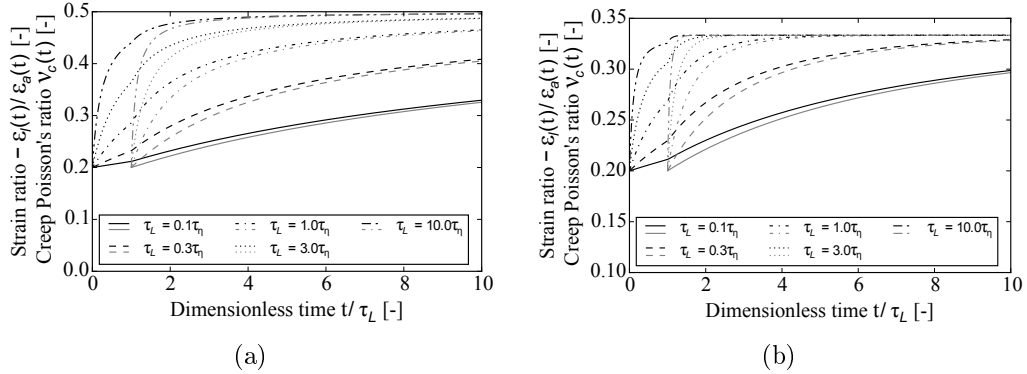


Figure 2.6 – Ratio $-\varepsilon_l(t)/\varepsilon_a(t)$ of the lateral to the axial strain (black lines) observed during creep experiments with various durations τ_L of the loading phase, and creep Poisson's ratio ν_c (gray lines) for a material that creeps deviatorically and whose deviatoric creep behavior is modeled by (a) the Maxwell unit, or (b) the Kelvin-Voigt unit.

2.4 Conclusions

Two time-dependent Poisson's ratios are defined for linear viscoelastic materials: the relaxation Poisson's ratio $\nu_r(t)$ and the creep Poisson's ratio $\nu_c(t)$. Those two Poisson's ratios were defined with respect to creep or relaxation experiments with an instantaneous loading. The following conclusions are drawn on their differences, in both theory and practice:

- Those two Poisson's ratios are not equal to each other. They can be expressed as functions of the creep compliances and relaxation moduli and are linked to each other through the exact expression 2.11.
- At the initial time of loading, both Poisson's ratios are equal to the elastic Poisson's ratio. Their long-time asymptotic values are identical. Their initial derivatives with respect to time are also identical, and so are their long-time asymptotic derivatives.

- The parametric study of virtual materials based on simple rheological models indicates that the two Poisson's ratios can differ significantly from each other. The maximum characteristic difference $\Delta\nu$ between them at a given time can be as large as 0.3. The creep Poisson's ratio evolves slower than the relaxation Poisson's ratio by a retard factor $f_{\Delta t}$, which is in the range $[1.44, 2.08]$.
- A study of multiaxial creep data on cementitious materials showed that, if the Poisson's ratios vary little over time, their difference is negligible. When the Poisson's ratios vary significantly over time, whether their difference must be taken into account in practice should be assessed with respect to the application considered. The significance of the difference must also be assessed by keeping in mind the accuracy of the measurement of creep strains.
- The use of each of the two Poisson's ratios is of interest: solving viscoelastic problems analytically can be performed much more easily by using the relaxation Poisson's ratio rather than the creep Poisson's ratio, since the elastic-viscoelastic correspondence principle is applicable to this parameter; in contrast, back-calculating the creep Poisson's ratio from experimental data is more straightforward than back-calculating the relaxation Poisson's ratio.
- For materials subjected to a triaxial loading, even if the load history is generic, from the uniaxial creep compliance $J_E(t)$ and the relaxation Poisson's ratio $\nu_r(t)$, one can calculate the evolution of the principal strains over time (see Eq. 2.29). However, given all confusion in the literature on how to manipulate viscoelastic Poisson's ratios, in the generic case, a wise choice to perform viscoelastic characterization or analytical calculations in viscoelasticity is to restrict oneself to the use of unambiguously defined creep compliances and relaxation moduli.
- The creep Poisson's ratio was defined on a creep experiment with an instantaneous loading. If the loading phase of the creep experiment is not instantaneous (which is the case in practice), the ratio of the lateral

dilation to the axial contraction during the creep phase differs from the creep Poisson's ratio. This difference may be significant only for times that are smaller than about 10 times the duration of the loading phase.

We calculated how the relaxation and creep Poisson's ratios of cementitious materials evolved over time. The analysis of those parameters could be translated in terms of volumetric and deviatoric creep behaviors, thus paving the way for a more rationale choice of creep models for those materials.

Chapter 3

Viscoelastic Poisson's ratio of concrete

THE VISCOELASTIC *Poisson's ratio of concrete is an essential parameter when it comes to study creep and loss of prestress in biaxially prestressed structures, e.g., the containment of nuclear power plants. Various definitions and evolutions with time are reported in the literature for this Poisson's ratio. The present work first aims to perform a comprehensive study of those definitions. We then analyze all creep data of concrete available in literature that make it possible to compute the evolutions of this non-aging isotropic viscoelastic Poisson's ratio of concrete, which is found to remain roughly constant or to slightly decrease over time, such as to reach a long-term value always comprised between 0.15 and 0.2.*¹

LE COEFFICIENT DE POISSON *viscoélastique du béton est un paramètre essentiel lorsqu'il s'agit d'étudier le fluage et la perte de précontrainte*

¹This chapter is published together with the next chapter as Aili, A., Vandamme, M., Torrenti, J. M., Masson, B., & Sanahuja, J. (2016). Time evolutions of non-aging viscoelastic Poisson's ratio of concrete and implications for creep of CSH. *Cement and Concrete Research*, 90, 144-161.

CHAPTER 3. VISCOELASTIC POISSON'S RATIO OF CONCRETE

dans des structures en bétons béton précontraint biaxialement comme l'enceinte de confinement de centrales nucléaires. Différentes définitions et évolutions avec le temps sont rapportées dans la littérature pour ce coefficient de Poisson. Le présent travail vise d'abord à mener une étude complète de ces définitions. Nous analysons ensuite toutes les données de fluage de béton disponibles dans la littérature qui permettent de calculer les évolutions de ce coefficient de Poisson viscoélastique isotrope non-vieillissant. Cette étude montre que le coefficient de Poisson viscoélastique du béton reste à peu près constant ou légèrement décroissant dans le temps, de manière à atteindre une valeur à long terme toujours comprise entre 0,15 et 0,2.

The containment of the typical French nuclear power vessel is a massive concrete structure which is biaxially prestressed and is designed to withstand an internal overpressure of 0.5 MPa in case of accident (Torrenti et al., 2014). To extend the service life of the containment, we need to ensure that the prestress remains sufficient in order to avoid tensile stress and thus limit cracks in the event of such an accident. However, the prestress decreases over time, because of a combination of relaxation of steel and delayed strain of concrete (i.e., creep and shrinkage). Here biaxial creep is considered. In this case, in order to predict the creep of concrete and the resulting loss of prestress, we need to know more than only the 1-dimensional creep behavior of the concrete: we need to know its full 3-dimensional creep behavior. Within the framework of isotropic linear viscoelasticity, this 3-dimensional creep behavior is fully characterized by two creep compliances or relaxation moduli: for instance, on top of the uniaxial creep compliance considered in most models, one can use a viscoelastic (i.e., time-dependent) Poisson's ratio. However, although numerous studies (e.g., (RILEM Technical Committee, 1995, 2015)) and models (e.g., FIB (2013), 1992-1-1:2005 (2004), ACI Committee 209 (2008)) are devoted to the uniaxial creep compliance, the evolution of the viscoelastic Poisson's ratio of concrete with time has been much less scrutinized.

A first issue when considering a viscoelastic Poisson's ratio is that its definition is not unique (Aili et al., 2015), even when considering simple uniaxial compression, and in spite of the fact that all authors define it through a ratio of axial strain to lateral strain. For instance, Neville et al. (1983) define it through a ratio of the creep strains only, while Jordaan and Illston (1969) define it through a ratio of the total mechanical strains (which are equal to the sum of the elastic strains and of the creep strains). For what concerns the value of this ratio or its evolution over time, a very large scatter is observed. For instance, with the definition he chose, Neville et al. (1983) gathered the following values for the viscoelastic Poisson's ratio: close to 0 (Ross, 1954; Furr, 1967), equal to 0.05 (Glanville and Thomas, 1939; L'Hermite, 1959), equal to the elastic Poisson's ratio (Duke and Davis, 1944; Polivka et al., 1963), increasing with time (Evans and Wood, 1937), or decreasing with

time (York et al., 1972). A possible reason that could partly explain this large scatter is that the various experiments gathered by Neville were performed under various —and sometimes uncontrolled— hydric conditions. In our present work, we will focus on the evolutions of a viscoelastic Poisson's ratio during basic creep experiments, during which no water is exchanged between sample and environment. Such condition is achieved either by sealing the sample (Jordaan and Illston, 1969, 1971; Kennedy, 1975; Ulm et al., 2000; Kim et al., 2005), or by controlling the relative humidity of the environment to the same relative humidity as that of the sample (Gopalakrishnan, 1968). As a prerequisite, we will need to clearly define the viscoelastic Poisson's ratio we will consider, and determine how our definition compares with definitions used elsewhere.

First, we define the viscoelastic Poisson's ratio we will consider in this study and compare it with alternative definitions found in the literature. Secondly, we perform an analysis of basic creep data on concrete from the literature, to determine how this viscoelastic Poisson's ratio evolves with time.

3.1 Definition of viscoelastic Poisson's ratio for creep tests

This section is devoted to clearly define a viscoelastic Poisson's ratio for creep studies. To do so, we consider ideal relaxation/creep experiments, i.e., experiments with an instantaneous loading. A more detailed introduction of those definitions and of their interest can be found in chapter 2. During an ideal creep experiment, the measured strains (referred to as the 'total' strains) can be separated into an elastic contribution (termed 'elastic' strains) and a delayed one (termed 'creep' strains). Next, we introduce a definition of viscoelastic Poisson's ratio based on total strains: we will use this definition throughout the chapter. In section 3.1.2, the introduced viscoelastic Poisson's ratio is compared to an alternative definition based on creep strains only.

Concrete is an aging material, i.e., its mechanical properties depend on

its age (Grasley and Lange, 2007; Li et al., 2015). However, mature concrete can be considered non-aging. Also, up to about at least 40% of its strength, concrete can reasonably be assumed to be linear viscoelastic (Neville et al., 1983). In this article, we restrict ourselves to a material that is isotropic linear non-aging viscoelastic.

3.1.1 Definition of viscoelastic Poisson's ratio for isotropic linear non-aging viscoelastic solids

Now, we consider an ideal uniaxial relaxation or an ideal creep experiment, i.e., an experiment in which the displacement or the load, respectively, is applied instantaneously and kept constant over time. Based on those two thought experiments, from the ratio of the radial dilation to the axial contraction, we can define two Poisson's ratios:

$$\nu_r(t) = -\frac{\varepsilon_l(t)}{\varepsilon_a^0} \text{ during a uniaxial relaxation experiment for which } \varepsilon_a(t) = \varepsilon_a^0 \quad (3.1a)$$

$$\nu_c(t) = -\frac{\varepsilon_l(t)}{\varepsilon_a(t)} \text{ during a uniaxial creep experiment for which } \sigma_a(t) = \sigma_a^0 \quad (3.1b)$$

which we termed relaxation Poisson's ratio ν_r and creep Poisson's ratio ν_c . They can be expressed as functions of the bulk and shear time-dependent properties:

$$\hat{\nu}_r(s) = \frac{3\hat{K}(s) - 2\hat{G}(s)}{2s(3\hat{K}(s) + \hat{G}(s))} \quad (3.2a)$$

$$\nu_c(t) = \frac{3J_G(t) - 2J_K(t)}{2(3J_G(t) + J_K(t))} \quad (3.2b)$$

where s is the Laplace variable and where $\hat{f}(s)$ represents the Laplace trans-

form of the function $f(t)$. Those two Poisson's ratios are related through the uniaxial creep compliance $J_E(t)$ by:

$$\nu_c(t) = (\nu_r(t) \otimes \dot{J}_E(t))/J_E(t) \quad (3.3)$$

Hilton (2001); Tschoegl et al. (2002); Hilton (2009, 2011); Aili et al. (2015) already discussed the difference between various definitions of Poisson's ratios, including the relaxation Poisson's ratio ν_r and creep Poisson's ratio ν_c . The principle of correspondence (Christensen, 1982), which is of great use for solving linear viscoelastic problems analytically, is only applicable to the relaxation Poisson's ratio ν_r , not to the creep Poisson's ratio ν_c (Hilton, 2001; Tschoegl et al., 2002; Hilton, 2009, 2011; Aili et al., 2015). Said otherwise, if we want to infer the solution to a linear viscoelastic problem from the solution to the corresponding elastic one, then we need to replace the elastic Poisson's ratio by the s -multiplied Laplace transform of the relaxation Poisson's ratio $s\widehat{\nu}_r$, not of the creep Poisson's ratio $s\widehat{\nu}_c$. Therefore, the relaxation Poisson's ratio ν_r is a material property, which can be used to predict the response of the material under a generic load history. In contrast, the correspondence principle cannot be applied to the creep Poisson's ratio ν_c .

In spite of the theoretical differences that exists between the two Poisson's ratios ν_r and ν_c , their initial and asymptotic values are equal, and so are their initial and asymptotic time-derivatives (Aili et al., 2015). Moreover, in practice, for all cementitious materials (i.e., cement paste, mortar, or concrete) on which we could analyze biaxial creep data, the difference between those two Poisson's ratios was negligible at all times. Therefore, in the following, we will not distinguish the two Poisson's ratios and will only refer to it as to the viscoelastic Poisson's ratio of the material: we will note it $\nu(t)$. Note however that, for innovative concretes or for immature ones, the fact that the creep and relaxation Poisson's ratio almost coincide is not guaranteed: consequently, even if the creep Poisson's ratio ν_c can easily be obtained with Eq. 3.4 from creep data, experimentalists should always calculate the relaxation Poisson's ratio ν_r as well (with the above relation via transforms or via a numerical fitting routine), to check if the difference between the two

3.1. DEFINITION OF VISCOELASTIC POISSON'S RATIO FOR CREEP TESTS

Poisson's ratio is indeed always negligible.

In the rest of the thesis, the viscoelastic Poisson's ratio of the material will be back-calculated from creep experiments by using Eq. 3.4 that was derived for the creep Poisson's ratio: we thus retrieve the definition 3.4 that we introduced. When needed, we will also consider that this viscoelastic Poisson's ratio $\nu(t)$ satisfies the elastic-viscoelastic correspondence principle, which can theoretically only be applied to the relaxation Poisson's ratio.

The viscoelastic Poisson's ratio $\nu(t)$ that we will use throughout this work relates strains and stresses for a triaxial creep experiment through:

$$\varepsilon_i(t) = J_E(t)\sigma_i^0 - (\sigma_j^0 + \sigma_k^0)\nu(t)J_E(t), \text{ where } i \neq j \neq k \in \{1, 2, 3\}, \quad (3.4)$$

where σ_i^0 , σ_j^0 , and σ_k^0 are the constant loads instantaneously applied in the principal directions, and $\varepsilon_i(t)$, $\varepsilon_j(t)$, and $\varepsilon_k(t)$ are the strains in those same principal directions. This definition makes it possible to retrieve a definition found elsewhere for uniaxial creep tests (Jordaan and Illston, 1969, 1971; Kim et al., 2005):

$$\nu(t) = -\frac{\varepsilon_2(t)}{\varepsilon_1(t)} = -\frac{\varepsilon_3(t)}{\varepsilon_1(t)} \text{ with a load applied in direction 1 only,} \quad (3.5)$$

and another definition found elsewhere for biaxial creep tests (Jordaan and Illston, 1969, 1971; Kim et al., 2005):

$$\nu(t) = -\frac{\varepsilon_3(t)}{\varepsilon_1(t) + \varepsilon_2(t) - \varepsilon_3(t)} \text{ with a load applied in directions 1 and 2.} \quad (3.6)$$

The viscoelastic Poisson's ratio here introduced is defined based on total strains: one cannot calculate it when only the creep strains are reported (as is the case, e.g., in Gopalakrishnan et al. (1969); Bernard et al. (2003a)), unless the elastic strains can be estimated.

3.1.2 Definition based on creep strain

One of the most reported Poisson's ratios in the literature is defined based on creep strains (L'Hermite, 1959; Hannant, 1967; Gopalakrishnan et al., 1969; Neville et al., 1983; Kogan, 1983; Granger, 1995; Bažant et al., 1997; Benboudjema, 2002; Hilaire, 2014). For instance, for uniaxial creep tests, Neville et al. (1983) defined a uniaxial creep-based Poisson's ratio as:

$$\tilde{\nu}(t) = -\frac{\varepsilon_l(t) - \varepsilon_l^0}{\varepsilon_a(t) - \varepsilon_a^0} \quad (3.7)$$

where $\varepsilon_l(t)$, $\varepsilon_a(t)$ are the total lateral and axial strain, respectively, and where $\varepsilon_l^0 = \varepsilon_l(0)$ and $\varepsilon_a^0 = \varepsilon_a(0)$ are the lateral and axial elastic strains, respectively. Thus, $\varepsilon_l(t) - \varepsilon_l^0$ and $\varepsilon_a(t) - \varepsilon_a^0$ are the lateral and axial creep strains, respectively. In comparison with the viscoelastic Poisson's ratio $\nu(t)$ that we introduced in Eq. (3.4), one could draw the following analogy: the creep-based Poisson's ratio corresponds to a creep function, while the viscoelastic Poisson's ratio corresponds to a creep compliance.

The main interest of the creep-based Poisson's ratio $\tilde{\nu}(t)$ is that only creep strains are needed to compute it. Thus, it can be reported for any creep experiment, even in absence of any information on the elastic properties of the material. But this interest is in fact a drawback, which is the same drawback as for any creep function compared with its corresponding creep compliance.

The first drawback is that, if one reports only the creep-based Poisson's ratio, he/she may omit to report the elastic Poisson's ratio. In such case, the creep-based Poisson's ratio becomes quite useless: if one does not keep the load constant after the initial loading, one would be unable to calculate how the ratio between lateral and axial strain would evolve over time. In contrast, such omission is not possible if the viscoelastic Poisson's ratio is reported, since this ratio includes the elastic data: indeed, $\nu(0)$ is the elastic Poisson's ratio.

Creep functions (and hence the creep-based Poisson's ratio) are sensitive to the duration of the loading, which, for any creep test, is never instantaneous.

3.1. DEFINITION OF VISCOELASTIC POISSON'S RATIO FOR CREEP TESTS

As a consequence, any creep function is associated to an apparent elastic modulus, which must be measured from the strain at the end of the loading phase. Yet, when creep functions are reported in the literature, the associated apparent elastic modulus is not always reported or measured, and, when it is measured, it is sometimes measured from a different test (Bažant et al., 1993). The error that may arise from such a wrong combination could be nonnegligible.

In conclusions, in the spirit of Bažant et al. (1993), who recommended to report creep compliances rather than creep functions, we recommend the use of the viscoelastic Poisson's ratio rather than the creep-based Poisson's ratio. In any case, if one chooses to report the creep-based Poisson's ratio, he/she should report meaningful elastic properties as well.

3.1.3 Potential anisotropy of time-dependent behavior

Gopalakrishnan (1968); Gopalakrishnan et al. (1969); Neville et al. (1983) wondered whether the creep-based Poisson's ratio of concrete is anisotropic during a multiaxial creep test. They reached the conclusion that it can be. Here, we discuss their results.

To reach their conclusions, the authors proposed, for triaxial loading, the following definition for a direction-specific creep-based Poisson's ratio $\tilde{\nu}_i$:

$$\varepsilon_i(t) - \varepsilon_i(0) = J_E^{cu}(\sigma_i^0 - \tilde{\nu}_i(\sigma_j^0 + \sigma_k^0)) \text{ where } i \neq j \neq k \in \{1, 2, 3\}. \quad (3.8)$$

which is a definition based on creep strains. Note that in this definition intervenes the uniaxial creep compliance J_E^{cu} , which is measured from an independent uniaxial creep test in which the axial load σ_a^0 is equal to the maximum load of the triaxial test (i.e., $\sigma_a^0 = \max_{i \in \{1, 2, 3\}} \{\sigma_i\}$).

For instance, Gopalakrishnan (1968) performed 13 different triaxial tests on a cubic concrete sample. Among these 13 tests, we consider the 11 tests that yielded an elastic Poisson's ratio between 0 and 0.3. His results showed that the direction-specific creep-based Poisson's ratios $\tilde{\nu}_i$ obtained in the

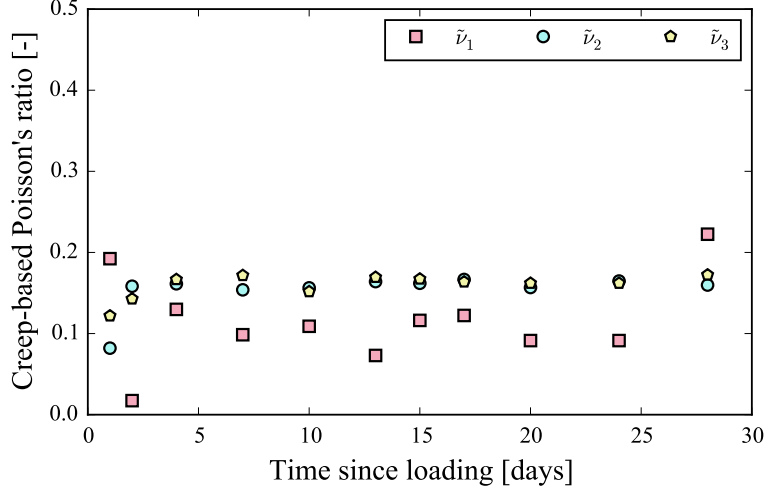
three directions $i \in \{1, 2, 3\}$ differ from each other. However, we believe that this anisotropy is mostly due to the fact that he only took into account creep strains, i.e., that he used uniaxial creep functions instead of uniaxial creep compliances.

Here, we propose an alternative way to analyze their data. This alternative relies on the data from the triaxial experiments only. First, we compute the volumetric strain $\varepsilon_v(t)$ and applied volumetric stress σ_v^0 , from which we obtain the volumetric creep compliance $J_K(t) = \varepsilon_v(t)/\sigma_v^0$. Second, we compute the von Mises strain $\varepsilon_d(t) = \sqrt{3J_2^\varepsilon(t)}$ (where $J_2^\varepsilon(t)$ is the second invariant of the deviatoric strain tensor e_{ij}) and von Mises stress $\sigma_d^0 = \sqrt{3J_2^{\sigma^0}}$ (where $J_2^{\sigma^0}$ is the second invariant of deviatoric stress tensor s_{ij}), from which we obtain the shear creep compliance $J_G(t) = 2\varepsilon_d(t)/\sigma_d^0$. Then, from the knowledge of the creep compliances $J_K(t)$ and $J_G(t)$, we obtain the uniaxial creep compliance $J_E(t) = J_K(t)/9 + J_G(t)/3$. Finally, by applying Eq. (3.4) while rotating the indices $i \neq j \neq k \in \{1, 2, 3\}$, we can obtain, from the triaxial data, 3 directional viscoelastic Poisson's ratios, which we note ν_1 , ν_2 , and ν_3 .

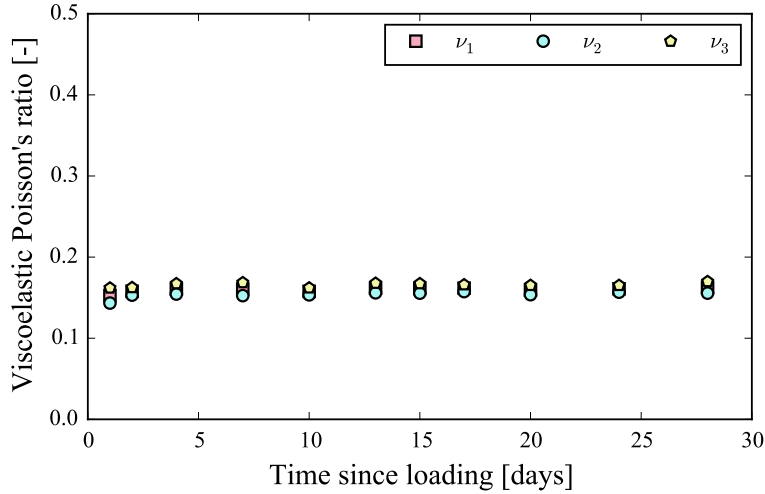
For instance, we consider the test TC10 in Gopalakrishnan (1968), in which the specimen is subjected to a triaxial compression: the 3 principal compression stresses are 13.24 MPa, 1.78 MPa and 1.83 MPa. We computed the 3 directional viscoelastic Poisson's ratios as explained above. Our results are displayed in Fig. 3.1, together with the 3 directional creep-based Poisson's ratio reported by Gopalakrishnan (1968). The maximum difference between the 3 creep-based Poisson's ratios (i.e., $\max_{i \neq j \in \{1, 2, 3\}} \{\tilde{\nu}_i(t) - \tilde{\nu}_j(t)\}$) displayed in Fig. 3.1a is 0.14. In contrast, the maximum difference between the 3 directional viscoelastic Poisson's ratios that we introduced (i.e., $\max_{i \neq j \in \{1, 2, 3\}} \{\nu_i(t) - \nu_j(t)\}$) and that are displayed in Fig. 3.1b is reduced to 0.019.

In fact, for the 11 tests considered from Gopalakrishnan (1968), we computed the 3 directional creep-based Poisson's ratios with Eq. (3.8) (as did the authors) and the 3 directional creep-based Poisson's ratios with Eq. (3.4) (see appendix C). For all 11 tests, the mean value of the maximum difference

3.1. DEFINITION OF VISCOELASTIC POISSON'S RATIO FOR CREEP TESTS



(a)



(b)

Figure 3.1 – Dependency of Poisson's ratio on the direction in experiment TC10 in Gopalakrishnan (1968): (a) Creep-based Poisson's ratio reported in Gopalakrishnan (1968), calculated from Eq. (3.8) for three directions; (b) viscoelastic Poisson's ratio calculated from Eq. (3.4) for three directions.

$\max_{i \neq j \in \{1,2,3\}} \{\tilde{\nu}_i(t) - \tilde{\nu}_j(t)\}$ between the 3 directional creep-based Poisson's ratio was 0.1182 and its standard deviation was 0.1245. In contrast, for the same 11 tests, the mean value of the maximum difference $\max_{i \neq j \in \{1,2,3\}} \{\nu_i(t) - \nu_j(t)\}$ between the 3 directional viscoelastic Poisson's ratios was 0.0367 and its

standard deviation was 0.0441.

Therefore, by working with viscoelastic Poisson's ratios rather than creep-based ones, and by consistently analyzing data from a unique test rather than from 2 independent ones, any potential anisotropy of a time-dependent Poisson's ratio vanished. In short: the viscoelastic Poisson's ratio of concrete can be considered as isotropic. Note that this conclusion is fully consistent with the theory of linear viscoelasticity, according to which, for an isotropic solid, the viscoelastic Poisson's ratio should have no reason to exhibit any anisotropy. Such conclusion is only valid for cases for which the load is lower than 30% of the strength, for which neither cracking nor damage is involved.

3.2 Evolution of viscoelastic Poisson's ratio of concrete

In this section, based on experimental results of basic creep of concrete available in the literature and for which the strains were measured in more than one direction, we analyze how the viscoelastic Poisson's ratio of concrete evolves over time. Here, following the reasoning explained in section 3.1.2, we consider only experiments for which both the creep strains and the elastic strains were measured. In these tests, the samples are either sealed (Jordaan and Illston, 1969, 1971; Kennedy, 1975; Ulm et al., 2000; Kim et al., 2005) or stored in an environment whose relative humidity is close to the relative humidity inside the sample (Gopalakrishnan, 1968). For each creep test, a reference specimen is used to measure autogenous shrinkage. This autogenous shrinkage is subtracted from the strain of the loaded specimen to obtain the strain only due to stress, i.e., the basic creep strain. Then, injecting the values of applied stress and stress-induced strains into Eq. (3.4), the evolution of the viscoelastic Poisson's ratio of the concrete samples with time is back-calculated. The data considered are the following:

- Gopalakrishnan (1968) performed triaxial creep tests on a cubic sample made of concrete with one mix design. The samples were always kept in a relative humidity of about 98%. The strain was measured by strain

3.2. EVOLUTION OF VISCOELASTIC POISSON'S RATIO OF CONCRETE

gauges of resolution $10\mu\text{m}/\text{m}$, with four strain gauges per surface. The load was applied by four high tensile steel rods whose relaxation was less than 0.2%. The load was provided by a 100-ton hydraulic jack and the load in the jack was indicated by a pressure gauge during the test. The loading age was 8 days.

- [Jordaan and Illston \(1969, 1971\)](#) measured the creep of a cubic sample of concrete with one mix design, under uniaxial and biaxial loads. The samples were coated with one layer of liquid plastic weatherproofing and several coats of resin. The strain was measured with strain gauges of sensitivity within $1\mu\text{m}/\text{m}$. The nominal stress was measured during the test in all three directions. The loading age was 16 days ([Jordaan and Illston, 1969](#)) or 7 days ([Jordaan and Illston, 1971](#)).
- [Kennedy \(1975\)](#) performed uniaxial and triaxial creep tests on cylindrical specimens of concrete with one mix design, but prepared with two types of curing conditions: "AsCast" denotes specimens cured under sealed conditions, while "AirDried" denotes specimens cured at a relative humidity of 50%. Before testing, all samples were coated with two layers of epoxy, then sealed in a copper jacket, placed in a neoprene sleeve and sealed at both ends with neoprene. At the end of each test, the author checked the mass loss of the specimens. The largest mass loss was 0.97% for the sample loaded at the age of 365 days and loaded during 1700 days. The strain was measured with vibrating wire strain gauges embedded in the sample, whose accuracy was $1\mu\text{m}/\text{m}$. The load was supplied by a hydraulic pressure which was regulated with a stability of $\pm 5\%$. A warning system was set to trigger an alarm if a 10% drop in pressure occurred, but the alarm was never triggered during the test.
- [Kim et al. \(2005\)](#) prepared cubic samples of concrete with three mix designs (noted C1, C2 and C3) and tested them under uniaxial, biaxial and triaxial loads. The samples were cured under water. Before the test, all exposed faces of the specimens were sealed with a base coat of

bituminous sealant and wrapped again in several layers of waterproof plastic film. They stated that they verified the reliability of the sealing method. The strain was measured with embedded gauges of sensitivity $1\mu\text{m}/\text{m}$. The load was applied with a spring-loaded creep frame and hydraulic cylinders with loading plates. The hydraulic cylinders were connected to accumulators that automatically compensated for the oil leakage of the cylinders. The authors also stated that they confirmed the effectiveness of their spring-loaded creep frame in providing reliable loads.

All cements that are used for the concretes above are equivalent of cement CEM I clinker in Eurocode. All experimental data are provided in appendix D.

The results are summarized in Fig. 3.2a, in which, for each experiment, the evolutions of the viscoelastic Poisson's ratio $\nu(t)$ with time are lumped into: elastic Poisson's ratio ν^0 (i.e., value at loading, displayed on the x-axis), long-term asymptotic viscoelastic Poisson's ratio ν^∞ (which is approximated by the value at the end of the test, displayed on the y-axis), and maximum and minimum viscoelastic Poisson's ratios over time (indicated with the error bars). For almost all experiments, the viscoelastic Poisson's ratio either remained quite constant and equal to its elastic value ν^0 at loading, or decreased continuously toward its long-term value ν^∞ .

For each mix design tested, a significant scatter was observed from experiment to experiment. In Fig. 3.2b, we display, averaged over experiments performed with each mix design, the long-term viscoelastic Poisson's ratio ν^∞ versus the elastic Poisson's ratio ν^0 . One can observe that the scatter from test to test was on the order of 0.05, for both the elastic Poisson's ratio and the long-term viscoelastic one. For all concretes tested by [Gopalakrishnan \(1968\)](#); [Jordaan and Illston \(1969, 1971\)](#); [Kim et al. \(2005\)](#), the elastic ν^0 and long-term viscoelastic ν^∞ Poisson's ratios were almost identical, as a consequence of the fact that, for those concretes, the viscoelastic Poisson's ratio remained almost constant over time. In contrast, for the two concretes tested by [Kennedy \(1975\)](#), the final viscoelastic Poisson's ratio ν^∞ was significantly

3.2. EVOLUTION OF VISCOELASTIC POISSON'S RATIO OF CONCRETE

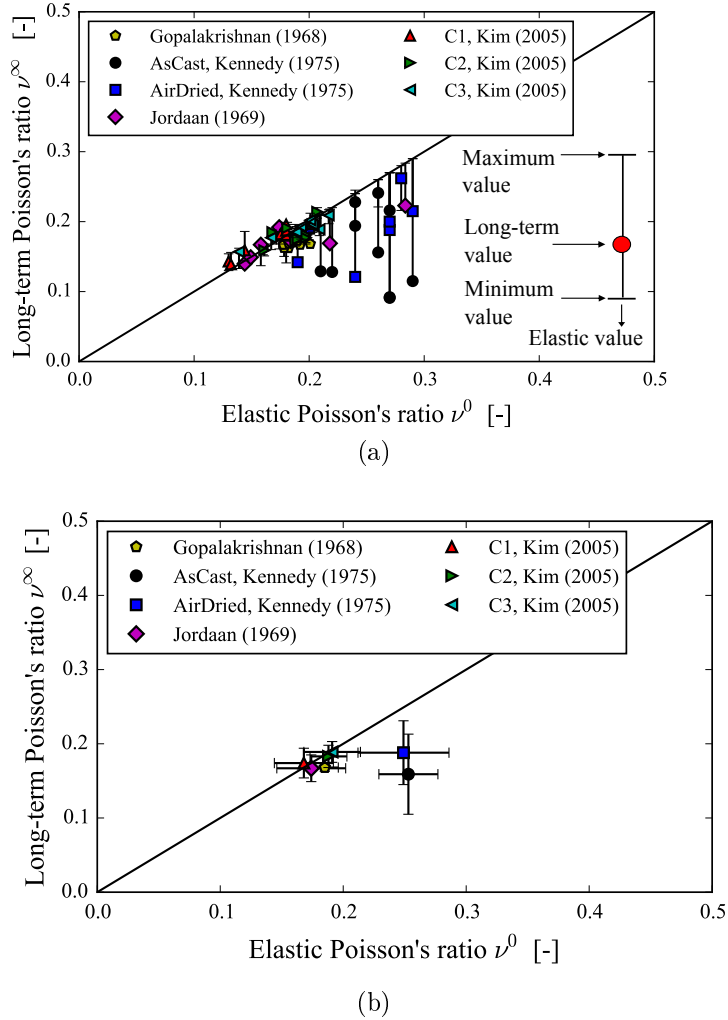


Figure 3.2 – Creep experiments on concrete of Gopalakrishnan (1968); Jordaan and Illston (1969); Kennedy (1975); Kim et al. (2005): Long-term asymptotic value of the viscoelastic Poisson's ratio versus elastic Poisson's ratio (a) for each individual experiment, and (b) averaged over all experiments performed with one mix design. In subfigure (a), y-axis error bars indicate the maximum and minimum values of the viscoelastic Poisson's ratio during the experiment.

lower than its elastic value ν^0 .

From Fig. 3.2, we observe that, in all cases, the long-term value ν^∞ of the viscoelastic Poisson's ratio was always equal to or smaller than the elastic value ν^0 . The variation of viscoelastic Poisson's ratio over time was non-

negligible for certain types of concrete. For all concretes studied here, the long-term value ν^∞ of the viscoelastic Poisson's ratio was comprised between 0.15 and 0.20. So, if the elastic Poisson's ratio of a concrete is in-between 0.15 and 0.20, considering that its viscoelastic Poisson's ratio is constant with time, as proposed by Bazant (1975); RILEM Technical Committee (1995), is a very reasonable assumption. We remind the reader that these conclusions are drawn by neglecting aging: they are therefore valid for a mature concrete (for which aging is negligible), but do not hold necessarily for early-age concrete (for which aging is significant).

These values of long-term viscoelastic Poisson's ratio ν^∞ of concrete show that the long-term creep of concrete is both deviatoric and volumetric. Indeed, if concrete were to creep only in a deviatoric manner with no asymptote, the long-term viscoelastic Poisson's ratio should theoretically converge toward $\nu^\infty = 0.5$ for infinite times (see section 4.1), and hence should at least, in practice, increase with time. However, the experiments here analyzed show that the viscoelastic Poisson's ratio remained constant or decreased slightly with time. Moreover, Fig. 3.3 highlights the fact that the long-term creep is not only deviatoric but also volumetric: out of the five tests plotted in Fig. 3.3, four showed an increasing volumetric strain, three of which evolved logarithmically with time during the creep experiment.

3.3 Conclusions

We analyzed the long-term viscoelastic Poisson's ratio of concrete from creep experiments from the literature. The analysis of all experimental results shows that:

- The time-dependent behavior of concrete is isotropic, as expected from the theory of linear viscoelasticity.
- The long-term creep of concrete is not only deviatoric, but also volumetric.
- The long-term viscoelastic Poisson's ratio of concrete is equal to or

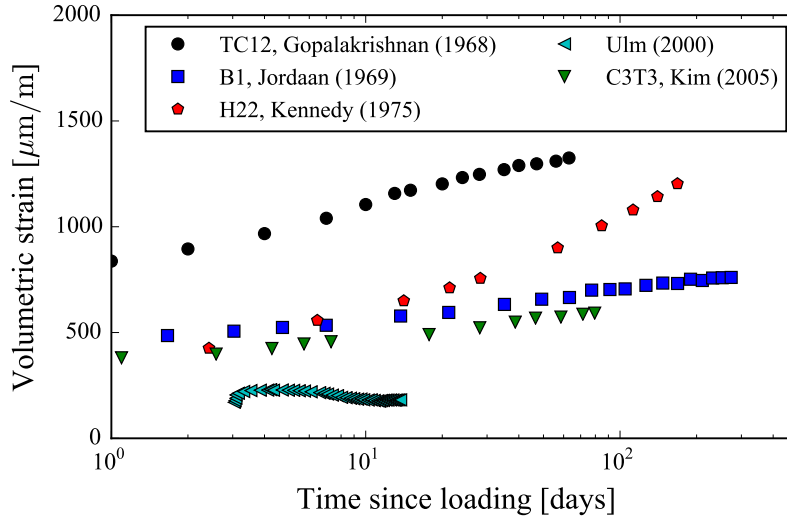


Figure 3.3 – Evolution of volumetric strain during creep experiment on concrete. Original data are from [Gopalakrishnan \(1968\)](#); [Jordaan and Illston \(1969\)](#); [Kennedy \(1975\)](#); [Ulm et al. \(2000\)](#); [Kim et al. \(2005\)](#).

smaller than its elastic Poisson's ratio, and comprised between 0.15 and 0.20.

- When the elastic Poisson's ratio of mature concrete is significantly greater than 0.20, the variation of its viscoelastic Poisson's ratio over time is non-negligible.
- When the elastic Poisson's ratio of mature concrete is comprised between 0.15 and 0.20, for practical applications, considering that its viscoelastic Poisson's ratio is constant over time, as proposed in particular by [Bazant \(1975\)](#); [RILEM Technical Committee \(1995\)](#), is a very reasonable assumption.

CHAPTER 3. VISCOELASTIC POISSON'S RATIO OF CONCRETE

Chapter 4

Long-term viscoelastic Poisson's ratio of C-S-H gel

THE LONG-TERM *viscoelastic Poisson's ratio of concrete is downscaled to the level of calcium silicate hydrates (noted C-S-H) with homogenization schemes. The long-term viscoelastic Poisson's ratio of the C-S-H gel is found to be comprised between 0 and 0.2. Finally, the downscaled long-term viscoelastic Poisson's ratio of the C-S-H gel is used to discuss various potential creep mechanisms at the level of the C-S-H particles.*¹

LE COEFFICIENT DE POISSON *viscoélastique à long terme du gel de silicate de calcium hydraté (noté comme C-S-H) est calculé à partir du coefficient de Poisson à long terme du béton par des schémas d'homogénéisation viscoélastique. Le coefficient de Poisson viscoélastique du gel de C-S-H se trouve entre 0 et 0,2. À la fin, en nous basant sur la valeur à long terme du*

¹This chapter is published together with the previous chapter as Aili, A., Vandamme, M., Torrenti, J. M., Masson, B., & Sanahuja, J. (2016). Time evolutions of non-aging viscoelastic Poisson's ratio of concrete and implications for creep of CSH. *Cement and Concrete Research*, 90, 144-161.

CHAPTER 4. LONG-TERM VISCOELASTIC POISSON'S RATIO OF
C-S-H GEL

coefficient de Poisson du gel de C-S-H, nous analysons différents mécanismes possibles de fluage à l'échelle de particules de C-S-H.

For concretes made with ordinary Portland cement paste, there is a consensus that the main phase responsible for the creep of concrete is the calcium silicate hydrates (noted C-S-H) (Mehta and Monteiro, 2006). C-S-H is layered at the nanometric scale —we will refer to stacks of C-S-H layers as to C-S-H ‘particles’— and forms a gel at a larger scale. We can reasonably wonder how the viscoelastic Poisson’s ratio of concrete is related to the viscoelastic Poisson’s ratio of the C-S-H gel and to the creep mechanism of the C-S-H particles. By performing some downscaling on the long-term viscoelastic Poisson’s ratio of concrete found in chapter 3, we aim at shedding some light on these relations.

First, we derive the relation between the long-term Poisson’s ratio of a composite and of its components using viscoelastic Mori-Tanaka scheme. Then, by performing three steps of downscaling of the long-term Poisson’s ratio of concrete, we infer the long-term viscoelastic Poisson’s ratio of the C-S-H gel. Finally, we consider various creep mechanisms at the scale of the C-S-H particles and assess, by upscaling, whether those mechanisms are possible or not.

4.1 Downscaling of long-term viscoelastic Poisson’s ratio

Knowing the long-term value of the viscoelastic Poisson’s ratio of concrete, a back-calculation of the long-term value of the viscoelastic Poisson’s ratio of the C-S-H gel is possible. As we shall see, from the knowledge of this long-term viscoelastic Poisson’s ratio, some physical conclusions can be inferred. Working with data on cement paste may have been more relevant, but we are aware of only one experimental data (Parrott, 1974) on cement paste that we could use. Therefore, in this section, an analysis of data on concrete is presented.

The elastic-viscoelastic correspondence principle (Christensen, 1982) is a tool that can transform a linear non-aging viscoelastic problem into a corresponding linear elastic problem. This principle consists in eliminating the

explicit time-dependence of the viscoelastic problem by replacing all time-dependent moduli by the s -multiplied Laplace transform (also called Carson transform) of their viscoelastic operator, thus yielding a corresponding elasticity problem in the Laplace domain. Using this principle makes it possible to tackle upscaling of viscoelastic creep compliances, by using corresponding elastic homogenization schemes in the Laplace domain.

Resulting relations in the Laplace domain need to be transformed back into the real time domain, which always remains hard to do analytically, because only a few types of functions can be transformed analytically from the Laplace domain back into the time domain. Nevertheless, one can use the final value theorem (Auliac et al., 2000) to find a relation between the long-term asymptotic values K^∞ and G^∞ of the relaxation moduli, J_K^∞ and J_G^∞ of the creep compliances, and ν^∞ of the viscoelastic Poisson's ratio. For instance, applying the final value theorem (Auliac et al., 2000) to Eq. 3.2a, we find the following relation between the long-term value ν^∞ of the viscoelastic Poisson's ratio and the long-term bulk K^∞ and shear G^∞ moduli:

$$\lim_{s \rightarrow 0} (s\hat{\nu}(s)) = \lim_{s \rightarrow 0} \left(\frac{3\hat{K} - 2\hat{G}s}{6\hat{K} + 2\hat{G}s} \right) = \frac{3K^\infty - 2G^\infty}{6K^\infty + 2G^\infty} = \nu^\infty \quad (4.1)$$

From this relation, we infer that, if the material creeps with no asymptote in time (which seems to be the case for most cementitious materials (Bazant et al., 2011; Müller et al., 2013; RILEM Technical Committee, 2015; Torrenti and Le Roy, 2015; Le Roy et al., 2017), see also Fig. 3.3), but in a deviatoric manner only (in which case $K^\infty \gg G^\infty$), the viscoelastic Poisson's ratio must converge toward $\nu^\infty = 0.5$. In contrast, if the material creeps with no asymptote in time but in a volumetric manner only (in which case $K^\infty \ll G^\infty$), the viscoelastic Poisson's ratio must converge toward $\nu^\infty = -1$.

In the experiments discussed in Sec. 3.2, the duration of the experiments is finite and the viscoelastic Poisson's ratio may not have reached its asymptotic value fully. However, as the viscoelastic Poisson's ratio $\nu(t)$ does not vary much with time, we will consider its value at the end of the experiment as its asymptotic value ν^∞ . Based on this approach, we will perform downscaling of the long-term asymptotic viscoelastic Poisson's ratio by using the elastic-

viscoelastic correspondence principle and the final value theorem.

To infer the long-term asymptotic value of the viscoelastic Poisson's ratio of the C-S-H gel from that of the concrete, the concrete is regarded as a multiscale composite material at four different scales, which are displayed in Fig. 4.1:

- At the largest scale of concrete (see Fig. 4.1a), the aggregates are considered as spherical inclusions that do not creep and are embedded into a matrix made of cement paste, which creeps.
- At a scale below, i.e., at the scale of the cement paste (see Fig. 4.1b), portlandite, calcium sulfoaluminates hydrates and the unhydrated clinker are considered as spherical inclusions that do not creep and are embedded into a matrix made of a mixture of C-S-H with capillary pores. This mixture is considered to creep.
- At another scale below (see Fig. 4.1c), the mixture of C-S-H with capillary pores is considered to be a matrix of C-S-H gel (that contains the gel porosity) that surrounds spherical capillary pores.

We downscaled then the Poisson's ratio from the scale of concrete (Fig. 4.1a) to the scale of C-S-H gel (Fig. 4.1c). As a prerequisite to the downscaling, we derive some theoretical results. It should be noted that we do not take into account any interfacial transition zone (ITZ) in this stage of downscaling but the effect of ITZ will be discussed in section 4.2.1. In section 4.1.1, we derive what the long-term viscoelastic Poisson's ratio is for a composite material made of a matrix that creeps and that embeds spherical inclusions that do not creep. In section 4.1.2, we derive what the long-term viscoelastic Poisson's ratio is for a composite material made of a matrix that creeps and that surrounds spherical pores.

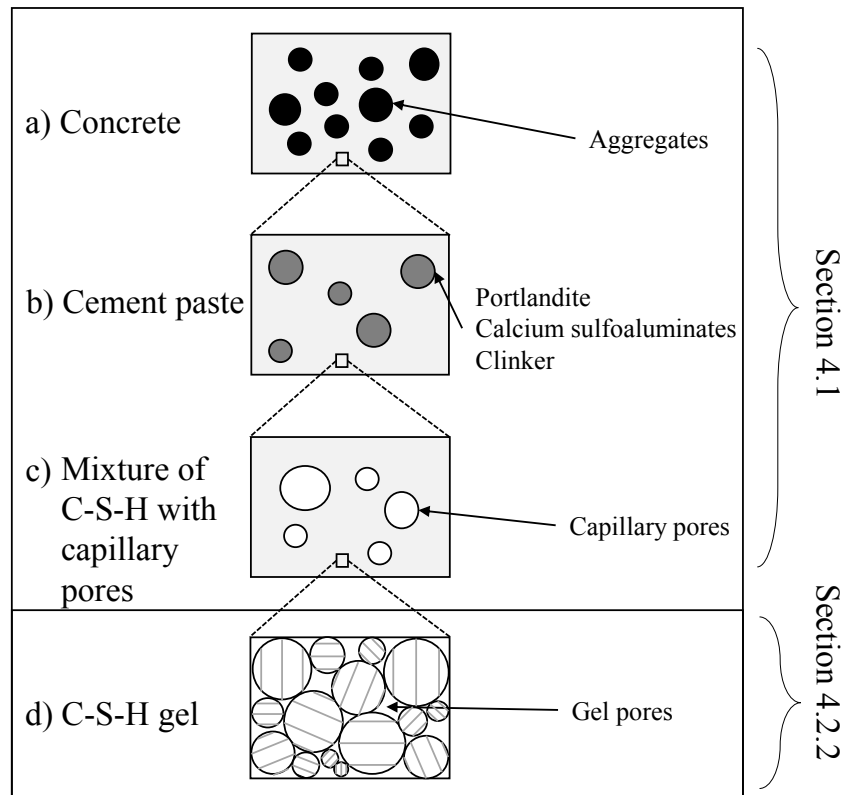


Figure 4.1 – Multiscale structure of concrete: (a) Concrete as a matrix of cement paste embedding aggregates, (b) cement paste as portlandite, calcium sulfoaluminates hydrates and unhydrated clinker embedded into a matrix made of a mixture of C-S-H with capillary pores, (c) mixture of C-S-H with capillary pores as a matrix of C-S-H gel surrounding capillary porosity, and (d) C-S-H gel as a mixture of C-S-H particles and gel pores. The scales (a) (b) (c) are considered in Sec. 4.1 for the downscaling of the long-term Poisson's ratio, while the scale (d) is considered in Sec. 4.2.2 for the analysis of long-term creep mechanism of C-S-H gel.

4.1.1 Viscoelastic Poisson's ratio of composite made of matrix embedding non-creeping inclusions

Here we consider a composite made of a matrix that embeds spherical inclusions. The matrix is considered to creep, and the inclusions are considered not to creep. The aim is to derive the relation between the long-term value ν_{com}^{∞} of the viscoelastic Poisson's ratio of the composite, the long-term value ν_m^{∞} of the viscoelastic Poisson's ratio of the matrix, and the volume fraction

f_i of the inclusions.

For such a microstructure, the Mori-Tanaka scheme has been shown to be applicable, for any volume fraction of inclusions (Bernard et al., 2003b; Sanahuja et al., 2007; Pichler and Hellmich, 2011). So, we apply the Mori-Tanaka scheme to calculate the properties of the composite as a function of the properties of its individual phases. The interface between inclusion and matrix is considered to be perfectly adhesive. Applying the correspondence principle to the elastic Mori-Tanaka homogenization scheme, one finds, in the Laplace domain, the solution to the viscoelastic homogenization problem of interest.

Applying the final value theorem (Auliac et al., 2000) to this relation, we obtain a relation between the long-term values K_{com}^∞ and G_{com}^∞ of the relaxation moduli of the composite, K_m^∞ and G_m^∞ of the relaxation moduli of the matrix, and K_i^∞ and G_i^∞ of the relaxation moduli of the inclusions:

$$K_{com}^\infty = K_m^\infty \frac{(1-f)(K_m^\infty + \alpha(K_i^\infty - K_m^\infty)) + fK_i^\infty}{(1-f)(K_m^\infty + \alpha(K_i^\infty - K_m^\infty)) + fK_m^\infty} \quad (4.2a)$$

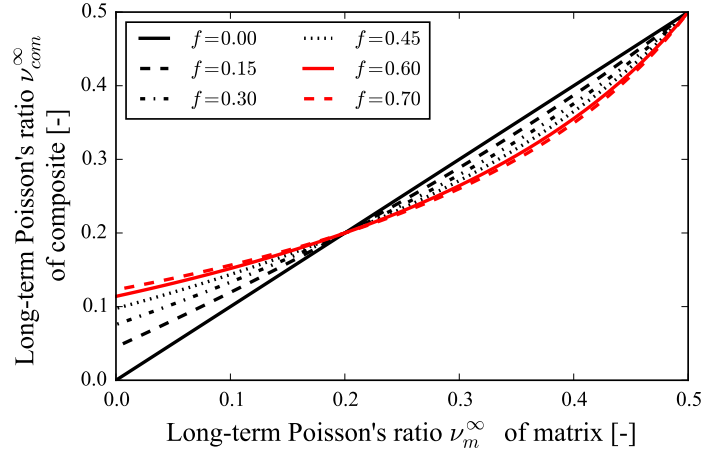
$$G_{com}^\infty = G_m^\infty \frac{(1-f)(G_m^\infty + \beta(G_i^\infty - G_m^\infty)) + fG_i^\infty}{(1-f)(G_m^\infty + \beta(G_i^\infty - G_m^\infty)) + fG_m^\infty} \quad (4.2b)$$

where $\alpha = (3K_m^\infty)/(3K_m^\infty + 4G_m^\infty)$ and $\beta = (6K_m^\infty + 12G_m^\infty)/(15K_m^\infty + 20G_m^\infty)$. Then, injecting the relaxation moduli K_{com}^∞ and G_{com}^∞ into Eq. (4.1), we get the expression of the long-term value ν_{com}^∞ of the viscoelastic Poisson's ratio of the composite. Supposing that the long-term volumetric and deviatoric creep functions of the matrix are non-asymptotic, we let $K_m^\infty/K_i^\infty \rightarrow 0$ and $G_m^\infty/G_i^\infty \rightarrow 0$ in the expression of ν_{com}^∞ and obtain:

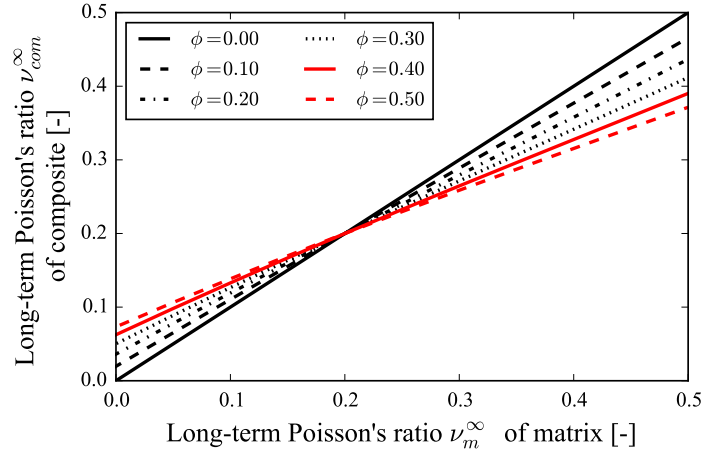
$$\nu_{com}^\infty = \frac{(10(\nu_m^\infty)^2 - 11\nu_m^\infty + 3)f + (8(\nu_m^\infty) - 10(\nu_m^\infty)^2)}{(30(\nu_m^\infty)^2 - 41\nu_m^\infty + 13)f + (8 - 10\nu_m^\infty)} \quad (4.3)$$

This equation indicates that the long-term viscoelastic Poisson's ratio of such a composite depends only on the long-term viscoelastic Poisson's ratio of the matrix and on the volume fraction of the inclusions. The relation between the long-term viscoelastic Poisson's ratio ν_{com}^∞ of the composite and

ν_m^∞ of the matrix is displayed in Fig. 4.2a for various volume fractions f of inclusion.



(a)



(b)

Figure 4.2 – (a) Long-term viscoelastic Poisson's ratio of a composite made of a creeping matrix that surrounds non-creeping spherical inclusions. f is the volume fraction of inclusions. (b) Long-term viscoelastic Poisson's ratio of a composite made of a creeping matrix that surrounds spherical pores. ϕ is the volume fraction of pores.

Figure 4.2a shows that if the matrix creeps only deviatorically (i.e., $\nu_m^\infty = 0.5$) at large times, then the composite must also creep deviatorically only.

As the basic creep of concrete is non-asymptotic (Le Roy, 1995; Zhang et al., 2014; Le Roy et al., 2017) and its long-term viscoelastic Poisson's ratio is strictly lower than 0.5 (see Fig. 3.2), we can consider that the cement paste creeps not only deviatorically but also volumetrically with no asymptote. Thus, the homogenization scheme developed in this section can be applied to downscale results from the scale of concrete to the scale of the cement paste and to the scale of the mixture of C-S-H with capillary porosity (see Fig. 4.1).

4.1.2 Viscoelastic Poisson's ratio of porous medium

Here we consider a composite made of a homogeneous matrix that embeds spherical pores. The aim is to relate the long-term viscoelastic Poisson's ratio ν_{com}^∞ of the composite to the long-term viscoelastic Poisson's ratio ν_m^∞ of the matrix and the volume fraction ϕ of pores (i.e. porosity).

Given the microstructure, we apply the Mori-Tanaka scheme to compute the properties of the composite as a function of the properties of its individual phases. Since the homogenization scheme is the same as that used in section 4.1.1, the long-term relaxation moduli K_{com}^∞ and G_{com}^∞ of the composite read as in Eq. (4.2). In this equation, taking into account the fact that $K_i^\infty = 0$ and $G_i^\infty = 0$ and injecting them into Eq. (4.1) yields:

$$\nu_{com}^\infty = \frac{((5\nu_m^\infty)^2 + 2\nu_m^\infty - 3)\phi + \nu_m^\infty(10\nu_m^\infty - 14)}{(15(\nu_m^\infty)^2 + 2\nu_m^\infty - 13)\phi + (10\nu_m^\infty - 14)} \quad (4.4)$$

This equation indicates that the long-term viscoelastic Poisson's ratio of such a composite depends only on the long-term viscoelastic Poisson's ratio of the matrix and on the volume fraction of the pores. The relation between the long-term viscoelastic Poisson's ratios ν_{com}^∞ of the composite and ν_m^∞ of the matrix is displayed in Fig. 4.2b for various values of volume fraction of pores. This figure shows that if the matrix creeps only deviatorically (i.e., $\nu_m^\infty = 0.5$) at large times, the porous medium may creep not only deviatorically, but also volumetrically. It is worth to keep in mind that a pure deviatoric creep at microscopic level does not imply always a pure deviatoric creep at macroscopic level.

4.1.3 Long-term viscoelastic Poisson's ratio: from concrete down to C-S-H gel

The long-term viscoelastic Poisson's ratio ν_{gel}^∞ of the C-S-H gel is computed from the results obtained at the scale of concrete by downscaling in three steps, by using the intermediate scales of the cement paste and of the mixture of C-S-H with the capillary porosity (see Fig. 4.1).

To downscale results from the scale of concrete to the scale of cement paste, we apply the viscoelastic homogenization scheme introduced in section 4.1.1. We use Eq. (4.3), in which the long-term viscoelastic Poisson's ratio used is that of concrete, which is displayed in Fig. 3.2a, and in which the volume fraction of aggregates is computed from the mix design (see Tab. 5.2). Thus, we back-calculate the long-term viscoelastic Poisson's ratio of the cement paste, which plays the role of the matrix in this step of downscaling (see Fig. 4.1a).

To downscale results from the scale of cement paste to the scale of the mixture of C-S-H with capillary porosity, we apply the viscoelastic homogenization scheme introduced in section 4.1.1 again. The volume fraction of each phase is computed by using Power's model (Powers and Brownyard, 1947; Taylor, 1997), which considers that the volume of cement paste is composed of bulk hydrate (i.e., solid hydrates plus gel pores), unhydrated clinker, and capillary pores. The sample is considered to be fully hydrated if the water-to-cement mass ratio w/c is superior to 0.38 for samples cured under water, and superior to 0.44 for samples cured under sealed conditions (Taylor, 1997). Otherwise, the long-term hydration degree α^∞ is taken to be equal to $(w/c)/0.38$ for samples cured under water, and to $(w/c)/0.44$ for samples cured under sealed conditions (Taylor, 1997). The bulk volume fraction of hydrates per volume of cement paste is $2.12(1-p)\alpha^\infty$, where $p = (w/c)/(w/c + \rho_w/\rho_c)$ and where ρ_w and ρ_c are the densities of water and cement, respectively. The volume fraction of portlandite per bulk volume of hydrates is estimated to be equal to 25%, which is a typical value for CEM I cement pastes (Mehta and Monteiro, 2006), from which the volume fraction f_{CH} of portlandite per volume of cement paste is $f_{CH} = 0.53(1-p)\alpha^\infty$.

The volume fraction of calcium sulfoaluminates hydrates per bulk volume of hydrate is estimated to be equal to 15% (Mehta and Monteiro, 2006), from which the volume fraction f_{alu} of sulfoaluminates hydrates per volume of cement paste is $f_{alu} = 0.32(1 - p)\alpha^\infty$. The volume fraction f_{cl} of unhydrated clinker per volume of cement paste is estimated also with Power's model (Powers and Brownyard, 1947; Taylor, 1997) to be equal to $f_{cl} = (1 - p)(1 - \alpha^\infty)$. Therefore, to downscale results from the scale of cement paste to the scale of the mixture of C-S-H with capillary porosity, we use Eq. (4.3) by considering that the volume fraction of inclusions is $f_{CH} + f_{alu} + f_{cl}$. Thus, we back-calculate the long-term viscoelastic Poisson's ratio of the mixture of C-S-H with the capillary porosity, which plays the role of the matrix in this step of downscaling (see Fig. 4.1b).

To downscale results from the scale of the mixture of C-S-H with the capillary porosity to the scale of the C-S-H gel, we apply the viscoelastic homogenization scheme introduced in section 4.1.2. The volume fraction V_{cp} of capillary pores per volume of cement paste is estimated with Powers' law (Powers and Brownyard, 1947; Taylor, 1997) as $V_{cp} = p - 1.12(1 - p)\alpha^\infty$. We use Eq. (4.4) by considering that the porosity $\phi = V_{cp}/(1 - V_{CH} - V_{alu} - V_{cl})$ is the volume fraction of capillary pores in the mixture. Thus, we back-calculate the long-term viscoelastic Poisson's ratio of the C-S-H gel, which plays the role of the matrix in this step of downscaling (see Fig. 4.1c).

Figure 4.3 displays the results of this downscaling. The long-term viscoelastic Poisson's ratio ν_{gel}^∞ of the C-S-H gel is comprised between -0.07 and 0.16 , while the long-term viscoelastic Poisson's ratio ν_c^∞ of concrete is comprised between 0.16 and 0.19 . As a result of the fact that the slope of the curves displayed in Figs. 4.2a and b is lower than 1 for Poisson's ratios around 0.2 , the long-term viscoelastic Poisson's ratio of C-S-H is more scattered than that of concrete, which indicates that the long-term viscoelastic Poisson's ratio of concrete is rather independent of that of C-S-H gel: the long-term viscoelastic Poisson's ratio of C-S-H has little influence on the long-term viscoelastic Poisson's ratio of concrete. The fact that the estimation of the Poisson's ratio of C-S-H gel is scattered is due to the scatter of the measurement at the level of the concrete.

CHAPTER 4. LONG-TERM VISCOELASTIC POISSON'S RATIO OF C-S-H GEL

Concrete	Cement type	Water-to-cement mass ratio	Volume fraction of aggregates	Volume fraction of portlandite, calcium sulfoaluminates hydrates and clinker	Volume fraction of capillary pores
Gopalakrishnan	Type III	0.72	0.725	0.259	0.474
AsCast, Kennedy	Type II	0.425	0.637	0.363	0.147
AirDried, Kennedy	Type II	0.425	0.637	0.363	0.147
Jordaan and Illston	OPC ¹	0.40	0.641	0.375	0.099
C1, Kim et al.	Type I	0.58	0.715	0.300	0.357
C2, Kim et al.	Type I	0.4	0.7	0.375	0.099
C3, Kim et al.	Type I	0.32	0.691	0.434	0.057

Table 4.1 – Concrete formulation data used for the downscaling of viscoelastic Poisson's ratio. The volume fraction of aggregates is expressed per unit volume of concrete. The volume fraction of portlandite, calcium sulfoaluminates hydrates and unhydrated clinker is expressed per unit volume of cement paste. The volume fraction of capillary pores is expressed per unit volume of mixture of C-S-H with capillary pores. ¹ OPC is ordinary Portland cement.

4.1. DOWNSCALING OF LONG-TERM VISCOELASTIC POISSON'S RATIO

Even when taking into account the scatter, for all materials considered, the sum of the long-term viscoelastic Poisson's ratio ν_{gel}^∞ of the C-S-H gel and of its standard deviation is found to be between -0.38 and 0.24 , which is significantly smaller than 0.5 and significantly greater than -1 . Therefore, given the fact that the creep of cementitious materials is known to exhibit no asymptote (Le Roy, 1995; Zhang et al., 2014; Le Roy et al., 2017), we infer that the long-term creep of the C-S-H gel is neither deviatoric only (in which case we would observe $\nu_{gel}^\infty = 0.5$), nor volumetric only (in which case we would observe $\nu_{gel}^\infty = -1$): in the long term, the C-S-H gel creeps both volumetrically and deviatorically.

We remind the reader that in the above downscaling approach, aging effect is neglected. It is possible to extend the downscaling of Poisson's ratio to the case of aging (Sanahuja, 2013).

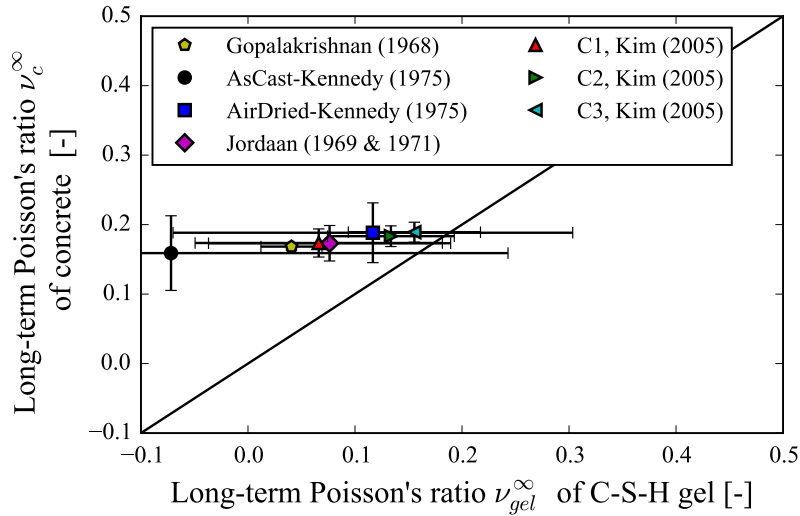


Figure 4.3 – Long-term viscoelastic Poisson's ratio ν_c^∞ of concrete versus long-term viscoelastic Poisson's ratio ν_{gel}^∞ of C-S-H gel.

4.2 Discussion

4.2.1 Influence of interface

The homogenization scheme introduced in section 4.1.1 was derived by considering that the interface between inclusion and matrix is perfectly adhesive. Said otherwise, by using this scheme, we considered that there is no discontinuity of displacement, neither at the interface between aggregates and cement paste (see Fig. 4.1a), nor at the interface between portlandite, calcium sulfoaluminates hydrates, clinker and the mixture of C-S-H with capillary porosity (see Fig. 4.1b). In practice, adhesion at those two interfaces may not be perfect. The objective of this section is to quantify how this imperfection could alter the findings obtained in section 4.1.3.

As was done in section 4.1.3, we consider a composite made of a matrix that creeps and surrounds spherical inclusions that do not creep, but we now consider that the interface between matrix and inclusion can be imperfect: a tangential stiffness $K_t(t)$ of the interface is introduced, with a long-term asymptotic value $\lim_{t \rightarrow +\infty} K_t(t) = K_t^\infty$. The normal displacement at the interface is considered to be continuous, i.e., there is no separation at the interface. The radius of the inclusions is noted R_i . The viscoelastic homogenization scheme is based on the equivalent inclusion method developed by [Duan et al. \(2007\)](#) for elastic solids. In his model, the imperfection of the interface is characterized by the dimensionless parameter $m_\theta = K_t R_i / G_m$, where G_m is the shear modulus of the matrix. Using the correspondence principle, the viscoelastic homogenization scheme with imperfect interfaces is derived in the Laplace domain by replacing all elastic parameters in Duan's scheme by the s -multiplied Laplace transform of their corresponding viscoelastic parameter. Then, using again the final value theorem ([Auliac et al., 2000](#)), we derive a relation between the long-term viscoelastic Poisson's ratio ν_{com}^∞ of the composite, ν_m^∞ of the matrix, the long-term interface property $m_\theta^\infty = \lim_{t \rightarrow +\infty} (K_t(t) R_i / G_m(t))$, and the volume fraction f of inclusions:

$$\nu_{com}^\infty = \frac{A_1(\nu_m^\infty)^2 + B_1\nu_m^\infty + C_1}{A_2(\nu_m^\infty)^2 + B_2\nu_m^\infty + C_2} \quad (4.5)$$

where the coefficients are:

- $A_1 = 10f^2m_\theta^\infty + 20f^2 - 20fm_\theta^\infty - 76f + 10m_\theta^\infty + 38$
- $B_1 = -11f^2m_\theta^\infty - 22f^2 + 19fm_\theta^\infty + 92f - 8m_\theta^\infty - 34$
- $C_1 = 3f^2m_\theta^\infty + 6f^2 - 3fm_\theta^\infty - 24f$
- $A_2 = 30f^2m_\theta^\infty + 60f^2 - 30fm_\theta^\infty - 96f$
- $B_2 = -41f^2m_\theta^\infty - 82f^2 + 31fm_\theta^\infty + 116f + 10m_\theta^\infty + 38$
- $C_2 = 13f^2m_\theta^\infty + 26f^2 - 5fm_\theta^\infty - 28f - 8m_\theta^\infty - 34$

In the above equation, letting the interface parameter m_θ^∞ tend toward $+\infty$, we retrieve Eq. (4.3), which is valid for perfectly adhesive interfaces. In contrast, letting the interface parameter m_θ^∞ tend toward 0, we obtain a relation valid in the case of perfectly smooth interfaces. We checked that the relation obtained in this latter case is consistent with the Poisson's ratio obtained by using the elastic homogenization scheme for perfectly smooth interface developed by Barthélémy (2005). Next, we study the influence of the interface conditions on the results when performing a homogenization 1) from the scale of the cement paste to that of the concrete, and 2) from the scale of the C-S-H gel to that of the cement paste.

For what concerns homogenization from the scale of cement paste to the scale of concrete, the interface that plays a role is that between aggregates and cement paste (see Fig. 4.1a). Here, in accordance with the experimental results of Parrott (1974), we consider a concrete made of aggregates at a typical volume fraction of 0.7 and of a cement paste with a long-term viscoelastic Poisson's ratio equal to 0.19. Using Eq. (4.5), we compute the long-term viscoelastic Poisson's ratio of the concrete as a function of the interface parameter m_θ^∞ . The results are displayed in Fig. 4.4a: to retrieve a long-term viscoelastic Poisson's ratio between 0.15 and 0.2 for concrete (as is observed experimentally, see Fig. 3.2), Fig. 4.4a suggests that the interface between aggregates and cement paste can be considered to be perfectly adhesive.

For what concerns homogenization from the scale of the C-S-H gel to the scale of the cement paste, the interfaces that play a role are those between portlandite, calcium sulfoaluminates hydrates, clinker and the mixture of C-S-H with the capillary porosity (see Fig. 4.1b). Here, in accordance again with the experimental results of Parrott (1974), we consider a cement paste with a long-term viscoelastic Poisson's ratio equal to 0.19. This long-term viscoelastic Poisson's ratio is downscaled down to the scale of the C-S-H gel in two steps, to obtain the long-term viscoelastic Poisson's ratio of the C-S-H gel (see Fig. 4.1b and c). For the first step, we consider the volume fraction of portlandite, calcium sulfoaluminates hydrates and clinker equal to 0.35 (which is the mean value of the volume fractions of portlandite, calcium sulfoaluminates hydrates and clinker in Tab. 5.2) and use Eq. (4.5) to back-calculate the long-term viscoelastic Poisson's ratio of the mixture of C-S-H with capillary porosity, as a function of the parameter m_{θ}^{∞} of its interface with portlandite, calcium sulfoaluminates hydrates and clinker. Then, considering the volume fraction of capillary pores equal to 0.21 (which is the mean value of the volume fractions of capillary pores in Tab. 5.2) and using Eq. (4.4), by downscaling we infer the long-term viscoelastic Poisson's ratio ν_{gel}^{∞} of the C-S-H gel. The results are displayed in Fig. 4.4b: the range over which the long-term viscoelastic Poisson's ratio ν_{gel}^{∞} of the C-S-H gel is almost the same as the scatter of the downscaled value, which is visible in Fig. 4.3. Said otherwise: the properties of the interface between portlandite, calcium sulfoaluminates hydrates and clinker on one hand, and the mixture of C-S-H with capillary porosity on the other hand, play a negligible role on the back-calculated value of the long-term viscoelastic Poisson's ratio of the C-S-H gel.

From the calculations performed above, we conclude that 1) the interface between aggregates and cement paste can be considered to be perfectly adhesive, and 2) the interface between portlandite, calcium sulfoaluminates hydrates and clinker on one hand, and the mixture of C-S-H with capillary porosity on the other hand, has little influence on the back-calculated long-term viscoelastic Poisson's ratio of the C-S-H gel. It should be noted that such conclusion is only valid for the long-term values of Poisson's ratio. As

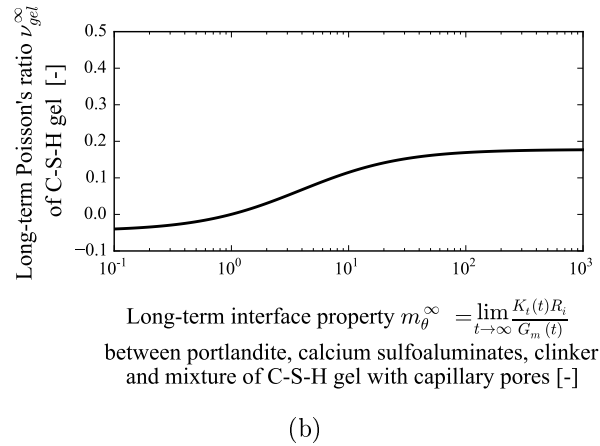
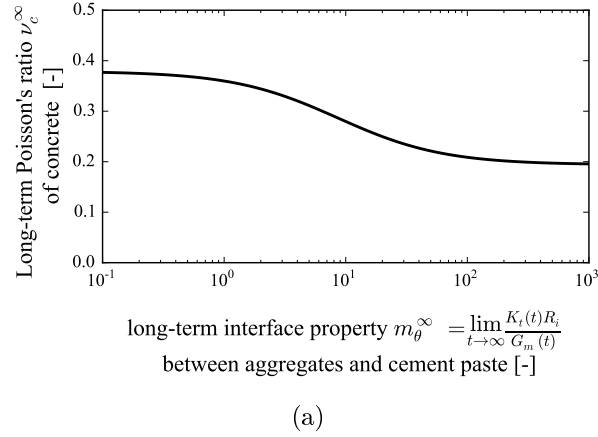


Figure 4.4 – (a) Upscaled long-term viscoelastic Poisson's ratio of concrete as a function of the property of the interface between aggregates and cement paste. (b) Downscaled long-term viscoelastic Poisson's ratio of C-S-H gel as a function of the property of the interface between portlandite, calcium sulfoaluminates hydrates and clinker on one hand, and the mixture of C-S-H with capillary pores on the other hand.

to whether the interface effect can be neglected or not for the whole time-evolution of Poisson's ratio, no information can be obtained from the above study.

4.2.2 Implications for creep mechanism of C-S-H gel at large times

Based on the back-calculated long-term viscoelastic Poisson's ratio of the C-S-H gel, which is found to lie between 0 and 0.18 (see sec. 4.1.3), we aim at inferring some implications for the creep mechanism of the C-S-H gel. In the spirit of the model proposed by Jennings (2000, 2004), we consider the C-S-H gel to be made of nanometer-sized C-S-H particles. Two potential creep mechanisms are considered next: long-term creep of the C-S-H gel is due to 1) creep of the C-S-H particles themselves, or 2) creep of the contact points between neighboring C-S-H particles. Note that those conclusions which will be drawn only hold if we consider that the experimental data at the concrete scale are sufficiently reliable.

Creep of C-S-H gel originating from creep of C-S-H particles

In this section, we consider that creep of the C-S-H gel originates from the creep of the C-S-H particles themselves, and that those particles are perfectly bonded to each other. We adopted the model proposed by Tennis and Jennings (2000); Jennings (2000) for the description of the microstructure of C-S-H gel. The C-S-H gel is composed of individual globules of C-S-H particles, which are stacks of C-S-H layers. The globules form zones of Low Density (LD) C-S-H and zones of High Density (HD) C-S-H, whose gel porosity (volume of gel pores over the sum of the volume of solid hydrates and gel pores) is 0.37 and 0.24, respectively (Tennis and Jennings, 2000). We consider that each globule of C-S-H particle can creep by having its C-S-H layers sliding over each other (see Fig. 4.5a): the shear relaxation modulus associated to this sliding is noted $G_{\text{CSH}}(t)$. In addition, we consider that the distance between solid C-S-H layers could vary over time: the uniaxial relaxation modulus associated to this type of deformation is noted $E_{\text{CSH}}(t)$. At large times, the shear and uniaxial relaxation moduli tend toward G_{CSH}^{∞} and E_{CSH}^{∞} , respectively.

Sanahuja (2008) developed a viscoelastic homogenization scheme for a composite material made of an assembly of transverse isotropic particles ran-

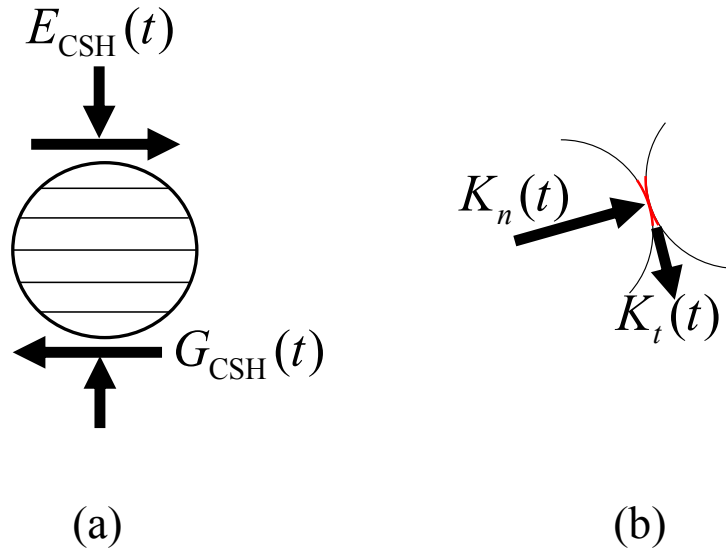


Figure 4.5 – (a) Layered structure of C-S-H particles. (b) Imperfect contact between C-S-H particles.

domly oriented, intermixed with spherical pores. He considered both spherical and aspherical particles. Here we extend his scheme to homogenization of the long-term viscoelastic behavior, again by using the correspondence principle and the final value theorem (Auliac et al., 2000). Thus, we obtain a relationship between long-term viscoelastic Poisson's ratio ν_{gel}^∞ of the C-S-H gel and long-term shear relaxation modulus G_{CSH}^∞ and uniaxial relaxation modulus E_{CSH}^∞ of the C-S-H particles.

For spherical C-S-H particles, we found that the long-term viscoelastic Poisson's ratio ν_{gel}^∞ of the C-S-H gel did not depend much on the gel porosity, in the range of its two extreme values, i.e., 0.24 and 0.37. We display this long-term viscoelastic Poisson's ratio ν_{gel}^∞ of the C-S-H gel in Fig. 4.6a, as a function of the ratio $G_{CSH}^\infty/E_{CSH}^\infty$, for a gel porosity of 0.28. If the ratio $G_{CSH}^\infty/E_{CSH}^\infty$ is equal to 0, i.e., if in the long term C-S-H layers can only slide over each other, the long-term viscoelastic Poisson's ratio of the C-S-H gel must be equal to $\nu_{gel}^\infty = 0.40$, which is not consistent with the experimental results obtained by downscaling and displayed in Fig. 4.3. In contrast, to retrieve the long-term viscoelastic Poisson's ratio ν_{gel}^∞ of the C-S-H gel observed experimentally, which is between -0.07 and 0.16 (see Fig. 4.3), and

if we still consider spherical C-S-H particles, in the long term both sliding of its C-S-H layers over each other and variations of the interlayer distance must occur.

For oblate C-S-H particles with still a gel porosity equal to 0.28, Fig. 4.6a displays the long-term viscoelastic Poisson's ratio of the C-S-H gel, as a function of the ratio $G_{\text{CSH}}^\infty/E_{\text{CSH}}^\infty$, for two aspect ratio: $r_s = 0.12$ (Sanahuja et al., 2007) and $r_s = 0.033$ (Sanahuja et al., 2007). We observe that, in such case, one can retrieve the long-term creep Poisson's ratio of the C-S-H gel observed experimentally, if $G_{\text{CSH}}^\infty/E_{\text{CSH}}^\infty = 0$, i.e., if the C-S-H layers are only allowed to slide over each other, with no variation of the interlayer distance.

In conclusion, if creep of the C-S-H gel is due to creep of the C-S-H particles themselves, evolutions of the viscoelastic Poisson's ratio observed experimentally cannot be explained if one considers that the C-S-H particles are spherical and that they creep by sliding of its C-S-H layers over each other: either the C-S-H particles need to be considered aspherical, or the interlayer distance between neighboring C-S-H layers must be considered to vary in the long term.

Creep of C-S-H gel originating from creep of contact points between neighboring C-S-H particles

In this section, we consider that creep of the C-S-H gel originates from creep of the contact points between C-S-H particles, and that C-S-H particles only deform elastically.

Maalej (2007) developed an elastic homogenization scheme for a composite material made of rigid spherical particles in contact through elastic contact points: to those contact points are associated a normal stiffness K_n and a tangential stiffness K_t (see Fig. 4.5b). In order to predict the viscoelastic behavior of the C-S-H gel here considered, in which contact points are considered viscoelastic, we extend Maalej's scheme to homogenization of the long-term viscoelastic behavior, again by using the correspondence principle and the final value theorem (Auliac et al., 2000). Thus, we obtain a relationship between the long-term viscoelastic Poisson's ratio ν_{gel}^∞ of the C-S-H gel,

its porosity, the long-term asymptotic values K_n^∞ of the normal stiffness and K_t^∞ of the tangential stiffness.

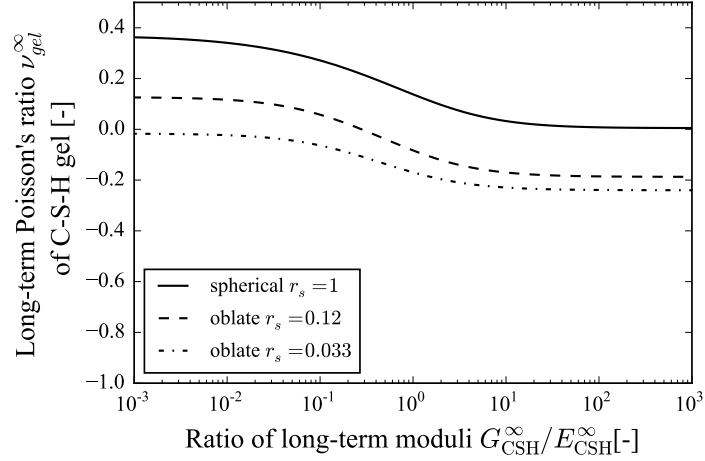
For spherical C-S-H particles and a gel porosity equal to 0.28, the long-term viscoelastic Poisson's ratio ν_{gel}^∞ of the C-S-H gel is displayed in Fig. 4.6b as a function of the ratio K_t^∞/K_n^∞ . If C-S-H particles can only slide over each other, i.e., if $K_t^\infty/K_n^\infty = 0$, the long-term viscoelastic Poisson's ratio of the C-S-H gel is predicted to be equal to 0.33, which is greater than the values observed experimentally, which lay between -0.07 and 0.16 (see Fig. 4.3). Therefore, if creep of the C-S-H gel originates from the creep of the contact points between C-S-H particles, if one considers that C-S-H particles are spherical, he/she cannot consider that C-S-H particles can only slide over each other: in the long term, the C-S-H particles must also be allowed to get closer to each other, i.e., to interpenetrate each other.

We found no homogenization scheme that predicts the elastic behavior of an assembly of rigid particles in contact through elastic contact points, when the particles are considered aspherical. Therefore, we do not know how the conclusions drawn in this section would hold if the assumption of sphericity of the C-S-H particles was relaxed. However, given the results obtained in section 4.2.2, conclusions are likely to significantly differ for aspherical particles. This elastic homogenization problem is difficult from a technical point of view. As a starting point, [Sidhom \(2014\)](#) proposed some bounds on the effective moduli, using energy approaches, but these bounds may not be tight enough to be directly applied to this study.

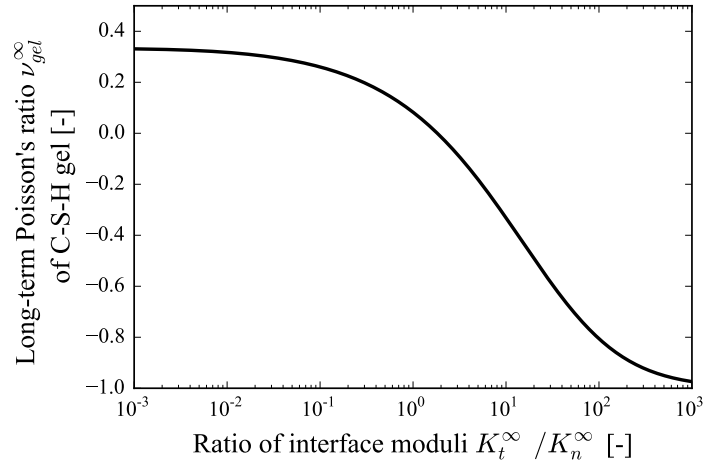
4.3 Conclusions

From the long-term viscoelastic Poisson's ratio of concrete we compute the long-term viscoelastic Poisson's ratio of C-S-H gel by downscaling with the help of elastic homogenization schemes extended to viscoelasticity. Several conclusions can be drawn.

For what concerns downscaling of the viscoelastic Poisson's ratio of concrete, if the aggregates, portlandite, calcium sulfoaluminates hydrates and clinker can be considered as spherical:



(a)



(b)

Figure 4.6 – Long-term viscoelastic Poisson's ratio ν_{gel}^{∞} of C-S-H gel: (a) in the case where creep is due to creep of the C-S-H particles themselves, and (b) in the case where creep is due to creep of contact points between neighboring C-S-H particles.

- The long-term viscoelastic Poisson's ratio of the C-S-H gel has little effect on the long-term viscoelastic Poisson's ratio of concrete.
- The interface between aggregates and cement paste can be considered adhesive for downscaling or upscaling the long-term viscoelastic Poisson's ratio.

- The interface between portlandite, calcium sulfoaluminates hydrates and clinker on one hand, and the mixture of C-S-H with the capillary porosity on the other hand, has little effect on the relation between the viscoelastic Poisson's ratio of concrete and that of the C-S-H gel.

For what concerns creep of the C-S-H gel, if we consider that the experimental data at the concrete scale are sufficiently reliable, downscaling of all experimental results obtained at the scale of concrete shows that:

- The long-term viscoelastic Poisson's ratio of the C-S-H gel is comprised between 0 and 0.2.
- The long-term creep of C-S-H gel in concrete is both deviatoric and volumetric.
- If creep of the C-S-H gel is due to creep of the C-S-H particles themselves, evolutions of the creep Poisson's ratio observed experimentally cannot be explained if one considers that the C-S-H particles are spherical and that they creep by sliding of its C-S-H layers over each other: either the C-S-H particles need to be considered aspherical, or the interlayer distance between neighboring C-S-H layers must be considered to vary in the long term.
- if creep of the C-S-H gel is due to creep of the contact points between C-S-H particles, and if one considers that C-S-H particles are spherical, he/she cannot consider that C-S-H particles can only slide over each other: in the long term, the C-S-H particles must also be allowed to get closer to each other, i.e., to interpenetrate each other.

CHAPTER 4. LONG-TERM VISCOELASTIC POISSON'S RATIO OF
C-S-H GEL

Chapter 5

Is long-term autogenous shrinkage a creep phenomenon induced by capillary effects due to self-desiccation?

LONG-TERM *shrinkage and creep of concrete can impact the lifetime of concrete structures. Basic creep of cementitious materials is now known to be non-asymptotic and evolve logarithmically with time at large times. However, the long-term kinetics of autogenous shrinkage is not systematically analyzed. Here we first aim at finding out how autogenous shrinkage evolves with time at long term. We analyze all experimental data available in the literature and find that autogenous shrinkage evolves logarithmically with respect to time at long term, like basic creep. Then, by considering concrete as a multiscale material, we obtain the bulk creep modulus of the calcium silicate hydrate gel. In the end, we show that the kinetics of long-term autogenous shrinkage can be a viscoelastic response to self-desiccation by comparing the mechanical stress that should be applied to explain this long-term kinetics of autogenous shrinkage with the capillary force due to self-desiccation.*

CHAPTER 5. IS LONG-TERM AUTOGENOUS SHRINKAGE A CREEP PHENOMENON INDUCED BY CAPILLARY EFFECTS DUE TO SELF-DESICCATION?

LE RETRAIT ET FLUAGE à long terme du béton peuvent avoir un impact sur la durée de vie des structures en béton. On sait maintenant que le fluage propre des matériaux cimentaires est non-asymptotique et évolue comme une fonction logarithmique du temps à long terme. Cependant, il n'y pas d'analyse systématique de la cinétique à long terme du retrait endogène dans la littérature. Dans ce chapitre, nous cherchons donc à comprendre comment le retrait endogène évolue au cours du temps à long terme. Nous analysons toutes les données expérimentales disponibles dans la littérature et trouvons que le retrait endogène évolue comme une fonction logarithmique du temps à long terme, de même que le fluage propre. Ensuite, en considérant le béton comme un matériau multi-échelle, nous obtenons le module de fluage volumétrique du gel de silicate de calcium hydraté. Au final, nous montrons que la cinétique du retrait endogène à long terme pourrait être une réponse viscoélastique à l'auto-dessiccation, en comparant la contrainte mécanique qui doit être appliquée pour expliquer cette cinétique à long terme du retrait endogène avec la force capillaire due à l'auto-dessiccation.

5.1 Introduction

Time-dependent behavior (i.e., creep and shrinkage) of cementitious materials has been studied for more than half a century. In most of the shrinkage-creep models (RILEM Technical Committee, 1995; Benboudjema et al., 2007; RILEM Technical Committee, 2015) and engineering design codes (1992-1-1:2005, 2004; ACI Committee 209, 2008; FIB, 2013), the time-dependent strain is decomposed into four components: autogenous shrinkage, basic creep, drying shrinkage and drying creep. In this present chapter, we focus only on autogenous shrinkage and basic creep, i.e., on time-dependent deformations of sealed sample for which drying is not involved.

Both autogenous shrinkage and basic creep are time-dependent strains that are measured on specimens that do not exchange water with its surroundings. Such condition is achieved either by sealing the sample, (e.g., by De Larrard (1990)), or by controlling the relative humidity of the environment to the same relative humidity as that of the sample (e.g., by Gopalakrishnan (1968)). For characterization of time-dependent behavior of cementitious materials under such condition, usually two specimens are needed: one reference specimen which is not loaded and another specimen which is loaded. The time-dependent strain of the reference specimen is called autogenous shrinkage. Basic creep is obtained by subtracting time-dependent strain of the reference specimen from the time-dependent strain of the loaded specimen. Basic creep is the time-dependent strain only due to the mechanical load.

For compressive stresses below 40% of the compressive strength, the basic creep of concrete is non-asymptotic and evolves logarithmically with time at large times (Bazant et al., 2011; Le Roy, 1995; Le Roy et al., 2017). By analyzing viscoelastic Poisson's ratio, we showed in chapter 3 that even the volumetric basic creep of concrete is non asymptotic. At the scale of microindentation and nanoindentation, Zhang et al. (2014); Frech-Baronet et al. (2017) and Vandamme and Ulm (2013) respectively showed that the basic creep of cement paste and of C-S-H gel evolves logarithmically with time after a transient period. In contrast, autogenous shrinkage is sometimes assumed to be

CHAPTER 5. IS LONG-TERM AUTOGENOUS SHRINKAGE A CREEP PHENOMENON INDUCED BY CAPILLARY EFFECTS DUE TO SELF-DESICCATION?

asymptotic (1992-1-1:2005, 2004; FIB, 2013; RILEM Technical Committee, 2015), while some experimental data (e.g. of De Larrard (1990); Mazloom et al. (2004); Brooks and Wainwright (1983); Brooks (1984)) show that autogenous shrinkage evolves logarithmically over time in the long term. For what concerns the modeling of autogenous shrinkage, several authors (Lin and Meyer, 2008; Stefan et al., 2009; Zhang et al., 2012; Wu et al., 2017) considered the autogenous shrinkage as the elastic strain under the action of capillary forces induced by self-desiccation, while others (Hua et al., 1995; Luan et al., 2013) suggested that autogenous shrinkage is the viscoelastic response of cement-based materials to the capillary forces. In comparison, drying shrinkage is modeled as elastic strain (Di Bella et al., 2017) or viscoelastic strain (Benboudjema et al., 2007; Sellier and Buffo-Lacarriere, 2009; Grasley and Leung, 2011; Sellier et al., 2016) under the action of capillary forces induced by desiccation. However, modeling autogenous shrinkage as elastic strain due to self-desiccation can model only asymptotic evolution of autogenous shrinkage at long term as self-desiccation stops at certain time. In any case, no consensus exists regarding the physical origin of autogenous shrinkage. In this chapter, we aim at shedding some light on the physical origin by starting from an exhaustive analysis of data from the literature.

In the first part, we perform an exhaustive analysis of autogenous shrinkage and basic creep data from the literature. Then, by considering concrete as a multi-scale material, we use micromechanics to identify a long-term creep property of the calcium silicate hydrates (C-S-H) gel. In the third part, we discuss if long-term autogenous shrinkage can be explained as a creep phenomenon under the action of capillary force caused by self-desiccation. To do so, we compare the magnitude of in-pore stress necessary to obtain the long-term creep kinetics of autogenous shrinkage with that of capillary forces.

5.2 Analysis of autogenous shrinkage and basic creep data

This section is devoted to analyze experimental data from literature and study the long-term evolution of autogenous shrinkage and basic creep.

5.2.1 Autogenous shrinkage

We selected autogenous shrinkage data from the comprehensive database on concrete creep and shrinkage (Bažant and Li, 2008) compiled by Prof. Bažant and his collaborators. We consider all the experiments that satisfy the following criteria:

- The tested concrete or cement paste is made with ordinary Portland cement, i.e., the cement must be of type CEM I according to Eurocode-2 (1992-1-1:2005, 2004), or of type I to type V according to ASTM (ASTM-C150-C150M-16e1, 2016).
- The tested concrete or cement paste contains no silica fume, fly ashes, filler or slag.
- The autogenous shrinkage must be measured at least until the age of 90 days.

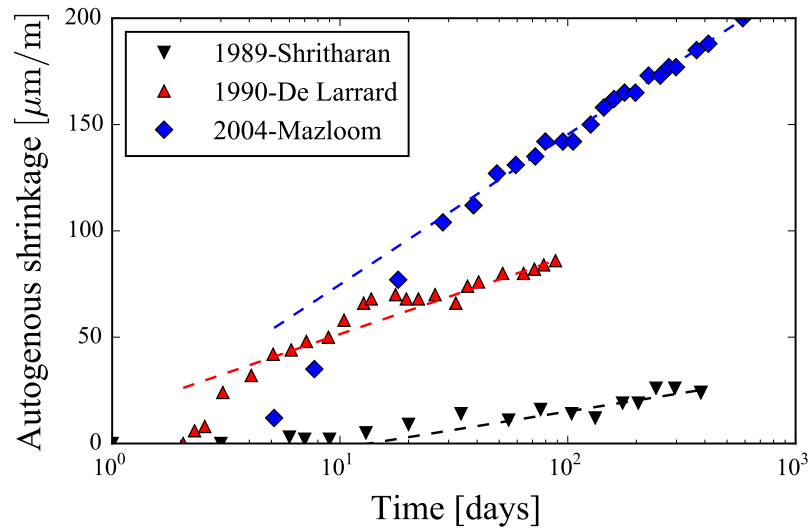
With these criteria, we selected in total 29 tests on concrete and 16 tests on cement paste.

Figure 5.1a shows time evolution of autogenous shrinkage for three representative tests. At large times, autogenous shrinkage evolves linearly with logarithm of time. Such feature was in fact observed for all concretes and cement pastes made with water-to-cement ratio below 0.5. Hence, we fitted the following empirical relation for all of the chosen tests:

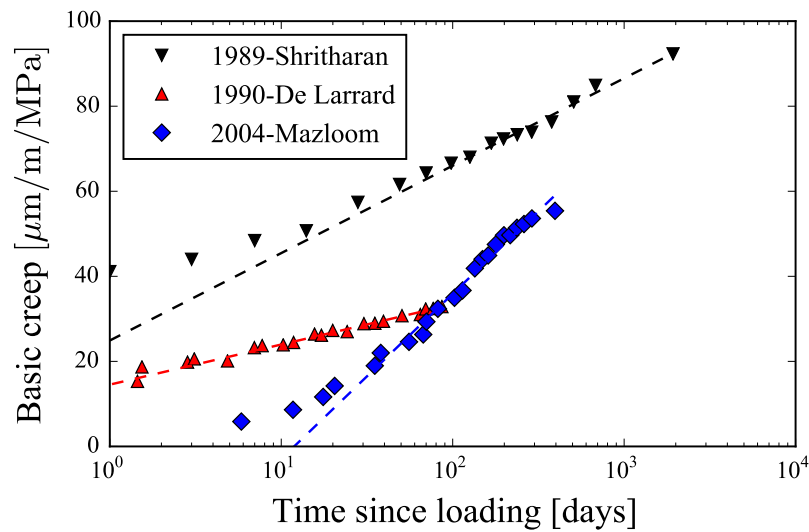
$$\varepsilon_{sh}(t) = \alpha_{sh} \log\left(\frac{t}{\tau_0}\right) + \beta_{sh}, \quad (5.1)$$

to all data points obtained at the age of more than 28 days. In Eq. 5.1, ε_{sh} is the autogenous shrinkage strain, α_{sh} is the slope of autogenous shrinkage

CHAPTER 5. IS LONG-TERM AUTOGENOUS SHRINKAGE A CREEP PHENOMENON INDUCED BY CAPILLARY EFFECTS DUE TO SELF-DESICCATION?



(a)



(b)

Figure 5.1 – (a) Example of autogenous shrinkage data; (b) Example of basic creep data. Data from [Shritharan \(1989\)](#); [De Larrard \(1990\)](#); [Mazloom et al. \(2004\)](#)

displayed versus $\log(t)$, t is age of concrete and $\tau_0 = 1$ day is a reference time. Table 5.1 summarizes the origin of data, mix design properties of concretes and the fitted parameter α_{sh} . For the sake of length, only the data of the

5.2. ANALYSIS OF AUTOGENOUS SHRINKAGE AND BASIC CREEP DATA

Author	File ¹	w/c ²	a/c ³	c ⁴	α_{cr} ⁶
Shritharan (1989)	e_079_06	0.47	5.09	393	7.51
De Larrard (1990)	A_022_05	0.35	3.96	450	15.96
Mazloom (2004)	A_031_02	0.35	3.70	500	30.64

Table 5.1 – Extract of autogenous shrinkage data. ¹File corresponds to the file number in the database compiled by Prof. Bažant and his collaborators (Bažant and Li, 2008); ²w/c: water-to-cement ratio; ³a/c: aggregate-to-cement mass ratio; ⁴c: cement per volume of mixture [kg/m³]; ⁵ α_{sh} : Fitted parameter in Eq. 5.1, [$\mu\text{m}/\text{m}$]

three tests displayed in Fig. 5.1a are given in Tab. 5.2. For the data of all 45 tests used in this study, please see Tabs. E.1 and E.2 in appendix E.

If the autogenous shrinkage can be explained as a creep phenomenon, we should be able to relate the fitted parameter α_{sh} with a stress Σ_h that is necessary to explain the long-term kinetics as following:

$$\Sigma_h = 3\alpha_{sh}C_c^K \quad (5.2)$$

where C_c^K is the bulk creep modulus of concrete which is defined, in a creep test under the stress σ_0 , as the asymptotic value of $\sigma_0/(t d\varepsilon/dt)$ in the long term. Hence, in order to obtain the stress Σ_h that is necessary to explain the long-term kinetics of autogenous shrinkage as a creep phenomenon, we need the bulk creep modulus C_c^K of concrete. In next section, we analyze basic creep data to obtain this parameter.

5.2.2 Basic creep

We selected basic creep data also from the comprehensive database on concrete creep and shrinkage (Bažant and Li, 2008) compiled by Prof. Bažant and his collaborators. We selected all the basic creep data that satisfy the following criteria:

- The tested concrete or cement paste is made with ordinary Portland cement, i.e., the cement must be of type CEM I according to Eurocode-2 (1992-1-1:2005, 2004), or of type I to type V according to ASTM

CHAPTER 5. IS LONG-TERM AUTOGENOUS SHRINKAGE A CREEP PHENOMENON INDUCED BY CAPILLARY EFFECTS DUE TO SELF-DESICCATION?

(ASTM-C150-C150M-16e1, 2016).

- The tested concrete or cement paste contains no silica fume, fly ashes, filler or slag.
- The basic creep must be measured even after 5 times age of loading.
- The applied stress does not exceed 40% of the compressive strength.

With these criteria, we selected in total 59 tests on concrete.

Figure 5.1b shows time evolution of basic creep for three representative tests. At large times, the evolution of basic creep is logarithmic with time for all of the selected tests. Hence, by choosing the data from the time equal to 5 times the age of loading till the end of test, we fitted the following empirical relation to all tests:

$$\varepsilon_{cr}(t) = \frac{1}{C_c^E} \log\left(\frac{t}{\tau_0}\right) + \beta_{cr} \quad (5.3)$$

where ε_{cr} is the specific basic creep strain, $\frac{1}{C_c^E}$ is the slope of basic creep displayed versus $\log(t)$, t is time since loading and $\tau_0 = 1$ day is reference time. The parameter C_c^E is equal to the uniaxial creep modulus of concrete. Table 5.2 summarizes the origin of data, mix design properties of concrete/cement paste, loading age and the fitted parameter $\frac{1}{C_c^E}$. For the sake of length, only the data of the three experiments displayed in Fig. 5.1a are given in Tab. 5.2. For data of all 59 tests used in this study, please see Tabs.F.1 and F.2 in appendix F.

In conclusion, we confirmed that basic creep evolves logarithmically with respect to time at long term. Our analysis of an exhaustive set of data shows that autogenous shrinkage also evolves logarithmically with respect to time at long term.

5.3. DOWNSCALING OF CREEP COMPLIANCE FROM THE SCALE OF CONCRETE TO THE SCALE OF C-S-H GEL

Author	File ¹	w/c ²	a/c ³	c ⁴	t ₀ ⁵	1/C _c ^{E6}
Shritharan (1989)	c_079_08	0.47	5.09	390	14	8.93
De Larrard (1990)	D_022_05	0.35	3.96	450	3	4.10
Mazloom (2004)	D_031_02	0.35	3.70	500	7	16.86

Table 5.2 – Extract of basic creep data. ¹File corresponds to the file number in the database compiled by Prof. Bažant and his collaborators (Bažant and Li, 2008); ²w/c: water-to-cement ratio; ³a/c: aggregate-to-cement mass ratio; ⁴c: cement per volume of mixture [kg/m³]; ⁵t₀: loading age [days]; ⁶1/C_c^E: Fitted parameter in Eq. 5.3, [μm/m/MPa].

5.3 Downscaling of creep compliance from the scale of concrete to the scale of C-S-H gel

The objective of this section is to estimate the long-term creep properties of C-S-H gel from the basic creep data on concrete presented in section 5.2.2. As the creep of concrete evolves logarithmically with respect to time in the long term, we can express the bulk creep compliance of concrete as $J_c^K = 1/K_c^0 + 1/C_c^K \log(1 + t/\tau_c)$, where C_c^K is the bulk creep modulus that characterizes long term kinetics of bulk creep strain.

Aili et al. (2016) showed that the viscoelastic Poisson’s ratio ν_c of concrete remains quite constant and comprised between 0.15 and 0.2. Hence, we take the viscoelastic Poisson’s ratio ν_c as constant and equal to 0.2. Then, making use of the elastic-viscoelastic correspondence principle, we replace in the elastic relation between bulk modulus and uniaxial modulus by s -multiplied Laplace transform of their corresponding parameters. Next, we apply finite value theorem and obtain the relation between the bulk creep modulus C_c^K and the uniaxial creep modulus C_c^E :

$$C_c^E = 3(1 - 2\nu_c)C_c^K \quad (5.4)$$

where ν_c is the viscoelastic Poisson’s ratio of concrete. The objective is to relate this bulk creep modulus C_c^K of concrete to the bulk creep modulus C_{gel}^K of the C-S-H gel.

We first present the multi-scale scheme of concrete that we are going to

use throughout the whole chapter. Then, we derive some theoretical result by adapting some elastic homogenization schemes to viscoelastic case via the correspondence principle (Christensen, 1982). In the end, we apply the derived equations to relate the bulk creep modulus C_c^K of concrete to bulk creep modulus C_{gel}^K of C-S-H gel.

5.3.1 Multiscale model for concrete

Concrete can be regarded as a multiscale composite material at three different scales, which are displayed in Fig. 5.2:

- At the largest scale of concrete (see Fig. 5.2a), the aggregates are considered as spherical inclusions that do not creep and are embedded into a matrix made of cement paste, which creeps.
- At a scale below, i.e., at the scale of the cement paste (see Fig. 5.2b), portlandite, calcium sulfoaluminate hydrates and the unhydrated clinker are considered as spherical inclusions that do not creep and are embedded into a matrix made of a mixture of C-S-H with capillary pores. This mixture is considered to creep.
- At another scale below (see Fig. 5.2c), the mixture of C-S-H with capillary pores is considered to be a matrix of C-S-H gel (that contains the gel porosity) that surrounds spherical capillary pores.

As explained before, here we take viscoelastic Poisson's ratios of concrete (Fig. 5.2a) equal to 0.2. Using the results displayed in Figs 4.2a and 4.2b, we can also take the viscoelastic Poisson's ratio of cement paste (Fig. 5.2b), of the mixture of C-S-H gel and capillary pores (Fig. 5.2c) and of C-S-H gel as constant, equal to 0.2.

5.3.2 Theoretical derivation

We consider a composite made of a matrix that embeds spherical inclusions. Given the microstructure, we employ the Mori-Tanaka scheme (Mori and

5.3. DOWNSCALING OF CREEP COMPLIANCE FROM THE SCALE OF CONCRETE TO THE SCALE OF C-S-H GEL

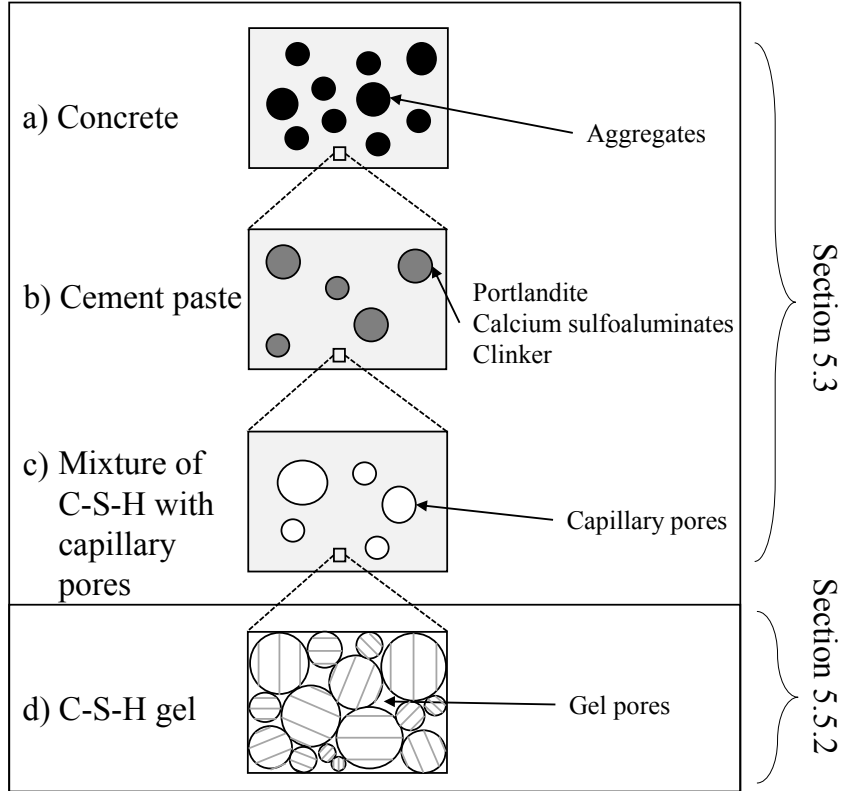


Figure 5.2 – Multiscale structure of concrete: (a) Concrete as a matrix of cement paste embedding aggregates, (b) cement paste as portlandite, calcium sulfoaluminates hydrates and unhydrated clinker embedded into a matrix made of a mixture of C-S-H with capillary pores, (c) mixture of C-S-H with capillary pores as a matrix of C-S-H gel surrounding capillary porosity, and (d) C-S-H gel as a mixture of C-S-H particles and gel pores. The scales (a) (b) (c) are considered in Sec. 5.3.1 for the downscaling of the creep modulus, while the scale (d) is considered in Sec. 5.5.2 for estimating the Biot coefficient of the mixture of C-S-H gel with capillary pores.

(Tanaka, 1973; Zaoui, 1999) to calculate the properties of the composite as a function of the properties of each phases (i.e., the matrix and inclusion). The interface between inclusion and matrix is considered to be perfectly adhesive. The viscoelastic Poisson's ratio ν_m of matrix is constant and equal to 0.2. Applying the correspondence principle (Christensen, 1982) to the elastic Mori-Tanaka homogenization scheme, making use of the fact that $\nu_m = 0.2$, replacing the elastic parameters by the s -multiplied Laplace transform of

CHAPTER 5. IS LONG-TERM AUTOGENOUS SHRINKAGE A CREEP PHENOMENON INDUCED BY CAPILLARY EFFECTS DUE TO SELF-DESICCATION?

their corresponding viscoelastic parameters, we get the viscoelastic homogenization scheme in the Laplace domain:

$$\widehat{K}_{com} = \frac{\widehat{K}_m(1 - f_i) + \widehat{K}_i(1 + f_i)}{\widehat{K}_m(1 + f_i) + \widehat{K}_i(1 - f_i)} \widehat{K}_m \quad (5.5)$$

where f_i is the volume fraction of inclusions; K_m , K_i and K_{com} are the viscoelastic bulk relaxation modulus of the matrix, of the inclusion and of the composite, respectively. \widehat{g} is the Laplace transform of the function g .

These bulk relaxation moduli K_j are related to bulk creep compliances J_j^K through:

$$s\widehat{J}_j^K = \frac{1}{s\widehat{K}_j} \quad (5.6)$$

where s is the Laplace variable, $j = m, i, com$ represents matrix, inclusion and composite, respectively.

We suppose that the bulk creep compliances J_j^K evolve logarithmically with respect to time at large times and can be expressed as $J_j^K = 1/K_j^0 + 1/C_j^K \log(1 + t/\tau_j)$, where $j = m, i, com$ and C_j^K is the bulk creep modulus. By using final value theorem (Auliac et al., 2000) and Laplace transform of a derivative, we obtain the following relation between the bulk creep modulus C_j^K and the Laplace transform of bulk relaxation modulus \widehat{J}_j^K :

$$\begin{aligned} \frac{1}{C_j^K} &= \lim_{t \rightarrow \infty} t\dot{J}_j^K = \lim_{s \rightarrow 0} s \left(t\widehat{J}_j^K \right) = \lim_{s \rightarrow 0} \left(-s \frac{d}{ds} \left(\widehat{J}_j^K \right) \right) \\ &= \lim_{s \rightarrow 0} \left(-s \frac{d}{ds} \left(s\widehat{J}_j^K - J_j^K|_{t=0} \right) \right) = \lim_{s \rightarrow 0} \left(-s \frac{d}{ds} \left(s\widehat{J}_j^K \right) \right) \end{aligned} \quad (5.7)$$

where \dot{g} is the derivative of the function g with respect to time. Equation 5.7 means that $d(s\widehat{J}_j^K)/ds$ can be approximated by $-1/sC_j^K$ for small s , from which follows that \widehat{J}_j^K can be approximated by $-\log(s)/C_j^K s$ for small s :

$$\widehat{J}_j^K \approx -\log(s)/C_j^K s, \text{ for } s \rightarrow 0 \quad (5.8)$$

Using the final value theorem (Auliac et al., 2000), letting $s \rightarrow 0$ in Eq. 5.5

5.3. DOWNSCALING OF CREEP COMPLIANCE FROM THE SCALE OF CONCRETE TO THE SCALE OF C-S-H GEL

and combining with Eqs. 5.8 and 5.6, we obtain:

$$C_{com}^K = \frac{C_m^K(1 - f_i) + C_i^K(1 + f_i)}{C_m^K(1 + f_i) + C_i^K(1 - f_i)} C_m^K \quad (5.9)$$

which make it possible to relate the bulk creep modulus C_{com}^K of the composite with that of its constituents.

We consider the following two cases:

- Case 1: Composite made of matrix embedding non-creeping inclusions. The matrix is considered to creep logarithmically with respect to time in the long term. The long-term volumetric creep kinetics of the matrix is characterized by its creep modulus C_m^K . Letting $C_m^K/C_i^K \rightarrow 0$, equation 5.9 yields:

$$C_{com}^K = \frac{1 + f_i}{1 - f_i} C_m^K \quad (5.10)$$

- Case 2: Porous composite made of a matrix embedding spherical pores. Letting $C_i^K/C_m^K \rightarrow 0$, equation 5.9 yields:

$$C_{com}^K = \frac{1 - f_i}{1 + f_i} C_m^K \quad (5.11)$$

5.3.3 From concrete to C-S-H gel

In this section, we derive a relation between the bulk creep modulus C_c^K of concrete and C_{gel}^K of the C-S-H gel, by performing three steps of downscaling following the multi-scale scheme displayed in Fig. 5.2.

- To relate the bulk creep modulus C_c^K of concrete to the bulk creep modulus of C_p^K of cement paste (Fig. 5.2a), we apply Eq. 5.10.
- To relate the bulk creep modulus C_p^K of cement paste to the bulk creep modulus C_{mix}^K of the mixture of C-S-H gel with capillary pores (Fig. 5.2b), we apply again Eq. 5.10.

CHAPTER 5. IS LONG-TERM AUTOGENOUS SHRINKAGE A
 CREEP PHENOMENON INDUCED BY CAPILLARY EFFECTS DUE
 TO SELF-DESICCATION?

- To relate the bulk creep modulus C_{mix}^K of the mixture of C-S-H gel with capillary pores to the bulk creep modulus C_{gel}^K of the C-S-H gel (Fig. 5.2c), we apply Eq. 5.11.

with these three steps of downscaling, we obtain:

$$C_c^K = \left(\frac{1 + f_a}{1 - f_a} \right) \left(\frac{1 + f_b}{1 - f_b} \right) \left(\frac{1 - \phi_c}{1 + \phi_c} \right) C_{gel}^K \quad (5.12)$$

where f_a is the volume fraction of aggregates (counted with respect to the volume of concrete); f_b is the volume fraction of portlandite, calcium sulfoaluminates and unhydrated clinker (counted with respect to the volume of cement paste); ϕ_c is the volume fraction of the capillary porosity (counted with respect to the volume of the mixture of C-S-H gel with capillary pores).

Combing Eqs. 5.12 and. 5.4, we obtain:

$$C_{gel}^K = \left(\frac{1 - f_a}{1 + f_a} \right) \left(\frac{1 - f_b}{1 + f_b} \right) \left(\frac{1 + \phi_c}{1 - \phi_c} \right) \frac{1}{3(1 - 2\nu_c)} C_c^E \quad (5.13)$$

This equation makes it possible to compute the bulk creep modulus C_{gel}^K of the C-S-H gel from the uniaxial creep modulus C_c^E obtained from the analysis of basic creep data, as long as the microstructural parameters f_a , f_b and ϕ_c are known.

To determine the microstructural parameters f_a , f_b and ϕ_c , we use followings:

- The volume fraction f_a of aggregates in concrete, is computed from the mix design properties of concrete: $f_a = 1 - c/\rho_c - c \times w/c/\rho_w$, where c and w/c are mass of clinker per volume of mixture and the water-to-cement mass ratio, $\rho_c = 3.15g/cm^3$ and $\rho_w = 1g/cm^3$ are the density of cement and of water, respectively.
- The volume fraction f_b of portlandite, calcium sulfoaluminates and unhydrated clinker (counted with respect to the volume of the cement paste), is the sum of the volume fraction of portlandite, of calcium sulfoaluminates and of unhydrated clinker. Each of them is computed by using Powers' model (Powers and Brownyard, 1947; Taylor, 1997),

5.3. DOWNSCALING OF CREEP COMPLIANCE FROM THE SCALE OF CONCRETE TO THE SCALE OF C-S-H GEL

which considers that the volume of cement paste is composed of bulk hydrates (i.e., solid hydrates plus gel pores), unhydrated clinker, and capillary pores. The long-term hydration degree ξ^∞ of the sample is taken to be equal to $\xi^\infty = 1 - \exp(-3.3w/c)$ (Waller, 1999). The volume fraction of bulk hydrates per unit volume of cement paste is $2.12(1-p)\alpha^\infty$, where $p = (w/c)/(w/c + \rho_w/\rho_c)$. The volume of portlandite per unit volume of bulk hydrates is estimated to be equal to 25%, which is a typical value for CEM I cement pastes (Mehta and Monteiro, 2006). Then, the volume fraction of portlandite (counted with respect to the volume of cement paste) is $0.53(1-p)\xi^\infty$. The volume of calcium sulfoaluminates hydrates per unit volume of bulk hydrates is estimated to be equal to 15% (Mehta and Monteiro, 2006), from which the volume fraction of sulfoaluminates hydrates (counted with respect to the volume of cement paste) reads $0.32(1-p)\xi^\infty$. The volume fraction of unhydrated clinker (still counted with respect to the volume of cement paste) is estimated also with Powers' model (Powers and Brownyard, 1947; Taylor, 1997) to be equal to $(1-p)(1-\xi^\infty)$. Therefore, volume fraction f_b of portlandite, calcium sulfoaluminates and unhydrated clinker (counted with respect to the volume of the cement paste) is $f_b = 0.85(1-p)\xi^\infty + (1-p)(1-\xi^\infty)$.

- The volume fraction ϕ_c of capillary porosity with respect to the volume of the mixture of C-S-H gel with capillary pores, is also computed by using Powers' model (Powers and Brownyard, 1947; Taylor, 1997). The volume fraction of capillary pores counted with respect to the volume of cement paste is estimated as $p - 1.12(1-p)\xi^\infty$. The volume fraction of the mixture of C-S-H gel with capillary pores (counted with respect to the volume of cement paste) is equal to $1 - f_b$. Hence, the capillary porosity ϕ_c (i.e., volume fraction of the capillary pores counted with respect to the volume of the mixture of C-S-H gel with capillary pores) is equal to $(p - 1.12(1-p)\xi^\infty)/(1 - f_b)$.

Inserting the uniaxial creep modulus C_c^E from Tab. 5.2, and the above-calculated microstructural parameters f_a , f_b and ϕ_c into Eq. 5.12, we ob-

CHAPTER 5. IS LONG-TERM AUTOGENOUS SHRINKAGE A CREEP PHENOMENON INDUCED BY CAPILLARY EFFECTS DUE TO SELF-DESICCATION?

tain the bulk creep modulus C_{gel}^K of C-S-H gel. The results are displayed in Fig. 5.3. The bulk creep modulus C_{gel}^K of C-S-H gel does not exhibit any specific trend with water-to-cement ratio. Its mean value is 13GPa.

The value of 13 GPa is lower than that obtained by Zhang (2014); Frech-Baronet et al. (2017), who measured contact creep modulus as a function of relative humidity. By downscaling their results as done here, we found that the mean value of the bulk creep modulus is constant around 32GPa for relative humidities over 75%. Flatt et al. (2011) showed that the relative humidity under autogenous condition remains beyond 80%, from which follows that the bulk creep moduli displayed in Fig. 5.3 should be comparable with those downscaled from the measurements of Zhang (2014); Frech-Baronet et al. (2017).

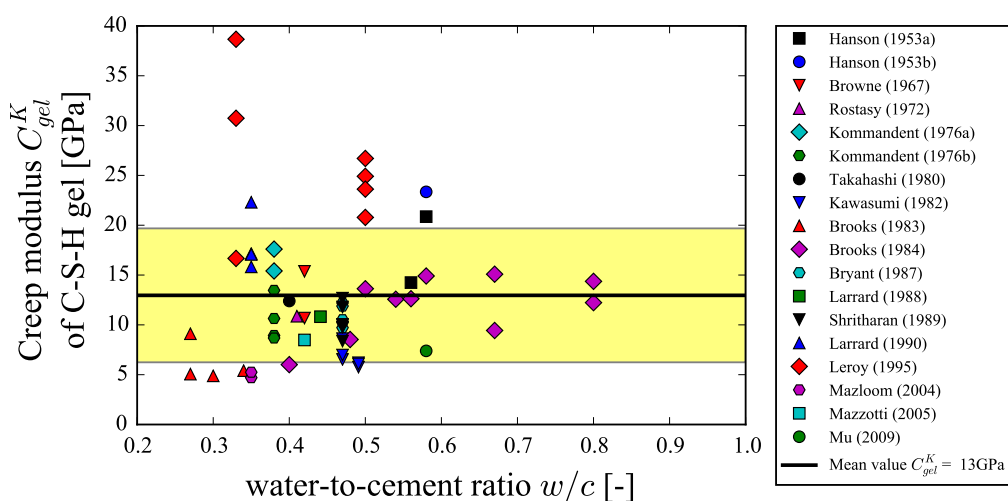


Figure 5.3 – Bulk creep modulus as a function water-to-cement ratio, computed from basic creep data in Hanson (1953); Browne (1967); Rostasy et al. (1973); Kommendant et al. (1976); Takahashi and Kawaguchi (1980); Kawasumi et al. (1982); Brooks (1984); Brooks and Wainwright (1983); Bryant and Vadhanavikkit (1987); De Larrard (1988); Shriitharan (1989); De Larrard (1990); Le Roy (1995); Mazloom et al. (2004); Mazzotti et al. (2005); Mu et al. (2009)

5.4 In-pore stress necessary to explain long-term kinetics of autogenous shrinkage

This section aims at testing the following hypothesis: may capillary forces due to self-desiccation be the driving force of the long-term kinetics of autogenous shrinkage? To do so, we compare the in-pore stress necessary to explain long-term kinetics of autogenous shrinkage with the capillary stress induced by self-desiccation of concrete under autogenous condition. In this section, we compute the in-pore mechanical stress σ_h that should act on the mixture of C-S-H gel with capillary pores to explain the long-term kinetics characterized by α_{sh} . The next section is devoted to compute the capillary stress due to self-desiccation.

We compute first the mechanical stress Σ_h that should act on concrete to explain the long-term kinetics of autogenous shrinkage, which was captured through the fitted parameter α_{sh} (see Tab. 5.1), using Eq. 5.2.

Then, we downscale the stress Σ_h to the scale of the C-S-H gel to which stress it may correspond. To do so, we perform two steps of downscaling. The two steps are the same as the first two steps of downscaling scheme that is described in section 5.3.1.

In each step, we are dealing with a composite made of a matrix that creeps with no asymptote and of spherical inclusions that do not creep. The matrix is subjected to a stress $\underline{\underline{\sigma}}$. We aim at computing an equivalent macroscopic stress $\underline{\underline{\Sigma}}$ that should act on the composite to obtain an identical strain response (Zaoui, 1999; Pichler et al., 2007).

In elastic case, the macroscopic stress reads:

$$\underline{\underline{\Sigma}} = (1 - f_i)\underline{\underline{\sigma}} : \langle \underline{\underline{A}} \rangle_m \quad (5.14)$$

where f_i is the volume fraction of inclusion; $\underline{\underline{A}}$ is the 4th order strain localization tensor; $\langle g \rangle_m$ is the mean value of the parameter g on the matrix domain. For an isotropic stress $\underline{\underline{\sigma}} = \sigma \underline{\underline{1}}$ where $\underline{\underline{1}}$ is the identity tensor (hence, $\underline{\underline{\Sigma}} = \Sigma \underline{\underline{1}}$), Eq. 5.14 can be simplified to scalar form by taking the spherical part A_i^{sph} of the localization tensor $\underline{\underline{A}}$ of inclusion in Mori-Tanaka's scheme

CHAPTER 5. IS LONG-TERM AUTOGENOUS SHRINKAGE A
 CREEP PHENOMENON INDUCED BY CAPILLARY EFFECTS DUE
 TO SELF-DESICCATION?

(Zaoui, 1999):

$$\Sigma = (1 - f_i)\sigma \left(\frac{1 - f_i A_i^{sph}}{1 - f_i} \right) = \frac{\left(1 + \frac{\alpha_m}{K_m} (K_i - K_m) \right) (1 - f_i)}{1 + \frac{\alpha_m}{K_m} (K_i - K_m) (1 - f_i)} \sigma \quad (5.15)$$

where $\alpha_m = 3K_m/(3K_m + 4G_m)$, for $\nu_m = 0.2$, we obtain $\alpha = 1/2$.

In viscoelastic case with the viscoelastic Poisson's ratio of the matrix $\nu_m(t) = 2$, using the elastic-viscoelastic correspondence principle, we replace all the elastic parameters in Eq. 5.15 by the s -multiplied Laplace transform of their corresponding viscoelastic parameters. Then, considering that at long term, the inclusion is much more rigid than the matrix, i.e., $K_i^\infty \gg K_m^\infty$, we use final value theorem and obtain:

$$\Sigma^\infty = \sigma^\infty \quad (5.16)$$

In two steps downscaling from the scale of concrete to the scale of the mixture of C-S-H gel with capillary pores, we use Eq. 5.16 twice. The in-pore stress Σ_h that should act on concrete to explain long-term kinetics of autogenous shrinkage corresponds to a stress $\sigma_h = \Sigma_h$ act on the mixture of C-S-H gel with capillary pores. Hence, combing Eqs. 5.2 and 5.12, we can relate this stress σ_h to the fitted parameter α_{sh} via the bulk creep modulus C_{gel}^K of the C-S-H gel:

$$\sigma_h = 3\alpha_{sh} C_{gel}^K \left(\frac{1 + f_a}{1 - f_a} \right) \left(\frac{1 + f_b}{1 - f_b} \right) \left(\frac{1 - \phi_c}{1 + \phi_c} \right) \quad (5.17)$$

This equation provides the mechanical stress σ_h that must act in the capillary pore system at the scale of the mixture of C-S-H gel with capillary pores to explain the long-term logarithmic kinetics of autogenous shrinkage, characterized by the parameter α_{sh} . For all autogenous shrinkage experiments considered in section 5.2.1, we compute the mechanical stress σ_h and display σ_h as a function of water-to-cement ratio in Fig. 5.6. This stress σ_h is going to be compared with the capillary forces due to self-desiccation in the next section.

5.5 Capillary stress due to self-desiccation

In this section, we first analyze experimental data that measure evolution of relative humidity under autogenous conditions in order to characterize the self desiccation. Then, making use of Power's hydration model (Powers and Brownyard, 1947) and theory of poromechanics (Coussy, 2011), we estimate capillary stress due to self-desiccation. By comparing this capillary stress with the mechanical stress σ_h , we check the hypothesis: may capillary forces due to self-desiccation be the driving force of the long-term kinetics of autogenous shrinkage?

5.5.1 Self-desiccation of cementitious materials

Hydration of cement is a water-consuming process. In sealed conditions, i.e., in absence of any external water supply, consumption of water desaturates the cement paste as the porosity decreases less slowly than the quantity of water. As a result, the relative humidity inside of cement paste (Jensen, 1995) decreases. Flatt et al. (2011) showed that hydration stops below a certain relative humidity. On the other hand, Jensen (1995) showed that the self-desiccation is limited by thermodynamics. Thus, we expect that under autogenous condition the relative humidity reaches an equilibrium value when hydration stops. The objective of this section is to relate this relative humidity at equilibrium to the water-to-cement ratio of the concrete or the cement paste.

Baroghel-Bouny (1994); Jensen and Hansen (1996, 1999); Persson (1997); Yssorche-Cubaynes and Ollivier (1999); Zhutovsky and Kovler (2013); Wyrzykowski and Lura (2016) measured relative humidity inside concrete or cement paste under autogenous conditions as a function of age. In addition, we have measured the evolution of the relative humidity of a cement paste (see appendix H). For each of these tests, author, year, water-to-cement ratio and duration of test are summarized in Tab. 5.3.

As the relative humidity stabilize at a certain value, we propose the following simple empirical relation for the evolution of relative humidity over

CHAPTER 5. IS LONG-TERM AUTOGENOUS SHRINKAGE A
 CREEP PHENOMENON INDUCED BY CAPILLARY EFFECTS DUE
 TO SELF-DESICCATION?

Author	w/c ¹ [-]	τ_T ² [days]	h_r^∞ ³ [-]	τ_{h_r} ⁴ [days]
Baroghel-Bouny (1991)	0.35	800	0.87	237
Baroghel-Bouny (1991)	0.49	365	0.94	52
Jensen (1996)	0.30	1	0.89	0.12
Jensen (1996)	0.35	14	0.93	0.71
Persson (1997)	0.25	450	0.76	40
Persson (1997)	0.33	450	0.82	62
Persson (1997)	0.47	450	0.88	135
Persson (1997)	0.58	450	0.94	98
Yssorche (1999)	0.33	365	0.84	15.24
Yssorche (1999)	0.44	365	0.90	0.95
Yssorche (1999)	0.59	365	0.99	0.57
Yssorche (1999)	0.75	337	0.99	0.06
Zhutovsky (2013)	0.21	7	0.81	0.44
Zhutovsky (2013)	0.25	7	0.84	0.61
Zhutovsky (2013)	0.33	7	0.86	0.62
Wyrzykowski (2016)	0.21	7	0.78	4
Wyrzykowski (2016)	0.24	7	0.79	5
Wyrzykowski (2016)	0.30	7	0.83	5
Wyrzykowski (2016)	0.35	7	0.88	4
Aili (see appendix H)	0.52	127	0.90	10

Table 5.3 – Summary of experimental data of evolution of relative humidity with respect to time under autogenous condition, and of the fitted parameters. Data from Baroghel-Bouny (1994); Jensen and Hansen (1996, 1999); Persson (1997); Yssorche-Cubaynes and Ollivier (1999); Zhutovsky and Kovler (2013); Wyrzykowski and Lura (2016) and appendix H. ¹w/c: water-to-cement ratio; ² τ_T : the duration of the test; ³ h_r^∞ : fitted parameter with Eq. 5.18, corresponding to the long-term relative humidity under autogenous conditions; ⁴ τ_{h_r} : fitted parameter with Eq. 5.18.

time under autogenous condition:

$$h_r(t) = h_r^\infty + (1 - h_r^\infty) \exp\left(-\frac{t}{\tau_{h_r}}\right) \quad (5.18)$$

where h_r^∞ and τ_{h_r} are fitted parameters, which depend on the water-to-cement ratio and correspond to the long-term relative humidity and to a characteristic time, respectively. For the sake of simplicity, in Fig. 5.4 we present only the experimental measure of Baroghel-Bouny (1994) and the corresponding fit with Eq. 5.18. However, we have analyzed a set of 20 experiments, see Fig. G.1 in appendix G.

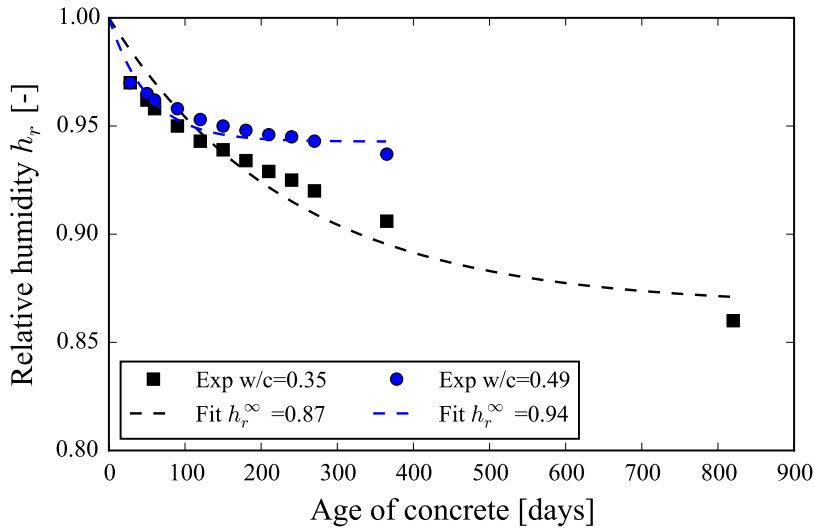


Figure 5.4 – Evolution of relative humidity under autogenous condition, data retrieved from Baroghel-Bouny (1994).

As we are interested in long-term kinetics of autogenous shrinkage, we listed the long-term relative humidity h_r^∞ in Tab. 5.3 and again plotted them against water-to-cement ratio in Fig. 5.5. From Fig. 5.5, we can see that the long-term relative humidity h_r^∞ for a concrete with water-to-cement ratio

CHAPTER 5. IS LONG-TERM AUTOGENOUS SHRINKAGE A CREEP PHENOMENON INDUCED BY CAPILLARY EFFECTS DUE TO SELF-DESICCATION?

w/c will be in between Eq. 5.19 and Eq. 5.20:

$$\text{Upper bound for } h_r^\infty : \begin{cases} 1 - (0.4 - w/c), & \text{if } w/c < 0.4, \\ 1, & \text{otherwise.} \end{cases} \quad (5.19)$$

$$\text{Lower bound for } h_r^\infty : \begin{cases} 1 - 0.45(0.75 - w/c), & \text{if } w/c < 0.75, \\ 1, & \text{otherwise.} \end{cases} \quad (5.20)$$

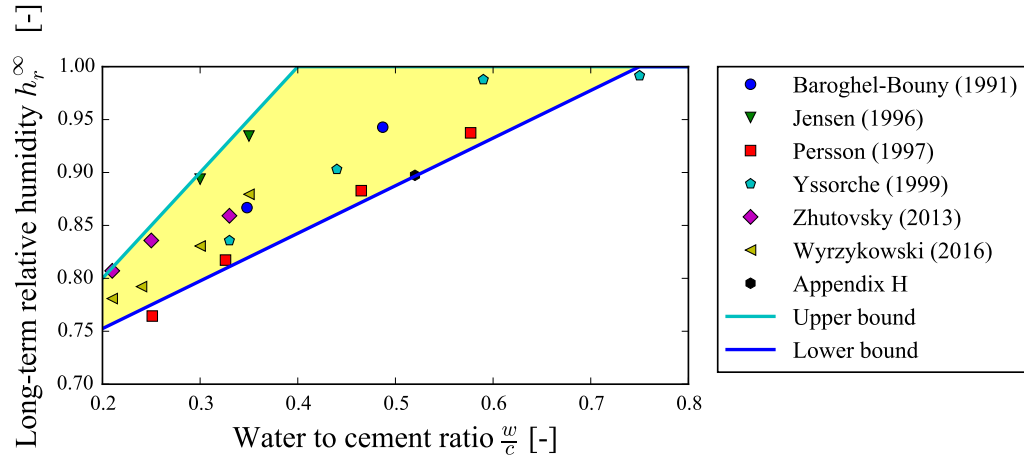


Figure 5.5 – Long-term relative humidity under autogenous condition as a function water-to-cement ratio, computed from experimental data in Baroghel-Bouny (1994); Jensen and Hansen (1996, 1999); Persson (1997); Yssorche-Cubaynes and Ollivier (1999); Zhutovsky and Kovler (2013); Wyrzykowski and Lura (2016) and in appendix H.

5.5.2 Estimation of capillary force

Knowing the relative humidity h_r^∞ at long term under autogenous conditions, we compute the long-term capillary pressure by using Kelvin's law (Coussy, 2011):

$$P_c = \frac{\rho_w RT}{M_w} \log(h_r^\infty) \quad (5.21)$$

$R = 8.314 \text{ J} \cdot \text{K}^{-1} \cdot \text{mol}^{-1}$, T and $M_w = 18 \text{ g/mol}$ are ideal gas constant, the absolute temperature and molar mass of water.

The saturation degree S_l (i.e., the volume fraction of the capillary and gel pores spaces that is occupied with liquid water with respect to the total volume of capillary and gel pores) is computed from Power's model as following: For a given volume V of cement paste, the volume V_p of total pore space is equal to total volume minus the volume $0.53(1-p)\xi^\infty V$ of portlandite, $0.32(1-p)\xi^\infty V$ of calcium sulfoaluminate, $(1-p)(1-\xi^\infty)V$ of clinker and $V_{\text{CSH}} = 1.52(1-p)(1-\alpha^\infty)V$ of C-S-H solid (i.e., C-S-H without its gel porosity). The volume of chemical shrinkage is equal to $V_{cs} = 0.20(1-p)\xi^\infty V$. The saturation degree S_l is then get by:

$$S_l = 1 - \frac{V_{cs}}{V_p} = \frac{p - 0.72(1-p)\alpha^\infty}{p - 0.52(1-p)\alpha^\infty} \quad (5.22)$$

The Biot coefficient is computed by two steps of upscaling:

- In the first step, at the scale of the C-S-H gel, we compute the porosity of C-S-H gel as mean value of the porosity of high-density C-S-H and low-density C-S-H: considering that 40% of C-S-H gel is high-density C-S-H with porosity 0.24, and the other 60% is low-density C-S-H with porosity 0.37 (Jennings, 2000), the mean porosity of C-S-H gel is estimated to be equal to $\phi_{gel} = 0.32$. Considering that the C-S-H gel is composed from spherical C-S-H particles and gel pores, we apply the self-consistent homogenization scheme and use the expression of the Biot coefficient developed by Ghabezloo (2010).

In elastic case, assuming the Poisson's ratio of the C-S-H gel equal to 0.2 (see section 5.3.1), we obtain the Biot coefficient of C-S-H gel:

$$b_{gel} = 2\phi_{gel} \quad (5.23)$$

In viscoelastic case, using the elastic-viscoelastic correspondence principle, we replace the elastic parameters in Eq. 5.23 with the s -multiplied Laplace transform of their corresponding viscoelastic parameters. At long term, we consider that the microstructure of material remains

CHAPTER 5. IS LONG-TERM AUTOGENOUS SHRINKAGE A CREEP PHENOMENON INDUCED BY CAPILLARY EFFECTS DUE TO SELF-DESICCATION?

constant, from which follows that the gel porosity ϕ_{gel} is constant over time. As a result, we can easily transform back the relation in the Laplace domain to real time. Hence, Eq. 5.23 holds true for viscoelastic case, under the hypothesis that the viscoelastic Poisson's ratio of the C-S-H gel is constant and equal to 0.2.

- In the second step, at the scale of the mixture of C-S-H gel with capillary pores (Fig. 5.2c), we consider the Biot coefficient of a composite made from porous matrix (i.e., C-S-H gel) and capillary pores. As done previous step, in elastic case, assuming the Poisson's ratio of the C-S-H gel equal to 0.2 (see section 5.3.1), making use of the derivations in Ghabezloo (2010), we apply the Mori-Tanaka's homogenization scheme and obtain the Biot coefficient b of the mixture of C-S-H gel with capillary pores:

$$b = 1 - \frac{1 - \phi_c}{1 + \phi_c}(1 - b_{gel}) \quad (5.24)$$

In viscoelastic case, using the elastic-viscoelastic correspondence principle, we replace the elastic parameters in Eq. 5.24 with the s -multiplied Laplace transform of their corresponding viscoelastic parameters. At long term, we consider that the microstructure of material remains constant, from which follows that the capillary porosity ϕ_c is constant over time. As a result, we can easily transform back the relation in the Laplace domain to real time. Hence, Eq. 5.24 holds true for viscoelastic case, under the hypothesis that the viscoelastic Poisson's ratio of the C-S-H gel is constant and equal to 0.2.

Knowing the capillary pressure P_c , the saturation degree S_l and the Biot coefficient b , the mechanical stress due to capillary force acting on the mixture of capillary pores with C-S-H gel is estimated as bS_lP_c according to the theory of poromechanics (Coussy, 2011).

Figure 5.6 compares the mechanical stress due to capillary force bS_lP_c , act on the mixture of C-S-H gel and capillary pores, with the mechanical stress σ_h that should act to explain the long-term kinetics of autogenous

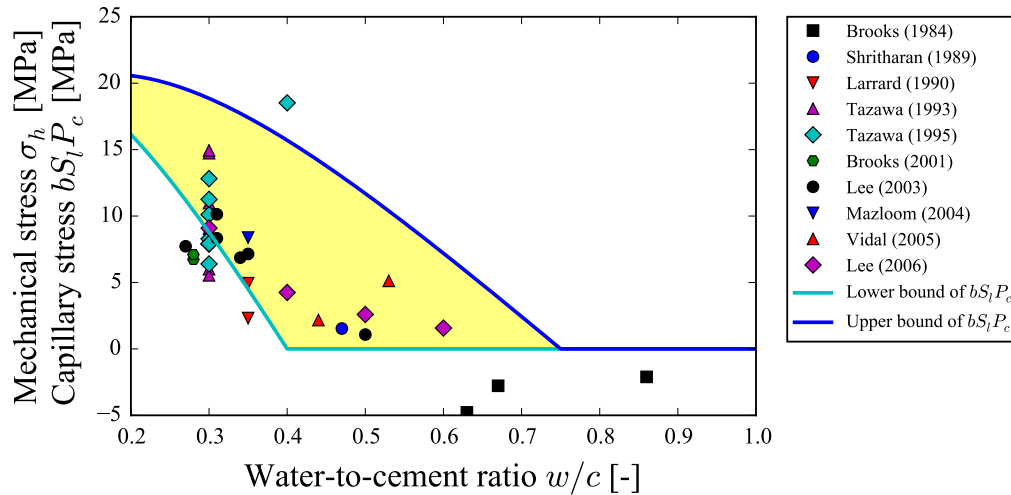


Figure 5.6 – Mechanical stress σ_h that should act on the mixture of C-S-H gel displayed together with capillary pores to explain the long-term kinetics of autogenous shrinkage of data in Brooks (1984); Shritharan (1989); De Larrard (1990); Tazawa and Miyazawa (1993, 1995); Weiss et al. (1999); Brooks and Johari (2001); Lee et al. (2003); Zhang et al. (2003); Mazloom et al. (2004); Vidal et al. (2005); Lee et al. (2006) with the capillary stress $bS_l P_c$.

shrinkage characterized by α_{sh} . The mechanical stress σ_h is of the same magnitude as the stress $bS_l P_c$ induced by capillary forces and exhibits identical trends with water-to-cement ratio. Therefore, we conclude that the long-term kinetics of autogenous shrinkage is compatible with the hypothesis of autogenous shrinkage being creep under the action of capillary forces due to self-desiccation.

5.6 Conclusions

We performed an exhaustive study of experimental data in literature on basic creep and autogenous shrinkage. We downscaled these results with help of elastic homogenization schemes extended to viscoelasticity and discussed the origin of long-term autogenous shrinkage using the theory of porous mechanics. Several conclusions can be drawn.

- For materials that are kept under autogenous condition, the creep mod-

CHAPTER 5. IS LONG-TERM AUTOGENOUS SHRINKAGE A CREEP PHENOMENON INDUCED BY CAPILLARY EFFECTS DUE TO SELF-DESICCATION?

ulus of C-S-H gel exhibits no specific trend with water-to-cement ratio, with a mean value around 13 GPa.

- The creep modulus, which is found by analyzing data of basic creep, is lower than the value obtained from microindentation testing, which is 32 GPa.
- For concretes made with a water-to-cement ratio below 0.5, the autogenous shrinkage is not asymptotic and evolves logarithmically with respect to time in the long term.
- The long-term kinetics of this logarithmically evolving autogenous shrinkage is compatible with the hypothesis of autogenous shrinkage being creep under the action of capillary forces due to self-desiccation.
- An upper bound and a lower bound are proposed for the long-term relative humidity under autogenous conditions by analyzing experimental data in the literature.
- The stress induced by the capillary forces due to self-desiccation is estimated by bS_lP_c for various water-to-cement ratio. The capillary stress bS_lP_c can be around 20 MPa for water-to-cement ratio of 0.2.

Chapter 6

Viscoelastic poromechanical model

THIS CHAPTER presents a viscoelastic poromechanical model to predict creep and shrinkage behavior of mature cement-based materials. The objective of the model is to unify the prediction of four types of delayed strain of classical decomposition. The model is going to be proposed at the scale of the mixture of the C-S-H gel and capillary pores at which scale the long-term creep originates. We start by listing major experimental tendencies that are to be captured by the model. Then, the influence of relative humidity on the long-term viscoelastic behavior of concrete is considered in two manners. The first one is through the dependence of the creep modulus on relative humidity. This dependence is characterized based on experimental results of microindentation tests from the literature. The second one is through the dependence of the effective stress on capillary effects. The third section is devoted to present the model at the scale of the mixture of the C-S-H gel and capillary pores with as few fitting parameters as possible. All of the components of delayed strains are regarded as viscoelastic response of material. Considering that the capillary stress transmitted to the solid skeleton is less important in non-loaded specimen than that in loaded specimen due to some sort of micro-damage, we introduce a coefficient noted κ . By doing so, the model is able to

capture well the Pickett effect. In the end, two ways are presented to apply the model at the scale of concrete before ending up calibrating the model with experimental results of delayed strain of concrete in literature.

CE CHAPITRE présente un modèle viscoélastique poromécanique pour prédire le comportement de retrait et fluage à long terme des matériaux cimentaires matures. L'objectif du modèle est d'unifier la prédiction des quatre composants classiques de la déformation différée. Le modèle est formulé à l'échelle du mélange du gel de C-S-H et des pores capillaires où se trouve l'origine du fluage à long terme. Nous commençons par lister les principales tendances expérimentales qui sont à capturer par le modèle. Puis, l'influence de l'humidité relative sur le comportement viscoélastique à long terme est considérée en deux volets. Le premier est via la dépendance du module de fluage sur l'humidité relative. La caractérisation de cette dépendance est basée sur les résultats expérimentaux des tests de microindentation de la littérature. Le second est via la dépendance de la contrainte effective à l'effet capillaire. La section suivante est dédiée à la présentation du modèle à l'échelle du mélange du gel de C-S-H et pores capillaires en utilisant le minimum possible de paramètres à calibrer. Toutes les composantes de la déformation différée sont considérées comme réponse viscoélastique du matériau. En supposant que, dû à un certain micro-endommagement, la contrainte capillaire transmise au squelette solide est moins importante dans un cas de séchage sans charge que dans un cas de séchage avec charge appliquée, nous introduisons un coefficient κ . Ainsi, le modèle est capable de bien capturer l'effet Pickett. À la fin, nous présentons deux manières d'appliquer le modèle à l'échelle du béton avant de finir par calibrer le modèle aux résultats expérimentaux de la déformation différée du béton de la littérature.

Long-term time-dependent strains of concrete are of great importance when it comes to analyze the security of major civil engineering concrete structures such as dams, nuclear power plants, nuclear waste storage tunnels and large bridges, as they are normally designed for service lifetime of several decades. Conventionally, the delayed behavior of concrete is decomposed into autogenous shrinkage, basic creep, drying shrinkage and drying creep. Most design codes (1992-1-1:2005, 2004; ACI Committee 209, 2008; FIB, 2013) and well know models such as the B4 model of RILEM Technical Committee (2015) follow such classical decomposition of delayed strains. In these models, each component of delayed strain is computed with different laws of kinetics separately. Then, by summing them up, we obtain the total delayed strain. However, the possible correlation between the four components of delayed strain is neglected. In this chapter, we aim at unifying the prediction law by deriving a predictive model that does not decompose the delayed strain.

Autogenous shrinkage is the time-dependent strain of a non-loaded specimen exchanging no water with outside. Autogenous shrinkage at long term can be modeled as viscoelastic strain under capillary effects due to self-desiccation (Hua et al., 1995; Luan et al., 2013) (see also chapter 5.).

Basic creep is the difference between the strain of a loaded specimen exchanging no water with the outside and the autogenous shrinkage. Basic creep is regarded as the viscoelastic strain response of material to the applied load.

Drying shrinkage is the difference between the strain of a non-loaded specimen exchanging water with outside and the autogenous shrinkage. The drying shrinkage can be modeled as viscoelastic strain under capillary effects due to desiccation (Benboudjema et al., 2007; Sellier and Buffo-Lacarriere, 2009; Grasley and Leung, 2011; Sellier et al., 2016).

Drying creep is the additional time-dependent strain of a loaded specimen exchanging water with outside with respect to the sum of autogenous shrinkage, basic creep and drying shrinkage. Drying creep is also known under the name of Pickett effect as it was observed at first by Pickett (1942). The most common two ways to model drying creep are: 1) the first one is that the variation \dot{h}_r of relative humidity with respect to time in presence of an

applied mechanical load induces an additional term in the creep compliance; 2), in a drying sample, the capillary effects in presence of a mechanical load is more important than in absence of a mechanical load. [Bažant and Chern \(1985\)](#) followed the first method while [Sellier et al. \(2016\)](#) used the second one. We choose the second way.

From the above we can see that each of the 4 components of delayed strain can be considered to be a viscoelastic response to applied external load or internal capillary effects. Each component is influenced by the internal relative humidity, which governs the material creep properties and the capillary effects. Thus, the various components of delayed strain can be modeled in a unified manner, which will be achieved based on poromechanics in the framework of non-aging isotropic linear viscoelasticity. The model starts at the scale of a porous material whose solid skeleton is homogenous, namely the mixture of C-S-H gel with capillary pores.

In the following, we start by listing the main experimental tendencies that are to be captured with the model. Then, the influence of relative humidity on delayed strain of concrete is reflected on two aspects: the creep compliance of material and the effective stress. In the end, the model is upscaled to be used at the scale of concrete from the scale of the mixture of C-S-H gel with capillary pores. In the last section, the model is calibrated with experimental results from the literature.

6.1 Objective of model

Being the final objective of the thesis, the predictive model of shrinkage and creep of cement-based material is based on poromechanics. The main feature of this model is to not suppose the decomposition of delayed strain of concrete. No kinetics will be separately assumed for autogenous shrinkage, drying shrinkage, basic creep and drying creep. Instead, we would like to capture these different strains via material properties that depend on relative humidity and capillary effect. Therefore, the model does not intend to improve accuracy of shrinkage and creep prediction but to capture main experimental tendencies, while considering the right physics behind with the

least possible fitting parameters.

Although a variety of experimental tendencies are observed in the literature for the delayed behavior of concrete, the model aims at capturing only the main ones as following.

For basic creep, we consider a logarithmic evolution over time at long term, as observed by [Hanson \(1953\)](#); [Browne \(1967\)](#); [Rostasy et al. \(1973\)](#); [Kommendant et al. \(1976\)](#); [Takahashi and Kawaguchi \(1980\)](#); [Kawasumi et al. \(1982\)](#); [Brooks \(1984\)](#); [Brooks and Wainwright \(1983\)](#); [Bryant and Vadhanavikkit \(1987\)](#); [De Larrard \(1988\)](#); [Shritharan \(1989\)](#); [De Larrard \(1990\)](#); [Le Roy \(1995\)](#); [Mazloom et al. \(2004\)](#); [Mazzotti et al. \(2005\)](#); [Mu et al. \(2009\)](#) and supported also by nanoindentation tests ([Vandamme and Ulm, 2013](#)) and microindentation tests ([Zhang, 2014](#); [Frech-Baronet et al., 2017](#)).

Autogenous shrinkage is regarded as creep under the action of capillary stress due to self desiccation, according to the findings of chapter 5. With this assumption, autogenous shrinkage evolves also logarithmically over time at long term, which is supported by the data of [Brooks \(1984\)](#); [Shritharan \(1989\)](#); [De Larrard \(1990\)](#); [Tazawa and Miyazawa \(1993, 1995\)](#); [Weiss et al. \(1999\)](#); [Brooks and Johari \(2001\)](#); [Lee et al. \(2003\)](#); [Zhang et al. \(2003\)](#); [Mazloom et al. \(2004\)](#); [Vidal et al. \(2005\)](#); [Lee et al. \(2006\)](#) (all gathered from the database of [Bažant and Li \(2008\)](#)).

For what concerns drying shrinkage, we consider the drying shrinkage as creep under the action of capillary stress due to desiccation, as done by [Benboudjema et al. \(2007\)](#); [Sellier and Buffo-Lacarriere \(2009\)](#); [Grasley and Leung \(2011\)](#); [Sellier et al. \(2016\)](#). Therefore, the drying shrinkage does not stop increasing when drying finishes, but slows down significantly over time.

Drying creep, i.e., Pickett effect appears when drying occurs in the presence of load. This part of time-dependent strain will be modeled as viscoelastic strain due to the higher effect of capillary stress comparing to non-loaded drying specimen, as done by [Sellier et al. \(2016\)](#).

The model is proposed for a porous material that is composed from a homogenous matrix and spherical inclusions, which corresponds to the mixture of C-S-H gel and capillary pores, scale (c) in the multi-scale scheme of

concrete in Fig. 5.2.

As the model is based on non-aging isotropic linear viscoelasticity, it is not applicable to the cases where the applied load exceeds 40% of the strength. The pore pressure does not take into account surface effects. So the range of applicability is limited to relative humidity over 40%.

This model is limited to hardened mature materials, i.e., mature materials whose microstructure does not change with time. So the model cannot simulate shrinkage and creep behavior related to or caused by the hydration at early age.

6.2 Influence of relative humidity

The influence of relative humidity on delayed behavior of concrete is twofold: on one hand, the creep compliance of cement-based material depends on the relative humidity, according to the experimental observation of Bažant et al. (1976) and Abiar (1986) that, under autogenous conditions, a wet specimen creeps more than a pre-dried specimen; on the other hand, the relative humidity governs the capillary effects.

6.2.1 Dependence of creep compliance on relative humidity

Experimental observations (Bažant et al., 1976; Abiar, 1986) showed that a pre-dried concrete creeps less than a wet concrete under autogenous condition. In this section, we aim at taking into account this dependence of creep compliance on the relative humidity.

Given that the basic creep evolves logarithmically over time at long term, we take the following form for the bulk creep compliance:

$$J^K(t) = \frac{1}{K} + \frac{1}{C^K} \log \left(1 + \frac{t}{\tilde{t}} \right) \quad (6.1)$$

where K is the bulk modulus; C^K is the bulk creep compliance; \tilde{t} is the creep characteristic time. The definition of creep compliance C^K is consistent

with the definition of Vandamme and Ulm (2009), where it is defined, for a creep test under the stress σ_0 , as the asymptotic value of $\sigma_0/(td\varepsilon/dt) = \sigma_0/d\varepsilon/d(\log(t))$ in the long term.

The influence of relative humidity h_r is taken into account by the dependence of the bulk creep modulus C^K on the relative humidity h_r . As wet concrete creeps faster than a pre-dried concrete at long term, the bulk creep modulus C^K should be higher for lower relative humidity h_r . In fact, this dependence is also supported by the results of microindentation test by Zhang (2014) and Frech-Baronet et al. (2017), as explained next.

Microindentation test of Zhang (2014) is on C₃S paste with water-to-cement ratio 0.42. The samples are prepared by cutting a cylindrical specimen at the age of 28 days into dish-like sample with thickness of 3 mm to 3.5 mm and are kept under various relative humidities in desiccator during 90 days, where the hydric equilibrium is reached. Then a load of 5 to 20 N is applied and kept constant for 300 seconds. The volume fraction of each phase is estimated by using the hydration degree which is measured by the method of chemical shrinkage (Parrott et al., 1990). The volume fractions given by Zhang (2014) are as follows: unhydrated clinker: 0.05; C-S-H gel: 0.55; Portlandite: 0.215; Capillary porosity: 0.185.

Microindentation test of Frech-Baronet et al. (2017) is on ordinary Portland cement paste with water-to-cement ratio 0.6. The samples are prepared by cutting a cylindrical specimen at the age of 3 months into cubic samples with 30 mm of edge size. Then the sample is kept under various relative humidities during 7 days before testing. The hydric equilibrium should be only established in a layer of thickness around 200 μm which is the characteristic size of the zone probed by microindentation. The applied load is equal to 8 N and kept constant for 300 seconds. We estimate the volume fraction of each phase using Powers' model (see chapter 1) by taking the hydration degree ξ equal to its long-term value ξ^∞ given in Eq. 1.10.

The experimental results of microindentation test provide the contact compliance $L(t)$ which is the inverse, in the Laplace domain, of the time-dependent indentation modulus $M(t)$. The contact creep modulus C^M is defined as the asymptotic value of $t\frac{dL}{dt} = \frac{dL}{d(\log(t))}$ at large times.

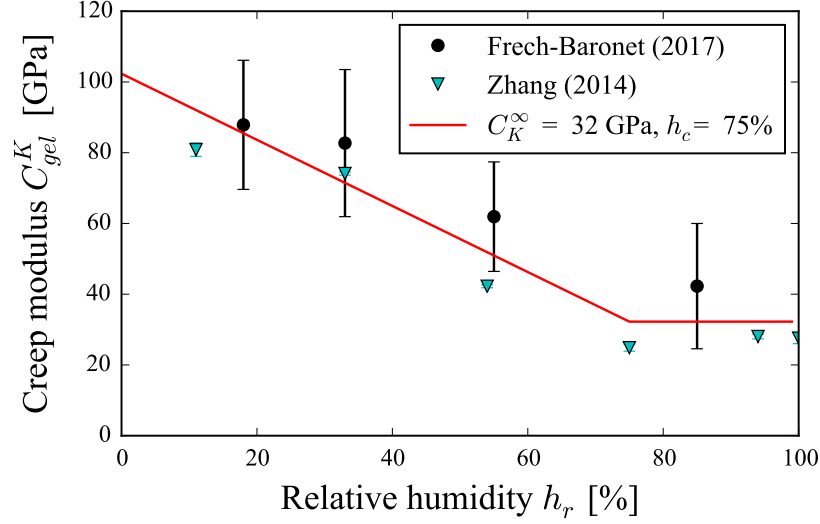


Figure 6.1 – Bulk creep modulus of C-S-H gel as a function of relative humidity obtained from microindentation results of Zhang (2014) and Frech-Baronet et al. (2017)

Taking the viscoelastic Poisson's ratio ν as a constant, Vandamme and Ulm (2013) derived the following relation between contact creep modulus C^M and bulk creep modulus C^K :

$$C^M = \frac{3(1 - 2\nu)}{1 - \nu^2} C^K \quad (6.2)$$

Knowing the contact creep modulus C_p^M of cement paste from the results of microindentation test of Zhang (2014) or Frech-Baronet et al. (2017), we compute the bulk creep modulus C_p^K of cement paste with Eq. 6.2. Then, using the microstructure of cement paste as shown in Fig. 5.2, we perform three steps of downscaling and obtain the bulk creep modulus C_{gel}^K of the C-S-H gel (for details of derivation, see section 5.3.3):

$$C_{gel}^K = \left(\frac{1 - f_b}{1 + f_b} \right) \left(\frac{1 + \phi_c}{1 - \phi_c} \right) C_p^K \quad (6.3)$$

where f_b is the volume fraction of unhydrated clinker and portlandite and calcium sulfoaluminate hydrates with respect to the volume of cement paste; ϕ_c is the volume fraction of capillary pores with respect to the volume of

the mixture of C-S-H gel with capillary pores. Inserting the values of ϕ_c and f_b (computed from experimental data for the test of Zhang (2014) or estimation from Powers' model for the test of Frech-Baronet et al. (2017)) and the creep modulus C_p^K of cement paste into Eq. 6.3, we obtain the creep modulus C_{gel}^K of the C-S-H gel as a function of relative humidity h_r . The results are displayed in Fig. 6.1. This result leads us to propose the following type of relationship for the dependence of creep modulus of the C-S-H gel on the relative humidity:

$$C_{gel}^K(h_r) = \begin{cases} C_{gel}^{K\infty} + \beta_{h_r}(h_c - h_r), & \text{if } h_r < h_c, \\ C_{gel}^{K\infty}, & \text{if } h_r \geq h_c \end{cases} \quad (6.4)$$

where $C_{gel}^{K\infty}$ is the creep modulus for the concretes that are kept at a relative humidity higher than a critical relative humidity h_c . Figure 6.1 suggests that the critical relative humidity h_c should be 75% while the creep modulus $C_{gel}^{K\infty}$ should be 32 GPa. Compared to this result, the creep modulus of 13 GPa obtained in Fig. 5.3 from the analysis of basic creep data in section 5.3.3, is significantly lower. Considering that the testing condition in the application of the model is closer to that of macroscopic basic creep test than that of microindentation test, we choose 13 GPa for the value of $C_{gel}^{K\infty}$. For what concerns the parameter β_{h_r} , by scaling the value of β_{h_r} obtained from the results of microindentation by a factor of 13/32, we obtain $\beta_{h_r} = 38$ GPa. Thus, in the model we take: $C_{gel}^{K\infty} = 13$ GPa, $\beta_{h_r} = 38$ GPa.

6.2.2 Capillary stress

This section is dedicated to take into account the influence of relative humidity on the effective stress. Considering the application of the model, we restrict the relative humidity between 100% and 40%. As mentioned in section 1.5.3, the pore pressure is taken to be equal to bS_lP_c , where b , S_l and P_c are Biot coefficient of the mixture of C-S-H gel with capillary pores, saturation degree and capillary pressure, respectively.

The Biot coefficient of the mixture of C-S-H gel with capillary pores, is computed by two steps of upscaling.

At a lower scale, C-S-H particles and gel pores are arranged together to form the C-S-H gel. We compute first the porosity of the C-S-H gel as the mean value of the porosity of high-density C-S-H and low-density C-S-H: taking 40% of C-S-H gel as high-density C-S-H with a porosity 0.24, and the other 60% as low-density C-S-H with a porosity 0.37 (Jennings, 2000), we obtain the porosity of the C-S-H gel equal to $\phi_{gel} = 0.32$. Then, supposing that the viscoelastic Poisson's ratio of the C-S-H gel is 0.2 and taking the self-consistent scheme, we obtain the Biot coefficient b_{gel} from Eq. 1.36, $b_{gel} = 2\phi_{gel}$.

At the scale of the mixture of the C-S-H gel with capillary pores, we consider the Mori-Tanaka scheme. Inserting the capillary porosity ϕ_c obtained from Power's model into Eq. 1.38, we obtain the Biot coefficient b of the mixture of the C-S-H gel with capillary pores:

$$b = 1 - \frac{1 - \phi_c}{1 + \phi_c}(1 - 2\phi_{gel}) \quad (6.5)$$

The saturation degree S_l depends on the relative humidity h_r as the thermodynamic equilibrium should be maintained between water vapor and liquid water in capillary pores. In fact, this dependence of the saturation degree S_l on the relative humidity h_r is known as sorption isotherm. Most often, the sorption isotherm is expressed by the water content w per dried hardened cement paste as a function of relative humidity. When the relative humidity decreased to 40% almost all capillary water has evaporated (Jennings, 2000). The water content w_{cr} remaining at this relative humidity of 40% can be regarded as absorbed water on the surface of solid hydrates. Therefore, the water content w_{cr} should depend only on the specific area of solid and be independent of the water-to-cement ratio w/c . That is to say, the sorption isotherms for various cement paste should merge to a same point when relative humidity is decreased to 40%. This is confirmed by experimental results of Baroghel-Bouny (2007) displayed in Fig. 6.2.

Baroghel-Bouny (2007) measured the desorption isotherm for cement pastes with various water-to-cement ratios. The desorption isotherms of cement pastes with various water-to-cement ratios differ from each other for

6.2. INFLUENCE OF RELATIVE HUMIDITY

relative humidities between 100% and 40%. When relative humidity drops below 40%, all desorption isotherms are reduced to a master curve. The results displayed in Fig. 6.2 suggest that the water content w_{cr} corresponding to $h_r = 40\%$ is 7.11 g/g.

In addition to the point at 40% of relative humidity, we can obtain also the water content w_{sat} at saturated state (i.e., all pores spaces are filled with water) $h_r = 100\%$ from hydration model of Powers:

$$w_{sat} = \frac{(f_{cs} + f_{cw} + f_{aw})\rho_w}{p\rho_w + (1-p)\rho_c - (f_{aw} + f_{gw})\rho_w} \quad (6.6)$$

where f_{cs} , f_{cw} and f_{gw} are the volume fraction of chemical shrinkage, of capillary water and of physically adsorbed water, respectively (for the computation, see Eqs. 1.2, 1.3 and 1.4); $p = \frac{w/c}{w/c + \rho_w/\rho_c}$ is the volume fraction of water in the initial mixture; ρ_w and ρ_c are the density of water and of clinker, respectively.

Knowing the two points, we could propose a linear model for the desorption isotherm. However, the experimental results of Baroghel-Bouny (2007) in Fig. 6.2 show that straight lines do not reflect well the desorption isotherm. Hence, we choose a second-order power function:

$$w(h_r) = a_{h_r}h_r^2 + b_{h_r}h_r + c_{h_r} \quad (6.7)$$

Since we know already two points, only one fitting parameter is needed. The least square method suggests that $c_{h_r}(w/c) = 56.8w/c - 11.4$. Then, the other two parameters in Eq. 6.7 read $a_{h_r} = -25w_{sat}/6 + 5w_{cr}/3 + 5c_{h_r}/2$ and $b_{h_r} = 25w_{sat}/6 - 2w_{cr}/3 + 7c_{h_r}/2$, respectively. The modeled desorption isotherms are compared with the experimental results in Fig. 6.2.

The saturation degree then can be computed as follows:

$$S_l(h_r) = \frac{w(h_r)}{w_{sat}} \quad (6.8)$$

For materials kept under autogenous condition, the relative humidity h_r^∞ at long term is computed first as the mean value of the upper limit and lower

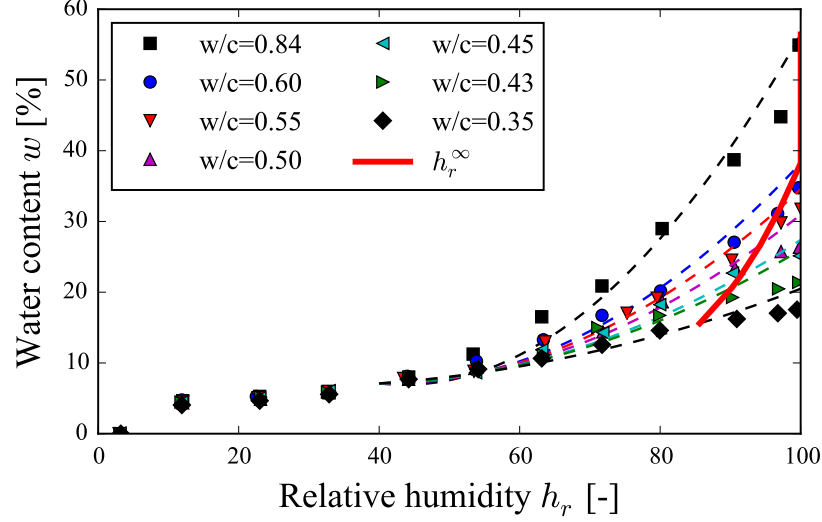


Figure 6.2 – Desorption isotherm for cement pastes with various water-to-cement ratio. Points are experimental results of [Baroghel-Bouny \(2007\)](#), dashed lines are the model fitted relation with Eq. 6.7, solid line h_r^∞ corresponds to the water content under autogenous condition at long term.

limit in Fig. 5.5:

$$h_r^\infty(w/c) = \min \{0.655 + 0.575w/c, 1\} \quad (6.9)$$

Then, inserting the long-term relative humidity h_r^∞ into Eq. 6.8, we obtain the corresponding saturation degree S_l^∞ under autogenous condition.

The capillary pressure P_c can be computed from Kelvin's law:

$$P_c = \frac{\rho_w R T}{M_w} \ln(h_r) \quad (6.10)$$

$R = 8.314 \text{ J} \cdot \text{K}^{-1} \cdot \text{mol}^{-1}$, T and $M_w = 18 \text{ g/mol}$ are ideal gas constant, the absolute temperature and molar mass of water.

Inserting Eqs. 6.5-6.10 into

$$\underline{\underline{\sigma_h}} = \sigma_h \underline{\underline{1}} = -b S_l P_c \underline{\underline{1}}, \quad (6.11)$$

we obtain the capillary stress.

6.3 Constitutive model

After having identified the influence of relative humidity, in this section, we present first the constitutive equations and the procedure to predict the shrinkage and creep strains. In second part, we discuss how the 4 components of delayed strains are considered in the model.

6.3.1 Constitutive equations

We recall that the model is proposed at the scale of the mixture of C-S-H gel and capillary pores, i.e., scale c in Fig. 5.2. The C-S-H gel is regarded as a matrix that embeds the spherical capillary pores.

The mixture of C-S-H gel and capillary pores, is regarded as non-aging linear isotropic viscoelastic. Under a known history $h_r(t)$ relative humidity, we compute first the effective stress (which will be defined in Eq. 6.15) according to poromechanics. Then, the strain response $\underline{\underline{\varepsilon}}(t)$ of the material is given as viscoelastic response to the effective stress as following:

$$\varepsilon_v(t) = J^K(0)\sigma'_v(t) - \int_0^t \sigma'_v(\tau) \frac{\partial J^K(t-\tau, h_r)}{\partial \tau} d\tau \quad (6.12a)$$

$$e_{ij}(t) = J^G(0)s_{ij}(t) - \int_0^t s_{ij}(\tau) \frac{\partial J^G(t-\tau, h_r)}{\partial \tau} d\tau \quad (6.12b)$$

where $\sigma'_v = \text{tr}(\underline{\underline{\sigma'}})/3$ and $\underline{\underline{s}}$ are the effective volumetric stress and deviatoric stress tensor, respectively. $\varepsilon_v = \text{tr}(\underline{\underline{\varepsilon}})$ and $\underline{\underline{e}}$ are the volumetric strain and deviatoric strain tensor, respectively. The decompositions of stress and strain tensors are same as in Eq. 2.3.

The remaining tasks are to compute the creep compliances $J^K(t)$, $J^G(t)$ of material and the effective stress σ'_v .

The creep compliances $J^K(t)$, $J^G(t)$ depend on water-to-cement ratio w/c and relative humidity $h_r(t)$. Using Powers' model (Powers and Brownyard, 1947), we compute first the volume fraction ϕ_c of capillary pores (with respect to the volume of the mixture of C-S-H with and capillary pores). Inserting

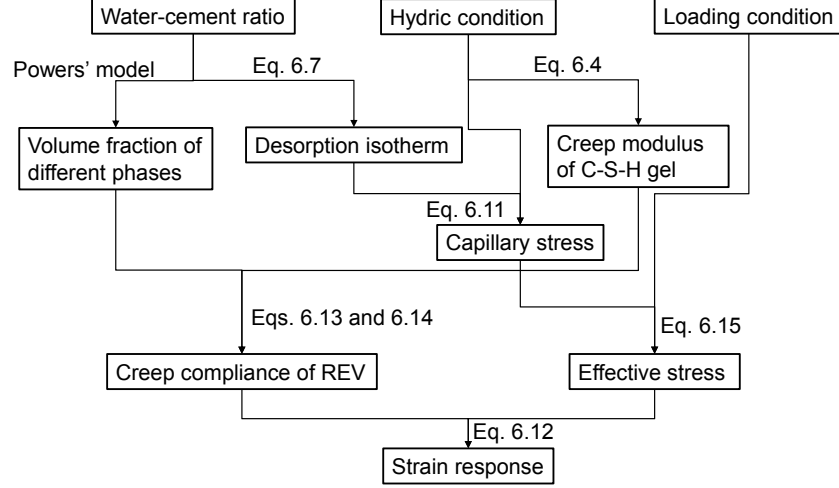


Figure 6.3 – The procedure to predict shrinkage and creep with the proposed model

the given history $h_r(t)$ of relative humidity in Eq. 6.4, we obtain the creep modulus $C_{gel}^K(t)$ of the C-S-H gel. Then, using the elastic Mori-Tanaka scheme for bulk modulus and the viscoelastic Mori-Tanaka scheme for creep modulus, we obtain the bulk modulus K and bulk creep compliance C^K of the mixture of C-S-H gel with capillary pores:

$$K = \frac{1 - \phi_c}{1 + \phi_c} K_{gel} \quad (6.13a)$$

$$C^K = \frac{1 - \phi_c}{1 + \phi_c} C_{gel}^K \quad (6.13b)$$

$$J^K(t) = \frac{1}{K} + \frac{1}{C^K} \ln \left(1 + \frac{t}{\bar{t}} \right) \quad (6.13c)$$

where K_{gel} is the bulk modulus of C-S-H gel. [Acker et al. \(2001\)](#) and [Constantinides and Ulm \(2004\)](#) provide the uniaxial elastic modulus E_{HD} of high-density C-S-H gel and E_{LD} of low-density C-S-H gel (see Tab. 6.1). Supposing the elastic Poisson's ratio of both high-density and low-density C-S-H gel equal to be 0.2, we compute the bulk modulus K_{HD} of high-density C-S-H and K_{LD} of low-density C-S-H, respectively. Then, taking the volume

6.3. CONSTITUTIVE MODEL

Reference	Component	Young's modulus [GPa]	Bulk modulus [GPa]
Acker et al. (2001)	LD C-S-H	20±2	11.1±1.1
Acker et al. (2001)	HD C-S-H	31±4	17.2±2.2
Constantinides and Ulm (2004)	LD C-S-H	21.7±2.2	12.1±1.2
Constantinides and Ulm (2004)	HD C-S-H	29.4±2.4	16.3±1.3

Table 6.1 – Young's modulus of C-S-H gel measured by Acker et al. (2001); Constantinides and Ulm (2004) and computed bulk modulus of C-S-H gel

ratio of high-density C-S-H and low-density C-S-H equal to 4:6, we compute the bulk modulus $K_{gel} = 0.4K_{HD} + 0.6K_{LD}$. We can take $K_{gel} = 13.6 \pm 1.6$ GPa according to the results of Acker et al. (2001) or $K_{gel} = 13.8 \pm 1.3$ GPa according to the results of Constantinides and Ulm (2004). Hence, the bulk modulus of C-S-H gel in Eq. 6.13 can be taken the average of those 2 values, i.e., $K_{gel} = 13.7$ GPa.

From the results of chapter 3, we take viscoelastic Poisson's ratios of concrete equal to 0.2. As explained in section 5.3, adapting the multi-scale scheme displayed in Fig. 5.2 and using the results displayed in Figs 4.2a and 4.2b, we can also take the viscoelastic Poisson's ratio of the mixture of C-S-H gel and capillary pores as constant, equal to 0.2. Inserting this value into the Laplace transform of the relation between bulk and shear modulus, we obtain the shear properties of the mixture of C-S-H gel with capillary

pores:

$$G = \frac{3(1-2\nu)}{2(1+\nu)}K = \frac{3}{4}K \quad (6.14a)$$

$$C^G = \frac{3(1-2\nu)}{2(1+\nu)}C^K = \frac{3}{4}C^K \quad (6.14b)$$

$$G(t) = \frac{1}{G} + \frac{1}{C^G} \ln \left(1 + \frac{t}{\bar{t}} \right) \quad (6.14c)$$

The effective stress $\sigma'_v(t)$ depends also on water-to-cement ratio w/c and the history $h_r(t)$ of relative humidity. Inserting the water-to-cement ratio into Eq. 6.7, we can predict the desorption isotherm. The given history $h_r(t)$ of relative humidity permits to compute the saturation degree S_l from Eqs. 6.7 and 6.8 and the capillary pressure P_c from Eq. 6.10. Then, we obtain the capillary stress from Eq. 6.11. The effective stress σ'_v is computed in incremental form:

$$d\underline{\underline{\sigma}}' = d\underline{\underline{\sigma}} - \kappa d\sigma_{h\underline{\underline{1}}} \quad (6.15)$$

where κ is a parameter to capture drying creep.

Sellier et al. (2016) suppose that the capillary pressure that is transferred to solid skeleton is greater in presence of mechanical load than in absence of mechanical load. The explanation he gives is that, for non-loaded drying specimen, micro-damage occurs as the relative humidity decreases. As a result, the transmitted capillary stress is less important than in a loaded drying specimen for which the load prevents partially micro-damage (Sellier et al., 2016). We employ the same explanation as Sellier et al. (2016) but formulate the equations in a slightly different way.

When drying takes place in the presence of mechanical load, we consider that κ is equal to 1, thus, making it possible to retrieve Eq. 1.34:

$$\underline{\underline{\sigma}}' = \underline{\underline{\sigma}} - \sigma_{h\underline{\underline{1}}} \quad (6.16)$$

In contrast, when drying takes place in absence of mechanical load, κ is

considered to be smaller than 1.

As the coefficient κ is intended to characterize the micro-damage of material, the magnitude of κ should be related to tensile strength of material and the intensity of drying. In case of drying, this coefficient κ should be a parameter varying over time, because of the desiccation varying over time. However, for the sake of simplicity, we will consider the coefficient κ to be constant over time.

Figure 6.3 summarizes the procedure of predicting delayed strain of the mixture of C-S-H gel and capillary pores. Water-to-cement ratio, evolution of relative humidity over time and loading condition are necessary to predict the delayed strain behavior with the proposed model.

6.3.2 Discussion about the 4 components of delayed strain

With such a model, the 4 components of delayed strain of cement-based material are predicted with a unified method.

For a non-loaded non-drying specimen, the strain response, which is equal to the autogenous shrinkage, is creep under the capillary stress due to self-desiccation. For a sufficiently mature specimen, this capillary stress is considered to remain constant, as the internal relative humidity does. If the relative humidity is equal to 100%, the delayed strain is 0. Otherwise, autogenous shrinkage evolves as a logarithmic function of time at long term, which is in agreement with the experimental observation displayed in Fig. 5.1a.

For a loaded non-drying specimen, the strain response, which is equal to the sum of autogenous shrinkage and basic creep, is creep under the constant stress that is equal to the sum of applied load and capillary stress. The basic creep evolves logarithmically over time at long term, which is in agreement with the experimental observation displayed in Fig. 5.1b.

For a non-loaded drying specimen, the strain response, which is equal to the sum of autogenous shrinkage and drying shrinkage, is creep under a capillary stress which is variable over time and only partially transmitted to the specimen. The drying shrinkage increases with no asymptote at long term but the increment rate slows down significantly due to the increase of

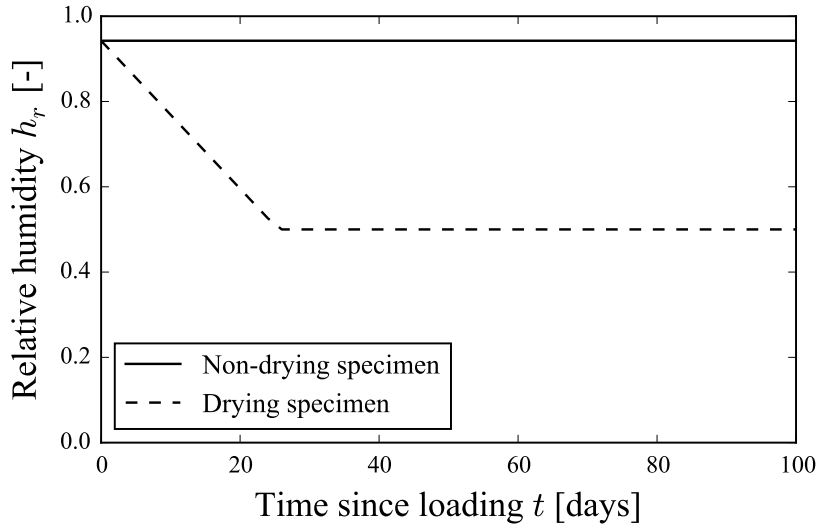
the creep modulus with the decrease of relative humidity.

For a loaded drying specimen, the strain response, which is the sum of autogenous shrinkage, drying shrinkage, basic creep, and drying creep, is creep under variable stress that is equal to the sum of applied load and capillary stress. The drying creep is due to the fact that the capillary stress is transmitted in a larger proportion to the specimen when the sample is drying and loaded than drying but non-loaded.

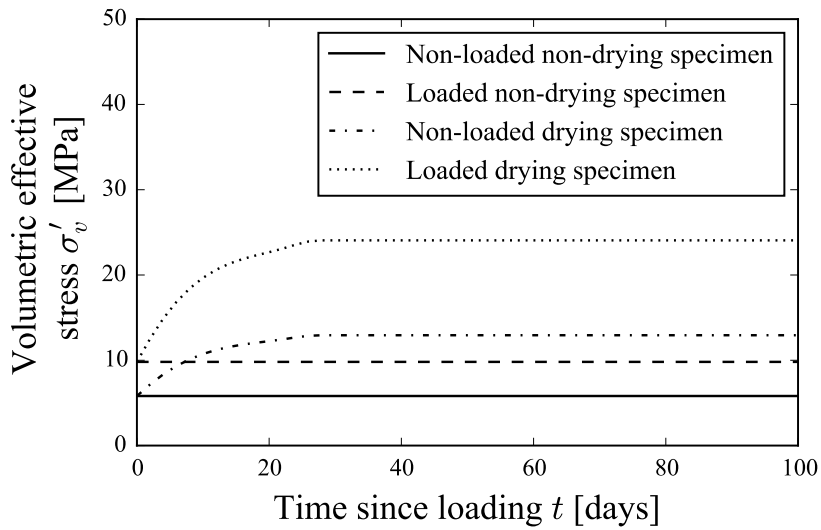
As an example, Figures 6.4 and 6.5 show the delayed strain of a mixture of C-S-H gel and capillary pores for four cases: non-loaded non-drying; loaded with $\sigma_1 = 12$ MPa and $\sigma_2 = \sigma_3 = 0$ but non-drying; non-load but drying specimen with drying kinetics presented in Fig. 6.4a; loaded with $\sigma_1 = 12$ MPa and $\sigma_2 = \sigma_3 = 0$ and drying specimen with drying kinetics presented in Fig. 6.4a. The volume fraction ϕ_c of capillary pores computed with respect to the volume of the mixture of C-S-H gel with capillary pores corresponds to that in cement paste with water-to-cement ratio $w/c = 0.5$. Under autogenous conditions, the relative humidity h_{r0} is computed to be equal to 94% from Eq. 6.9. The coefficient κ is taken to be equal to $\kappa = 0.5$. As displayed in Fig. 6.5b, the delayed strain of loaded drying specimen is higher than the sum of autogenous shrinkage, drying shrinkage and basic creep. Therefore, the model is able to exhibit drying creep.

6.4 Application to concretes

The model presented in previous section is proposed to the scale of the mixture of the C-S-H gel and capillary pores so that the physical phenomena at play can be taken into account with the least fitted parameters. The industrial background of the thesis being the long-term delayed behavior of concrete structures, we aim at applying the above proposed model to concretes in this section. Two methods of applying the model to concrete are going to be presented in the first part. The second part is dedicated to the calibration of the model with experimental results from the literature.

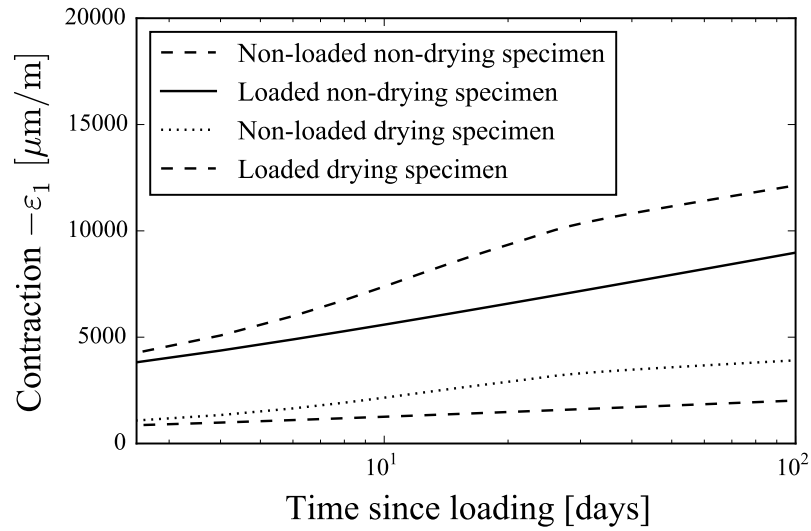


(a)

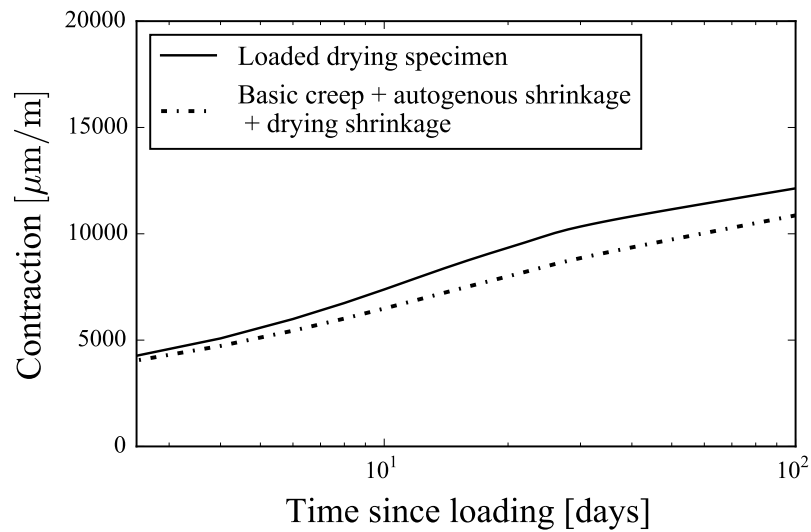


(b)

Figure 6.4 – Application of model on the mixture of C-S-H gel and capillary pores submitted to the histories of relative humidity displayed in Fig. (a). (b) volumetric effective stress acting on the mixture of C-S-H gel with capillary pores. When the specimen is mechanically loaded, the applied stress is uniaxial and of magnitude 12 MPa.



(a)



(b)

Figure 6.5 – Application of model on the mixture of C-S-H gel and capillary pores submitted to histories of relative humidity and mechanical load displayed in Fig. 6.4. (a) strain of various specimens; (b) illustration of Pickett effect.

6.4.1 Methodology

At the scale of concrete, when this concrete is sufficiently mature, the nature of delayed strain is exactly the same as at the scale of the mixture of the

C-S-H gel and capillary pores: non-aging linear isotropic viscoelastic strain of a porous medium. The porous medium, here concrete, is composed from capillary pores and a solid skeleton which is composed from aggregates and cement paste. Hence, the model is, in theory, also applicable to concretes. However, the solid skeleton differs from concrete to concrete, not only because of the variability of aggregates but also because of differences in water-to-cement ratio and hydration degree of cement. Hence, we cannot provide a unique creep property of this solid skeleton, as was done in section 6.3 for the C-S-H gel. In contrast, the computation of capillary stress may remain the same as at the scale of the mixture of C-S-H gel with capillary pores, according to Eq. 5.16. To use the model at the scale of concrete, we need to know the creep compliance of concrete. In the following, we propose two methods to obtain the creep compliance of concrete.

The first method consists of upscaling the creep compliance of the mixture of the C-S-H gel and capillary pores to the scale of concrete. This upscaling can be performed in two steps.

In the first step, we consider the cement paste (see Fig. 5.2b) as a composite made from spherical inclusions that are embedded in a matrix that is the mixture of the C-S-H gel and capillary pores. The inclusions are unhydrated clinker, portlandite and calcium sulfoaluminates and supposed to be elastic. Then, we use viscoelastic Mori-Tanaka scheme to upscale the creep compliances in Eqs. 6.13 and 6.14. This step requires the knowledge of elastic modulus of unhydrated clinker, portlandite and calcium sulfoaluminates. Numerical inversion of viscoelastic Mori-Tanaka scheme from Laplace domain to time domain is also needed.

In the second step, we consider the concrete (see Fig. 5.2a) as a composite made of spherical inclusions that are embedded in a matrix of cement paste. The inclusions are aggregates and supposed to be elastic. Then, inserting the elastic modulus of aggregates and creep compliances of cement paste into viscoelastic Mori-Tanaka scheme, we obtain the creep compliance of concrete. This step requires the knowledge of the elastic modulus of aggregates as well as a numerical inversion of viscoelastic Mori-Tanaka scheme from Laplace domain to time domain.

The desorption isotherm of the mixture of the C-S-H gel and capillary pressure can be adapted for the concrete by supposing that the aggregates do not influence the water migration in the material. If the desorption isotherm is expressed by water content per dried material, we need to scale the mass of dried material taking into account the mass of unhydrated clinker, portlandite, calcium sulfoaluminates and aggregates. If the desorption isotherm is expressed by degree of saturation, we can use directly the same desorption isotherm.

Knowing the creep compliances of the concrete and the desorption isotherm, the delayed strain of concrete can be computed for given stress and history of relative humidity. However, the estimated delayed strain is not satisfactory, as the predicted creep compliance deviates largely from the one measured experimentally. A deeper investigation of homogenization schemes would be needed to improve the quality of estimation of the creep compliance.

The second method is based on macroscopic experimental results. We obtain the uniaxial creep compliance of concrete from the experimental results of basic creep. Then, supposing the viscoelastic Poisson's ratio equal to 0.2, we obtain the bulk and shear creep compliances of the concrete.

In the same spirit, if experimental results of desorption isotherm are available for the concrete, we can use them instead of using the theoretical desorption isotherm of Eq. 6.7. In this case, we suppose that the capillary pressure P_c and the saturation degree S_l follow the following law proposed by [Van Genuchten \(1980\)](#):

$$P_c(S_l) = b_1 \left(S_l^{-\frac{1}{a_1}} - 1 \right)^{1-a_1} \quad (6.17)$$

where a_1 and b_1 are material parameters, which are dimensionless and express in Pascal, respectively.

The delayed strain of drying specimen can also provide information about the isotherm of desorption. When the delayed strain of loaded drying specimen is known, combining this delayed strain with the creep compliances fitted from basic creep test, we can fit the value of material parameters a_1 and b_1 with least square method. In the end, using experimental results on

Concrete	Water-to-cement ratio [-]	Saturated water content [m ³ /m ³]	Porosity [%]
Flamanville	0.48	0.106	15.2
Chooz	0.543	0.118	21.0
Civaux B11	0.557	0.129	20.0
Penly	0.577	0.133	18.5

Table 6.2 – Mix design of concretes used in Granger (1995)

delayed strain of non-loaded drying specimen, we can fit the coefficient κ .

Compared to the first method, the second method requires more experimental investigation, not only on delayed strain but also mass loss of drying specimen.

In the next section, we fit the model to macroscopic experimental results on concrete employing this second method.

6.4.2 Example of application

Granger (1995) studied the delayed behavior of six different concretes. The mix design of each of the six concretes corresponds to the concretes that are used in containment building of nuclear power stations. Excluding the concretes with silica fume, we focus ourselves on Civaux B11, Flamanville and Chooz. The mix design properties of these concretes are displayed in Tab. 6.2.

For each of the concretes, Granger (1995) measured the delayed strain under four different conditions: non-loaded non-drying condition, loaded non-drying condition, non-loaded drying condition and loaded drying condition. All specimens are kept sealed until the age of loading, i.e., 28 days. For the loaded specimen, an axial load of 12 MPa is applied instantaneously via a hydraulic pressure tank and kept constant afterwards. Drying starts also at the time of loading under an ambient relative humidity of 50%. The specimens are cylindrical specimens with a diameter of 16 cm and a height of 1 m.

Beside the four tested specimen, another drying specimen is placed in the same room to measure mass loss over time. Combining the history of

mass loss over time with the water content at saturation given in Tab. 6.2, we obtain the evolution of saturation degree $S_l(t)$ over time.

The first step of calibration is to obtain the creep properties of concrete from the basic creep strain. We obtain the axial basic creep strain ε_1^{bc} by subtracting the strain of non-loaded non-drying specimen from the total strain of loaded non-drying specimen. As proposed in section 6.3.1, the following relation is fitted to the basic creep data:

$$\varepsilon_1^{bc} = \sigma_1 \otimes j^E(t) = \frac{\sigma_1}{E} + \frac{\sigma_1}{C^E} \log \left(1 + \frac{t}{\tilde{t}^E} \right) \quad (6.18)$$

where E , C^E and \tilde{t}^E are Young's modulus, uniaxial creep modulus and characteristic time, respectively. Using the least square method, we obtain all three parameters. Then supposing that the viscoelastic Poisson's ratio of concrete is constant and equal to 0.2, we obtain the bulk $J^K(t)$ and shear $J^G(t)$ creep compliances.

The dependence of creep compliance on relative humidity is taken into account in the same way as Eq. 6.4. The creep modulus $C^{K\infty}$ at saturated state is taken to be equal to the bulk creep modulus C^K obtained from basic creep test. The fitting parameter β_{h_r} is rescaled, i.e., $\beta_{h_r} = \frac{C^{K\infty}}{13} \text{GPa} \times 38 \text{GPa}$.

The next step consists in calibrating the Van Genuchten parameters a_1 , b_1 and the coefficient κ from the strain of drying specimens. We propose two types of calibration.

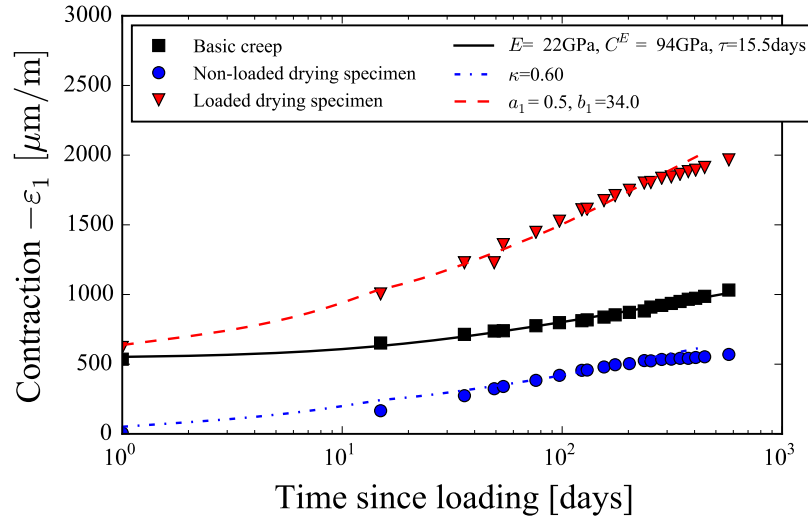
The first one is to calibrate those three parameters a_1 , b_1 and κ . Knowing the history $S_l(t)$ of saturation degree for drying specimen, we obtain the history $P_c(t)$ of capillary pressure as a function of Van Genuchten parameters from Eq. 6.17. The Kelvin's law in Eq. 6.10 gives then the history $h_r(t)$ of relative humidity. As a result, we obtain the capillary stress as a function of the Van Genuchten parameters and then, inserting the capillary stress in Eq. 6.16, we obtain the effective stress σ'_v . The dependence $C^K(t)$ of creep compliance on relative humidity is also obtained from the history $h_r(t)$ of relative humidity using Eq. 6.4. Combining the effective stress with the creep compliance obtained from basic creep strain and inserting them

into the viscoelastic stress-strain relation Eq. 6.12, we compute the strain of a loaded drying specimen. Finally using the least square method, we calibrate the value of Van Genuchten parameters a_1 and b_1 . For non-loaded drying specimen, knowing the Van Genuchten parameters a_1 and b_1 , the capillary stress σ_h is known. Then, the effective stress σ'_v is computed from Eq. 6.15 as a function of the coefficient κ . Inserting this effective stress and humidity-dependent creep compliance into the viscoelastic relation Eq. 6.12, we compute the strain of a non-loaded drying specimen. Finally using the least square method, we calibrate the value of the coefficient κ . The results of calibration are displayed in Fig. 6.6a-6.7a-6.8a-6.9a.

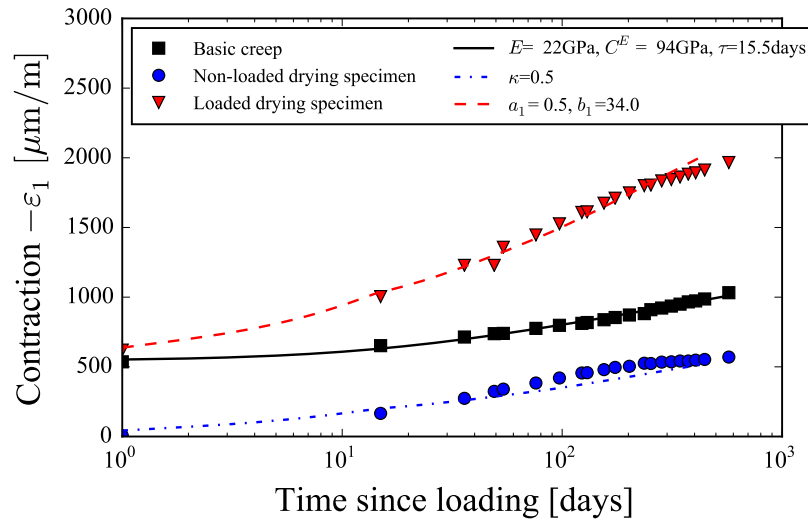
In the second type of calibration, we suppose a unique value 0.5 for the coefficient κ . Then, we calibrate a_1 and b_1 from the strain of non-loaded drying specimen. In this case, without any additional information, we can predict the strain of loaded drying specimen. The prediction results are compared with experimental measurement in Fig. 6.6b-6.7b-6.8b-6.9b. An alternative choice could have been the inverse: we could have calibrated a_1 and b_1 from the strain of loaded drying specimen. In this case, the strain of non-loaded drying specimen could be predicted.

By comparing the two types of calibration in Fig. 6.6, we can see that, by considering a unique value for the coefficient $\kappa = 0.5$ of all concretes, we can predict reasonably well the drying creep and drying shrinkage. Therefore, setting $\kappa = 0.5$ is a reasonable choice if all types of delayed strain test have not been performed. We can thus predict the delayed strain under a different hydric and loading condition from other tests. In contrast, when all types of delayed strain tests are available, we can calibrate all parameters from experimental results. The calibrated parameters are then used to model the behavior of structures made of this type of concrete.

In the framework of the VERCORS project, [Charpin et al. \(2017\)](#) have tested delayed strain behavior of the VERCORS concrete, whose water-to-cement ratio is equal to 0.52. The delayed strains are measured under four different conditions: non-loaded non-drying condition, loaded non-drying condition, non-loaded drying condition and loaded drying condition. All specimens are kept sealed until the age of loading, i.e., 90 days. For the



(a)

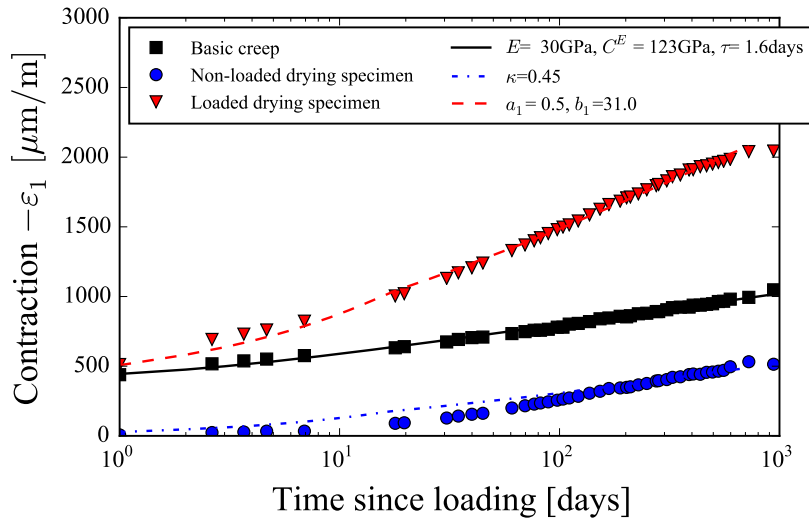


(b)

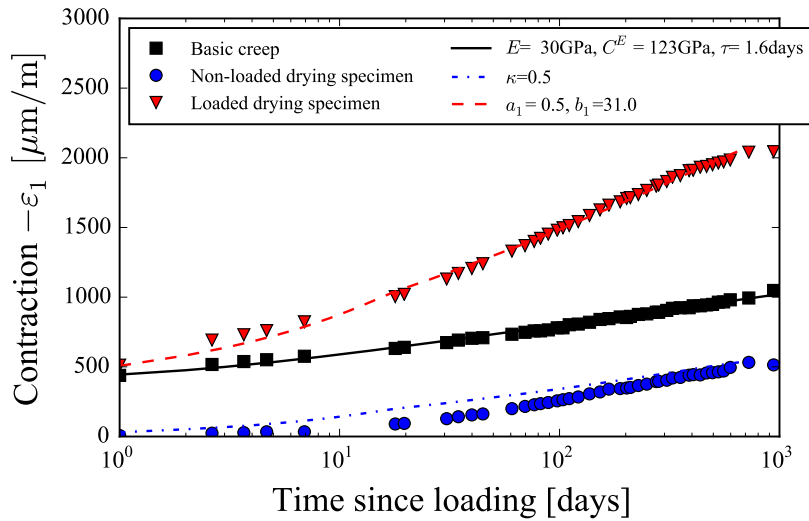
Figure 6.6 – Calibration of the model with the experimental results of Flamanville (Granger, 1995): (a) when the coefficient κ is also fitted, (b) when the coefficient κ is set to $\kappa = 0.5$.

loaded specimen, an axial load of 12 MPa is applied instantaneously via a hydraulic pressure tank and kept constant afterwards. Drying starts also at the time of loading under an ambient relative humidity of 50%. The specimens are cylindrical specimens with a diameter of 16 cm and a height of 1

6.4. APPLICATION TO CONCRETES



(a)



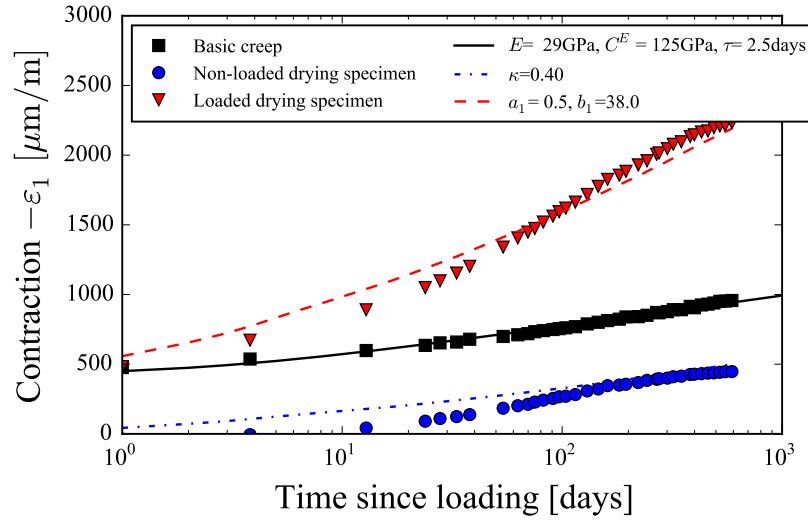
(b)

Figure 6.7 – Calibration of the model with the experimental results of Chooz (Granger, 1995): (a) when the coefficient κ is also fitted, (b) when the coefficient κ is set to $\kappa = 0.5$.

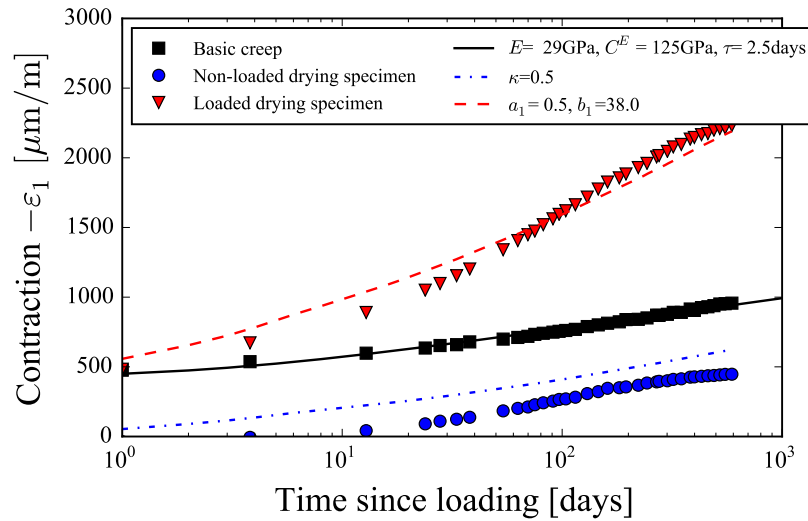
m.

The desorption isotherm was measured on other specimens made with same concrete. Fig. 6.10a displays the desorption isotherm.

The first step is to calibrate creep compliance from basic creep strains. We



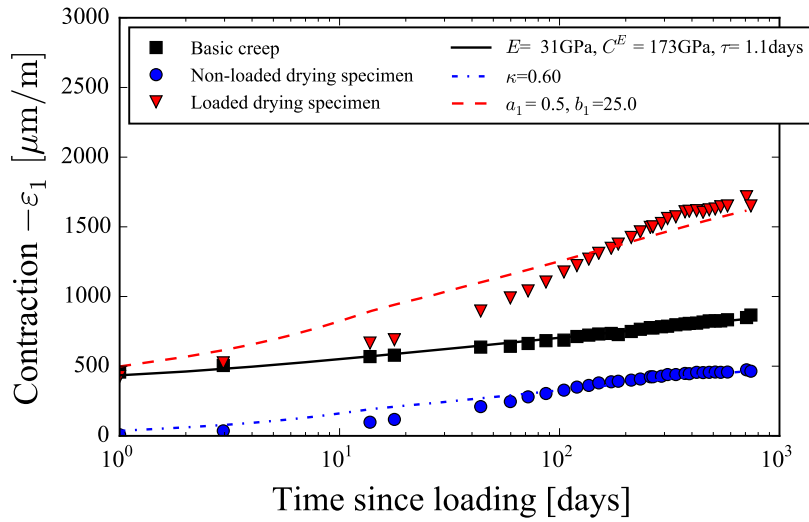
(a)



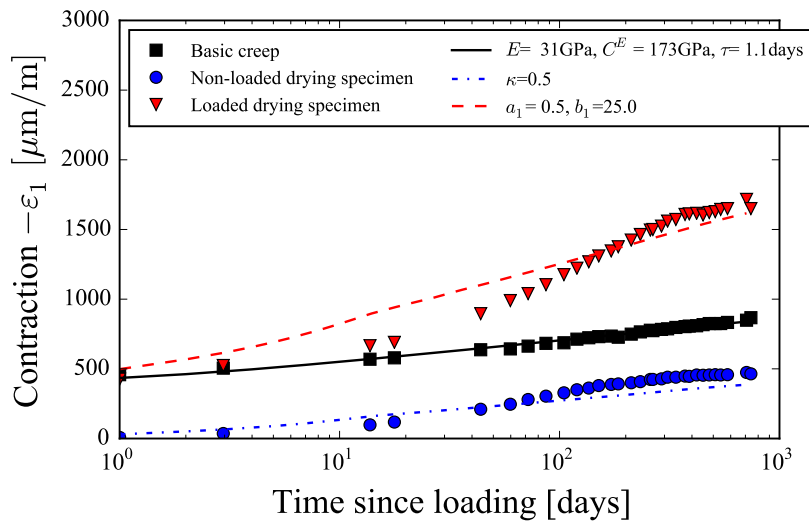
(b)

Figure 6.8 – Calibration of the model with the experimental results of Civaux B11 (Granger, 1995): (a) when the coefficient κ is also fitted, (b) when the coefficient κ is set to $\kappa = 0.5$.

obtain the axial basic creep ε_1^{bc} strain by subtracting the strain of non-loaded non-drying specimen from the total strain of loaded non-drying specimen. Then, using least square method, we fit the relation in Eq. 6.18 to obtain Young's modulus E , uniaxial creep modulus C^E and characteristic time τ_E .



(a)

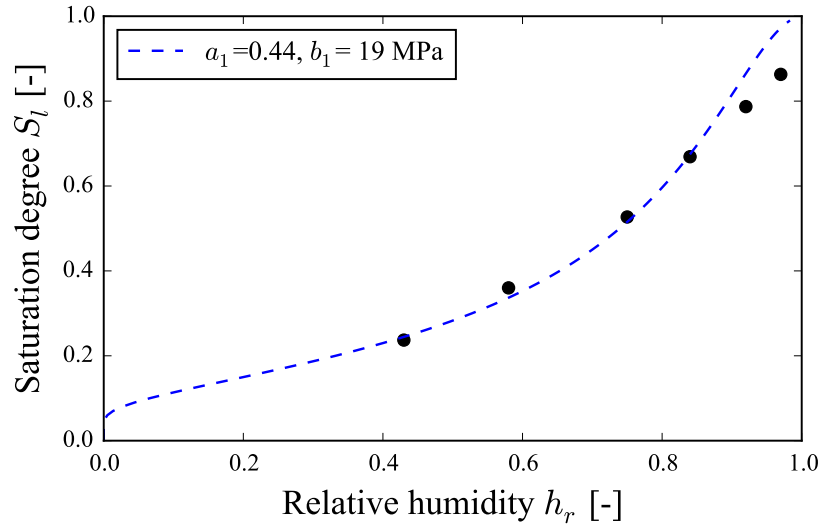


(b)

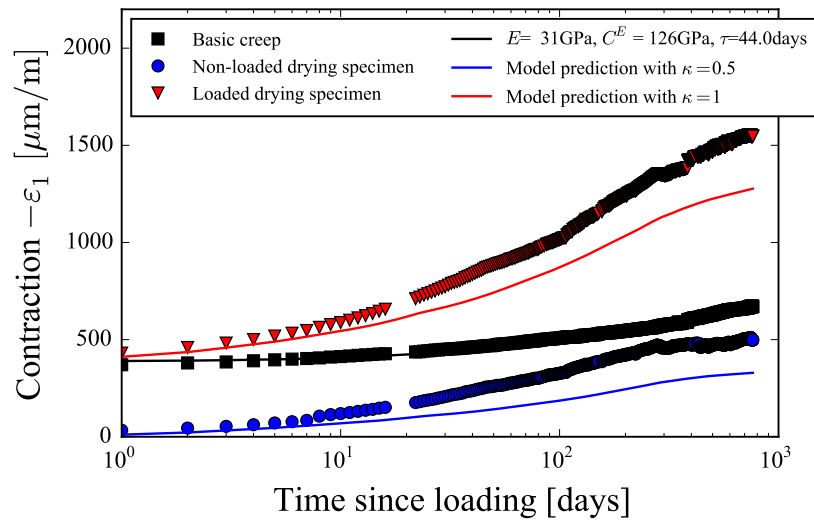
Figure 6.9 – Calibration of the model with the experimental results of Penly (Granger, 1995): (a) when the coefficient κ is also fitted, (b) when the coefficient κ is set to $\kappa = 0.5$.

Then supposing that the viscoelastic Poisson's ratio of concrete is constant and equal to 0.2, we obtain the bulk $J^K(t)$ and shear $J^G(t)$ creep compliances.

The dependence of creep compliance on relative humidity is taken into account in the same way as done for the results of Granger (1995).



(a)



(b)

Figure 6.10 – Calibration of the model with the experimental results on VERCORS concrete: (a) measured desorption isotherm, (b) Calibration of creep properties from basic creep strains and prediction of the strain of non-loaded drying specimen and of loaded drying specimen

As we know the desorption isotherm, combining the desorption isotherm with the creep compliance obtained by fitting the basic creep strain, we can predict the delayed strain of non-loaded drying specimen and loaded

drying specimen. We consider the coefficient κ equal to 0.5 for non-loaded drying specimen. The results are displayed in Fig. 6.10b. Taking $\kappa = 0.5$ gives a reasonable prediction of the strain of non-loaded drying specimen. Comparison between the measured strain and predicted strain supports the idea of unifying the four types of delayed strain as viscoelastic strain under the action of the applied mechanical load and/or capillary stress.

6.5 Conclusions

In this chapter, we proposed a non-aging linear viscoelastic model to predict the delayed strain of cement-based material, without decomposing the delayed strain. The model is based on poromechanics and developed initially at the scale of the mixture of the C-S-H gel and capillary pores. In the last section the model is upscaled to the scale of concrete and calibrated with experimental results from the literature.

At the scale of the mixture of the C-S-H gel and capillary pores, the model takes into account the dependence of creep modulus on relative humidity and also capillary effects. Based on physical phenomena, the model aims at reducing as much as possible the number of the parameters to fit. In total, there are two parameters to calibrate: first one is already fitted, the parameter c_{hr} in desorption isotherm (see section 6.2.2); second one is the coefficient κ .

At the scale of concrete, we proposed two ways of using the model: based on viscoelastic upscaling of the model developed at the level of the mixture of C-S-H gel with capillary pores, and by direct calibration on macroscopic results on concrete. The former method requires the knowledge of elastic modulus of clinker, portlandite, calcium sulfoaluminate and aggregates. Numerical inversion of Laplace transform is also needed. The latter method requires experimental investigation of delayed strain of concrete and drying kinetics.

In the end, we calibrated the model to the experimental results of [Granger \(1995\)](#). The results support the idea of unifying the four types of delayed strain as viscoelastic strain under the action of mechanical applied load

and/or capillary stress.

However, at least three points need to be improved in the model: the creep characteristic time, the coefficient κ , and structural effects.

At the scale of the mixture of C-S-H gel and capillary pores, the creep characteristic time \tilde{t} in Eq. 6.13 is not known. In fact, if the creep characteristic time related to C-S-H gel was known from microindentation test, the creep characteristic time of the mixture of C-S-H gel and capillary pores in Eq. 6.13 could have been computed by numerical inverting the Laplace transform of the viscoelastic Mori-Tanaka scheme.

The coefficient κ is taken as a constant both at the scale of the mixture of C-S-H gel and capillary pores and at the scale of concrete. However, as the coefficient κ is related to micro-damage, it should depend on the tensile strength of material as well as the intensity of drying. Therefore, the coefficient κ may vary over time during a test. Though taking a constant value 0.5 apparently provides satisfactory results at the scale of concrete, some more efforts could be devoted to the study of this parameter and to its physical origin.

The calibration neglects the fact that the drying is not homogenous in the testing specimen. The relative humidity decreases faster at the edge of the specimen than in its middle. Some tensile stress is generated by the gradient of the relative humidity, reducing the effective section (Bažant and Yunping, 1994; Granger et al., 1997). This effect is known as structural effect and not negligible. Including this structural effect should be the very next point to take into account in order to improve the model.

Chapter 7

Conclusions and perspectives

7.1 Conclusions

In the context of evaluation and extension of service lifetime of nuclear pressure vessels, we aimed in this thesis at better understanding long-term delayed strain behavior of cement-based materials. We contributed to the current state of the art by exhaustive analysis of experimental data from the literature and by micromechanical analysis and poromechanical modeling.

Considering the biaxial prestress in the nuclear vessel, we started by studying the viscoelastic Poisson's ratio. We first looked at the definition of Poisson's ratio in non-aging isotropic viscoelasticity. The definition of Poisson's ratio in isotropic linear viscoelasticity is not unique. We compared two most intuitive definitions: the relaxation Poisson's ratio $\nu_r(t)$ and the creep Poisson's ratio $\nu_c(t)$. Those two Poisson's ratios were defined with respect to creep or relaxation experiments with an instantaneous loading. Those two Poisson's ratios are not equal to each other. They can be expressed as functions of the creep compliances and relaxation moduli and are linked to each other through an exact expression. For cementitious materials, we showed through a study of multiaxial creep data that, if the Poisson's ratios vary little over time, their difference is negligible. Hence, throughout the whole thesis, we do not distinguish the two Poisson's ratios.

In a second step, we compared the above definition of Poisson's ratio in

viscoelasticity with other definitions based on creep strain that are widely used in concrete creep testing. Then, we analyzed all experimental data from the literature in which the delayed strains are measured in more than one direction. The analysis of all experimental results shows that the long-term viscoelastic Poisson's ratio of concrete is equal to or smaller than its elastic Poisson's ratio, and comprised between 0.15 and 0.20. If the elastic Poisson's ratio of a mature concrete is comprised between 0.15 and 0.20, considering for practical applications that its viscoelastic Poisson's ratio is constant over time, as proposed in particular by [Bazant \(1975\)](#); [RILEM Technical Committee \(1995\)](#), is a very reasonable assumption. This long-term value of Poisson's ratio indicates that the long-term creep of concrete is not only deviatoric, but also volumetric.

Knowing the long-term Poisson's ratio of concrete, we computed the long-term viscoelastic Poisson's ratio of C-S-H gel by downscaling with the help of elastic homogenization schemes extended to viscoelasticity. If the aggregates, portlandite, calcium sulfoaluminates hydrates and clinker can be considered as spherical, then the long-term viscoelastic Poisson's ratio of the C-S-H gel has little effect on the long-term viscoelastic Poisson's ratio of concrete. The value of the long-term viscoelastic Poisson's ratio of the C-S-H gel is comprised between 0 and 0.2. The long-term creep of C-S-H gel in concrete is both deviatoric and volumetric.

From the long-term Poisson's ratio of C-S-H gel, we analyzed different possible mechanisms of creep at the scale of C-S-H particles. If creep of the C-S-H gel is due to creep of the C-S-H particles themselves, evolutions of the creep Poisson's ratio observed experimentally cannot be explained if we consider that the C-S-H particles are spherical and that they creep by sliding of its C-S-H layers over each other: either the C-S-H particles need to be considered aspherical, or the interlayer distance between neighboring C-S-H layers must be considered to vary in the long term. If creep of the C-S-H gel is due to creep of the contact points between C-S-H particles, and if we consider that C-S-H particles are spherical, we cannot consider that C-S-H particles can only slide over each other: in the long term, the C-S-H particles must also be allowed to get closer to each other, i.e., to interpenetrate each

other.

In the second part of the thesis, which is devoted to the development of the model, we started by identifying the major experimental tendencies that are to be captured with the model. With this aim in mind, we performed an exhaustive study of experimental data from the literature on basic creep and autogenous shrinkage. The basic creep of concrete, as well as the autogenous shrinkage, is not asymptotic and evolves logarithmically with respect to time at long term. Then, we downscaled these results to the scale of C-S-H gel with the help of elastic homogenization schemes extended to viscoelasticity. For materials that are kept under autogenous conditions, the creep modulus of C-S-H gel remains approximately constant, around 13 GPa. For what concerns autogenous shrinkage, we computed the stress that is needed to explain long-term kinetics of autogenous shrinkage. Comparing this stress with the capillary force due to self desiccation computed as $bS_l P_c$ from poromechanics, we concluded that the autogenous shrinkage can be explained as creep under the action of capillary effects.

In the end, we proposed a non-aging linear viscoelastic model to predict the delayed strain of cement-based materials, without decomposing the delayed strain into its classical components. The model is based on poromechanics and developed initially at the scale of the mixture of the C-S-H gel and capillary pores. In the last section the model is upscaled to the scale of concrete and calibrated with experimental results from the literature. Calibration of the model on experimental results of [Granger \(1995\)](#) showed that the model is able to capture well the magnitude of drying creep. The calibration results support the idea of unifying the four types of delayed strain as viscoelastic strain under the action of the applied mechanical load and/or capillary stress.

7.2 Perspectives

Several improvements can be done to complete the work of the thesis, both on the part dedicated to the Poisson's ratio and on the proposed poroviscoelastic model.

In the thesis, we analyzed basic creep data to draw conclusions on the evolution of viscoelastic Poisson's ratio of concrete. The question of multi-axiality is not explicitly studied for other components of delayed strain.

Autogenous shrinkage is considered to be isotropic since there is no privileged direction for internal capillary pressure under autogenous conditions. However, as we know, the only measurement of lateral autogenous shrinkage, performed by [Ulm et al. \(2000\)](#), showed that lateral autogenous shrinkage differs from axial autogenous shrinkage. At that time, [Ulm et al. \(2000\)](#) attributed this inequality to non-homogenous radial aggregate distribution, but suggested to check by testing autogenous shrinkage of cored cylindrical samples. This could be a direct extension of the work on viscoelastic Poisson's ratio of concrete.

Drying shrinkage is also considered to be isotropic at the material level (i.e., if the structural effect is not taken into account) for the same reason: there is no privileged direction in drying. As far as we know, there is no experimental studies on this point. [Charpin et al. \(2015, 2017\)](#) studied the delayed strain behavior of concrete under biaxial load where drying shrinkage is measured in three directions. However, the drying took place through two opposite surfaces of the rectangular cuboid sample while the other four surfaces were wrapped with four layers of aluminum sheets, thus inducing anisotropic drying. Therefore, the results of the tests need careful analysis to infer some conclusions on any potential multiaxial feature.

For what concerns drying creep, since the coefficient κ is identical in all directions in Eq. 6.15, drying creep is considered to be isotropic in the thesis. However, there are very few tests on multiaxial drying creep in the literature. [Charpin et al. \(2017\)](#) analyzed ten years shrinkage and creep measurement of concrete and suggested that the Poisson's ratio related to drying shrinkage is equal to the viscoelastic Poisson's ratio of basic creep. Hence, we could calibrate the model to the data of [Charpin et al. \(2017\)](#) to improve the prediction of multiaxial drying creep.

For what concerns the model, we never discussed the value of the creep characteristic time \tilde{t} in Eq. 6.13. Analyzing experimental data from microindentation and nanoindentation tests may provide information about the creep

characteristic time of C-S-H gel. Then, numerically inverting viscoelastic Mori-Tanaka scheme from the Laplace domain to time domain, we could deduce the creep characteristic time of the mixture of C-S-H gel with capillary pores.

The calibration of the model neglects any structural effects that are related to the inhomogeneous drying of specimen due to its finite size. The gradient of relative humidity due to the inhomogeneous drying causes tensile stresses in the skin of the concrete. As a result, damage occurs when the tensile stress is higher than the tensile strength of concrete; Consequently, the effective section decreases. [Bažant and Yunping \(1994\)](#); [Granger et al. \(1997\)](#); [Benboudjema et al. \(2005\)](#) showed that an important part of drying creep is related to the structural effect. Incorporating this structural effect into the analysis of experimental data such as the ones of [Granger \(1995\)](#) (see section [6.4.2](#)), should be the very next point to take into account to better predict the strain behavior of a drying concrete specimen.

CHAPTER 7. CONCLUSIONS AND PERSPECTIVES

Appendix A

Relaxation and creep Poisson's ratios in rheological models

This section is devoted to present the analytical expression of the relaxation Poisson's ratio ν_r and the creep Poisson's ratio ν_c based on the rheological models that are presented in Fig. 2.1. For a material whose both volumetric and deviatoric behaviors are governed by Maxwell units (see Fig. 2.1a), the Poisson's ratios read:

$$\nu_r(t) = -\frac{(G_0 + 3K_0)(2\eta_G - 3\eta_K) + 9(\eta_G K_0 - \eta_K G_0) \exp\left(-\frac{G_0 K_0 (\eta_G + 3\eta_K)}{\eta_G \eta_K (G_0 + 3K_0)} t\right)}{2(\eta_G + 3\eta_K)(G_0 + 3K_0)} \quad (\text{A.1})$$

$$\nu_c(t) = -\frac{\eta_G \eta_K (2G_0 - 3K_0) + G_0 K_0 (2\eta_G - 3\eta_K) t}{\eta_G \eta_K (G_0 + 3K_0) + G_0 K_0 (\eta_G + 3\eta_K) t} \quad (\text{A.2})$$

For a material whose volumetric and deviatoric behaviors are governed by a Maxwell unit and a Kelvin-Voigt unit, respectively (see Fig. 2.1b), the Poisson's ratios are expressed as:

$$\nu_r(t) = -1 + \frac{9K_0}{2(G_0 + 3K_0)} \exp(-\Omega_1 t) (\cosh(\Omega_2 t) + \Omega_3 \sinh(\Omega_2 t)) \quad (\text{A.3})$$

APPENDIX A. RELAXATION AND CREEP POISSON'S RATIOS IN RHEOLOGICAL MODELS

$$\nu_c(t) = -\frac{2\eta_K G_0 - 6\eta_K K_0 + 2G_0 K_0 t + 3\eta_K K_0 \exp\left(-\frac{G_0 t}{\eta_G}\right)}{2\left(\eta_K G_0 + 6\eta_K K_0 + G_0 K_0 t - 3\eta_K K_0 \exp\left(-\frac{G_0 t}{\eta_G}\right)\right)} \quad (\text{A.4})$$

where the parameters $\Omega_1, \Omega_2, \Omega_3$ are function of K_0, G_0, η_K, η_G :

$$\begin{aligned} \Omega_1 &= \frac{G_0 (6K_0\eta_K + \eta_G K_0 + G_0\eta_K)}{2\eta_G\eta_K (G_0 + 3K_0)} \\ \Omega_2 &= \frac{\sqrt{G_0^2 (36\eta_K^2 K_0^2 + 12\eta_K^2 G_0 K_0 + \eta_G^2 K_0^2 - 2\eta_G\eta_K G_0 K_0 + \eta_K^2 G_0^2)}}{2\eta_G\eta_K (G_0 + 3K_0)} \\ \Omega_3 &= \frac{(3\eta_K G_0 + 6\eta_K K_0 - \eta_G K_0)}{\sqrt{(36\eta_K^2 K_0^2 + 12\eta_K^2 G_0 K_0 + \eta_G^2 K_0^2 - 2\eta_G\eta_K G_0 K_0 + \eta_K^2 G_0^2)}} \end{aligned}$$

For a material whose volumetric and deviatoric behaviors are governed by a Kelvin-Voigt unit and a Maxwell unit, respectively (see Fig. 2.1c), the Poisson's ratios read:

$$\nu_r(t) = \frac{1}{2} - \frac{3G_0}{2(G_0 + 3K_0)} \exp(-\Omega_4 t) (\cosh(\Omega_5 t) - \Omega_6 \sinh(\Omega_5 t)) \quad (\text{A.6})$$

$$\nu_c(t) = \frac{3\eta_G K_0 - 4\eta_G G_0 + 3K_0 G_0 t + 2\eta_G G_0 \exp\left(-\frac{K_0 t}{\eta_K}\right)}{2\left(3\eta_G K_0 + 2\eta_G G_0 + 3K_0 G_0 t - \eta_G G_0 \exp\left(-\frac{K_0 t}{\eta_K}\right)\right)} \quad (\text{A.7})$$

where the parameters $\Omega_4, \Omega_5, \Omega_6$ are function of K_0, G_0, η_K, η_G :

$$\begin{aligned}\Omega_4 &= \frac{K_0 (3K_0\eta_G + 3\eta_K G_0 + 2G_0\eta_G)}{2\eta_G\eta_K (G_0 + 3K_0)} \\ \Omega_5 &= \frac{\sqrt{K_0^2 (9\eta_G^2 K_0^2 - 18\eta_K\eta_G K_0 G_0 + 12\eta_G^2 K_0 G_0 + 9\eta_K^2 G_0^2 + 4\eta_G^2 G_0^2)}}{2\eta_G\eta_K (G_0 + 3K_0)} \\ \Omega_6 &= \frac{K_0 (3\eta_K G_0 - 9\eta_G K_0 - 2\eta_G G_0)}{\sqrt{K_0^2 (9\eta_G^2 K_0^2 - 18\eta_K\eta_G K_0 G_0 + 12\eta_G^2 K_0 G_0 + 9\eta_K^2 G_0^2 + 4\eta_G^2 G_0^2)}}\end{aligned}$$

For a material whose both volumetric and deviatoric behaviors are governed by Kelvin-Voigt units (see Fig. 2.1d), the Poisson's ratios read:

$$\nu_r(t) = \frac{3K_0 - 2G_0}{2(3K_0 + G_0)} + \frac{9K_0 G_0}{3K_0 + G_0} \Omega_9 \exp(-\Omega_7 t) \sinh\left(\frac{\Omega_8}{\eta_K \eta_G (3K_0 + G_0)}\right) \quad (\text{A.9})$$

$$\nu_c(t) = \frac{6K_0 - 4G_0 - 3K_0 \exp\left(-\frac{K_0}{\eta_K} t\right) + 2G_0 \exp\left(-\frac{G_0}{\eta_G} t\right)}{2\left(6K_0 + 2G_0 - 3K_0 \exp\left(-\frac{K_0}{\eta_K} t\right) - G_0 \exp\left(-\frac{G_0}{\eta_G} t\right)\right)} \quad (\text{A.10})$$

where the parameters $\Omega_4, \Omega_5, \Omega_6$ are function of K_0, G_0, η_K, η_G :

$$\begin{aligned}\Omega_7 &= \frac{3K_0^2\eta_G + 6K_0 G_0\eta_K + G_0^2\eta_K + 2K_0 G_0\eta_G}{2\eta_K\eta_G(3K_0 + G_0)} \\ \Omega_8 &= 9K_0^4\eta_G^4 - 36K_0^3 G_0\eta_K\eta_G - 18K_0^2 G_0^2\eta_K\eta_G + 12K_0^3 G_0\eta_G^2 \\ &\quad + 36K_0^2 G_0^2\eta_K^2 + 12K_0 G_0^3\eta_K^2 + G_0^4\eta_K^2 - 4K_0 G_0^3\eta_K\eta_G + 4K_0^2 G_0^2\eta_G^2 \\ \Omega_9 &= \frac{G_0\eta_K - K_0\eta_G}{\Omega_8}\end{aligned}$$

APPENDIX A. RELAXATION AND CREEP POISSON'S RATIOS IN
RHEOLOGICAL MODELS

Appendix B

Calculation of the two Poisson's ratios from the experimental results

This section is devoted to present how the relaxation Poisson's ratio ν_r and the creep Poisson's ratio ν_c are calculated from the experimental results. By using Eq. (2.24b), the creep Poisson's ratio $\nu_c(t)$ and the uniaxial creep compliance J_E are computed directly from the experimental measurement of principals strains $\varepsilon_1(t)$, $\varepsilon_2(t)$, $\varepsilon_3(t)$ and applied stress values σ_{10} , σ_{20} , σ_{30} . Then, to the experimental values of the uniaxial creep compliance J_E is fitted the following analytical expression:

$$J_E(t) = \alpha_1 t + \alpha_2 + \alpha_3 \exp\left(-\frac{t}{\tau_1}\right) \quad (\text{B.1})$$

where α_1 , α_2 , α_3 and τ_1 are fitted parameters.

Further, in order to capture the asymptotic behavior of the Poisson's ratio, it is assumed that the relaxation Poisson's ratio $\nu_r(t)$ has an exponential form, as follows:

$$\nu_r(t) = \nu_f + \alpha_0 \exp\left(-\frac{t}{\tau_0}\right) \quad (\text{B.2})$$

where ν_f , α_0 , and τ_0 are parameters to fit.

APPENDIX B. CALCULATION OF THE TWO POISSON'S RATIOS FROM THE EXPERIMENTAL RESULTS

Substituting Eqs. (B.1) and (B.2) into Eq. (2.17), the creep Poisson's ratio ν_c is computed analytically. By changing the parameters ν_f , α_0 , and τ_0 in Eq. (B.2), a best fit which gives the minimum variance for the fitted creep Poisson's ratio ν_c is obtained.

Appendix C

Comparison of Poisson's ratio and creep-based Poisson's ratio in different directions

In this section, for the 11 tests in [Gopalakrishnan \(1968\)](#), we computed the 3 directional creep-based Poisson's ratios with Eq. 17 (as did the authors) and the 3 directional creep-based Poisson's ratios with Eq. 5. The results are plotted in Figs. [C.1-C.4](#).

APPENDIX C. COMPARISON OF POISSON'S RATIO AND CREEP-BASED POISSON'S RATIO IN DIFFERENT DIRECTIONS

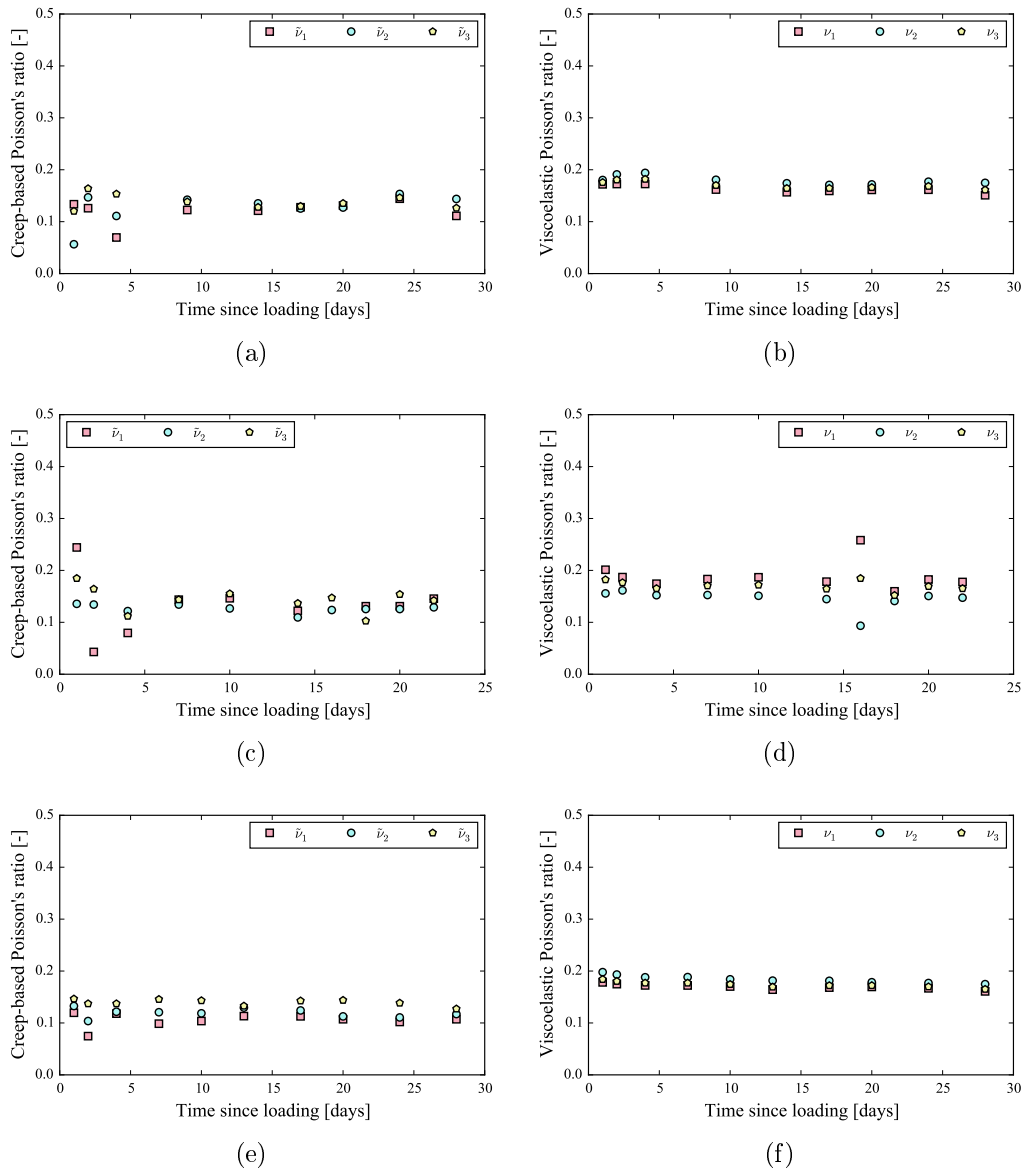


Figure C.1 – Dependency of Poisson's ratio on the direction: (a)(c)(e) creep-based Poisson's ratio reported in [Gopalakrishnan \(1968\)](#), calculated from Eq. (17) for three directions; (b)(d)(f) viscoelastic Poisson's ratio calculated from Eq. (5) for three directions. Data (a)(b) from experiment TC1, (c)(d) from experiment BC4, (e)(f) from experiment TC5 in [Gopalakrishnan \(1968\)](#):

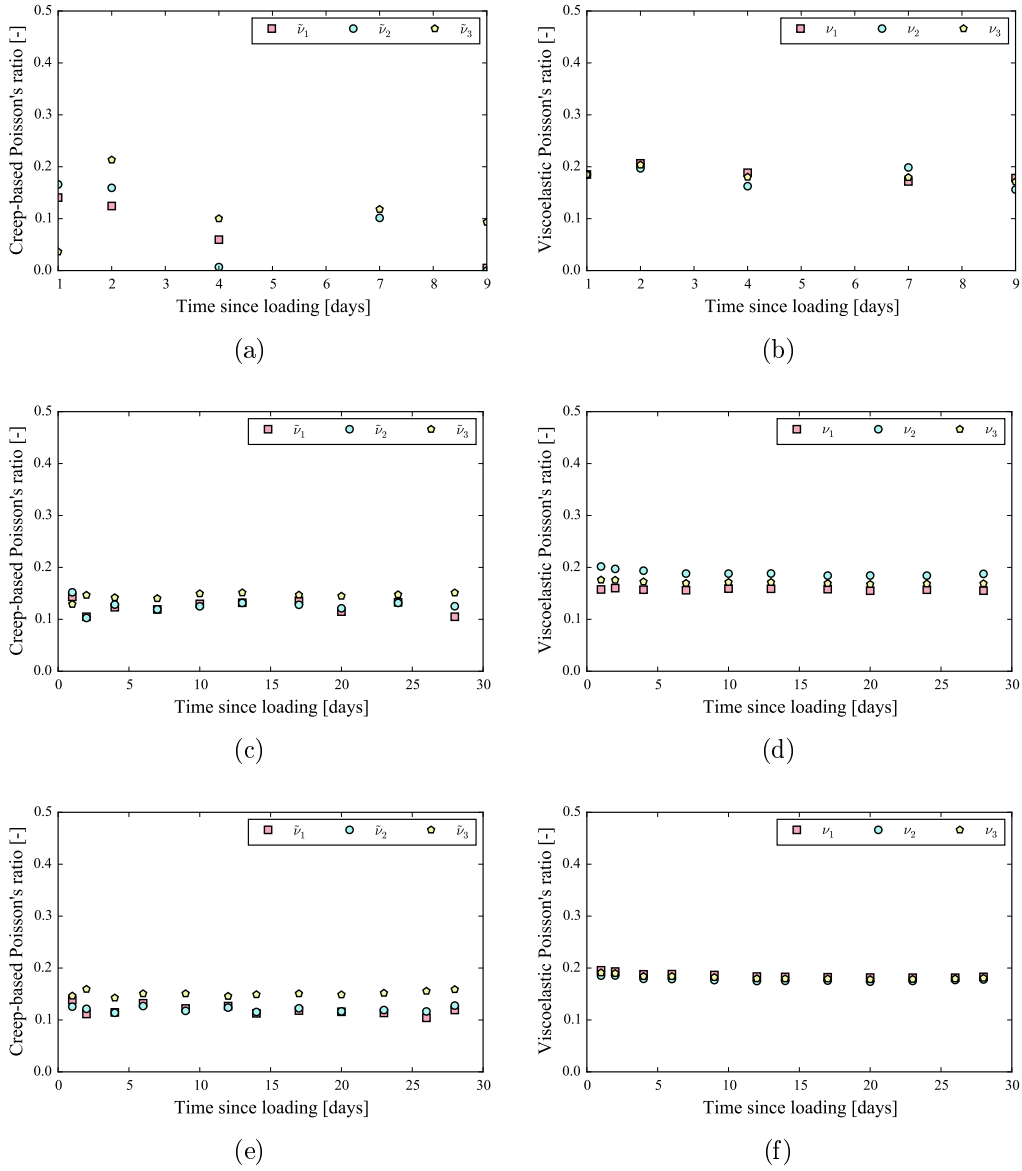


Figure C.2 – Dependency of Poisson’s ratio on the direction: (a)(c)(e) creep-based Poisson’s ratio reported in [Gopalakrishnan \(1968\)](#), calculated from Eq. (17) for three directions; (b)(d)(f) viscoelastic Poisson’s ratio calculated from Eq. (5) for three directions. Data (a)(b) from experiment TC5R, (c)(d) from experiment TC6, (e)(f) from experiment TC7 in [Gopalakrishnan \(1968\)](#):

APPENDIX C. COMPARISON OF POISSON'S RATIO AND CREEP-BASED POISSON'S RATIO IN DIFFERENT DIRECTIONS

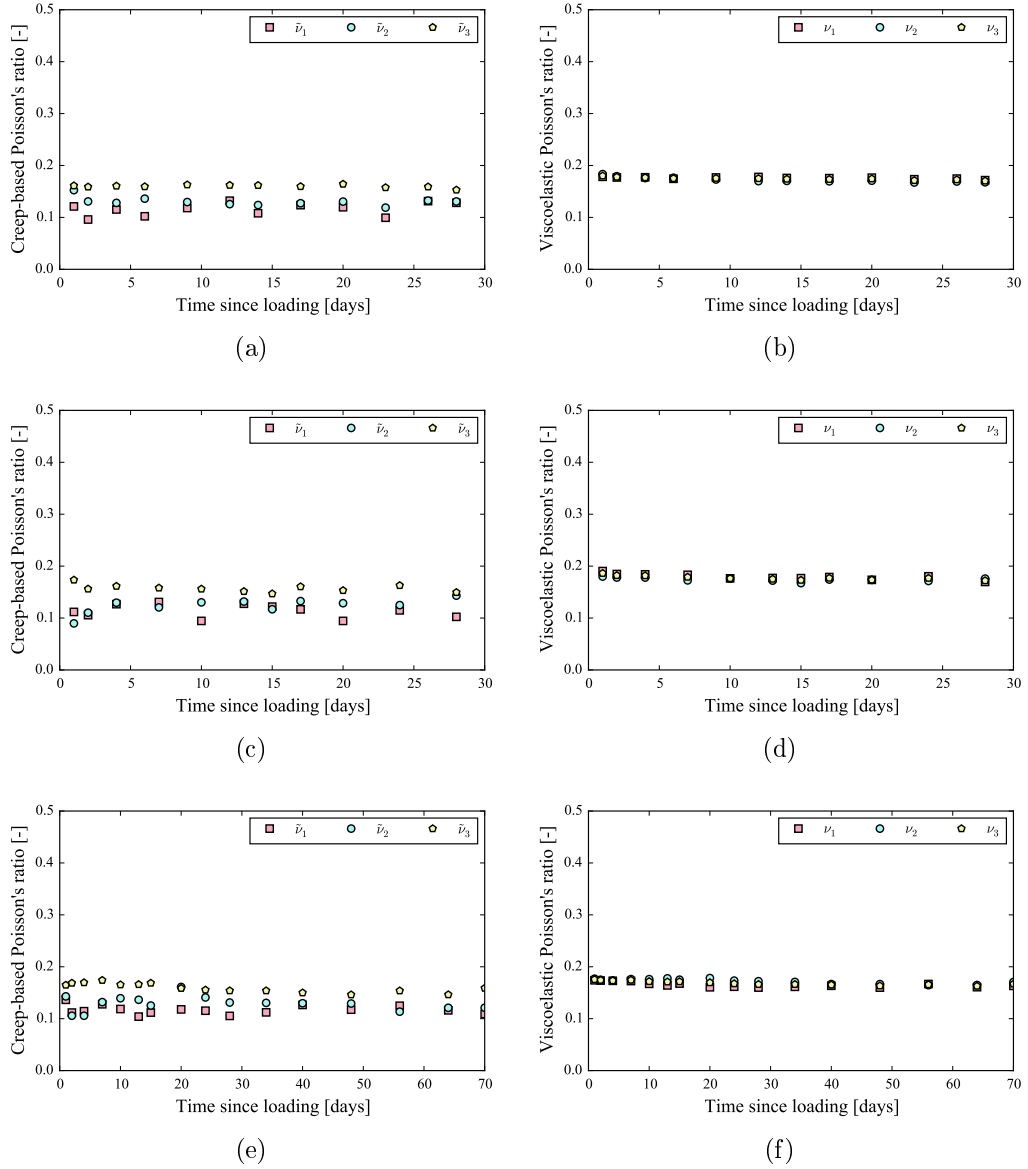


Figure C.3 – Dependency of Poisson's ratio on the direction: (a)(c)(e) creep-based Poisson's ratio reported in [Gopalakrishnan \(1968\)](#), calculated from Eq. (17) for three directions; (b)(d)(f) viscoelastic Poisson's ratio calculated from Eq. (5) for three directions. Data (a)(b) from experiment BC8, (c)(d) from experiment BT9, (e)(f) from experiment TC11 in [Gopalakrishnan \(1968\)](#):

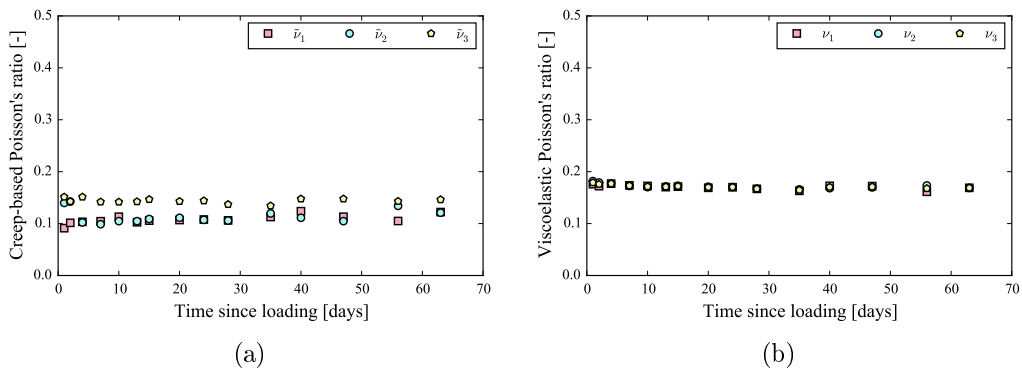


Figure C.4 – Dependency of Poisson's ratio on the direction in experiment TC12 in Gopalakrishnan (1968): (a) creep-based Poisson's ratio reported in Gopalakrishnan (1968), calculated from Eq. (17) for three directions; (b) viscoelastic Poisson's ratio calculated from Eq. (5) for three directions.

APPENDIX C. COMPARAISON OF POISSON'S RATIO AND
CREEP-BASED POISSON'S RATIO IN DIFFERENT DIRECTIONS

Appendix D

Experimental data of concrete Poisson's ratio from literature

In this section, we present all the experimental data of the evolution of Poisson's ratio of concrete. The evolution of the Poisson's ratio is computed from Eq. 3.2. Each test is described briefly in the following:

The tests of [Gopalakrishnan \(1968\)](#) are on cubic sample concrete. The load is applied at the age of 8 days in three direction consequently. The values of load are:

- Test TC1: $\sigma_1 = -5.69$ MPa, $\sigma_2 = -5.55$ MPa, $\sigma_3 = -3.59$ MPa;
- Test BC4: $\sigma_1 = -5.21$ MPa, $\sigma_2 = -3.59$ MPa, $\sigma_3 = -0$;
- Test TC5: $\sigma_1 = -10.0$ MPa, $\sigma_2 = -7.72$ MPa, $\sigma_3 = -3.14$ MPa;
- Test TC5R: $\sigma_1 = -9.89$ MPa, $\sigma_2 = -7.55$ MPa, $\sigma_3 = -3.03$ MPa;
- Test TC6: $\sigma_1 = -11.2$ MPa, $\sigma_2 = -9.72$ MPa, $\sigma_3 = -2.10$ MPa;
- Test TC7: $\sigma_1 = -12.55$ MPa, $\sigma_2 = -11.45$ MPa, $\sigma_3 = -2.45$ MPa;
- Test BC8: $\sigma_1 = -12.58$ MPa, $\sigma_2 = -7.24$ MPa, $\sigma_3 = 0$;
- Test BT9: $\sigma_1 = -8.41$ MPa, $\sigma_2 = -5.62$ MPa, $\sigma_3 = 0$;
- Test TC10: $\sigma_1 = -13.24$ MPa, $\sigma_2 = -1.76$ MPa, $\sigma_3 = -1.83$ MPa;

APPENDIX D. EXPERIMENTAL DATA OF CONCRETE POISSON'S RATIO FROM LITERATURE

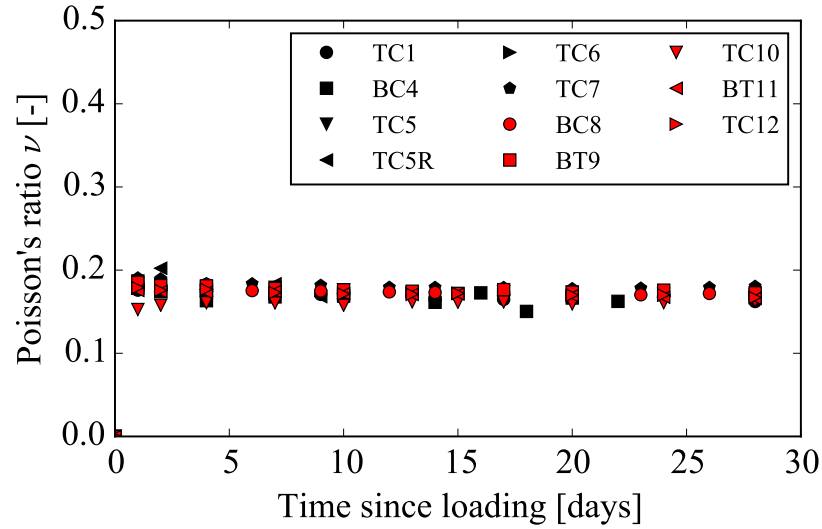


Figure D.1 – Poisson's ratio of concrete versus time. Data retrieved from [Gopalakrishnan \(1968\)](#)

- Test BT11: $\sigma_1 = -13.38$ MPa, $\sigma_2 = -13.89$ MPa, $\sigma_3 = 0$;
- Test TC12: $\sigma_1 = -12.82$ MPa, $\sigma_2 = -13.24$ MPa, $\sigma_3 = -6.34$ MPa;

The evolution of Poisson's ratio in these test are displayed in Fig. D.1.

[Jordaan and Illston \(1969, 1971\)](#) tested cubic sample of concrete under uniaxial and biaxial load. Loading age is 16 days. The load values for the tests from [Jordaan and Illston \(1969\)](#) are:

- Serie 1, uniaxial test: $\sigma_1 = -10.0$ MPa, $\sigma_2 = \sigma_3 = 0$;
- Serie 1, biaxial test: $\sigma_1 = \sigma_2 = -9.50$ MPa, $\sigma_3 = 0$;
- Serie 2, uniaxial test: $\sigma_1 = -10.6$ MPa, $\sigma_2 = \sigma_3 = 0$;
- Serie 2, biaxial test: $\sigma_1 = -10.6$ MPa, $\sigma_2 = -3.32$ MPa, $\sigma_3 = 0$;

The load values for the tests from [Jordaan and Illston \(1971\)](#) are:

- Uniaxial test: $\sigma_1 = -5.2$ MPa, $\sigma_2 = \sigma_3 = 0$;
- Biaxial test: $\sigma_1 = -5.2$ MPa, $\sigma_2 = -6.9$ MPa, $\sigma_3 = 0$;

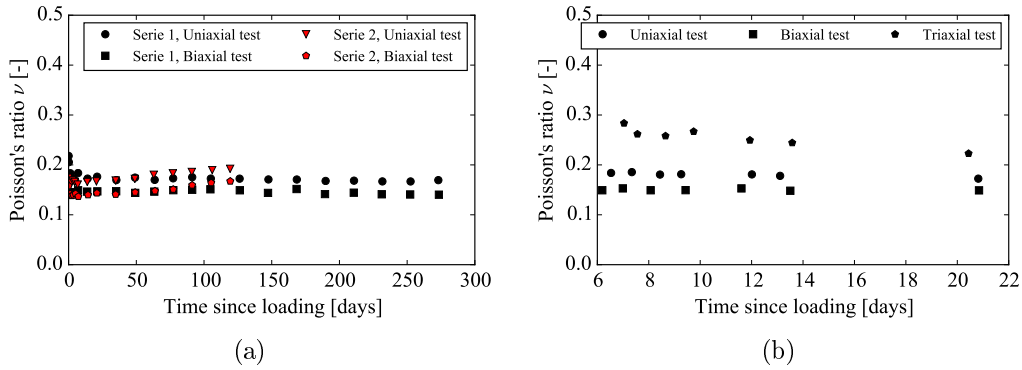


Figure D.2 – (a) Poisson’s ratio versus time. Data retrieved from [Jordaan and Illston \(1969\)](#). (b) Poisson’s ratio versus time. Data retrieved from [Jordaan and Illston \(1971\)](#).

- Triaxial test: $\sigma_1 = -5.2$ MPa, $\sigma_2 = -6.9$ MPa, $\sigma_3 = 3.5$ MPa;

The evolution of Poisson’s ratio for the test from [Jordaan and Illston \(1969\)](#) are displayed in Fig. D.2a and those from [Jordaan and Illston \(1971\)](#) are displayed in Fig. D.2b.

[Kennedy \(1975\)](#) performed uniaxial and triaxial creep tests on cylindrical specimen. The axial load σ_a and radial load σ_r are list in the following list, as well as loading age:

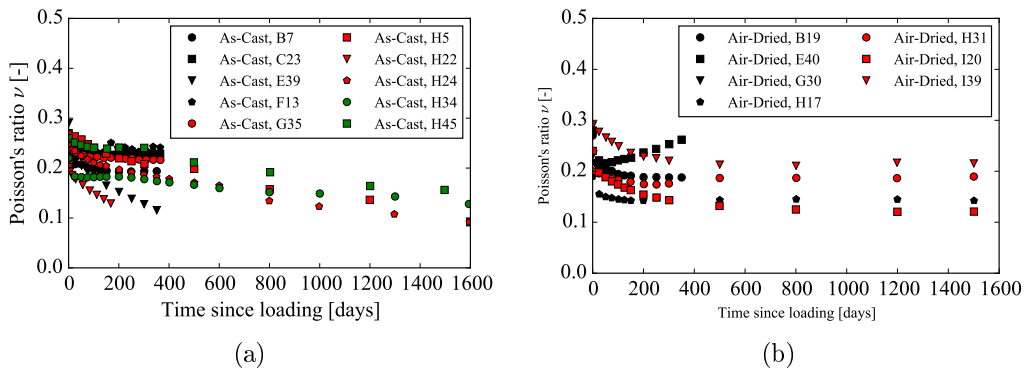


Figure D.3 – (a) Poisson’s ratio versus time for As-Cast concrete specimens. Data retrieved from [Kennedy \(1975\)](#). (b) Poisson’s ratio versus time for Air-Dried specimens. Data retrieved from [Kennedy \(1975\)](#).

APPENDIX D. EXPERIMENTAL DATA OF CONCRETE POISSON'S RATIO FROM LITERATURE

- As-Cast, B7: $\sigma_a = -16.55$ MPa, $\sigma_r = 0$, loading age 90 days;
- As-Cast, C23: $\sigma_a = 0$, $\sigma_r = -16.55$ MPa, loading age 90 days;
- As-Cast, E39: $\sigma_a = 4.14$ MPa, $\sigma_r = 0$, loading age 90 days;
- As-Cast, F13: $\sigma_a = 0$, $\sigma_r = -4.14$ MPa, loading age 90 days;
- As-Cast, G35: $\sigma_a = -4.14$ MPa, $\sigma_r = -24.82$ MPa;
- As-Cast, H5: $\sigma_a = -4.14$ MPa, $\sigma_r = 0$, loading age 365 days;
- As-Cast, H22: $\sigma_a = 0$, $\sigma_r = -24.82$ MPa;
- As-Cast, H24: $\sigma_a = -16.55$ MPa, $\sigma_r = 0$, loading age 365 days;
- As-Cast, H34: $\sigma_a = -16.55$ MPa, $\sigma_r = 0$, loading age 183 days;
- As-Cast, H45: $\sigma_a = -4.14$ MPa, $\sigma_r = 0$, loading age 183 days;
- Air-Dried, B19: $\sigma_a = -16.55$ MPa, $\sigma_r = 0$, loading age 90 days;
- Air-Dried, E40: $\sigma_a = 4.14$ MPa, $\sigma_r = 0$, loading age 90 days;
- Air-Dried, G30: $\sigma_a = -4.14$ MPa, $\sigma_r = -24.82$ MPa;
- Air-Dried, H17: $\sigma_a = -16.55$ MPa, $\sigma_r = 0$, loading age 365 days;
- Air-Dried, H31: $\sigma_a = -4.14$ MPa, $\sigma_r = 0$, loading age 365 days;
- Air-Dried, I20: $\sigma_a = -16.55$ MPa, $\sigma_r = 0$, loading age 183 days;
- Air-Dried, I39: $\sigma_a = -4.14$ MPa, $\sigma_r = 0$, loading age 183 days;

The evolution of the Poisson's ratio for As-Cast samples are displayed in Fig. D.3a and those for Air-Dried samples are displayed in Fig. D.3b.

Kim et al. (2005) tested cubic concrete sample which are cured until age of 28 days under water. The loading age is 28 days. The load values for each test are:

- Concrete C1, uniaxial test 1: $\sigma_1 = -4.90$ MPa, $\sigma_2 = \sigma_3 = 0$;

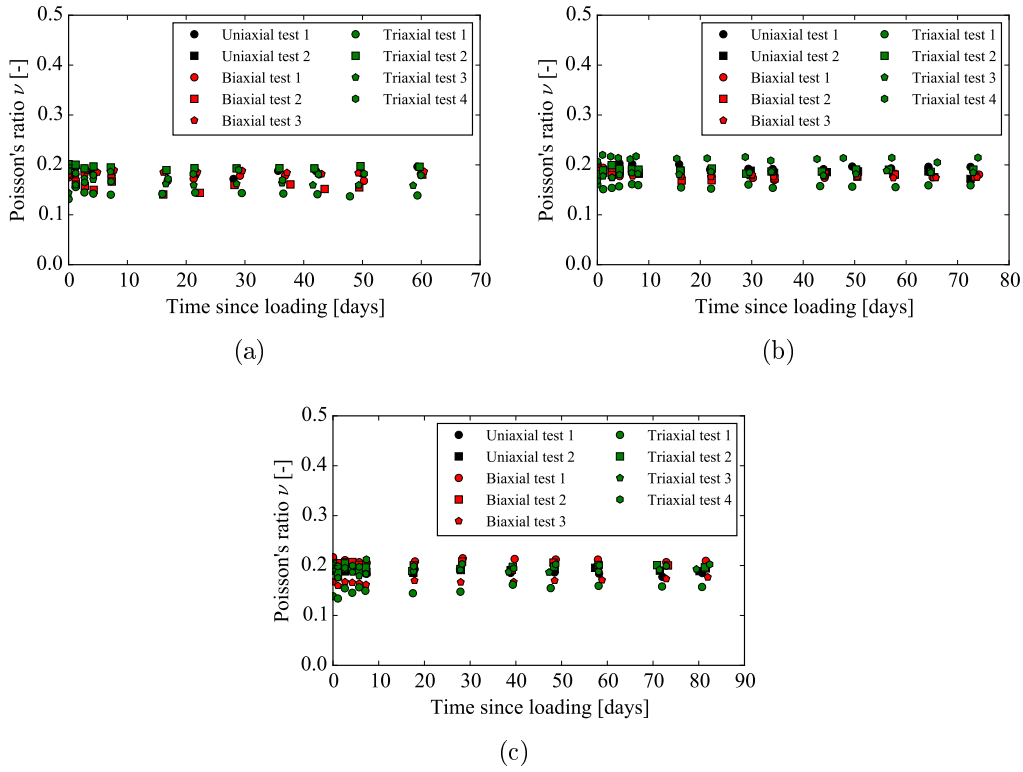


Figure D.4 – (a) Poisson’s ratio versus time for C1 concrete specimens. Data retrieved from [Kim et al. \(2005\)](#). (b) Poisson’s ratio versus time for C2 concrete specimens. Data retrieved from [Kim et al. \(2005\)](#). (c) Poisson’s ratio versus time for C3 concrete specimens. Data retrieved from [Kim et al. \(2005\)](#).

- Concrete C1, uniaxial test 2: $\sigma_1 = -9.80$ MPa, $\sigma_2 = \sigma_3 = 0$;
- Concrete C1, biaxial test 1: $\sigma_1 = -4.90$ MPa, $\sigma_2 = -0.98$ MPa, $\sigma_3 = 0$;
- Concrete C1, biaxial test 2: $\sigma_1 = -4.90$ MPa, $\sigma_2 = -1.96$ MPa, $\sigma_3 = 0$;
- Concrete C1, biaxial test 3: $\sigma_1 = -9.80$ MPa, $\sigma_2 = -1.96$ MPa, $\sigma_3 = 0$;
- Concrete C1, triaxial test 1: $\sigma_1 = -4.90$ MPa, $\sigma_2 = \sigma_3 = -0.49$ MPa;
- Concrete C1, triaxial test 2: $\sigma_1 = -4.90$ MPa, $\sigma_2 = \sigma_3 = -0.98$ MPa;
- Concrete C1, triaxial test 3: $\sigma_1 = -4.90$ MPa, $\sigma_2 = \sigma_3 = -1.96$ MPa;

APPENDIX D. EXPERIMENTAL DATA OF CONCRETE POISSON'S RATIO FROM LITERATURE

- Concrete C1, triaxial test 4: $\sigma_1 = -4.90$ MPa, $\sigma_2 = -1.96$ MPa, $\sigma_3 = -0.98$ MPa;
- Concrete C2, uniaxial test 1: $\sigma_1 = -7.35$ MPa, $\sigma_2 = \sigma_3 = 0$;
- Concrete C2, uniaxial test 2: $\sigma_1 = -9.80$ MPa, $\sigma_2 = \sigma_3 = 0$;
- Concrete C2, biaxial test 1: $\sigma_1 = -7.35$ MPa, $\sigma_2 = -1.47$ MPa, $\sigma_3 = 0$;
- Concrete C2, biaxial test 2: $\sigma_1 = -7.35$ MPa, $\sigma_2 = -2.94$ MPa, $\sigma_3 = 0$;
- Concrete C2, biaxial test 3: $\sigma_1 = -9.80$ MPa, $\sigma_2 = -2.94$ MPa, $\sigma_3 = 0$;
- Concrete C2, triaxial test 1: $\sigma_1 = -7.35$ MPa, $\sigma_2 = \sigma_3 = -0.74$ MPa;
- Concrete C2, triaxial test 2: $\sigma_1 = -7.35$ MPa, $\sigma_2 = \sigma_3 = -1.47$ MPa;
- Concrete C2, triaxial test 3: $\sigma_1 = -7.35$ MPa, $\sigma_2 = \sigma_3 = -2.94$ MPa;
- Concrete C2, triaxial test 4: $\sigma_1 = -7.35$ MPa, $\sigma_2 = -2.94$ MPa, $\sigma_3 = -1.96$ MPa;
- Concrete C3, uniaxial test 1: $\sigma_1 = -9.80$ MPa, $\sigma_2 = \sigma_3 = 0$;
- Concrete C3, uniaxial test 2: $\sigma_1 = -12.25$ MPa, $\sigma_2 = \sigma_3 = 0$;
- Concrete C3, biaxial test 1: $\sigma_1 = -9.80$ MPa, $\sigma_2 = -1.96$ MPa, $\sigma_3 = 0$;
- Concrete C3, biaxial test 2: $\sigma_1 = -9.80$ MPa, $\sigma_2 = -3.92$ MPa, $\sigma_3 = 0$;
- Concrete C3, biaxial test 3: $\sigma_1 = -12.25$ MPa, $\sigma_2 = -3.92$ MPa, $\sigma_3 = 0$;
- Concrete C3, triaxial test 1: $\sigma_1 = -9.80$ MPa, $\sigma_2 = \sigma_3 = -0.98$ MPa;
- Concrete C3, triaxial test 2: $\sigma_1 = -9.80$ MPa, $\sigma_2 = \sigma_3 = -1.96$ MPa;
- Concrete C3, triaxial test 3: $\sigma_1 = -9.80$ MPa, $\sigma_2 = \sigma_3 = -3.92$ MPa;
- Concrete C3, triaxial test 4: $\sigma_1 = -9.80$ MPa, $\sigma_2 = -3.92$ MPa, $\sigma_3 = -1.96$ MPa;

The evolution of Poisson's ratio for concrete C1, C2 and C3 are displayed in Fig. [D.4a](#), b and c, respectively.

APPENDIX D. EXPERIMENTAL DATA OF CONCRETE POISSON'S
RATIO FROM LITERATURE

Appendix E

Autogenous shrinkage database

This section is devoted to present autogenous shrinkage data that are displayed in Fig. 5.6. For each data are given author and year of the work, file number that corresponds database (Bažant and Li, 2008) collected in Northwestern University, mix design properties and long-term log-slope of autogenous shrinkage, see Tab. E.1 and E.2.

APPENDIX E. AUTOGENOUS SHRINKAGE DATABASE

Author	File ¹	w/c ²	a/c ³	c ⁴	α_{cr} ⁶
Brooks (1984)	e_074_20	0.67	4.75	366	-26.3
Brooks (1984)	e_074_29	0.76	4.75	383	-98.94
Brooks (1984)	e_074_30	0.62	4.75	344	-83.22
Brooks (1984)	e_074_33	0.86	4.75	457	-46.73
Brooks (1984)	e_074_35	0.63	4.75	387	-42.43
Shritharan (1989)	e_079_6	0.47	5.09	393	7.51
Larrard (1990)	A_022_2	0.35	3.96	450	82.13
Larrard (1990)	A_022_3	0.35	3.96	450	7.49
Larrard (1990)	A_022_5	0.35	3.96	450	15.96
Tazawa (1993)	A_062_6	0.3	0	533	129.92
Tazawa (1993)	A_062_7	0.3	0	533	221.16
Tazawa (1993)	A_062_8	0.3	0	533	224.33
Tazawa (1993)	A_062_9	0.3	0	533	90.08
Tazawa (1993)	A_062_12	0.3	0	533	83.14
Tazawa (1993)	A_062_13	0.3	0	533	136.05
Tazawa (1993)	A_062_14	0.3	0	533	132.06
Tazawa (1993)	A_062_15	0.3	0	533	164.82
Tazawa (1995)	A_063_22	0.3	0	NAN	1.71
Tazawa (1995)	A_063_27	0.4	0	NAN	1.69
Tazawa (1995)	A_063_39	0.3	0	NAN	4.35
Tazawa (1995)	A_063_42	0.3	0	NAN	2.42
Tazawa (1995)	A_063_44	0.3	0	NAN	0.03
Tazawa (1995)	A_063_49	0.3	0	NAN	9.01
Tazawa (1995)	A_063_50	0.3	0	NAN	8.49
Tazawa (1995)	A_063_51	0.3	0	NAN	8.85

Table E.1 – Details of autogenous shrinkage data (first part). ¹File corresponds to the file number in the database compiled by Prof. Bažant and his collaborators (Bažant and Li, 2008); ²w/c: water-to-cement ratio; ³a/c: aggregate-to-cement mass ratio; ⁴c: cement per volume of mixture [kg/m³]; ⁵ α_{sh} : Fitted parameter in Eq. 5.1, [$\mu\text{m}/\text{m}$]

Author	File ¹	w/c ²	a/c ³	c ⁴	α_{sh} ⁶
Weiss (1998)	A_068_1	0.3	3.04	485	63.01
Weiss (1998)	A_068_16	0.3	3.04	485	59.57
Weiss (1998)	A_068_19	0.3	3.04	485	61.54
Brooks (2001)	A_007_8	0.28	4	450	14.39
Brooks (2001)	A_007_12	0.28	4	450	15.18
Lee (2003)	A_023_1	0.5	4.66	370	5.59
Lee (2003)	A_023_2	0.35	3.85	450	23.07
Lee (2003)	A_023_3	0.31	3.4	500	24.23
Lee (2003)	A_023_4	0.27	3.05	550	19.58
Lee (2003)	A_023_8	0.34	3.73	440	20.44
Lee (2003)	A_023_9	0.31	3.4	500	29.5
Zhang (2003)	A_072_1	0.26	3.7	496	38.97
Zhang (2003)	A_072_2	0.3	3.6	497	40.17
Mazloom (2004)	A_031_2	0.35	3.7	500	30.64
Vidal (2005)	A_065_3	0.44	3.7	450	10.95
Vidal (2005)	A_065_5	0.53	5.25	350	27.99
Lee (2006)	A_024_1	0.3	2.73	583	29.96
Lee (2006)	A_024_2	0.4	3.92	438	17.17
Lee (2006)	A_024_3	0.5	5.09	350	12.57
Lee (2006)	A_024_4	0.6	6.43	292	9

Table E.2 – Details of autogenous shrinkage data (second part). ¹File corresponds to the file number in the database compiled by Prof. Bažant and his collaborators (Bažant and Li, 2008); ²w/c: water-to-cement ratio; ³a/c: aggregate-to-cement mass ratio; ⁴c: cement per volume of mixture [kg/m³]; ⁵ α_{sh} : Fitted parameter in Eq. 5.1, [$\mu\text{m}/\text{m}$]

APPENDIX E. AUTOGENOUS SHRINKAGE DATABASE

Appendix F

Basic creep database

This section is devoted to present basic creep data that are displayed in Fig. 5.3. For each data are given author and year of the work, file number that corresponds database (Bažant and Li, 2008) collected in Northwestern University, mix design properties, age of loading and long-term log-slope of basic creep, see Tabs. F.1 and F.2.

APPENDIX F. BASIC CREEP DATABASE

Author	File ¹	w/c ²	a/c ³	c ⁴	t ₀ ⁵	1/C _c ^{E6}
Hanson (1953a)	C_002_1	0.58	5.62	346	28	6.76
Hanson (1953a)	C_002_3	0.56	6.14	320	7	8.39
Hanson (1953b)	C_101_1	0.58	9.6	362	28	6.37
Browne (1967)	C_025_15	0.42	4.4	418	28	5.94
Browne (1967)	C_025_16	0.42	4.4	418	60	8.54
Rostasy (1972)	C_043_3	0.41	5.59	332	28	6.13
Kommendant (1976a)	C_104_1	0.38	4.34	419	28	4.88
Kommendant (1976a)	C_104_2	0.38	4.34	419	90	4.28
Kommendant (1976b)	C_054_1	0.38	4.34	419	28	8.42
Kommendant (1976b)	C_054_2	0.38	4.34	419	90	8.67
Kommendant (1976b)	C_054_14	0.38	4.03	449	28	6.07
Kommendant (1976b)	C_054_15	0.38	4.03	449	90	7.67
Takahashi (1980)	J_015_3	0.4	4.45	400	30	6.35
Kawasumi (1982)	J_018_1	0.47	6.01	304	7	9.16
Kawasumi (1982)	J_018_2	0.47	6.01	304	28	12.08
Kawasumi (1982)	J_018_3	0.47	6.01	304	91	11.32
Kawasumi (1982)	J_018_9	0.49	6.79	286	7	12.96
Kawasumi (1982)	J_018_10	0.49	6.79	286	28	13.95
Kawasumi (1982)	J_018_11	0.49	6.79	286	91	13.21
Brooks (1983)	C_072_2	0.27	3.3	535	28	5.83
Brooks (1983)	C_072_3	0.34	2.6	608	28	17.62
Brooks (1983)	C_072_4	0.27	2.6	628	28	12.75
Brooks (1983)	C_072_5	0.3	2.08	725	28	19.21
Brooks (1984)	C_074_19	0.8	4.75	405	14	24.09
Brooks (1984)	C_074_20	0.67	4.75	366	14	13.61
Brooks (1984)	C_074_21	0.58	4.75	337	14	9.17
Brooks (1984)	C_074_22	0.54	4.75	326	14	9.01
Brooks (1984)	C_074_23	0.5	4.75	311	14	6.73
Brooks (1984)	C_074_24	0.8	4.75	389	14	26.88
Brooks (1984)	C_074_25	0.67	4.75	351	14	20.68
Brooks (1984)	C_074_26	0.56	4.75	317	14	9.36

Table F.1 – Details of basic creep data (first part). ¹File corresponds to the file number in the database compiled by Prof. Bažant and his collaborators (Bažant and Li, 2008); ²w/c: water-to-cement ratio; ³a/c: aggregate-to-cement mass ratio; ⁴c: cement per volume of mixture [kg/m³]; ⁵t₀: loading age [days]; ⁶1/C_c^E: Fitted parameter in Eq. 5.3, [μm/m/MPa].

Author	File ¹	w/c ²	a/c ³	c ⁴	t ₀ ⁵	1/C _c ^{E6}
Brooks (1984)	C_074_27	0.48	4.75	292	14	9.21
Brooks (1984)	C_074_28	0.4	4.75	267	14	8.29
Bryant (1987)	D_075_1	0.47	1.37	390	8	8.63
Bryant (1987)	D_075_2	0.47	1.37	390	14	8.86
Bryant (1987)	D_075_3	0.47	1.37	390	21	10.83
Bryant (1987)	D_075_4	0.47	1.37	390	28	10.28
Bryant (1987)	D_075_5	0.47	1.37	390	84	10.01
Larrard (1988)	C_122_4	0.44	3.75	410	28	9.08
Shritharan (1989)	C_079_7	0.47	5.09	390	8	8.3
Shritharan (1989)	C_079_8	0.47	5.09	390	14	8.93
Shritharan (1989)	C_079_9	0.47	5.09	390	21	12.57
Shritharan (1989)	C_079_10	0.47	5.09	390	28	10.47
Shritharan (1989)	C_079_11	0.47	5.09	390	84	10.78
Larrard (1990)	D_022_2	0.35	3.96	450	5	4.42
Larrard (1990)	D_022_3	0.35	3.96	450	3	3.14
Larrard (1990)	D_022_4	0.35	3.96	450	7	4.08
Larrard (1990)	D_022_5	0.35	3.96	450	3	4.1
Leroy (1995)	C_123_1	0.5	5.46	342	0.83	4.11
Leroy (1995)	C_123_3	0.5	5.46	342	3	3.83
Leroy (1995)	C_123_4	0.5	5.46	342	7	4.33
Leroy (1995)	C_123_5	0.5	5.46	342	28	4.92
Leroy (1995)	C_123_34	0.33	4.35	426	3	1.52
Leroy (1995)	C_123_35	0.33	4.35	426	7	1.91
Leroy (1995)	C_123_36	0.33	4.35	426	28	3.52
Mazloom (2004)	D_031_2	0.35	3.7	500	7	16.86
Mazloom (2004)	D_031_10	0.35	3.7	500	28	15.1
Mazzotti (2005)	D_033_3	0.42	4.32	418	7	10.75
Mu (2009)	D_036_11	0.58	7.15	275	3	14.61

Table F.2 – Details of basic creep data (second part). ¹File corresponds to the file number in the database compiled by Prof. Bažant and his collaborators (Bažant and Li, 2008); ²w/c: water-to-cement ratio; ³a/c: aggregate-to-cement mass ratio; ⁴c: cement per volume of mixture [kg/m³]; ⁵t₀: loading age [days]; ⁶1/C_c^E: Fitted parameter in Eq 5.3, [μm/m/MPa].

APPENDIX F. BASIC CREEP DATABASE

Appendix G

Experimental data of evolution of relative humidity with respect to time under autogenous condition

This section is devoted to present the experimental data of evolution of relative humidity under autogenous condition. For each data, the fitted long-term relative humidity h_r^∞ is displayed in legend of figure, see Fig. [G.1](#)

APPENDIX G. EXPERIMENTAL DATA OF EVOLUTION OF RELATIVE HUMIDITY WITH RESPECT TO TIME UNDER AUTOGENOUS CONDITION

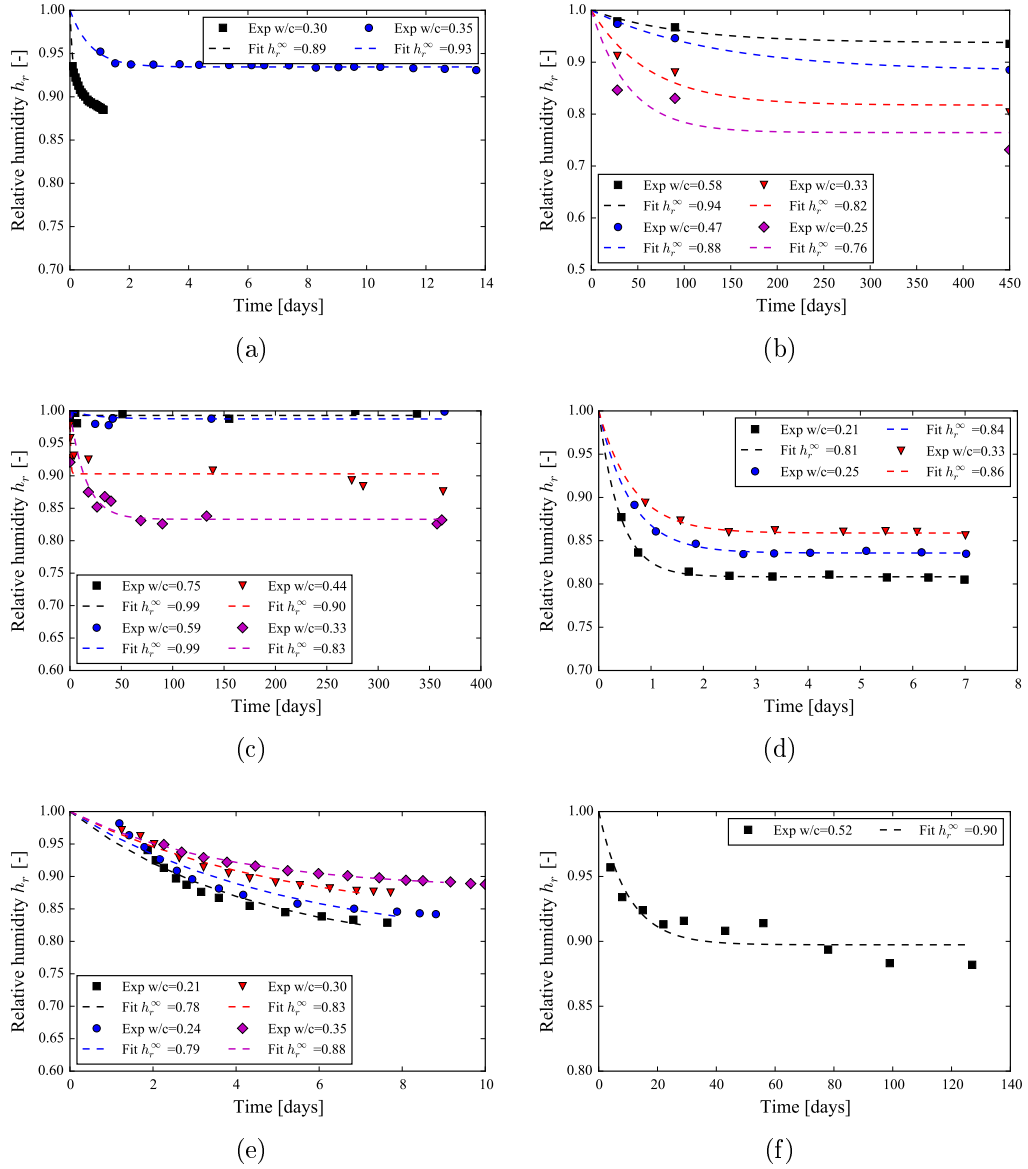


Figure G.1 – Evolution of relative humidity with respect to time under autogenous condition. Data from (a) Jensen and Hansen (1996, 1999), (b) Persson (1997), (c) Yssorche-Cubaynes and Ollivier (1999), (d) Zhutovsky and Kovler (2013), (e) Wyrzykowski and Lura (2016), (f) appendix H.

Appendix H

Experimental study of the influence of relative humidity on creep compliance of cement paste

[Bažant et al. \(1976\)](#); [Bažant and Chern \(1985\)](#); [Abiar \(1986\)](#) observed experimentally that, under autogenous condition, a pre-dried concrete creeps much more slowly than a humid concrete. This observation suggests that the creep modulus (see the definition in [chapter 5](#)) depends on relative humidity inside the porous network of concrete. In this study, we want to identify experimentally this dependency by tests on cement paste.

H.1 Material and methods

As a part of the VERCORS project, we prepare cement paste with cement CEM I and water. The water-to-cement ratio is 0.52. In total, 12 samples (see the notation of sample in [Fig. H.2.](#)) are casted into cylindrical molds whose diameter is 20 mm and height is 100 mm. The samples are rotated with a rotating device during the first 7 hours to avoid segregation and obtain a better homogeneity (see the setup for rotation in [Fig. H.1a](#)). We removed the samples from the molds at the age of 24 hours and wrapped each of them with four layers of aluminum and kept them wrapped until the age of 28

APPENDIX H. EXPERIMENTAL STUDY OF THE INFLUENCE OF RELATIVE HUMIDITY ON CREEP COMPLIANCE OF CEMENT PASTE

days. Then, we removed the aluminum layers from 9 samples and put them into three different desiccation boxes: 3 samples (1c, 1s, 1r) into the box in which relative humidity is controlled at 50%; 3 samples (2c, 2s, 2r) into the box in which relative humidity is controlled at 75%; 3 samples (3c, 3s, 3r) into the box in which relative humidity is controlled at 100%. The other left 3 specimens (4c, 4s, 4r) are kept wrapped. The relative humidity in boxes are controlled by saline solution: saturated solution of $Mg(NO_3)_2$ for $h_r = 50\%$, saturated solution of NaCl for $h_r = 75\%$ and tap water for $h_r = 100\%$. The room temperature is controlled at 20 ± 1 °C.

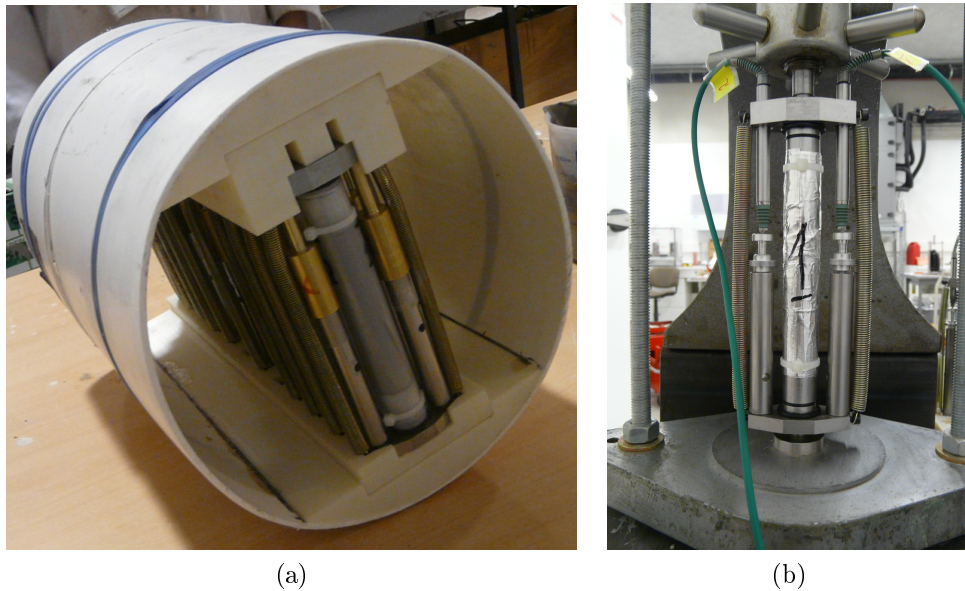


Figure H.1 – (a) Set up to rotate all 12 samples during the first 7 hours after casting. (b) LVDT to measure the strain of specimen.

The mass of each specimen is measured from time to time. At the end of the 4th month, the variation of mass of the specimens (1c, 1s, 1r) in the box of 50% of relative humidity was less than 0.05% during 30 days. Thus, we consider that the specimens reached hydric equilibrium with relative humidity of 50% (see Fig. H.3). Specimens that are in the box of 75% and of 100% of relative humidity have reached hydric equilibrium before. At the end of the 4th month, we rewrapped all of the 9 unwrapped specimens (1c, 1s, 1r, 2c, 2s, 2r, 3c, 3s, 3r) with four layers of aluminum. The curing and loading

history of the specimens are described in Fig. H.2. Then, the following tests are performed.

Specimen \ Age	1 - 28 days	28 – 142 days	142 – 336 days
	Cure	Drying	Test
1c	Sealed	Drying at 50% RH	Sealed, loaded
1s			Sealed, no load
1r			Characterize
2c		Drying at 75% RH	Sealed, loaded
2s			Sealed, no load
2r			Characterize
3c		Drying at 100% RH	Sealed, loaded
3s			Sealed, no load
3r			Characterize
4c		Sealed	Sealed, loaded
4s			Sealed, no load
4r			Characterize

Figure H.2 – Summary of storage and testing condition of the specimens

We took one specimen from each relative humidity (1c, 2c, 3c, 4c) and put them under a load of 12.56 MPa. The uniaxial compressive strength strength of cement paste at 28 days is measured and we found that the mean value of the strength is 40 MPa. As the applied load is around 30% of the uniaxial compressive strength, we consider that the delayed strain of the specimens are in the regime of linear viscoelasticity. The strain of each of these 4 specimen are measured by two LVDT. The accuracy of all of the LVDT is checked just before tests and found to be equal to 1 μm (see Fig. H.1b).

Next, we took one specimen from each relative humidity (1s, 2s, 3s, 4s) and measured the strain by two LVDT, the same measuring system as the above loaded test.

The strain of non-loaded specimen (1s, 2s, 3s, 4s) is the autogenous shrinkage of pre-dried specimen, whereas the strain of loaded specimen (1c, 2c, 3c, 4c) is the sum of autogenous shrinkage and basic creep of same pre-dried specimens. By subtracting the strain of former specimen from that of later specimens, we obtain the basic creep of predried specimens.

APPENDIX H. EXPERIMENTAL STUDY OF THE INFLUENCE OF RELATIVE HUMIDITY ON CREEP COMPLIANCE OF CEMENT PASTE

The other left four specimens (1r, 2r, 3r, 4r) are used to measure the hydration degree and water porosity.

The hydration degree is measured by thermogravimetric analysis. We put a small portion (around 200 mg) of grinded sample at the temperature of 80 °C until the mass of specimen stabilized to be M_{80} (approximately 2 hours). Then temperature is increased continuously till 550 °C in 45 minutes and kept under this temperature until the mass of specimen stabilized to be M_{550} (approximately 0.5 hour). The hydration degree is estimated by Eq. H.1 according to [Baroghel-Bouny et al. \(2002\)](#):

$$\xi = \frac{(M_{80} - M_{550})(1 + w/c)}{M_{80}E} \quad (\text{H.1})$$

where E is a coefficient related to the quantity of water for full hydration. For cement CEM I, we can take $E = 0.25$ ([Baroghel-Bouny et al., 2002](#)).

The water porosity of the sample is measured according to the French standard NF P 18-459. First we submerged a portion of sample (around 15 g) into water for 24 hours and measured the weight $M_w g$ in water (g is the gravity, [m/s²]). Then, we take the sample out of water and immediately measured the mass M_a . Finally, we dried sample at 105 °C until the mass stabilized at M_d . The water porosity reads:

$$\phi = \frac{M_a - M_d}{M_a - M_w} \quad (\text{H.2})$$

In addition to the above tests on cylindrical specimen, we casted at the same time cement pasts into cups with diameter of 4 cm and depth of 1.5 cm (filled depth is around 1 cm). The cups are closed with their own cap and wrapped up with fours layers of aluminum. At every due date, we opened two cups and measured the relative humidity inside the sample with dew point potential meter WP4C. Just after, one of the two samples is crushed into powder and used to measure the hydration degree by thermogravimetric analysis. By doing so, we follow up the evolution of relative humidity and degree of hydration under autogenous condition.

H.2 Results

Figure H.3 display the mass loss over time during the period of drying in desiccators. In the beginning of drying period in order to know approximately the date when we may stop drying, we performed finite element simulations of drying kinetics. The desorption isotherm of cement paste is modeled by Eq. 6.17 proposed by Van Genuchten (1980). The fitted parameters are: $a_1=0.36$, $b_1=36$ MPa.

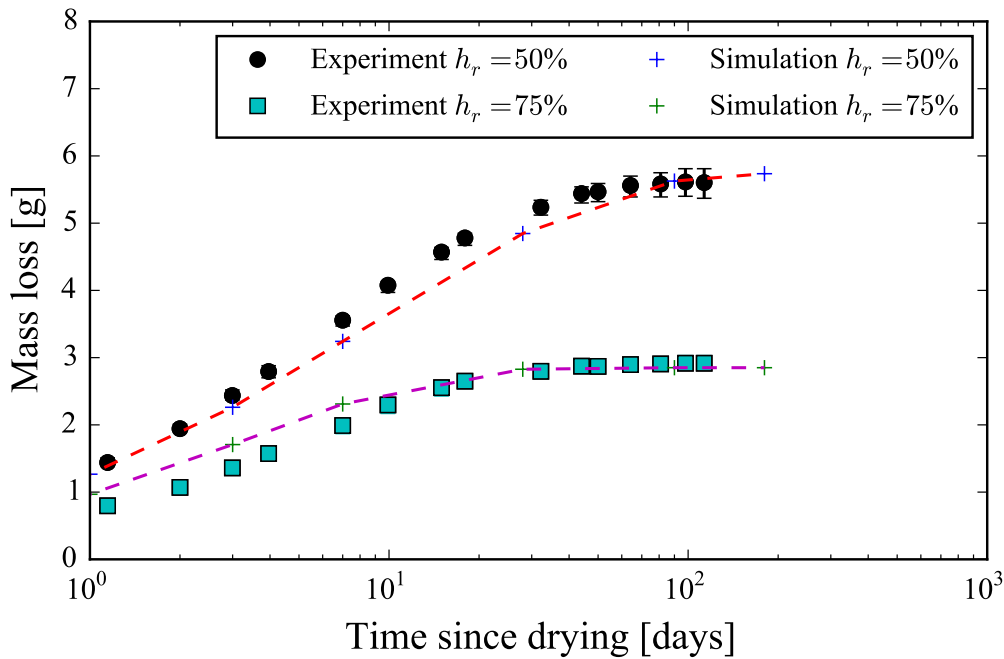
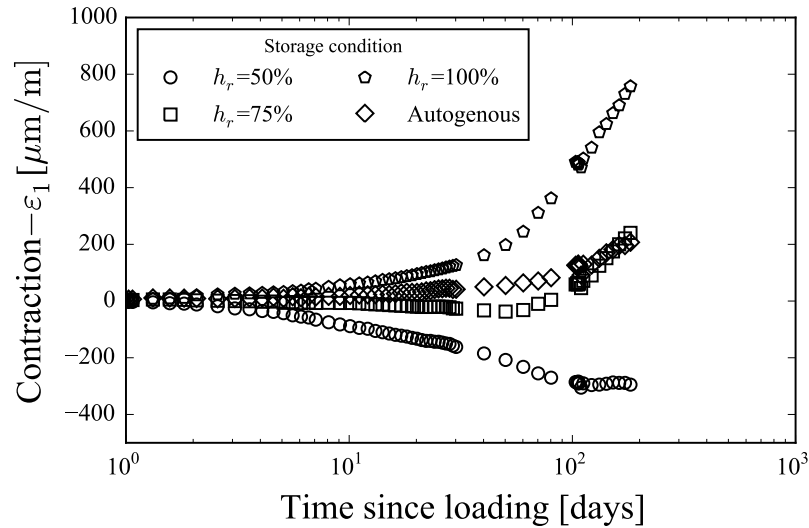


Figure H.3 – Mass loss over time. The experimental curve is the mean value of the three specimens in the same desiccator.

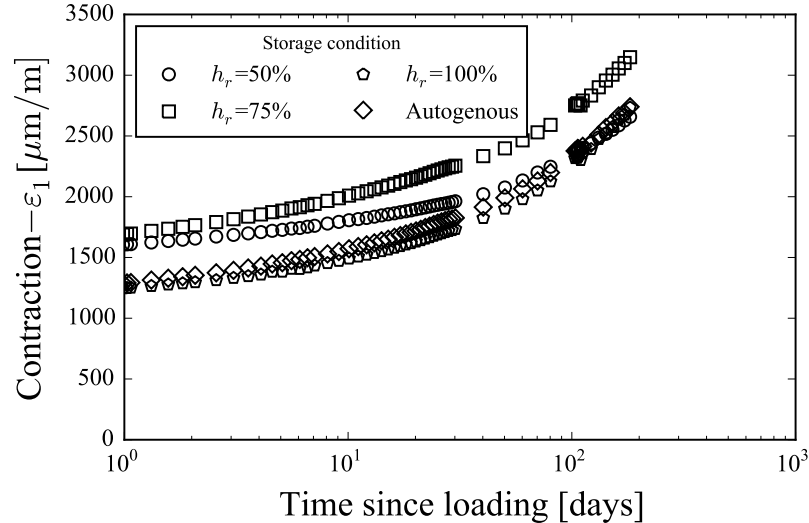
The measured strains are displayed in Fig. H.4. All of the 4 non-loaded specimens deformed during the test. The sample 1s that is kept under $h_r = 50\%$ expanded during the whole test. The sample 2s that is kept under $h_r = 75\%$ expanded at first then contracted. The sample 3s that is kept under $h_r = 100\%$ and the sample 4s that is kept sealed contracted. All of the 4 loaded sample showed logarithmic kinetics of strain at long term. However, the value of elastic modulus and creep modulus of these 4 specimens did not

APPENDIX H. EXPERIMENTAL STUDY OF THE INFLUENCE OF RELATIVE HUMIDITY ON CREEP COMPLIANCE OF CEMENT PASTE

show a simple correlation with the relative humidity h_r .



(a)



(b)

Figure H.4 – Measured total strain of (a) non-loaded specimens (b) loaded specimen.

The evolution of hydration degree ξ under autogenous condition is displayed in Fig. H.5. The hydration degree ξ was 0.7 at the age of 4 days and reached 0.9 at the age of 24 days.

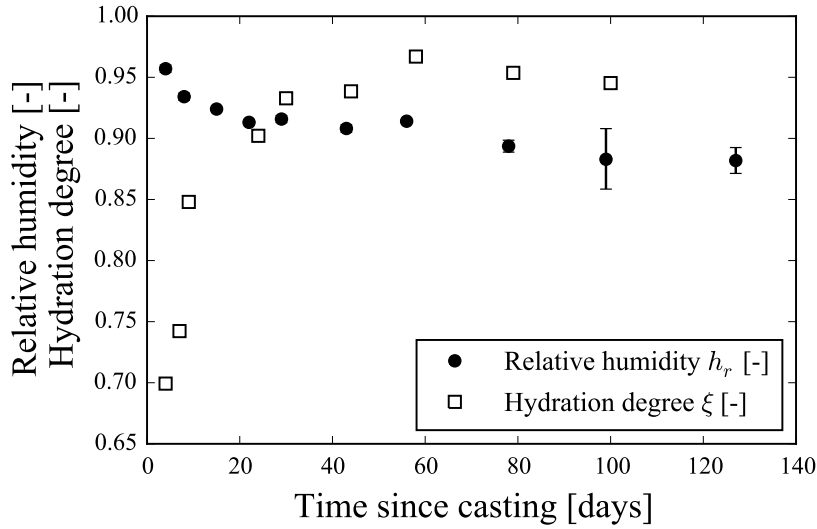


Figure H.5 – Evolution of hydration degree and relative humidity under autogenous condition

Figure H.5 shows also the mean value of relative humidity measured on two different cups at same age. Using Eq. 5.18, we found the long-term relative humidity $h_r^\infty = 0.88$.

H.3 Discussions

As described in Fig. H.2, we started the measurement of the strain of non-loaded specimen from the age of 142 days. Moreover, the water-to-cement ratio of the cement paste is 0.52. Hence we were expecting that the strain of non-loaded specimen would be much smaller comparing to the strain of loaded specimen. However, the amplitude of autogenous shrinkage of the sample 3s reached 25% of the strain the corresponding loaded sample 3c. In addition, the specimen 1c expands while others contract during the test. To understand the reason of these unexpected results, we checked if the specimens were well sealed during the test, if the relative humidity inside samples remained constant.

Table H.1 summarizes the mass loss of samples in each period. All of the four non-loaded samples lost mass during the test: sample 1s lost 0.25% of

APPENDIX H. EXPERIMENTAL STUDY OF THE INFLUENCE OF RELATIVE HUMIDITY ON CREEP COMPLIANCE OF CEMENT PASTE

Period	In Mold	Cure	Drying	Test	After test
Age	0-1 days	1-28 days	28-142 days	142-357 days	357-366 days
1c	0.17%	0.20%	9.07%	0.63%	0.32%
1s	0.17%	-0.02%	9.62%	0.25%	0.38%
2c	0.00%	0.07%	5.17%	0.68%	0.28%
2s	0.00%	0.19%	4.80%	0.62%	0.42%
3c	0.00%	0.03%	-2.20%	0.50%	-0.15%
3s	0.00%	-0.02%	-2.57%	1.02%	-0.17%
4c	0.17%	0.00%	-0.05%	0.36%	-
3s	0.00%	0.00%	-0.03%	0.15%	-

Table H.1 – Mass loss of specimens per period. A positive value corresponds to decrease of mass whereas a negative value to mass increase. The mass variation during a period is normalized with respect to the mass of sample at the beginning of this period

its mass, 2s lost 0.62%, 3s lost 1.02% and 4c lost 0.15%. Comparing to the mass loss of 1s, 2s and 4s, the sample 3s lost more mass which may explain a larger strain. However, this is not compatible with the fact that the sample 1s expands while losing mass during the test.

In order to check if the relative humidity inside sample at the end of the test is higher or lower than the supposed relative humidity, we put back all samples again in the same desiccator as during the period of drying and measured the mass during ten days. The results in Tab. H.1 show that the sample 1s and 2s are losing again mass whereas the 3s is gaining mass. We suppose from this result that, in the end of the test, the relative humidity of the sample 1s is higher than 50%. This is contradictory with the fact that the sample 1s lost mass during the test.

Other physical phenomenon may be needed to explain the fact that sample 1s lost mass during the test but the relative humidity increased and the sample itself expanded. For example, during the test, the sample 1c lost water in capillary pores which explains the mass loss. In the same time, water migrated from gel pores to capillary pores with a delayed kinetics so that the relative humidity increased in capillary pores. However, a further theoretical investigation is necessary to support this idea.

As to the strain of loaded specimen, no clear relation can be found between the elastic strain and the relative humidity of the sample. Neglecting the autogenous shrinkage of these specimen, we fitted for each specimen creep compliance in the same form as Eq. 6.1. The bulk creep modulus of specimen 1c, 2c, 3c, 4c are 13.0 GPa, 9.8 GPa, 8.9 GPa, 9.9 GPa, respectively. From these values of creep modulus, we cannot conclude on the dependence of the creep modulus on relative humidity.

APPENDIX H. EXPERIMENTAL STUDY OF THE INFLUENCE OF
RELATIVE HUMIDITY ON CREEP COMPLIANCE OF CEMENT
PASTE

Bibliography

- 1992-1-1:2005, E. (2004). *Eurocode 2: Design of Concrete Structures: Part 1-1: General Rules and Rules for Buildings*. CEN.
Cited pages 63, 82, 117, 159, 160, 161, 163, and 185
- Abiar, G. (1986). *Cinétique de dessiccation et déformations différées du béton (analyse et modélisation)*. PhD thesis, École Nationale des Ponts et Chaussées.
Cited pages 60, 188, and 251
- ACI Committee 209 (2008). *Guide for Modeling and Calculating Shrinkage and Creep in Hardened Concrete (ACI 209.2R-08)*. American Concrete Institute.
Cited pages 59, 63, 82, 117, 159, and 185
- Acker, P. (1988). *Comportement mécanique du béton: apports de l'approche physico-chimique*. Number 152.
Cited page 62
- Acker, P. et al. (2001). Micromechanical analysis of creep and shrinkage mechanisms. *Creep, Shrinkage and Durability Mechanics of Concrete and other quasi-brittle Materials, Cambridge, MA*, pages 15–25.
Cited pages 32, 196, and 197
- Aili, A., Vandamme, M., Torrenti, J.-M., and Masson, B. (2015). Theoretical and practical differences between creep and relaxation poisson's ratios in linear viscoelasticity. *Mechanics of Time-Dependent Materials*, 19(4):537–555.
Cited pages 117 and 120
- Aili, A., Vandamme, M., Torrenti, J.-M., Masson, B., and Sanahuja, J. (2016). Time evolutions of non-aging viscoelastic poisson's ratio of con-

BIBLIOGRAPHY

- crete and implications for creep of c-s-h. *Cement and Concrete Research*, 90:144 – 161. *Cited page 165*
- ASTM-C150-C150M-16e1 (2016). Standard specification for portland cement, astm international. *ASTM International*, West Conshohocken, PA. *Cited pages 161 and 164*
- Auliac, G., Avignat, J., and Azoulay, É. (2000). *Techniques mathématiques pour la physique*. Ellipses. *Cited pages 96, 136, 139, 146, 151, 152, and 168*
- Baroghel-Bouny, V. (1994). *Caractérisation des pâtes de ciment et des bétons-Méthodes, analyse, interprétations*. PhD thesis, École Nationale des Ponts et Chaussées. *Cited pages 25, 32, 175, 176, 177, and 178*
- Baroghel-Bouny, V. (2007). Water vapour sorption experiments on hardened cementitious materials: Part i: Essential tool for analysis of hygral behaviour and its relation to pore structure. *Cement and Concrete Research*, 37(3):414–437. *Cited pages 26, 192, 193, and 194*
- Baroghel-Bouny, V., Chaussadent, T., Croquette, G., Divet, L., Gawsewitch, J., Godin, J., Henry, D., Platret, G., and Villain, G. (2002). Caractéristiques microstructurales et propriétés relatives à la durabilité des bétons(méthodes de mesure et d’essai de laboratoire). *Techniques et méthodes des Laboratoires des ponts et chaussées. Méthode*. *Cited page 254*
- Barthélémy, J.-F. (2005). *Approche micromécanique de la rupture et de la fissuration dans les géomatériaux*. PhD thesis, École Nationale des Ponts et Chaussées. *Cited page 147*
- Bazant, Z. P. and Li, G.-H. (2008). Comprehensive database on concrete creep and shrinkage. *ACI Materials Journal*, 105(6):635–637. *Cited pages 31, 32, 33, 161, 163, 165, 187, 241, 242, 243, 245, 246, and 247*
- Bazant, Z. P., Xi, Y.-P., Baweja, S., and Carol, I. (1993). Preliminary guidelines and recommendation for characterizing creep and shrinkage in structural design codes. In *RILEM Proceedings*, pages 805–805. CHAPMAN & HALL. *Cited pages 67 and 123*

- Bažant, Z. (1988). Material models for structural creep analysis. mathematical modeling of creep and shrinkage of concrete, ed. zp bazant. *Cited pages 65 and 82*
- Bažant, Z., Asghari, A., and Schmidt, J. (1976). Experimental study of creep of hardened portland cement paste at variable water content. *Materials and Structures*, 9(4):279–290. *Cited pages 60, 188, and 251*
- Bažant, Z. and Chern, J. (1985). Concrete creep at variable humidity: constitutive law and mechanism. *Materials and structures*, 18(1):1–20. *Cited pages 60, 62, 186, and 251*
- Bazant, Z. P. (1975). Theory of creep and shrinkage in concrete structures: A precis of recent developments. *Mechanics today*, 2:1–93. *Cited pages 130, 131, and 216*
- Bažant, Z. P., Hauggaard, A. B., Baweja, S., and Ulm, F.-J. (1997). Microprestress-solidification theory for concrete creep. i: Aging and drying effects. *Journal of Engineering Mechanics*, 123(11):1188–1194. *Cited pages 62, 82, and 122*
- Bazant, Z. P., Hubler, M. H., and Yu, Q. (2011). Pervasiveness of excessive segmental bridge deflections: Wake-up call for creep. *ACI Structural Journal*, 108(6):766–774. *Cited pages 136 and 159*
- Bažant, Z. P. and Prasannan, S. (1989). Solidification theory for concrete creep. i: Formulation. *Journal of engineering mechanics*, 115(8):1691–1703. *Cited page 82*
- Bažant, Z. P. and XI, Y. (1994). Drying creep of concrete: constitutive model and new experiments separating its mechanisms. *Materials and structures*, 27(1):3–14. *Cited pages 60 and 62*
- Bažant, Z. P. and Yunping, X. (1994). Drying creep of concrete: constitutive model and new experiments separating its mechanisms. *Materials and structures*, 27(1):3–14. *Cited pages 214 and 219*

BIBLIOGRAPHY

- Benboudjema, F. (2002). *Modélisation des déformations différées du béton sous sollicitations biaxiales. Application aux enceintes de confinement de bâtiments réacteurs des centrales nucléaires*. PhD thesis, Université de Marne-la-Vallée. *Cited pages 109 and 122*
- Benboudjema, F., Meftah, F., and Torrenti, J.-M. (2005). Interaction between drying, shrinkage, creep and cracking phenomena in concrete. *Engineering structures*, 27(2):239–250. *Cited pages 82 and 219*
- Benboudjema, F., Meftah, F., and Torrenti, J.-M. (2007). A viscoelastic approach for the assessment of the drying shrinkage behaviour of cementitious materials. *Materials and Structures*, 40(2):163–174. *Cited pages 61, 159, 160, 185, and 187*
- Bernard, O., Ulm, F.-J., and Germaine, J. T. (2003a). Volume and deviator creep of calcium-leached cement-based materials. *Cement and Concrete Research*, 33(8):1127–1136. *Cited pages 23, 104, 106, and 121*
- Bernard, O., Ulm, F.-J., and Lemarchand, E. (2003b). A multiscale micromechanics-hydration model for the early-age elastic properties of cement-based materials. *Cement and Concrete Research*, 33(9):1293 – 1309. *Cited pages 21, 76, 77, and 139*
- Brooks, J. (1984). Accuracy of estimating long-term strains in concrete. *Magazine of Concrete Research*, 36(128):131–145. *Cited pages 25, 26, 160, 172, 181, and 187*
- Brooks, J. and Johari, M. M. (2001). Effect of metakaolin on creep and shrinkage of concrete. *Cement and Concrete Composites*, 23(6):495–502. *Cited pages 26, 181, and 187*
- Brooks, J. and Wainwright, P. (1983). Properties of ultra-high-strength concrete containing a superplasticizer. *Magazine of Concrete Research*, 35(125):205–213. *Cited pages 25, 160, 172, and 187*

BIBLIOGRAPHY

- Browne, R. (London,1967). Properties of concrete in reactor vessels. In *Conference on Prestressed Concrete Pressure Vessels*, pages 11–31. Group C Institution of Civil Engineers. *Cited pages 25, 172, and 187*
- Bryant, A. H. and Vadhanavikkit, C. (1987). Creep, shrinkage-size, and age at loading effects. *Materials Journal*, 84(2):117–123. *Cited pages 25, 172, and 187*
- Budiansky, B. (1965). On the elastic moduli of some heterogeneous materials. *Journal of the Mechanics and Physics of Solids*, 13(4):223–227. *Cited page 74*
- Charpin, L., Le Pape, Y., Coustabeau, E., Masson, B., and Montalvo, J. (2015). Edf study of 10-year concrete creep under unidirectional and biaxial loading: Evolution of the poisson coefficient under sealed and unsealed conditions. In *CONCREEP 10*, pages 1381–1390. *Cited page 218*
- Charpin, L., Sow, T., D'estève De Pradel, X., Hamon, F., and Mathieu, J.-P. (Paris, France, July 2017). *Numerical simulation of 12 years long biaxial creep tests. Efficiency of assuming a constant Poisson's ratio*, pages 1–6. *Cited pages 207 and 218*
- Christensen, R. (1982). *Theory of viscoelasticity: an introduction*. Elsevier. *Cited pages 65, 66, 67, 93, 94, 104, 120, 135, 166, and 167*
- Constantinides, G. and Ulm, F.-J. (2004). The effect of two types of csh on the elasticity of cement-based materials: Results from nanoindentation and micromechanical modeling. *Cement and concrete research*, 34(1):67–80. *Cited pages 21, 32, 76, 77, 196, and 197*
- Coussy, O. (2004). *Poromechanics*. John Wiley & Sons. *Cited pages 79, 80, and 81*
- Coussy, O. (2011). *Mechanics and physics of porous solids*. John Wiley & Sons. *Cited pages 175, 178, and 180*

BIBLIOGRAPHY

- Coussy, O., Dangla, P., Lassabatère, T., and Baroghel-Bouny, V. (2004). The equivalent pore pressure and the swelling and shrinkage of cement-based materials. *Materials and structures*, 37(1):15–20. *Cited page 80*
- De Larrard, F. (1988). *Formulation et propriétés des bétons à très hautes performances*. PhD thesis, École Nationale des Ponts et Chaussées. *Cited pages 25, 172, and 187*
- De Larrard, F. (1990). Creep and shrinkage of high-strength field concretes. *Special Publication*, 121:577–598. *Cited pages 25, 26, 159, 160, 162, 172, 181, and 187*
- Di Bella, C., Wyrzykowski, M., and Lura, P. (2017). Evaluation of the ultimate drying shrinkage of cement-based mortars with poroelastic models. *Materials and Structures*, 50(1):52. *Cited pages 61 and 160*
- Duan, H., Yi, X., Huang, Z., and Wang, J. (2007). A unified scheme for prediction of effective moduli of multiphase composites with interface effects. part i: Theoretical framework. *Mechanics of Materials*, 39(1):81–93. *Cited page 146*
- Duke, C. M. and Davis, H. E. (1944). Some properties of concrete under sustained combined stresses. *ASTM Proc. 44*, pages 888–896. *Cited pages 64 and 117*
- Eshelby, J. D. (1957). The determination of the elastic field of an ellipsoidal inclusion, and related problems. In *Proceedings of the Royal Society of London A: Mathematical, Physical and Engineering Sciences*, volume 241, pages 376–396. The Royal Society. *Cited page 73*
- Evans, R. H. and Wood, R. H. (1937). Transverse elasticity of building materials. *Engineering*, 143:161–3. *Cited pages 64 and 117*
- Feldman, R. F. and Sereda, P. J. (1968). A model for hydrated portland cement paste as deduced from sorption-length change and mechanical properties. *Materials and structures*, 1(6):509–520. *Cited page 50*

FIB (2013). Model code for concrete structures 2010. *Ernst and Son*.
Cited pages 59, 63, 82, 117, 159, 160, and 185

Flatt, R. J., Scherer, G. W., and Bullard, J. W. (2011). Why alite stops hydrating below 80% relative humidity. *Cement and Concrete Research*, 41(9):987–992.
Cited pages 56, 172, and 175

Frech-Baronet, J., Sorelli, L., and Charron, J.-P. (2017). New evidences on the effect of the internal relative humidity on the creep and relaxation behaviour of a cement paste by micro-indentation techniques. *Cement and Concrete Research*, 91:39–51.
Cited pages 26, 159, 172, 187, 189, 190, and 191

Furr, H. L. (1967). Creep tests of two-way prestressed concrete. In *ACI Journal Proceedings*, volume 64. ACI.
Cited pages 64 and 117

Gardner, N. and Lockman, M. (2001). Design provisions for drying shrinkage and creep of normal-strength concrete. *Materials journal*, 98(2):159–167.
Cited page 82

Ghabezloo, S. (2010). Association of macroscopic laboratory testing and micromechanics modelling for the evaluation of the poroelastic parameters of a hardened cement paste. *Cement and Concrete research*, 40(8):1197–1210.
Cited pages 21, 77, 78, 80, 179, and 180

Glanville, W. and Thomas, F. (1939). Studies in reinforced concrete: Further investigations on the creep or flow of concrete under load. iv. In *Building Research Technical Paper No.21*, London.
Cited pages 64 and 117

Gopalakrishnan, K. S. (1968). *Creep of concrete under multiaxial compressive stresses*. PhD thesis, Civil Engineering, University of Calgary.
Cited pages 23, 27, 28, 65, 118, 123, 124, 125, 126, 128, 129, 131, 159, 227, 228, 229, 230, 231, 233, and 234

Gopalakrishnan, K. S., Neville, A. M., and Ghali, A. (1969). Creep Poisson's ratio of concrete under multiaxial compression. *ACI Journal*, 66(66):1008–1020.
Cited pages 104, 121, 122, and 123

BIBLIOGRAPHY

- Granger, L. (1995). *Comportement différé du béton dans les enceintes de centrales nucléaires: analyse et modélisation*. PhD thesis, Ecole Nationale des Ponts et Chaussées. Cited pages [26](#), [27](#), [32](#), [82](#), [122](#), [205](#), [208](#), [209](#), [210](#), [211](#), [213](#), [217](#), and [219](#)
- Granger, L., Torrenti, J.-M., and Acker, P. (1997). Thoughts about drying shrinkage: experimental results and quantification of structural drying creep. *Materials and structures*, 30(10):588. Cited pages [214](#) and [219](#)
- Grasley, Z. C. and Lange, D. A. (2007). Constitutive modeling of the aging viscoelastic properties of portland cement paste. *Mechanics of Time-Dependent Materials*, 11(3):175–198. Cited pages [65](#) and [119](#)
- Grasley, Z. C. and Leung, C. K. (2011). Desiccation shrinkage of cementitious materials as an aging, poroviscoelastic response. *Cement and Concrete Research*, 41(1):77–89. Cited pages [61](#), [160](#), [185](#), and [187](#)
- Hannant, D. (1967). Strain behaviour of concrete up to 95 °c under compressive stresses. In *Proc. Conference on Prestressed Concrete Pressure Vessels Group C, Institution of Civil Engineers, London*, pages 57–71. Cited page [122](#)
- Hanson, J. (1953). A ten-year study of creep properties of concrete. Technical Report No. SP-38, Concrete Laboratory, US Department of the Interior, Bureau of Reclamation, Denver. Cited pages [25](#), [172](#), and [187](#)
- Heukamp, F. H. (2003). *Chemomechanics of calcium leaching of cement-based materials at different scales: The role of CH-dissolution and CSH degradation on strength and durability performance of materials and structures*. PhD thesis, Massachusetts Institute of Technology. Cited page [106](#)
- Hilaire, A. (2014). *Etude des déformations différées des bétons en compression et en traction, du jeune au long terme: application aux enceintes de confinement*. PhD thesis, Cachan, Ecole normale supérieure. Cited pages [109](#) and [122](#)

- Hill, R. (1965). A self-consistent mechanics of composite materials. *Journal of the Mechanics and Physics of Solids*, 13(4):213–222. Cited page [74](#)
- Hilton, H. H. (2001). Implications and constraints of time-independent Poisson ratios in linear isotropic and anisotropic viscoelasticity. *Journal of Elasticity*, 63:221–251. Cited pages [63](#), [91](#), [109](#), and [120](#)
- Hilton, H. H. (2009). The elusive and fickle viscoelastic Poisson’s ratio and its relation to the elastic-viscoelastic corresponding principle. *Journal of Mechanics of Materials and Structures*, 4(September):1341–1364. Cited pages [109](#) and [120](#)
- Hilton, H. H. (2011). Clarifications of certain ambiguities and failings of Poisson’s ratios in linear viscoelasticity. *Journal of Elasticity*, 104(1-2):303–318. Cited pages [91](#), [109](#), and [120](#)
- Hua, C., Acker, P., and Ehlacher, A. (1995). Analyses and models of the autogenous shrinkage of hardening cement paste: I. modelling at macroscopic scale. *Cement and Concrete Research*, 25(7):1457–1468. Cited pages [61](#), [160](#), and [185](#)
- Jennings, H. M. (2000). A model for the microstructure of calcium silicate hydrate in cement paste. *Cement and Concrete Research*, 30(1):101 – 116. Cited pages [50](#), [51](#), [52](#), [150](#), [179](#), and [192](#)
- Jennings, H. M. (2004). Colloid model of c-s-h and implications to the problem of creep and shrinkage. *Materials and Structures*, 37(1):59–70. Cited page [150](#)
- Jensen, O. M. (1995). Thermodynamic limitation of self-desiccation. *Cement and Concrete Research*, 25(1):157–164. Cited pages [56](#) and [175](#)
- Jensen, O. M. and Hansen, P. F. (1996). Autogenous deformation and change of the relative humidity in silica fume-modified cement paste. *ACI Materials Journal*, 93(6):539–543. Cited pages [25](#), [28](#), [32](#), [175](#), [176](#), [178](#), and [250](#)

BIBLIOGRAPHY

Jensen, O. M. and Hansen, P. F. (1999). Influence of temperature on autogenous deformation and relative humidity change in hardening cement paste. *Cement and Concrete Research*, 29(4):567–575.

Cited pages 25, 28, 32, 175, 176, 178, and 250

Jirásek, M. and Bazant, Z. P. (2002). *Inelastic analysis of structures*. John Wiley & Sons.

Cited page 82

Jordaan, I. J. and Illston, J. M. (1969). The creep of sealed concrete under multiaxial compressive stresses. *Magazine of Concrete Research*, 21(69):195–204.

Cited pages 23, 28, 64, 104, 105, 106, 107, 117, 118, 121, 126, 127, 128, 129, 131, 234, and 235

Jordaan, I. J. and Illston, J. M. (1971). Time dependent strains in sealed concrete under systems of variable multiaxial stress. *Magazine of Concrete Research*, 23(75-76):79–88.

Cited pages 28, 64, 118, 121, 126, 127, 128, 234, and 235

Kawasumi, M., Kasahara, K., and Kuriyama, T. (1982). Creep of concrete at elevated temperatures, part 3, the influence of ages at loading and water/cement ratios. Technical Report CRIEPI Report, No.382008.

Cited pages 25, 172, and 187

Kennedy, T. W. (1975). An evolution and summary of a study of the long-term multiaxial creep behavior of concrete. Technical report, Oak Ridge National Laboratory.

Cited pages 23, 28, 64, 104, 105, 118, 126, 127, 128, 129, 131, and 235

Kim, J. K., Kwon, S. H., Kim, S. Y., and Kim, Y. Y. (2005). Experimental studies on creep of sealed concrete under multiaxial stresses. *Magazine of Concrete Research*, 57(10):623–634.

Cited pages 23, 28, 64, 104, 105, 118, 121, 126, 127, 128, 129, 131, 236, and 237

Kogan, E. A. (1983). Creep of concrete under multiaxial compression. *Hydrotechnical construction*, 17(9):448–452.

Cited page 122

- Kommendant, G., Polivka, M., and Pirtz, D. (1976). Study of concrete properties for prestressed concrete reactor vessels. Technical Report No. UCSESM 76-3, Department of Civil Engineering, University of California, Berkeley. *Cited pages 25, 172, and 187*
- Lakes, R. S. and Wineman, A. (2006). On poisson's ratio in linearly viscoelastic solids. *Journal of elasticity*, 85(1):45–63. *Cited pages 63, 91, and 109*
- Le Bellego, C. (2001). *Couplages chimie-mécanique dans les structures en béton attaquées par l'eau: Etude expérimentale et analyse numérique*. Cachan, Ecole normale supérieure. *Cited page 106*
- Le Roy, R. (1995). *Déformations instantanées et différées des bétons à hautes performances*. PhD thesis, École Nationale des Ponts et Chaussées. *Cited pages 25, 82, 141, 145, 159, 172, and 187*
- Le Roy, R., Le Maou, F., and Torrenti, J.-M. (2017). Long term basic creep behavior of high performance concrete: data and modelling. *Materials and Structures*, 50(1):85. *Cited pages 136, 141, 145, and 159*
- Lee, H., Lee, K., and Kim, B. (2003). Autogenous shrinkage of high-performance concrete containing fly ash. *Magazine of Concrete Research*, 55(6):507–515. *Cited pages 26, 181, and 187*
- Lee, Y., Yi, S.-T., Kim, M.-S., and Kim, J.-K. (2006). Evaluation of a basic creep model with respect to autogenous shrinkage. *Cement and concrete research*, 36(7):1268–1278. *Cited pages 26, 181, and 187*
- L'Hermite, R. (1959). What do we know about the plastic deformation and creep of concrete. In *RILEM Bulletin*, number 1, pages 888–896, Paris. *Cited pages 64, 117, and 122*
- Li, X., Grasley, Z., Bullard, J., and Garboczi, E. (2015). Computing the time evolution of the apparent viscoelastic/viscoplastic poisson's ratio of hydrating cement paste. *Cement and Concrete Composites*, 56:121–133. *Cited page 119*

BIBLIOGRAPHY

- Lin, F. and Meyer, C. (2008). Modeling shrinkage of portland cement paste. *ACI materials journal*, 105(3):302–311. *Cited pages 61 and 160*
- Luan, Y., Ishida, T., Li, C.-H., Fujikura, Y., Oshita, H., Nawa, T. I. T., and Sagawa, T. (2013). Enhanced shrinkage model based on early age hydration and moisture status in pore structure. *Journal of Advanced Concrete Technology*, 11(12):1–13. *Cited pages 61, 160, and 185*
- Lura, P., Jensen, O. M., and van Breugel, K. (2003). Autogenous shrinkage in high-performance cement paste: an evaluation of basic mechanisms. *Cement and Concrete Research*, 33(2):223–232. *Cited pages 60 and 61*
- Maalej, Y. (2007). *Mechanical behaviour of a grouted granular medium : experimental study and micromechanical modelization*. PhD thesis, Ecole Nationale des Ponts et Chaussées. *Cited page 152*
- Mantellato, S., Palacios, M., and Flatt, R. J. (2015). Reliable specific surface area measurements on anhydrous cements. *Cement and Concrete Research*, 67:286–291. *Cited page 51*
- Mazloom, M., Ramezani-pour, A., and Brooks, J. (2004). Effect of silica fume on mechanical properties of high-strength concrete. *Cement and Concrete Composites*, 26(4):347–357. *Cited pages 25, 26, 160, 162, 172, 181, and 187*
- Mazzotti, C., Savoia, M., and Ceccoli, C. (2005). A comparison between long-term properties of self-compacting concretes and normal vibrated concretes with same strength. In *Proceedings of the International Conference on Creep, Shrinkage and Durability of Concrete and Concrete Structures*, pages 523–528. Nantes, France. *Cited pages 25, 172, and 187*
- Mehta, P. K. and Monteiro, P. J. (2006). *Concrete: microstructure, properties, and materials*. McGraw-Hill New York, 3 edition. *Cited pages 50, 51, 52, 65, 135, 142, 143, and 171*

- Mori, T. and Tanaka, K. (1973). Average stress in matrix and average elastic energy of materials with misfitting inclusions. *Acta metallurgica*, 21(5):571–574. *Cited pages 73 and 166*
- Mu, R., Forth, J., and Beeby, A. (2009). Designing concrete with special shrinkage and creep requirements. In *Proceedings of 8th International Conference on Creep, Shrinkage and Durability of Concrete and Concrete Structures*. Ise-Shima, Japan. *Cited pages 25, 172, and 187*
- Muller, A. C., Scrivener, K. L., Gajewicz, A. M., and McDonald, P. J. (2012). Densification of c–s–h measured by 1h nmr relaxometry. *The Journal of Physical Chemistry C*, 117(1):403–412. *Cited page 53*
- Müller, H. S., Anders, I., Breiner, R., and Vogel, M. (2013). Concrete: treatment of types and properties in fib model code 2010. *Structural concrete*, 14(4):320–334. *Cited page 136*
- Neville, A. M. (1995). *Properties of concrete*. Longman London, 4 edition. *Cited page 104*
- Neville, A. M., Dilger, W. H., and Brooks, J. J. (1983). *Creep of plain and structural concrete*. Construction Press. *Cited pages 64, 65, 104, 117, 119, 122, and 123*
- Parrott, L. (1974). Lateral strains in hardened cement paste under short- and long-term loading. *Magazine of Concrete Research*, 26(89):198–202. *Cited pages 23, 104, 105, 106, 107, 135, 147, and 148*
- Parrott, L. J., Geiker, M., Gutteridge, W. A., and Killoh, D. (1990). Monitoring portland cement hydration: comparison of methods. *Cement and Concrete Research*, 20(6):919–926. *Cited page 189*
- Persson, B. (1997). Moisture in concrete subjected to different kinds of curing. *Materials and Structures*, 30(9):533–544. *Cited pages 25, 28, 32, 175, 176, 178, and 250*

BIBLIOGRAPHY

- Pichler, B. and Hellmich, C. (2011). Upscaling quasi-brittle strength of cement paste and mortar: A multi-scale engineering mechanics model. *Cement and Concrete Research*, 41(5):467 – 476.
Cited pages 21, 76, 77, 78, and 139
- Pichler, C., Lackner, R., and Mang, H. A. (2007). A multiscale micromechanics model for the autogenous-shrinkage deformation of early-age cement-based materials. *Engineering fracture mechanics*, 74(1):34–58.
Cited pages 21, 76, 77, and 173
- Pickett, G. (1942). The effect of change in moisture-content on the crepe of concrete under a sustained load. In *Journal Proceedings*, volume 38, pages 333–356.
Cited pages 59 and 185
- Polivka, M., Pirtz, D., and Adams, R. F. (1963). Studies of creep in mass concrete. *ACI Special Publication*, 6:257–283. *Cited pages 64 and 117*
- Powers, T. C. and Brownyard, T. L. (1947). Studies of the hardened paste by means of specific-volume measurements. *Portland Cement Association Bulletin*, pages 669–712.
Cited pages 52, 53, 54, 55, 56, 142, 143, 170, 171, 175, and 195
- RILEM Technical Committee (1995). Creep and shrinkage prediction model for analysis and design of concrete structures-model b3. *Materials and Structures*, 28:357–365. *Cited pages 63, 82, 117, 130, 131, 159, and 216*
- RILEM Technical Committee (2015). RILEM draft recommendation: TC-242-MDC multi-decade creep and shrinkage of concrete: material model and structural analysis. *Materials and Structures*, 48(4):753–770.
Cited pages 63, 82, 117, 136, 159, 160, and 185
- Ross, A. (1954). Experiments on the creep of concrete under two-dimensional stressing. *Magazine of Concrete Research*, 6(16):3–10.
Cited pages 64 and 117
- Rostasy, F., K.Th., T., and Engelke, H. (1973). Beitrag zur klarung des zusammenhanges von kriechen und relaxation bei normal-beton. Technical

- Report Heft 139, mtliche Forschungs-und Materialpr Aufungsanstalt fur das Bauwesen. *Cited pages 25, 172, and 187*
- Salençon, J. (1983). *Viscoélasticité*. Presse de l'École Nationale des Ponts et Chaussées. *Cited page 95*
- Sanahuja, J. (2008). *Impact de la morphologie structurale sur les performances mécaniques des matériaux de construction : application au plâtre et à la pâte de ciment*. PhD thesis, École Normale Supérieure de Cachan. *Cited page 150*
- Sanahuja, J. (2013). Effective behaviour of ageing linear viscoelastic composites: Homogenization approach. *International Journal of Solids and Structures*, 50(19):2846–2856. *Cited page 145*
- Sanahuja, J., Dormieux, L., and Chanvillard, G. (2007). Modelling elasticity of a hydrating cement paste. *Cement and Concrete Research*, 37(10):1427 – 1439. *Cited pages 21, 76, 77, 139, and 152*
- Sellier, A. and Buffo-Lacarriere, L. (2009). Towards a simple and unified modelling of basic creep, shrinkage and drying creep of concrete. *European Journal of Environmental and Civil Engineering*, 13(10):1161–1182. *Cited pages 61, 82, 160, 185, and 187*
- Sellier, A., Multon, S., Buffo-Lacarrière, L., Vidal, T., Bourbon, X., and Camps, G. (2016). Concrete creep modelling for structural applications: non-linearity, multi-axiality, hydration, temperature and drying effects. *Cement and Concrete Research*, 79:301–315. *Cited pages 21, 61, 62, 82, 84, 85, 86, 160, 185, 186, 187, and 198*
- Shritharan, S. (1989). Structural effects of creep and shrinkage on concrete structures. Master's thesis, University Auckland. *Cited pages 25, 26, 162, 172, 181, and 187*
- Sidhom, M. (2014). *Multi-scale approaches of granular composites with interface effects : application to nanocomposites and cement based composites*. PhD thesis, Université Paris-Est. *Cited page 153*

BIBLIOGRAPHY

- Stefan, L., Benboudjema, F., Torrenti, J.-M., and Bissonnette, B. (2009). Behavior of concrete at early stage using percolation and biot's theory. In *Proceedings of the 4th Biot conference on Poromechanics*.
Cited pages 61 and 160
- Stockl, S., Lanig, N., and Kupfer, H. (1989). Creep behavior of concrete under triaxial compressive stresses. In *Transactions of the 10th international conference on structural mechanics in reactor technology*. *Cited page 105*
- Takahashi, H. and Kawaguchi, T. (1980). Study on time-dependent behavior of high strength concrete (part 1) - application of the time - dependent linear viscoelasticity theory of concrete creep behavior. Technical Report No.21, Ohbayashi-Gumi Research Institute. *Cited pages 25, 172, and 187*
- Taylor, H. F. (1997). *Cement chemistry*. Thomas Telford.
Cited pages 142, 143, 170, and 171
- Tazawa, E. and Miyazawa, S. (1993). Autogenous shrinkage of concrete and its importance in concrete technology. In *Proceedings of 5th International Conference on Creep, Shrinkage and Durability of Concrete and Concrete Structures*, pages 159–174. Barcelona, Spain. *Cited pages 26, 181, and 187*
- Tazawa, E.-i. and Miyazawa, S. (1995). Influence of cement and admixture on autogenous shrinkage of cement paste. *Cement and Concrete Research*, 25(2):281–287. *Cited pages 26, 181, and 187*
- Tennis, P. D. and Jennings, H. M. (2000). A model for two types of calcium silicate hydrate in the microstructure of portland cement pastes. *Cement and concrete research*, 30(6):855–863. *Cited pages 52 and 150*
- Torrenti, J. and Le Roy, R. (2015). Analysis and modelling of basic creep. In *CONCREEP 10*, pages 1400–1409. *Cited page 136*
- Torrenti, J. M., Benboudjema, F., Barré, F., and Gallitre, E. (2014). On the very long term delayed behaviour of concrete. In *Proceedings of the International Conference on Ageing of Materials & Structures*, number 218885. *Cited pages 92, 109, and 117*

- Tschoegl, N. W., Knauss, W. G., and Emri, I. (2002). Poisson's ratio in linear viscoelasticity - a critical review. *Mechanics of Time-Dependent Materials*, 7(6):3–51. *Cited pages 63, 91, 108, 109, and 120*
- Ulm, F., Le Maou, F., and Boulay, C. (2000). Creep and shrinkage of concrete-kinetics approach. *ACI Special Publication*, 194:135–153. *Cited pages 23, 64, 118, 126, 131, and 218*
- Van Genuchten, M. T. (1980). A closed-form equation for predicting the hydraulic conductivity of unsaturated soils. *Soil science society of America journal*, 44(5):892–898. *Cited pages 204 and 255*
- Vandamme, M. and Ulm, F.-J. (2009). Nanogranular origin of concrete creep. *Proceedings of the National Academy of Sciences*, 106(26):10552–10557. *Cited pages 67 and 189*
- Vandamme, M. and Ulm, F.-J. (2013). Nanoindentation investigation of creep properties of calcium silicate hydrates. *Cement and Concrete Research*, 52:38 – 52. *Cited pages 159, 187, and 190*
- Varst, P. T. and Kortsmit, W. (1992). Notes on the lateral contraction of linear isotropic visco-elastic materials. *Archive of Applied Mechanics*, 62(5):338–346. *Cited pages 91 and 95*
- Vidal, T., Assié, S., and Pons, G. (2005). Creep and shrinkage of self-compacting concrete and comparative study with model code. In *Proceedings of the Seventh International Conference, Ecole Centrale de Nantes, France*, pages 541–546. *Cited pages 26, 181, and 187*
- Vlahinić, I., Thomas, J. J., Jennings, H. M., and Andrade, J. E. (2012). Transient creep effects and the lubricating power of water in materials ranging from paper to concrete and kevlar. *Journal of the Mechanics and Physics of Solids*, 60(7):1350–1362. *Cited page 62*
- Waller, V. (1999). *Relations entre composition des bétons, exothermique en cours de prise et résistance en compression*. PhD thesis, Ecole Nationale des Ponts et Chaussées. *Cited pages 57 and 171*

BIBLIOGRAPHY

- Walraven, J. and Shen, J. (1991). On the applicability of the superposition principle in concrete creep. *Mechanics of Creep Brittle Materials 2*, pages 282–295. *Cited pages 21, 65, and 69*
- Weiss, W. J., Borichevsky, B. B., and Shah, S. P. (1999). The influence of a shrinkage reducing admixture on early-age shrinkage behavior of high performance concrete. In *5th International Symposium on Utilization of High Strength/High Performance Concrete*, volume 2, pages 1339–1350. *Cited pages 26, 181, and 187*
- Wu, L., Farzadnia, N., Shi, C., Zhang, Z., and Wang, H. (2017). Autogenous shrinkage of high performance concrete: A review. *Construction and Building Materials*, 149:62–75. *Cited pages 60, 61, and 160*
- Wyrzykowski, M. and Lura, P. (2016). Effect of relative humidity decrease due to self-desiccation on the hydration kinetics of cement. *Cement and Concrete Research*, 85:75–81. *Cited pages 25, 28, 32, 175, 176, 178, and 250*
- York, G. P., Kennedy, T. W., Perry, E. S., and Thompson, J. N. (1972). Experimental determination of poisson’s ratio for creep. *ACI Journal Special Publication*, 34:535–546. *Cited pages 64 and 118*
- Yssorche-Cubaynes, M. P. and Ollivier, J. (1999). La microfissuration d’autodessiccation et la durabilité des bhp et bthp. *Materials and Structures*, 32(1):14–21. *Cited pages 25, 28, 32, 175, 176, 178, and 250*
- Zaoui, A. (1999). *Matériaux hétérogènes et composites: Majeure de Mécanique, option" matériaux et structures*. École polytechnique, département de mécanique. *Cited pages 74, 167, 173, and 174*
- Zhang, J., Hou, D., and Han, Y. (2012). Micromechanical modeling on autogenous and drying shrinkages of concrete. *Construction and Building Materials*, 29:230–240. *Cited pages 61 and 160*
- Zhang, M., Tam, C., and Leow, M. (2003). Effect of water-to-cementitious materials ratio and silica fume on the autogenous shrink-

- age of concrete. *Cement and Concrete Research*, 33(10):1687–1694.
Cited pages 26, 181, and 187
- Zhang, Q. (2014). *Creep properties of cementitious materials : effect of water and microstructure : An approach by microindentation*. PhD thesis, Université Paris-Est. *Cited pages 26, 67, 172, 187, 189, 190, and 191*
- Zhang, Q., Roy, R. L., Vandamme, M., and Zuber, B. (2014). Long-term creep properties of cementitious materials: Comparing microindentation testing with macroscopic uniaxial compressive testing. *Cement and Concrete Research*, 58:89 – 98. *Cited pages 141, 145, and 159*
- Zhutovsky, S. and Kovler, K. (2013). Hydration kinetics of high-performance cementitious systems under different curing conditions. *Materials and structures*, 46(10):1599–1611. *Cited pages 25, 28, 32, 175, 176, 178, and 250*